# Characterization of spontaneous tumor antigen-reactive T cell responses in melanoma patients and treatment of human melanoma with optimized T cell receptor transgenic T cells in a xenotransplantation model

**Inaugural Dissertation**

for the degree of
doctor rerum naturalium (Dr. rer. nat.)

submitted to the
Combined Faculties for the Natural Sciences and for Mathematics
of the Ruperto-Carola University of Heidelberg, Germany

**presented by**

**Diplom-Biologist Christina Pfirschke**

**born 24.02.1981 in Weimar, Germany**

**August 2011**

The work has been carried out in the laboratory of Prof. Dr. Philipp Beckhove in the Unit of Translational Immunology at the German Cancer Research Center (DKFZ) and National Center for Tumor Diseases (NCT), Heidelberg, Germany.

Referees: Prof. Dr. Philipp Beckhove
Prof. Dr. Stefan Wölfl

Oral examination: 25.10.2011

**Parts of this thesis have been published in:**

**Pfirschke C** and Schirrmacher V. (2009) Cross-infection of tumor cells by contact with T lymphocytes loaded with Newcastle disease virus. *Int J Oncol.* 34:951-962.

Voss RH, Thomas S, **Pfirschke C**, Hauptrock B, Klobuch S, Kuball J, Grabowski M, Engel R, Guillaume P, Romero P, Huber C, Beckhove P and Theobald M. (2010) Coexpression of the T-cell receptor constant alpha domain triggers tumor reactivity of single-chain TCR-transduced human T cells. *Blood*. 115:5154-5163.

Witzens-Harig M, Juenger S, Hose D, **Pfirschke C**, Conrad H, Seckinger A, Condomines M, Meißner T, Hundemer M, Ho AD, Rossi JF, Neben K, Bernhardt H, Goldschmidt H, Klein B and Beckhove P. Human tumour cells inhibit T cell recognition through expression of carcinoembryonic-antigen-related cell adhesion molecule-6. *submitted*

Do not go where the path may lead
go instead where there is no path and leave a trail.

**Ralph Waldo Emerson (1803 - 1882)**

**Dedicated to my parents**

# 1. Table of contents

## 2. Abbreviations and definitions

| | |
|---|---|
| $A_{260/280}$ | absorption at 260 and 280 nm |
| aa | amino acids |
| AB | human serum type AB |
| Ab(s) | antibody(ies) |
| ACAD | activated cell-autonomous death |
| ACK | ammonium chloride potassium phosphate |
| ADI | adoptive immunotherapy |
| AEC | 3-amino-9-ethylcarbazole |
| AICD | activation-induced cell death |
| AJCC | American Joint Committee on Cancer |
| ANCA | anti-neutrophilic cytoplasmic auto-Abs |
| ANA | anti-nuclear auto-Abs |
| APC | Allophycocyanin |
| Arg | arginine, amino acid |
| ATCC | American Type Culture Collection |
| aT cell(s) | activated T cell(s) |
| BCIP | 5-bromo-4-chloro-3-indoyl phosphate |
| BD | Becton Dickinson |
| bp(s) | base pair(s) |
| BSA | bovine serum albumine |
| C | constant part of TCR |
| $Ca^{2+}$ | calcium |
| CAM | cell adhesion molecule |
| cAMP | cyclic adenosine monophosphate |
| CCR | chemokine receptor |
| CD | cluster of differentiation |
| cDNA | complementary DNA |
| CEACAM | carcinoembryonic antigen-related cell adhesion molecule |
| cf. | Latin "*confer*", - „bring together" |
| Chim | chimeric |
| cm | centimeter |
| $cm^2$ | square centimeter |
| CMV | cytomegalovirus |
| $CO_2$ | carbon dioxide |
| cpm | count per minute |
| CTC | circulating tumor cells |
| cTECs | cortical thymic epithelial cells |
| CTL(s) | cytotoxic T cell(s) |
| CTLA-4 | cytotoxic T lymphocyte associated antigen 4 |
| Cy | cyanine |
| d | day(s) |
| DAPI | 4', 6-diamidino-2-phenylindole |
| dc | double chain |
| DC | dendritic cells |
| $ddH_2O$ | double distilled water |
| DKFZ | German Cancer Research Center |
| DMEM | dulbecco's modified Eagle's medium |
| DMSO | dimethyl sulfoxide |
| DN | double negative |
| DNA | deoxyribonucleic acid |
| dNTP | deoxyribonucleoside triphosphate |
| DP | double positive |
| DPN | dysplastic nevus/nevi |
| DTT | dithiothreitol |
| E:T | effector to target ratio |
| ECL | enhanced chemiluminescence |
| ECM | extracellular matrix |
| E. coli | Escherichia coli |
| EDTA | ethylenediaminetetraacetic acid |
| e.g. | Latin "*exempli gratia*", - "for example" |
| EGFP | enhanced green fluorescent protein |
| ELISPOT | enzyme-linked immunospot assay |
| EMT | epithelial-to-mesenchymal transition |
| env | amphotropic virus envelope |
| et al. | Latin "*et alii*", - "and others" |
| F protein | fusion protein of NDV |
| $F(ab´)_2$ | 2 coupled variable Ab fragment regions |
| FACS | fluorescence activated cell sorting/flow cytometry |
| Fc | constant Ab fragment region |
| FCS | fetal calf serum |
| FDA | Food and Drug Administration |
| Fig(s). | figure(s) |
| FITC | fluorescein isothiocyanate |
| Foxp3 | forkhead box P3 |
| g | gram |
| gag | retroviral group-specific antigen |
| GAGE-1 | G antigen 1 |
| GALV | Gibbon ape leukemia virus |

| | |
|---|---|
| GITR | glucocorticoid-induced TNFR |
| Gly | glycine, amino acid |
| GM-CSF | granulocyte macrophage colony-stimulating factor |
| GnT-V | N-acetyl glucosaminyl-transferase V gene |
| gp100 | glycoprotein 100 |
| Gy | gray |
| G-418 | geneticin sulfate |
| h | hour(s) |
| HD | healthy donor |
| HLA-A2 | human leukocyte antigen A2 |
| HRP | horseradish peroxidase |
| HU | hemagglutination unit |
| Hygro | hygromycin |
| i.e. | Latin "*id est*", - "that is; in other words" |
| i.d. | intradermal |
| IDO | indoleamine 2,3-dioxygenase |
| IFN | interferon |
| Ig(A/G/M) | immunoglobulin (A/G/M) |
| IHC | immunohistochemistry |
| IL | interleukin |
| IL-2/IL-7Rα | α chain of IL-2/IL-7 receptor |
| i.p. | intraperitoneal |
| IRES | internal ribosomal entry site |
| iTreg | inducible Treg |
| i.v. | intraveneous |
| kb | kilobase |
| kDa | kilodalton |
| kV | kilovolt |
| L1CAM | L1 cell adhesion molecule |
| l | liter |
| LAG3 | lymphocyte-activation gene 3 |
| LB | Luria Bertani |
| luc | luciferase |
| Lys | lysine, amino acid |
| m | mouse |
| M | molar |
| *M.* | mycoplasma |
| mA | milliampere |
| mAb(s) | monoclonal antibody(ies) |
| MAGE | melanoma antigen family |
| Maxi Prep | Maxi DNA preparation |
| MBq | megabecquerel |
| McCT | multiplex cell contamination test |
| mCi | millicurie |
| MDSC | myeloid-derived suppressor cells |
| MDM2 | murine double minute 2 |
| Melan-A/ | tumor-associated |
| MART-1 | melanocytic differentiation antigen |
| mg | milligram |
| $Mg^{2+}$ | magnesium |
| M gene | matrix gene of NDV |
| MHC | major histocompatibility complex |
| MIF | macrophage migration inhibitory factor |
| min | minute(s) |
| ml | milliliter |
| mm | millimeter |
| mM | millimolar |
| MM | malignant melanoma |
| MoMuLV | moloney murine leukemia virus |
| mol/l | molar/liter |
| MPO | myeloperoxidase |
| mRNA | messanger RNA |
| Mt | mutated |
| mTECs | medullary thymic epithelial cells |
| Mu | murine |
| MW | molecular weight |
| n | number |
| NA17-A | melanoma antigen from patient NA17 |
| NBT | nitroblue tetrazolium |
| NC | negative control |
| NCT | National Center for Tumor Diseases |
| nd | not detectable |
| n.d. | not determined |
| NDV | Newcastle disease virus |
| NEAA | non-essential amino acid |
| NEB | New England Biolabs |
| NK | natural killer |
| nm | nanometer |
| NOD | non-obese diabetic |
| NSG | NOD-SCID gamma |
| nTreg | naturally occurring Treg |
| NY-Eso-1 | cancer/testis antigen |
| OD | optical density |
| p53 | protein 53 |
| p/sec/$cm^2$/sr | photons/second/square centimeter/steradian |
| PAGE | polyacrylamide gel electrophoresis |
| p-ANCA | perinuclear anti-neutrophilic cytoplasmic auto-Abs |

| | |
|---|---|
| PB | peripheral blood |
| PBMC | PB mononuclear cells |
| PBS | phosphate buffered saline |
| PC | positive control |
| PCR | polymerase chain reaction |
| PD-1 | programmed cell death-1 |
| PE | phycoerythrin |
| Pen/Strep | Penicillin/Streptomycin |
| PerCP-Cy5.5 | peridinin-chlorophyll-protein-complex-cyanine 5.5 |
| pH | Latin "*potentia hydrogenii*" |
| PI | propidium iodide |
| pmel17 | melanocyte-specific glycoprotein 17 |
| pmol | picomol |
| pol | retroviral reverse transcriptase polymerase |
| PVDF | polyvinylidene difluoride |
| r | recombinant |
| RAB38/ NY-Mel-1 | melanocyte differentiation antigen |
| rb | rabbit |
| rIL | recombinant interleukin |
| RLU | relative light units |
| RNA | ribonucleic acid |
| rpm | rounds per minute |
| RPMI | roswell park memorial institute |
| ROI | region of interest |
| ROS | reactive oxygen species |
| RT | room temperature |
| sc | single chain |
| s.c. | subcutaneous |
| SCID | severe combined immune-deficient |
| SD | standard deviation |
| SDS | sodium dodecyl sulfate |
| SEB | staphylococcal enterotoxin B |
| sec | second |
| SEM | standard error of the mean |
| S.O.C. | super optimal broth medium with catabolite repression |
| SP | single positive |
| TAAs | tumor-associated antigens |
| Tab(s). | table(s) |
| TAE | Tris-Acetate-EDTA |
| TAP | transporter associated with antigen processing |
| TC | T cell |
| TCR | T cell receptor |
| TE | Tris-EDTA |
| TGFβ | transforming growth factor β |
| Th/$T_H$ | T helper cells |
| TILs | tumor-infiltrating lymphocytes |
| TNA | tumor neutralization assay |
| TNF(R) | tumor necrosis factor (receptor) |
| TNM | tumor-node-metastases |
| TRAIL | TNF-related apoptosis-inducing ligand |
| Treg | regulatory T cells |
| Tris | tris(hydroxymethyl) aminomethane |
| TRP2 | tyrosinase related protein 2 |
| U | unit |
| UICC | International Union against Cancer |
| UV | ultraviolet |
| V | volt |
| VEGF | vascular endothelial growth factor |
| VLA | very late antigen |
| $V_\beta$ | variable part of TCR β chain |
| W | watt |
| WHO | World Health Organization |
| Wt/WT | wild type |
| x | times |
| X | x-fold |
| $^3H$ | tritium, hydrogen-3 |
| 7-AAD | 7-aminoactinomycin D |
| $^{51}Cr$ | radioactive chromium isotope 51 |
| α | alpha or anti |
| β | beta |
| $\beta_2m$ | $\beta_2$ microglobulin |
| γ | gamma |
| δ | delta |
| ε | epsilon |
| ζ | zeta |
| λ | lambda |
| π | pi |
| µCi | microcurie |
| µg | microgram |
| µl | microliter |
| µm | micrometer |
| µM | micromolar |
| ~ | approximately |
| °C | degree celsius |
| Ø | diameter |
| % | percentage |

## 3. Summary

One of the leading human malignancies is cancer, a disease characterized by mostly uncontrolled growth of abnormal cells in the body, often forming metastases. It´s interaction with the immune system, that can influence the disease progression, has repeatedly been reported and gained increasing importance over the last decades. However, most of the current immunotherapeutic approaches for cancer treatment are limited, partly due to the immune controlling capacities of tumors. The development of novel experimental approaches and therapeutic strategies, that support and complement the tumor-directed pre-existing abilities of the immune system, will be critical for the success of future cancer immunotherapies. Therefore, and because of the general need of novel treatment strategies, the presented thesis focused on four different approaches to optimize cancer immune therapeutic interventions.

Functionally competent tumor-specific memory T cells have been reported to efficiently control tumor growth and be required for a durable prevention of tumor recurrence and metastasis formation. Therefore, the first project dealed with spontaneously induced tumor antigen-reactive memory T cell responses in the peripheral blood (PB) of melanoma and dysplastic nevi patients. Thereby, using a short-term IFNγ ELISPOT assay, high frequencies of pre-existing T cell responses were detected in both cohorts *ex vivo*. As antigen-presenting cells, I have used autologous dendritic cells, generated from monocytes which were pulsed with 13 different 50 amino acid long synthetic melanoma polypeptides, derived from immunodominant regions of tumor-associated antigens (TAAs). Thereby, the nature of the identified T cell responses revealed to be polyvalent and HLA-unrestricted. Moreover, the designed polypeptide sequences, that covered MHC class I- and II-restricted epitopes, are optimal for presentation on a wide range of HLA types and therefore, were recognized by $CD4^+$ and $CD8^+$ T cells. I have shown that the long peptide sequence of the NA17-A antigen induce high frequencies of NA17-A-reactive memory T cells, but not NA17-A-specific regulatory T cell (Treg) responses. Thus, particular importance for future vaccination approaches might therefore have to be considered. Furthermore, the demonstration that the TAA-reactive T cell frequencies increased after resection of the non-metastasized tumors or dysplastic nevi indicates that the presence of the lesions controls pre-existing T cell responses. Additionally, these investigations also showed antigen-specific Treg in the PB and revealed that, in some patients, Treg have an immunosuppressive potential. In general, however, an essential role of Treg in controlling spontaneous T cell responses in non-metastasized melanoma and dysplastic nevi patients could not be detected. Based on these findings, besides Treg, the tumor- or lesion-mediated TAA-reactive memory T cell suppression might also be facilitated through other potential effectors of immunosuppression, including combinations of soluble and cellular mediators. Summarized, the investigated polypeptides efficiently elucidated pre-existing T cell responses in melanoma and dysplastic nevi patients and thus indicate that those polyvalent responses could be therapeutically reactivated in consequence of an appropriate peptide vaccination treatment.

For the second optimization approach a human melanoma murine xenotransplantation model has been established. Thereby, the *in vivo* efficiency and biologic relevance of human T cells,

which were transduced with functionally expressed, *in vitro* optimized, T cell receptor (TCR) constructs, specific for the antigens MDM2 or gp100 were investigated. For the first time *in vivo*, two novel strategies that aimed to avoid hybrid mispaired TCR chain formation and thereby potential autoimmune disease-causing “off-target” reactions were tested. These approaches comprised the molecular design of the TCR αβ interphase and a single chain TCR framework. Thereby, optimized MDM2 as well as gp100 transgenic T cells revealed the ability to significantly control human melanoma tumor growth. Moreover, the engineered T cells persisted *in vivo* and controlled in the same animals even a secondary tumor growth in a memory T cell-like manner. I could also demonstrate that a combinational treatment of adoptive T cell therapy using TCR gene-modified human T cells with local low dose tumor irradiation (2 Gy), led to an improved T cell targeting into the tumor and additionally further increased the tumor growth control. Consequently, in order to improve adoptive cancer immunotherapeutic approaches the *in vivo* experiments confirmed the feasibility and efficiency of the applied TCR design.

In the third project presented in this thesis, a novel tumor cell-mediated immunosuppressive mechanism, facilitated by the cell adhesion molecules CEACAM6 and L1CAM, was addressed. Thereby, these molecules were detected in various tumor cell lines and using short-term IFNγ ELISPOT and $^{51}$Cr release cytotoxicity assays it could be shown that their specific blockade resulted in increased, functional effector T cell responses. Therefore, in order to modulate the strength of T cell responses against malignant edited tumor cells that escaped immune recognition, CEACAM6 and L1CAM may consequently be attractive targets for novel immunotherapeutic interventions.

Finally, to increase the capacity of oncolytic virotherapies, in a fourth project, I optimized the viral transport of the Newcastle disease virus (NDV) to human tumor cells. In this approach, the loading of human T cells with NDV was specified for the first time in an *in vitro* co-culture system. Moreover, in a “hitchhiking”-like mechanism T cells have shown to be capable to transfer cell surface-attached NDV to MCF-7 tumor cells. In addition, monolayers of tumor cells were efficiently destroyed through oncolytic NDV-modified activated T cells. Based on this combinational therapy, it can be proposed that effector T cells can facilitate as potent carrier vehicles to transport NDV to tumor sites, resulting in focused tumor cell destruction.

In summary, the findings of the four different approaches, presented in this thesis, indicate novel perspectives for the optimization of future immunotherapeutic interventions in order to elicit and support protective T cell responses against clinically apparent malignant tumors.

# 4. Zusammenfassung

Krebs stellt eine der führenden malignen Erkrankungen beim Menschen dar und ist durch unkontrolliertes Wachstum von entarteten Körperzellen und die Bildung von Metastasen gekennzeichnet. Die Wechselwirkung von Krebs mit dem Immunsystem, welche die Krankheitsentwicklung beeinflussen kann, wurde wiederholt beschrieben und hat in den letzten Jahrzehnten an zunehmender Bedeutung gewonnen. Dennoch zeigen gegenwärtig die meisten immuntherapeutischen Ansätze zur Krebsbehandlung nur eine begrenzte Wirksamkeit, teilweise hervorgerufen durch immunkontrollierende Eigenschaften von Tumoren. Die Entwicklung von neuen experimentellen Ansätzen und therapeutischen Strategien, welche die vorhandenen, tumorgerichteten Fähigkeiten des Immunsystems unterstützen und zusätzlich ergänzen, wird für den Erfolg zukünftiger Krebsimmuntherapien von entscheidender Bedeutung sein. Aus diesem Grund und wegen des generellen Bedarfs an neuen Strategien, beschäftigte sich die vorliegende Doktorarbeit mit vier verschiedenen Ansätzen zur Optimierung von immuntherapeutischen Interventionen für die Behandlung von Krebserkrankungen.

Es wurde gezeigt, dass funktionell kompetente tumorspezifische Gedächtnis-T-Zellen das Tumorwachstum effizient kontrollieren können und für einen anhaltenden Schutz vor einem erneuten Auftreten von Tumoren und einsetzender Metastasierung benötigt werden. Das erste Projekt befasste sich daher mit spontan induzierten, Tumorantigen-reaktiven Gedächtnis-T-Zellantworten im peripheren Blut (PB) von Melanom- und dysplastischen Nävipatienten. Unter Verwendung von IFNγ ELISPOT-Kurzzeituntersuchungen wurden *ex vivo* in beiden Patientengruppen hohe Frequenzen von präexistierenden, tumor-spezifischen T-Zellantworten nachgewiesen. Als antigenpräsentierende Zellen habe ich autologe dendritische Zellen verwendet, welche aus Monozyten generiert wurden. Diese wurden mit 13 verschiedenen 50 Aminosäure-langen synthetischen Melanompolypeptiden beladen, welche von immundominanten Regionen von Tumor-assoziierten Antigenen (TAAs) abgeleitet wurden. Die resultierenden T-Zellantworten waren polyvalent und HLA-unrestringiert. Darüber hinaus umfassten die generierten Polypeptidsequenzen MHC-Klasse I und II-restringierte Epitope, welche effizient von einer Vielzahl von HLA-Molekülen präsentiert werden können und daher von $CD4^+$ und $CD8^+$ T-Zellen erkannt wurden. Weiterhin konnte ich zeigen, dass die lange NA17-A Peptidsequenz zur Induktion von erhöhten, NA17-A reaktiven Gedächtnis-T-Zellfrequenzen führte, wohingegen keine NA17-A spezifischen Antworten durch regulatorische T-Zellen (Treg) hervorgerufen wurden. Diese Erkenntnis könnte für zukünftige Vakzinierungsansätze von entscheidender Bedeutung sein. Nach Entfernung des nicht-metastasierten Tumors oder dysplastischen Nävus sind die TAA-reaktiven T-Zellfrequenzen stark angestiegen, wodurch gezeigt werden konnte, dass präexistierende T-Zellantworten durch das Vorhandensein der Läsionen kontrolliert werden. Des Weiteren wurden Antigen-spezifische Treg im PB nachgewiesen und bei einigen Patienten ein immunsuppressives Potenzial dieser Zellen aufgezeigt. Im Allgemeinen konnte jedoch keine wesentliche Rolle von Treg bei der Kontrolle von spontanen T-Zellantworten bei Patienten mit nicht-metastasierten Melanomen oder dysplastischen Nävi nachgewiesen werden. Basierend auf diesen Ergebnissen, ist eine tumor- oder läsionsabhängige Suppression von TAA-reaktiven Gedächtnis-T-Zellantworten, neben Treg, vermutlich auch durch andere potentielle immunsuppressive Effektoren vermittelt. Dabei spielen voraussichtlich Kombinationen von löslichen und zellulären Mediatoren eine entscheidende Rolle. Zusammenfassend zeigen diese Untersuchungen, dass die generierten langen Peptide effizient dazu verwendet werden können, um präexistierende Gedächtnis-T-Zellantworten bei Melanom-

und dysplastischen Nävipatienten nachzuweisen. Darüber hinaus könnten diese polyvalenten T-Zellantworten infolge einer geeigneten Peptidvakzinierung therapeutisch reaktiviert werden.

Für einen zweiten Optimierungsansatz, wurde ein humanes Melanom-Maus-Xenotransplantationsmodell etabliert, um die Wirksamkeit und biologische Relevanz von humanen T-Zell-Rezeptor-(TCR) transduzierten T-Zellen, welche spezifisch für die Antigene MDM2 oder gp100 sind, *in vivo* zu untersuchen. Die in T-Zellen funktionell-exprimierten TCR-Konstrukte wurden zuvor *in vitro* optimiert. In diesem Zusammenhang wurden zum ersten Mal zwei neuartige Strategien *in vivo* verfolgt, welche beabsichtigten eine Fehlpaarung von TCR-Ketten zu vermeiden, um somit möglichen Autoimmunkrankheit-verursachenden, vom zielabweichenden, „off-target" Reaktionen vorzubeugen. Bei diesen Ansätzen handelte es sich um eine molekular veränderte TCR-αβ-Struktur und ein Einzelketten-TCR-Konstrukt. Unter deren Verwendung konnte das Wachstum von humanen Melanomzellen sowohl durch die optimierten MDM2 als auch gp100 TCR-transgenen T-Zellen signifikant kontrolliert werden. Darüber hinaus überdauerten die optimierten T-Zellen *in vivo* und konnten in den gleichen Tieren in einer Gedächtnis-T-zellvermittelten Art und Weise das Wachstum eines sekundären Tumors kontrollieren. Weiterhin war es mir möglich zu zeigen, dass eine Kombinationsbehandlung aus adoptiven T-Zelltransfer mit TCR-genmodifizierten humanen T-Zellen und einer lokalen, niedrig dosierten Tumorbestrahlung (2 Gy) zu einer verbesserten T-Zelleinwanderung in den Tumor und einer verstärkten Tumorwachstumskontrolle führte. Diese *in vivo* Experimente bestätigten die Realisierbarkeit und Effizienz des angewandten TCR-Designs in Hinblick auf die Optimierung von adoptiven Krebsimmuntherapien.

Im dritten Projekt der vorliegenden Arbeit, wurde ein neuer Tumorzell-vermittelter immunsuppressiver Mechanismus, welcher auf den Zelladhäsionsmolekülen CEACAM6 und L1CAM basierte, untersucht. Zunächst konnten diese Moleküle auf verschiedenen Tumorzelllinien nachgewiesen werden. Unter Verwendung von Kurzzeit IFNγ ELISPOT- und $^{51}$Cr Zytotoxizitäts-experimenten konnte anschließend gezeigt werden, dass ihre spezifische Blockade in erhöhten funktionellen Effektor-T-Zellantworten resultierte. Infolgedessen, um die Intensität von T-Zell-antworten gegen maligne Tumorzellen, welche sich einer Immunerkennung entzogen haben, zu stärken, könnten CEACAM6 und L1CAM attraktive Ziele für neue immuntherapeutische Interventionen darstellen.

Um die Kapazität von onkolytischen Virustherapien zu erhöhen, optimierte ich in einem vierten Projekt den viralen Transport des Newcastle Disease Virus (NDV) zu humanen Tumorzellen. In diesem Ansatz wurde zum ersten Mal in einer *in vitro* Kokultur die Beladung von humanen T-Zellen mit NDV untersucht. Nachfolgend konnte in einem als „hitchhiking" definierten Transport-mechanismus gezeigt werden, dass T-Zellen in der Lage sind zelloberflächengebundenes NDV an MCF-7 Tumorzellen zu übertragen. Darüber hinaus wurden Tumorzellmonolayer effizient durch aktivierte T-Zellen, welche mit einem onkolytischen NDV Stamm modifiziert wurden, zerstört. Basierend auf dieser Kombinationstherapie könnten Effektor-T-Zellen als effiziente „Transportsysteme" eingesetzt werden, um NDV zu Tumorzellen zu transportieren, um so eine gezielte Zerstörung von Tumoren einzuleiten.

Zusammenfassend zeigen die Untersuchungen der vier unterschiedlichen Ansätze, die in dieser Arbeit vorgestellt wurden, neue Perspektiven für die Optimierung zukünftiger immun-therapeutischer Interventionen, um protektive T-Zellantworten gegen klinisch-erkennbare maligne Tumore auszulösen und zusätzlich zu unterstützen.

# 5. Introduction

The human immune system represents a complex, dynamic communication network and protects against diseases caused by bacterial, parasitic, fungal and viral infections. Moreover, it protects the organism from tumor cell growth. Thereby, it has to distinguish transformed cells from healthy cells and tissues (Murphy et al., 2008). The functions of the immune system are facilitated through diverse mechanisms of innate and adaptive immune responses (Fig. 1.). Cells of the innate immune system including mast cells, macrophages, dendritic cells, granulocytes and natural killer (NK) cells defend infections in a non-specific manner, and do not confer long-lasting or protective immunity. In contrast, the adaptive immunity is based on the characteristics of specificity, diversity, memory and the ability to discriminate between foreign and self antigens. Thereby, mainly T and B lymphocytes conduct the specialized responses, while B cells mediate the antibody (Ab)-driven humoral and T cells the cellular immunity. T cell-mediated immunity is characterized by a highly specific antigen-mediated clonal selection and proliferation of T cells, including the development of immunological memory, which shows enhanced responses on subsequent encounters with the antigen (Abbas and Lichtman, 2005; Murphy et al., 2008).

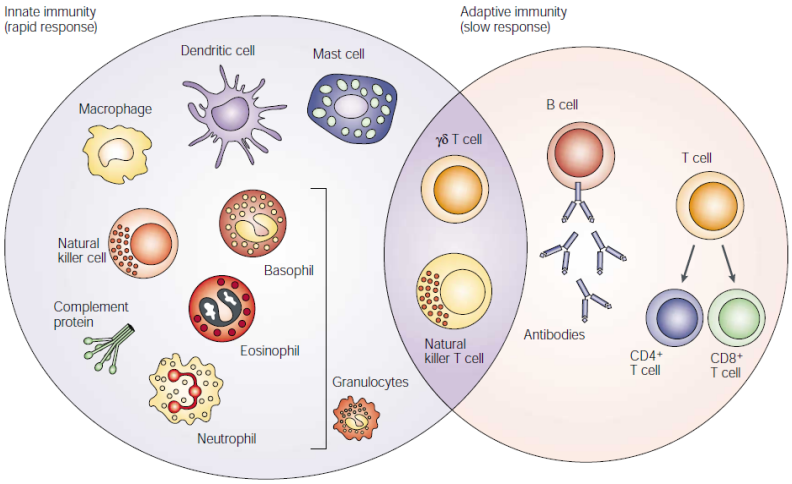


**Figure 1**. **The innate and adaptive immune response.** The innate immune response represents the first line of defense against infection. It consists of soluble factors (e.g., complement proteins) and cellular components (e.g., mast cells, macrophages, dendritic cells, granulocytes, natural killer cells). In contrast, the adaptive immune response develops slower, but manifests as increased antigenic specificity and memory. It consists of, e.g., antibodies, B cells, and T cells. The figure is taken from Dranoff, 2004.

During the last years, T cells have been described to mount anti-tumor responses that can efficiently destroy tumor cells (e.g., Boon et al., 2006). Therefore, in the course of the presented thesis, tumor-reactive T cells were investigated, and utilized as central mediators of cancer-directed immune interventions. The next paragraphs will describe how T cells mature, recognize their specific antigen, get activated and gain specific effector and memory cell functions, which are required to influence cancer progression.

## 5.1. T cell maturation and selection

T cells carry a highly diverse repertoire of T cell receptors (TCR), which they use to recognize foreign or self-antigens as peptide fragments bound to proteins of the major histocompatibility complex (MHC). The MHC is located on antigen-presenting cells including dendritic cells, macrophages and B cells.

In the bone marrow, lymphoid progenitor cells arise from pluripotent hematopoietic stem cells, followed by the migration to the thymus, where the generation and maturation of the T cell repertoire occurs (Abbas and Lichtman, 2005; Murphy et al., 2008). The thymus supports T cell differentiation, T cell repertoire selection and central tolerance induction to tissue-specific antigens (e.g., Miller, 1961; Zinkernagel et al., 1978; Kyewski and Derbinski, 2004). The lymphocytes in the thymus, the thymocytes, represent immature T cells at various stages of maturation. They perform a complex and highly ordered chemokine receptor-dependent, dynamic relocation through defined thymic regions (Plotkin et al., 2003; Benz et al., 2004; Misslitz et al., 2004). Thereby, they make intercellular contacts with cells of epithelial and mesenchymal origin including cortical and medullary thymic epithelial cells (cTECs, mTECs) as well as dendritic cells (cf., Fig. 2). The somatic recombination of TCR gene cassettes (TCR gene rearrangement) occurs in the subcapsular zone of the thymic cortex, followed by the assembly of a functional pre-TCR complex (von Boehmer and Fehling, 1997).

During the initial development, thymocytes are double negative (DN) for the cluster of differentiation 4 and 8 ($CD4^-CD8^-$), then become $CD4^+CD8^+$ double positive (DP) and undergo a positive and negative selection. This step ensures the deletion of thymocytes from the repertoire that bind peptide/MHC with insufficient avidity as well as the deletion of self-reactive thymocytes (Bousso et al., 2002). If low-avidity TCR-mediated interactions occur, DP thymocytes receive signals for survival, downregulate one of their co-receptors and become single positive (SP) $CD4^+$ or $CD8^+$ thymocytes (cf., Fig. 2; see also Ueno et al., 2004; Kurobe et al., 2006). The positive selection process leads to the maturation of thymocytes which carry a TCR with sufficient avidity to bind peptide/MHC. The majority of thymocytes cannot bind with sufficient avidity, and therefore undergo death by neglect (Kisielow et al., 1988; Jameson et al., 1995). Furthermore, self-reactive thymocytes undergo apoptosis, a non-inflammatory form of programmed cell death, in response to signals generated by high-avidity binding. This process, called “negative selection” or “clonal deletion”, is important for the induction of central T cell tolerance (von Boehmer et al., 1989; Robey and Fowlkes, 1994). Positively selected SP thymocytes mature to naive T cells with functional TCRs on their surface while undergoing further clonal deletion of self-reactive thymocytes. This additional elimination process is important to establish central T cell tolerance to peripheral tissue-specific antigens. Thereby, diverse tissues are presented by “promiscuous gene expression” (Zyklys et al., 2000; Kyewski and Derbinski, 2004; Derbinski et al., 2005). Moreover, the induction of naturally occurring regulatory T cells (nTreg) takes place in the thymus (Kyewski and Klein, 2006). Finally, naive $CD4^+$ T cells, $CD8^+$ T cells and nTreg, with a TCR αβ repertoire diversity of ~$2x10^7$ TCRs, leave the thymus (Arstila et al., 1999).

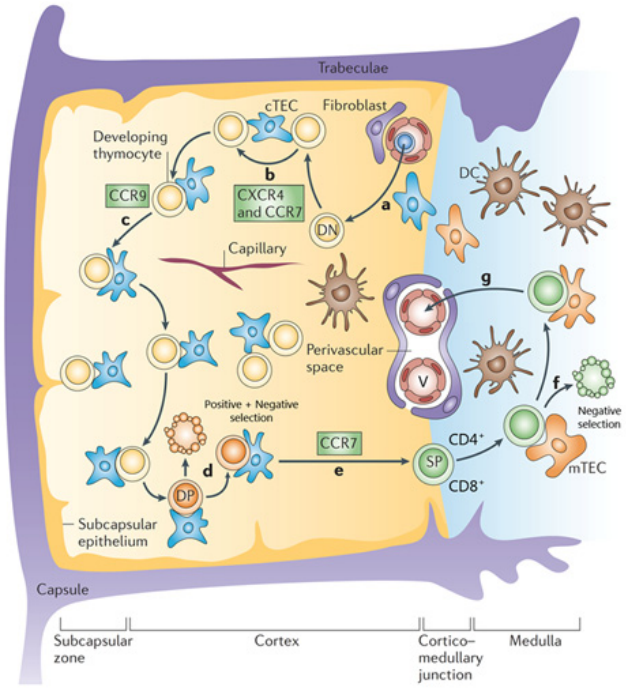


**Figure 2**. **Migration of thymocytes for T cell maturation and selection.** The circulation of thymocytes is indicated (**a**-**g**). Lymphoid progenitor cells enter the thymus at the cortico-medullary junction. $CD4^{-}CD8^{-}$ double-negative (DN) thymocytes migrate to the subcapsular zone. $CD4^{+}CD8^{+}$ double-positive (DP) thymocytes are generated in the outer cortex, and interact with cortical thymic epithelial cells (cTEC) and dendritic cells (DC) for positive and negative selection. Positively selected DP thymocytes differentiate into $CD4^{+}$ or $CD8^{+}$ single positive (SP) thymocytes, and migrate to the medulla were they undergo further negative selection through interaction with medullary thymic epithelial cells (mTEC) and DC. Finally, mature naive T cells leave the thymus through blood vessels. Chemokine receptors: CXCR4, CCR7 and CCR9. The figure is adapted from Takahama, 2006.

## 5.2. T cell antigen recognition and T cell activation

Naive T cells continuously migrate between secondary lymphatic organs (e.g., lymph nodes, spleen), the bone marrow, peripheral blood (PB) and the lymph in a blood-to-lymph recirculation. They get activated upon encounter of specific foreign peptide/MHC, which is presented on antigen-presenting cells, followed by the proliferation and differentiation into effector T cells (Butcher and Picker, 1996; Feuerer et al., 2003; Schirrmacher et al., 2003).

The recognition of antigens by T cells is conducted through an intercellular contact with antigen-presenting cells, mediated by cell adhesion molecules. This highly organized and dynamic cellular structure, formed at the T cell-antigen-presenting cell interface, is termed as the “immunological synapse” (for overview see Fig. 3; see also Monks et al., 1998; Bromley et al., 2001). This structure plays an important role in T cell activation and delivery of effector functions.

The TCR complex consists of two separate αβ heterodimeric peptide chains, bearing constant and variable regions. The chains are noncovalently associated with the cluster of differentiation 3 (CD3) proteins that consist of the two heterodimers γε and δε as well as the homodimer ζζ (Acuto et al., 2008). For antigen recognition, T cells need a MHC-restricted presentation of peptide

fragments. Moreover, the TCR/CD3-peptide/MHC complex has to be ligated to the co-receptors, either CD4 or CD8. $CD4^+$ T cells specifically respond to peptides presented by MHC class II molecules, while $CD8^+$ T cells need MHC class I for peptide presentation. In general, peptides loaded to MHC class I molecules derive from defective ribosomal products or normal turnover of endogenous intracellular proteins (Yewdell et al., 2003). In contrast, peptides loaded to MHC class II molecules mainly originate from endocytosed extracellular proteins or autophagy (Jensen, 2007). Nonetheless, some potent antigen-presenting cells are capable of presenting fragments of internalized extracellular proteins, on MHC class I, to $CD8^+$ T cells. This process has been introduced as “cross-presentation” (Carbone et al., 1998; Knutson and Disis, 2005).

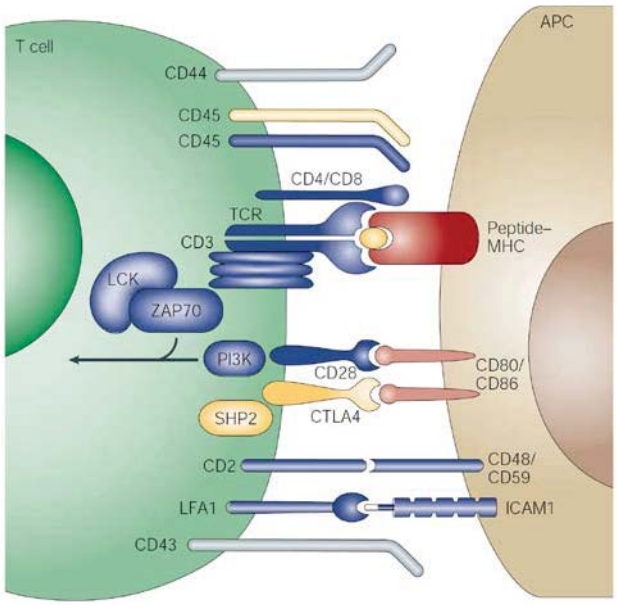


**Figure 3**. **The overview of an immunological synapse.** A selection of the key ligand pairs and signaling molecules, involved in T cell antigen recognition, followed by T cell activation are shown. APC, antigen-presenting cell; CD, cluster of differentiation; CTLA-4, cytotoxic T lymphocyte antigen 4; ICAM1, intercellular adhesion molecule 1; LFA1, leukocyte function-associated antigen 1; PI3K, phosphatidylinositol 3-kinase; SHP2, SRC homology 2-domain-containing protein tyrosine phosphatase 2; TCR, T cell receptor; ZAP70, ζ-chain-associated protein 70. The figure, exemplarily presented, is taken from Huppa and Davis, 2003.

In order to activate T cells, upon antigen recognition through TCR engagement, co-stimulatory signals from B7 molecules (CD80, CD86), presented by antigen-presenting cells are needed. These molecules bind to the CD28 surface receptor on T cells (Frauwirth et al., 2002). Besides CD28, the inhibitory molecule cytotoxic T lymphocyte antigen 4 (CTLA-4) can also bind B7 molecules, but with a higher avidity. CTLA-4 delivers inhibitory signals that make the T cell less sensitive to stimulation by antigen-presenting cells and lead to a decreased T cell-dependent production of the cytokine interleukin 2 (IL-2). The cytokine IL-2 is crucial for T cell proliferation (Robb et al., 1981; Smith, 1984; Teft et al., 2006). Furthermore, a comparable inhibitory function was also shown for the interaction of the CD28-related co-stimulatory molecule programmed death-1 (PD-1) on T cells with PD-ligand 1 (PD-L1) or PD-L2. These ligands, presented by antigen-

presenting cells, also belong to the B7 molecule family (Okazaki and Honjo, 2007). The here described mechanisms are critical for T cell proliferation control and self-tolerance maintenance.

To functional activate T cells, besides a specific cytokine milieu (including IL-2 and IL-15), further co-stimulatory/adhesion molecules on T cells are needed that bind to complementary molecules on antigen-presenting cells including CD2, CD27, CD40L, ICOS, LFA-1, OX40 and 4-1BB. Some of these molecules act as essential signals for T cell activation, while other stabilize the immunological synapse formation or enhance TCR signaling (Chambers and Allison, 1999; Watts and DeBenedette, 1999; Coyle and Gutierrez-Ramos, 2001; Croft, 2009). The signaling via the TCR complex is not a linear event from the receptor to the nucleus; it rather presents a complex feedback and feed forward regulation at each step of the signal transduction pathways (Smith-Garvin et al., 2009). Consequently, activated T cells that receive all the required signals start to proliferate and differentiate into effector T cells. Thereby, the context in which the T cells recognize their antigen, the abundance of antigen and the duration of antigen exposure are critical parameters that can affect the magnitude and nature of the T cell response. In contrast, T cells that do not receive the required signals become anergic, which results in a functional inactivation or clonal deletion.

## 5.3. Effector and memory T cells

Naive T cells have to pass three different stages until they differentiate into memory T cells (Ahmed and Gray, 1996; Kaech et al., 2002; Murphy et al., 2008). During the first, the “T cell expansion phase”, naive T cells that have encountered antigens, in course of a primary infection, clonally expand and differentiate into short-lived effector T cells. These are the $CD4^+$ T helper (Th) or the $CD8^+$ cytotoxic T cells (CTLs). Effector T cells are able to efficiently secrete inflammatory cytokines and kill infected cells. They migrate in a tissue-homing molecule-dependent way to sites of antigen exposure to deliver the appropriate effector and regulatory functions. After pathogen clearance, the majority of effector T cells rapidly die. These second phase is termed “T cell death” or “contraction phase”. Only a minority of T cells survives and enters the “memory phase” that characterizes the third stage of T cell response. The number of long-lived functional memory T cells stabilizes, and maintain for long periods of time. They represent the immunological memory, and provide ongoing protection against recurrent antigen stimuli (Sprent and Miller, 1976a, b; Kaech et al., 2002; for recent review see Taylor and Jenkins, 2011).

### 5.3.1. $CD4^+$ effector T cells

Th cells exert their function mainly through the secretion of cytokines and chemokines. They help other immune cells including B cells, macrophages and CTLs to express their functional activities at full strength (for review see Kaufmann, 2007). At the side of antigen recognition, different subsets of $CD4^+$ effector T cells, with unique functions, are generated in response to cytokines.

Peripheral $CD4^+$ T cells can differentiate into three main Th cell lineages: Th1, Th2 and Th17 or into inducible Treg (iTreg; for overview see Fig. 4; see also Zhou et al., 2009; Zou and Restifo, 2010).

Interferon γ (IFNγ) and IL-12 trigger the differentiation of Th1 cells. Th1 cells produce IFNγ, IL-2, tumor necrosis factor (TNF) and granulocyte macrophage colony-stimulating factor (GM-CSF) and stimulate for instance the activation of $CD8^+$ T cells. In contrast, Th2 cells are differentiated by the help of IL-4. They secrete IL-4, IL-5 and IL-13 and help for example B cells in Ab production and downregulate pro-inflammatory responses, induced by Th1 cells. Transforming growth factor β (TGFβ), IL-1, IL-6, IL-21 and IL-23 trigger the differentiation of Th17 cells. They produce IL-17 and IL-6, and, e.g., promote inflammation and activate neutrophiles. Besides different cytokine requirements, all three Th cell subsets are characterized by unique transcription factors (Th1: T-bet, Th2: GATA3, Th17: RORγt; for further details see also Weaver et al., 2006; Zhu and Paul, 2008; Zou and Restifo, 2010). Moreover, $CD4^+$ T cells differentiate into iTreg in the absence of proinflammatory cytokines but high concentrations of TGFβ. These cells secrete TGFβ and IL-10, and are characterized by the transcription factor forkhead box p3 (Foxp3). They control and counteract immune responses by other effector T cells, and are involved in the prevention of autoimmunity (cf., Fig.4; Kaufmann, 2007).

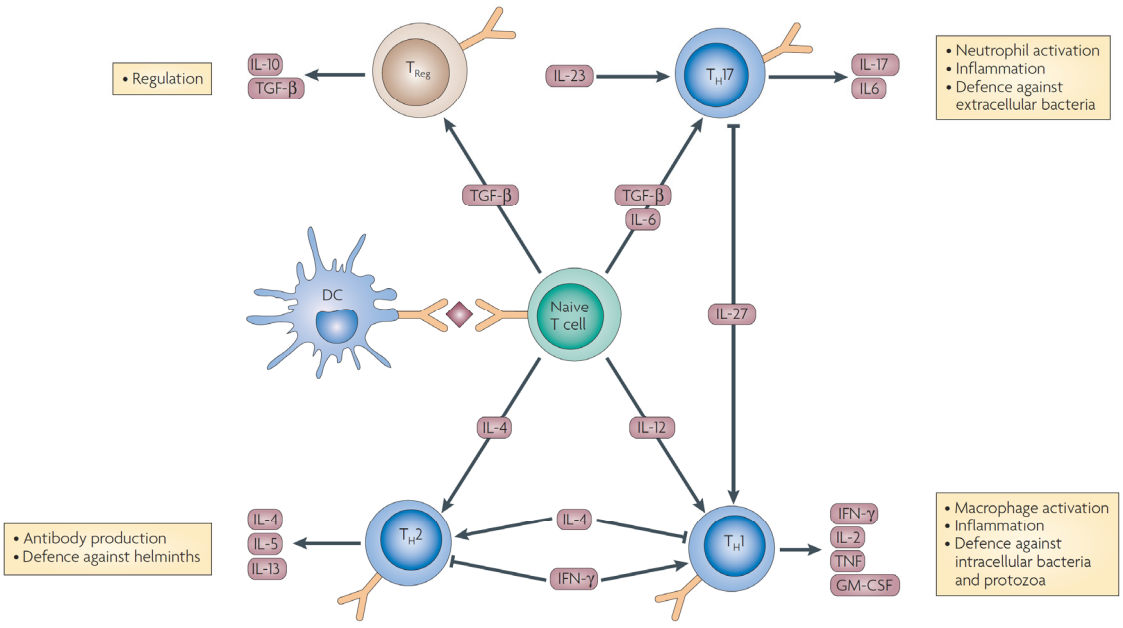


**Figure 4. Subpopulations of $CD4^+$ T cells.** The main populations of $CD4^+$ T cells are T helper 1 (Th1 or $T_H1$), Th2 and Th17 cells as well as inducible Treg (iTreg). Treg control the responses of immune effector cells. Th1 cells are responsible for cell-mediated immunity, and Th2 cells for humoral immunity and defense against parasites. Th17 cells are involved in the defense against bacteria. DC, dendritic cell; GM-CSF, granulocyte-macrophage colony-stimulating factor; IFN, interferon; IL, interleukin; TGF, transforming growth factor; TNF, tumor necrosis factor. The figure, exemplarily presented, is taken from Kaufmann, 2007.

### 5.3.2. $CD8^+$ effector T cells

Naive peripheral $CD8^+$ T cells differentiate into CTLs upon antigen recognition and additional factors produced through CD4 T cell help, especially by Th1 cells. The main effector function of CTLs is the direct destruction and elimination through lysis of target cells that express the specific peptide/MHC class I complex, against which the CD8 T cell response was generated. Through exocytosis, they release cytolytic effector molecules including perforin and granzyme, stored in cytoplasmic granules. Moreover, CTLs produce cytokines with cytotoxic action including IFNγ and TNF (Abbas and Lichtman, 2005; Murphy et al., 2008).

Perforin is a calcium-sensitive, membanolytic, pore-forming protein and granzymes are serine proteinases. Granzymes enter target cells either through perforin pores or by receptor-mediated endocytosis. They get activated intracellularly, then cleave and activate caspases, and induce target cell apoptosis (Barry and Bleackley, 2002; Kaufmann, 2007). Target cell apoptosis is further induced through various pathways that display complex networks. For example, besides the granule-exocytosis-mediated pathway, CTLs also induce, e.g., FAS ligand (FASL, CD95L), TNF and TNF-related apoptosis-inducing ligand (TRAIL)-mediated apoptosis in target cells through binding of FAS (CD95, APO-1), TNF or TRAIL cell death receptors, respectively (Barry and Bleackley, 2002).

To maintain immune homeostasis and not to compromise the response of naive T cells to new pathogen stimuli, after clonal T cell expansion and antigen clearance, most of the activated effector T cells must be rapidly deleted (Krueger et al., 2003; Strasser and Pellegrini, 2004). To induce the death of peripheral T cells, several extrinsic and intrinsic apoptotic pathways have been described, including extrinsic cell-death-receptor- and caspases-dependent apoptosis (Kroemer and Jaattela, 2005; Arnold et al., 2006; Krammer et al., 2007). Furthermore, autonomous cell death occurs in the absence of appropriate survival signals, termed “death by neglect” or “activated cell-autonomous death” (ACAD; for details see Hildeman et al., 2002). Moreover, “activation-induced cell death” (AICD) has been described, a process mainly mediated by IL-2. Thereby, activated and expanded TCR restimulated T cells, without appropriate co-stimulation, undergo cell death after engagement of cell-death receptors including CD95 or after exposure to reactive oxygen species (ROS; Schmitz et al., 2003; Krammer et al., 2007).

### 5.3.3. Memory T cells

After pathogen elimination, only a small proportion of effector T cells that is resistant to apoptosis induced cell death remain and survive, called “memory T cells” (for reviews see, e.g., Krueger et al., 2003; Strasser and Pellegrini, 2004; Pepper and Jenkins, 2011). These long-lived antigen-specific T cells are more responsive and sensitive to antigens, less dependent on co-stimulatory signals and able to functionally respond rapidly to a subsequent encounter with the same antigen. Thereby, memory T cells mount a more effective immune recall response than naive antigen-specific T cells (Beckhove et al., 2004; Ahmed et al., 2009). Moreover, in contrast to effector

T cells, they are capable of producing multiple cytokines (Kaufmann, 2007; Zielinski et al., 2011). In addition, the precursor frequency of memory T cells is much greater compared to naive T cells (Becker et al., 2005). Once memory T cells are differentiated, they can persist without antigen stimulation while undergoing homeostatic proliferation (Lau et al., 1994; Swain et al., 1999).

Two different main subpopulations, the effector and the central memory T cell, exist. They have different biological functions with distinct homing potentials and can, based on homing receptors, phenotypically be characterized. On the one hand, effector memory T cells are negative for L-selectin ($CD62L^-$), chemokine receptor 7 ($CCR7^-$) and positive for CD45RO ($CD45RO^+$). They migrate to inflamed nonlymphoid tissues, replicate less efficiently but can exert immediate rapid effector functions without further differentiation. Moreover, they can give rise to central memory T cells (Sallusto et al., 2004; Schwendemann et al., 2005; Ahmed et al., 2009). Furthermore, effector memory T cells are potent producers of IFNγ within the first hours of activation. On the other hand, central memory T cells circulate from the PB to secondary lymphoid organs and are $CD62L^+$, $CCR7^+$ and $CD45RO^+$. They lack immediate effector functions, but, after restimulation with antigens, can efficiently proliferate and mediate rapid recall responses while developing the phenotype and function of terminally differentiated effector T cells (Sallusto et al., 1999, 2004; Ahmed et al., 2009). Besides a balanced cytokine milieu, especially the cytokines IL-7 and IL-15 are important factors for T cell memory maintenance (Marrack and Kappler, 2004; Becker et al., 2005; Zielinski et al., 2011). However, the regulation of memory T cell differentiation, maintenance and the lineage relationship represent complex processes that are still under scientific debate (for discussion see, e.g., Kaech et al., 2002; Ahmed et al., 2009; Prlic and Bevan, 2011).

## 5.4. Regulatory T cells

$CD4^+$ Treg constitutively express the IL-2 receptor α chain (IL-2Rα, CD25), glucocorticoid-induced TNFR (GITR), CTLA-4 and are positive for Foxp3. They have the ability to control and suppress adaptive immune responses against self or foreign antigens and maintain peripheral self tolerance (Hori et al., 2003; Sakaguchi, 2004; Chai et al., 2005).

Two main populations of $CD4^+CD25^+Foxp3^+$ Treg have been described, the nTreg and the iTreg, that both strongly depend on IL-2. The nTreg develop in the thymus, and display a diverse TCR repertoire that is specific for self antigens. In contrast, iTreg are generated in an extrathymic development in the periphery from the naive $CD4^+$ T cell pool in the presence of TGFβ and the absence of proinflammatory cytokines (cf., Fig 4, see also, e.g., Chen et al., 2003; Fontenot et al., 2003; Hori et al., 2003). However, the biological importance of the different Treg subtypes for the revealed suppressive mechanisms, responsible for the physiological and the pathological role of Treg in humans, is still under discussion (Zhu and Paul, 2008). The transmembrane glycoprotein CD127 can be used to distinguish Treg from activated $CD4^+$ effector T cells that also upregulate CD25 (Liu et al., 2006). CD127 is the α chain of the IL-7 receptor (IL-7Rα) and is expressed on the

majority of mature T cells, but is absent on Treg. Moreover, CD127 is inversely correlated with the occurrence of Foxp3 (Liu et al., 2006; Seddiki et al., 2006).

The induction of Treg activation and function depends on antigen-specific TCR stimulation. In contrast, the subsequent suppressive activity, exerted by Treg, is antigen unspecific, and characterized by local bystander suppression of target cells (Thornton and Shevach, 2000; von Herrath and Harrison, 2003; Kretschmer et al., 2006; Josefowicz and Rudensky, 2009). Treg mediate their suppressive function through inhibitory mechanisms that depend on direct cell contact and soluble molecules including inhibitory cytokines, cytolysis, metabolic disruption and targeting of dendritic cells (Fig. 5; Vignali et al., 2008). Thereby, preferentially inhibitory cytokines including IL-10, TGFβ and IL-35, cytolysis through secretion of granzymes, perforin, galectins and induction of death-receptor pathway-mediated apoptosis in effector T cells are used (Collison et al., 2007; Ren et al., 2007; Vignali et al., 2008). Furthermore, Treg functions are mediated by metabolic disruption of the effector T cell target while consuming IL-2 through binding to CD25 on Treg. IL-2 is needed for T cells to survive, to proliferate and to maintain effector functions. Moreover, Treg can release adenosine nucleosides, which suppress effector T cell functions by activating the adenosine receptor and by transferring the inhibitory second messenger cyclic adenosine monophosphate (cAMP; cf., Fig. 5; see also Bopp et al., 2007; Deaglio et al., 2007; Vignali et al., 2008; Ring et al., 2009).

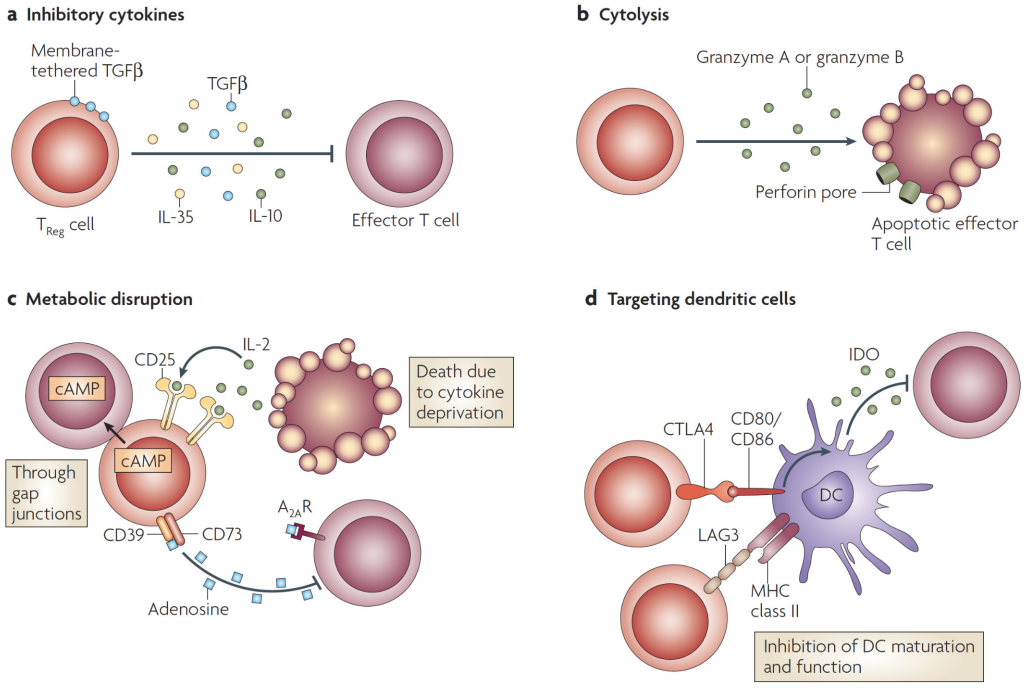


**Figure 5**. **Treg-mediated immunosuppression.** The basic mechanisms of Treg functions are: inhibitory cytokines (**a**), cytolysis (**b**), metabolic disruption of effector T cells (**c**) and dendritic cell (DC) targeting (**d**). $A_{2A}R$, adenosine receptor 2A; cAMP, cyclic adenosine monophosphate; CTLA4, cytotoxic T lymphocyte antigen 4; IDO, indoleamine 2,3-dioxygenase; IL, interleukin; ; LAG3, lymphocyte-activation gene 3; TGFβ, transforming growth factor β. The figure is taken from Vignali et al., 2008.

In addition, Treg can modulate dendritic cell maturation and function. Thereby, they can condition dendritic cells in a CTLA-4-dependent manner, leading to the expression of indoleamine 2,3-dioxygenase (IDO), a potent immunosuppressive regulatory molecule. Besides CTLA-4, Treg also express further negative co-stimulatory molecules like PD-L1. Furthermore, Treg are able to downregulate molecules, presented by dendritic cells, including CD80, CD86 and CD40. In addition, dendritic cell maturation can be blocked through Treg-mediated expression of lymphocyte-activation gene 3 (LAG3) while binding to MHC class II on dendritic cells (cf., Fig. 5; see also Cederbom et al., 2000; Fallarino et al., 2003; Liang et al., 2008; Vignali et al., 2008). Moreover, Treg have the ability to influence immune responses by recruiting other immune cells such as mast cells (Lu et al., 2006).

## 5.5. Cancer development and immunoediting

According to the World Health Organization (WHO), cancer is a leading cause of death worldwide and accounted for 7.6 million deaths (~13 % of all deaths) in 2008. The worldwide cancer deaths are expected to rise to more than 11 million by the year 2030 (WHO, 2011) and therefore, cancer represents a major public health problem (Jemal et al., 2011). The development of cancer is a complex multi-stage process that leads to the transformation of normal cells into invasive malignant tumors via pre-malignant stages. A tumor is characterized to be a benign or malign neoplasm of a tissue, generated through dysregulation of cell growth. Thereby, the term “cancer” is used synonymously to “malignant tumor” that can become invasive and metastatic. In general, metastases indicate the major cause for cancer death. The cancer development can be initiated by external agents including physical, chemical and biological carcinogens (e.g., ultraviolet radiation, components of tobacco smoke, chronic viral infections) as well as inherited genetic factors. Moreover, many types of cancer show an age-dependent incidence (cf., WHO, 2011).

More than ten years ago, Hanahan and Weinberg (2000) defined the concept of “the hallmarks of cancer” that can collectively cause malignant cell growth. This indicates that carcinogenesis requires crucial events that are most likely shared by all types of human tumors. They highlighted the six essential alterations in cell physiology and mechanistic strategies, i.e., “sustaining proliferative signaling”, “evading growth suppressors”, “resisting cell death”, “enabling replicative immortality”, “inducing angiogenesis” and “activating invasion and metastasis formation” (Hanahan and Weinberg, 2000). Recently, further emerging hallmarks were added that are acquired during the multistep cancer development. They are defined as “the reprogramming of cellular energy metabolism” and “the avoiding of immune destruction” in particular by T cells and B cells, macrophages and NK cells. Additionally, two enabling characteristics that support the multiple hallmark capabilities were specified, defined as “genome instability and mutation” as well as “tumor-promoting inflammation” caused by cells such as macrophages, mast cells and neutrophiles (cf., Fig. 6; see also Hanahan and Weinberg, 2011).

The course of the multi-stage carcinogenesis is strongly dependent on the tumor microenvironment which contributes to the biology of many tumors and to the acquisition of the cancer hallmarks (Hanahan and Weinberg, 2011). To understand the biology of tumor growth, one has to realize the tumor not as an isolated structure consisting only of cancer cells, rather as an independent organ comprising a variety of different cell types that interact with each other and with the entire organism (Egeblad et al., 2010; Pietras and Ostman, 2010; see therein for further informations). Besides cancer cells and neoplastic cancer stem cells, the microenvironment consists of cell types that form the tumor-associated stroma including endothelial cells, cancer-associated fibroblasts, pericytes and immune inflammatory cells (Pietras and Ostman, 2010). Cancer stem cells have been described to be more resistant to radio- and chemotherapies than conventional cancer cells. They can invasively disseminate from primary tumors, form micro-metastases and can clonally expand, caused by their self-renewal and tumor-initiating capability. This process can then lead to the formation of macro-metastases (Hanahan and Weinberg, 2011). Moreover, cancer stem cells can persist in a latent state before they start to give rise for metastases formation by activating the cellular program of “epithelial-to-mesenchymal transition” (EMT). This process is characterized by a loss of cell-cell adhesion and a gain of cell mobility that involves invasion (Hanahan and Weinberg, 2011).

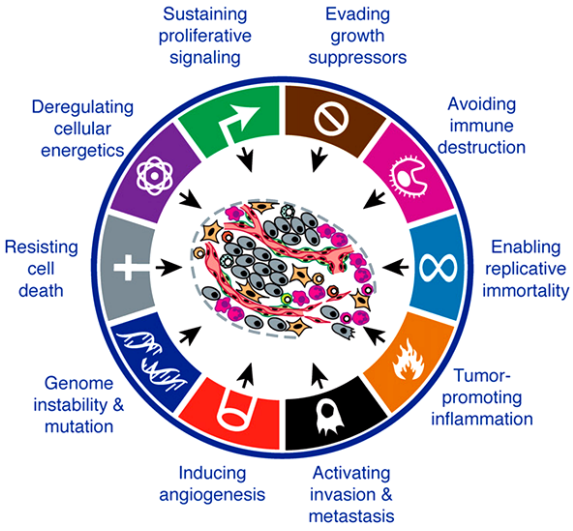


**Figure 6**. **The concept of the hallmarks of cancer.** Overview of the essential alterations, acquired during the multistep cancer development. The tumor growth and progression depends on defined capabilities that are acquired by cancer cells and shared by most malignant tumors. The figure is adapted from Hanahan and Weinberg, 2011.

Furthermore, Cavallo et al. (2011) focused on the “immune hallmarks of cancer”, and defined three major immune capabilities that are important for cancer progression, i.e., “the ability of cancer to develop in a chronically inflamed microenvironment”, “escape immune recognition control” and “suppress immune reactivity” (see also Schreiber et al., 2011). This highlights that the immune system, importantly participates in the development and growth of tumors, summarized as the “cancer immunoediting” hypothesis. Thereby, in terms of tumor cell growth, the immune system plays a dual extrinsic role in cancer development. It can suppress the tumor growth, but also

promotes the tumor progression (Schreiber et al., 2011). In general, tumor immunology is based on a balance between immune mediators that promote tumor progression (e.g., Treg, Th2, type 2 NK T cells, myeloid-derived suppressor cells (MDSC), M2/tumor-associated macrophages, mast cells), and mediators that promote tumor rejection (e.g., CTLs, Th1, NK cells, type 1 NK T cells, M1 macrophages; for review see Ostrand-Rosenberg, 2008). The cancer immunoediting process is characterized by three distinct phases, i.e., “elimination” (cancer immunosurveillance), “equilibrium” (cancer persistence/dormancy) and “escape” (cancer progression; Fig. 7; see also Smyth et al., 2006; Vesely et al., 2011).

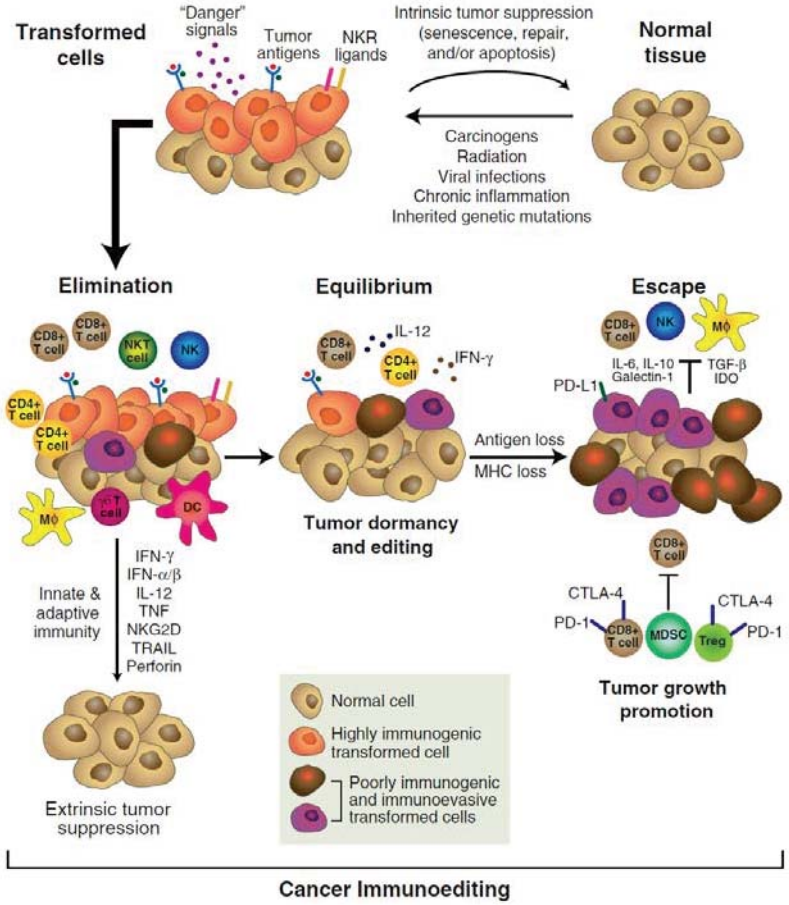


**Figure 7**. **The concept of cancer immunoediting.** The cancer immunoediting, an extrinsic tumor suppressor mechanism, consist of three phases (elimination, equilibrium, escape), and occurs when intrinsic mechanisms have failed. In the elimination phase, innate and adaptive immunity work together, to destroy developing tumors. When tumor cells survive, they will enter the equilibrium, in which their growth is prevented by adaptive immune cells that maintain tumor cells in a state of functional dormancy. In this phase, editing of tumor immunogenicity occurs. Tumor cells that enter the escape phase are no longer recognized by the adaptive immunity, and become insensitive to immune effector mechanisms. Moreover, within the tumor microenvironment, the tumor cells induce an immunosuppressive state, and start an aggressive uncontrolled tumor growth, which results in cancer formation. The figure is taken from Schreiber et al., 2011.

Thereby, the elimination phase is characterized by a “cancer immunosurveillance”, mediated by innate and adaptive immune cells. These cells fight against the developing tumor in response to danger signals, directly released by dying tumor cells including type I IFN cytokines, heat-shock

proteins and mitochondrial products (Matzinger, 1994, 2002; Schirrmacher et al., 2003). Moreover, effector T cells get activated by tumor antigens, proliferate and protect the host against the developing tumor. If tumor cells survive the elimination phase, they enter the equilibrium were they survive in a functional stage of “tumor dormancy”. Controlled by adaptive immunity, this state can last for decades (Aguirre-Ghiso, 2007). During the escape phase, tumor cells that have acquired the ability to circumvent immune recognition (tumor editing) start to aggressively grow, resulting in cancer formation. Thereby, the tumor cell escape of poorly immunogenic tumor cell variants is achieved by reduced immune recognition, driven by genetic instabilities (e.g., loss of antigen, MHC or antigen processing function and co-stimulation). Additionally, the escape phase is mediated by increased resistance to cytotoxic effects of immunity, through induction of anti-apoptotic mechanisms or defective death receptor signaling and cancer-induced immunosuppression (Khong and Restifo, 2002; Zitvogel et al., 2006; Schreiber et al., 2011; Vesely et al., 2011). Moreover, in this stage, tumor cells are able to control and suppress anti-tumor T cell responses. They produce immunosuppressive cytokines including vascular endothelial growth factor (VEGF), TGFβ, galectins, IDO, and can recruit regulatory immune cells such as Treg and MDSC (Schreiber et al., 2011; Vesely et al., 2011).

In the course of the last years, human anti-tumor-directed T cell responses have been detected in many tumor entities (e.g., Schmitz-Winnenthal et al., 2005; Boon et al., 2006; Bonertz et al., 2009). Their reactivation through peptide-based vaccination approaches or utilization through adoptive immunotherapeutic therapies has successfully been performed, but still with clinically limited efficiency (cf., Yee, 2005; Caspi, 2008; Rosenberg et al., 2008; Eggermont, 2009). The next paragraphs will highlight important strategies, used for cancer immunotherapy, and in addition will illustrate their limitations in terms of tumor targeting and treatment. Thereby, the main focus will recline on immune therapies for melanoma. Because melanoma, as one of the most immunogenic solid tumors, indicate a model entity for cancer immunotherapy, and has extensively been studied (cf., Eggermont, 2009). Moreover, the optimization of immune therapeutic approaches for melanoma is still be crucial and therefore will be addressed during this thesis.

## 5.6. Cancer immunotherapy

In addition to conventional cancer therapies including surgery, radiation- and chemotherapy, also immunotherapy can be used for cancer treatment. To obtain optimized treatment results, often different approaches are used in combination. Thereby, cancer immunotherapy attempts to harness and direct immune mechanisms to eradicate malignant tumors. Various immunotherapeutic approaches for cancer treatment exist, including triggering of inflammation, anti-angiogenic therapy, cytokine therapy, monoclonal Ab (mAb) therapy, cellular immunotherapy and anti-tumor vaccination (for reviews see, e.g., Mahabeleshwar and Byzova, 2007; Caspi, 2008).

### 5.6.1. Adoptive immunotherapy

The adoptive T cell transfer approach belongs to the cellular immunotherapies of cancer. Thereby, patient-derived T cells with anti-tumor activity are expanded *ex vivo,* followed by a T cell re-infusion into the lymphodepleted cancer patients. The strategy of adoptive T cell therapy is shown in Fig. 8. Thereby, tumor antigen-specific T cells, defined by *in vitro* specificity tests, have to be obtained from tumor tissue (tumor-infiltrating lymphocytes, TILs) or patient-derived PB and expanded to large numbers *ex vivo*. Lymphodepletion before adoptive cell therapy provides an optimal environment for the transferred cells. It leads to the elimination of the remaining lymphoid compartment such as immunosuppressive Treg and lymphocytes, which would compete with the transferred antigen-specific T cells for homeostatic cytokines. Preferentially, the non-myeloablative lymphodepletion is conducted through total body irradiation or cytotoxic drugs that suppress the immune system for a short period of time. Besides patient-derived tumor antigen-specific T cells, genetically modified human T cells can also be used as effector cells for adoptive immunotherapy. Thereby, TCR transgenic T cells have to be generated with defined cancer-antigen specificities, mainly by the help of viral particles. The approach of adoptive T cell therapy has proven to be functional for the treatment of cancer in experimental animal models and in cancer patients, but so far, only low response rates have been revealed (cf., Caspi, 2008; Rosenberg et al., 2008).

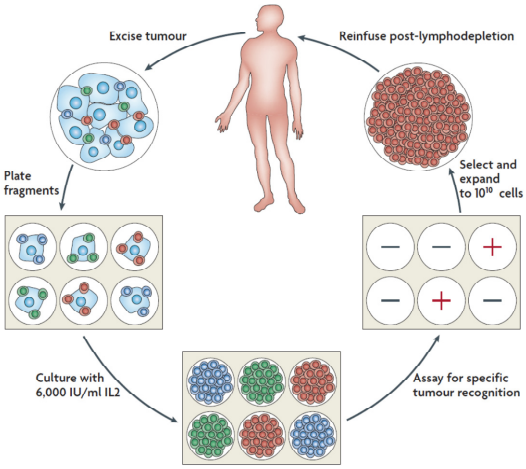


**Figure 8**. **The generation of anti-tumor T cells used for adoptive immunotherapy.** Tumor cell cultures have to be established *ex vivo* and assayed for specific tumor recognition. Cultures with high anti-tumor reactivity were then expanded and reinfused into cancer patients. The figure is taken from Rosenberg et al., 2008.

### 5.6.2. Tumor antigen-reactive TCR transgenic T cells

Genetically engineered TCR transgenic T cells are used for cancer treatment. Thereby, the TCR gene therapy is a method to produce antigen-specific T cells for adoptive T cell transfer immunotherapy by introducing high affine tumor-antigen reactive TCRs into human T cells. Different approaches have been used for TCR gene therapies that mainly depend on vector systems including retroviral vectors that facilitate a stable gene transfer (Schumacher, 2002;

Kieback and Uckert, 2010). Thereby, most TCR-transfer studies used Moloney murine leukemia virus (MoMuLV)-based retroviral vector systems (Schumacher, 2002). Recent work has provided first evidence for the clinical potential of TCR gene therapy (Morgan et al., 2006; Johnson et al., 2009). For example, a phase I clinical trial with metastatic melanoma patients showed a successful tumor rejection in the patient cohort, treated with autologous T cells engineered to express a TCR specific for the melanocyte differentiation antigen MART-1 (Morgan et al., 2006; de Witte et al., 2008).

Nevertheless, a current challenge of TCR gene therapy is a potential hybrid/mixed dimer formation between the introduced exogenous TCR α and β chains with the endogenous patient-derived chains (Fig. 9). This formation can occur during the transfer of double chain (dc) TCRs into human T cells (Schumacher, 2002). The resulting hybrid or mispaired TCRs will have unpredictable specificities that may cause “off-target” reactivities, potentially leading to autoimmune reactions Schumacher, 2002; Bendle et al., 2009). To avoid misspairing and promote preferential pairing of introduced chains, currently different strategies are investigated for TCR optimization including murinization of constant TCR regions, modification of the molecular design of the TCR αβ interface (e.g., additional cysteine bonds or inverse exchange of amino acids) and the generation of TCR-like molecules as single chain (sc) TCR constructs (Kieback and Uckert, 2010).

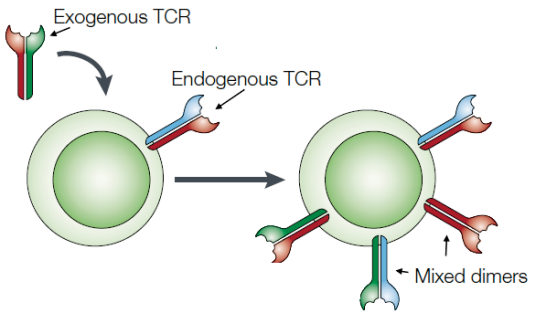


**Figure 9**. **The formation of hybrid/mixed TCR dimers.** Hybrid TCR formation can occur between exogenous and endogenous TCR chains. Thereby, mixed TCR dimers with unpredictable and potentially self-reactive specificities can result. The figure is adapted from Schumacher, 2002.

### 5.6.3. Peptide-based immunotherapy

The peptide-based immunotherapy belongs to the anti-tumor vaccination treatment, indicating an active immunization process of cancer patients against their autologous cancers using specifically designed peptides derived from tumor-associated antigens (TAAs). In the context of MHC molecules, those TAA peptides are recognized by T cells (Parmiani et al., 2002). Using peptide-based immunotherapy, in some studies, expansions of circulating antigen-specific $CD8^+$ T cells could be induced (Jandus et al., 2009). Thereby, a first evidence of a clinical benefit has recently been reported in a melanoma trial using glycoprotein 100 (gp100) peptide vaccinations together with IL-2 (Schwarzentruber et al., 2009). Besides these promising results, most of the other peptide-based vaccination trials failed so far, or showed only limited overall success (Lienard et al., 2004; Rosenberg et al., 2004; Eggermont, 2009).

Several reasons for this lack of response have been assumed, and will subsequently be discussed. Up to now, mainly human leukocyte antigen A2 (HLA-A2)-restricted peptide vaccines were tested in late stage cancer patients (Kirkwood et al., 2008; Jandus et al., 2009). Therefore, patients have to be selected accordingly to their expression of defined HLA molecules, and only HLA-A2$^+$ patients can receive the vaccinations. A further limitation using HLA-A2-restricted peptide vaccines is that only CD8$^+$, but not CD4$^+$ T cell responses are induced (Melief and van der Burg, 2008). The structure of the MHC class I molecule HLA-A2, discovered by Bjorkman and co-workers in the late 1980s, allowed to explain how MHC restricts the recognition of foreign antigens by T cells (Bjorkman et al., 1987a, b). In this context, HLA-A2 presents peptides specifically to CD8$^+$ T cells. CD4$^+$ T cells are not able to recognize peptides presented by MHC class I, they rather need for presentation MHC class II molecules. Historically, cancer-directed immune-based therapies have focused on eliciting a cytotoxic CTL response, primarily due to the fact that those cells can directly kill tumors (Knutson and Disis, 2005). Recently, increasing importance in cancer immunotherapy has been given to the stimulation of CD4$^+$ Th cells (Bos and Sherman, 2010). Th cells are central for the development of an immune response by activating antigen-specific effector cells as macrophages, mast cells and support CTLs (Kaufmann, 2007). Moreover, Th1 can also directly kill tumors, via release of cytokines that activate death receptors on tumor cells (Knutson and Disis, 2005; Haabeth et al., 2011). Based on these informations, a combined induction of CD4$^+$ and CD8$^+$ T cell stimulation will be essential for a successful immune response against cancer.

In addition, recently, large interests and efforts have been given to detect tumor-reactive memory T cells in cancer patients. After the surgical removal of the primary tumor, these cell responses might be required for a durable prevention of tumor recurrence and metastasis formation (Côté et al., 2008). Memory T cells, that can persist for decades, are particularly sensitive to antigens while exhibiting a faster activation and proliferation rate that is less dependent on co-stimulatory signals (Beckhove et al., 2004). Galon et al. (2006) showed that the infiltration of memory T cells into tumors can predict the clinical outcome of patients. Moreover, it could be revealed that the blockade of CTLA-4 by anti-CTLA-4 Abs enhance anti-tumor T cell responses in tumor-bearing mice, and led to the rejection of already well established tumors (Peggs et al., 2009). These findings demonstrate the clinical efficiency of pre-existing T cell responses.

Moreover, it has been shown that *ex vivo* reactivated pre-existing memory T cells of breast cancer patients selectively home to autologous human breast tumors in xenotransplanted mice, followed by an efficient tumor rejection (Beckhove et al., 2004). This observation indicated that memory T cells can be reactivated *ex vivo* and revealed a therapeutic potential upon reactivation. In this context, spontaneously induced tumor-reactive memory T cells have been detected in several human tumors including breast, pancreatic and colon carcinomas as well as multiple myeloma and melanoma (Choi et al., 2005; Schmitz-Winnenthal et al., 2005; Mueller-Berghaus et al., 2006; Bonertz et al., 2009; Schuetz et al., 2009). Thereby, the tumor-reactive patient-derived memory T cell repertoire was polyvalent and accordingly demonstrated a highly therapeutic repertoire that diminishes immune evasion phenomena (Sommerfeldt et al., 2006). Thus, in

summary, spontaneously induced tumor-reactive memory T cells provide a repertoire of functional and potentially protective immune cells that can therapeutically be reactivated. Thereby, for further optimization of cancer immunotherapies, in particular peptide-based immunotherapies, it will be essential to understand the regulation of those spontaneous T cell responses and to identify relevant antigens for reactivation.

Further limitations for an effective cancer immunotherapy are for example immunosuppressive mechanisms, facilitated through, e.g., a Treg blockade of immune reactions (Andrews et al., 2008). Treg can inhibit the development and effector functions of tumor-specific T cells (e.g., Nicholaou et al., 2009; Nishikawa and Sakaguchi, 2010). Moreover, in murine models of cancer it could be shown that the depletion of Treg permits immune-mediated tumor rejection (e.g., Kline et al., 2008). Since the role of Treg for controlling spontaneous T cell responses in melanoma is rather unclear in particular the presence and role of antigen-specific Treg, these should be addressed in future approaches in more detail.

Moreover, in general, the interactions between cancer and immune cells are very complex and can affect the success of immunotherapeutic interventions. In most experimental model systems the growth of tumors is accompanied by the induction of T cell tolerance towards the tumor (e.g., Kammertoens and Blankenstein, 2009). In this context, the inefficient T cell homing to the tumor area might be responsible for the limited success of immune therapeutic approaches (Mora and von Adrian, 2006). In addition, in order to gain clinical efficacy, T cells used for adoptive therapy should be equipped with the ability to persist for prolonged periods of time *in vivo* (Berger et al., 2008). Therefore, a main focus of current research is how tolerance to tumors is induced and how tolerance and various immunosuppressive conditions at the tumor side can be broken by cancer immunotherapy as well as to optimize methods that increase T cell targeting to the tumor area.

## 5.7. Malignant melanoma

Malignant melanoma, also termed as “melanoma”, a malignancy of melanocytes, the neural crest-derived melanin pigment-producing cells, is the most aggressive form of skin cancer and belongs to the most treatment-resistant human cancers (Ernfors, 2010; Ko and Fisher, 2011). Melanoma is less frequent than non-melanoma skin cancers, but cause the majority (more than 75 %) of skin cancer-related deaths (Jerant et al., 2000). The incidence of melanoma in the white population has more than tripled during the last two decades, posing a major threat to public health (Jemal et al., 2010). Melanocytes are preferentially located in the basal layer of the epidermis, hair bulb, eye, ear and meninges (Nordlund and Boissy, 2001; Bandarchi et al., 2010). Depending on the presence of melanocytes, melanoma can arise on different anatomic sides including cutaneous or uveal melanoma. Distinct melanoma subtypes have currently been summarized (Whitman et al., 2011).

To define the stages of melanoma, different classification systems and scales are used including the “Breslow scale” and the “tumor-node-metastases (TNM) staging”. The Breslow scale comprises the thickness of the melanoma in the skin. The TNM melanoma staging is based on

guidance of the American Joint Committee on Cancer (AJCC) and the International Union against Cancer (UICC), and describes the size and the nature of the primary tumor. It furthermore, provides informations whether tumor cells have spread to the lymph nodes or distant parts of the body, while forming metastases. Using the TNM classification, melanoma can be grouped into different stages: “stage 0” (melanoma *in situ*), “stage I/II” (invasive melanoma), “stage II” (high risk melanoma), “stage III” (regional metastases formation in lymph nodes) and “stage IV” (distant metastases formation). In the non-metastasized stages (stages 0, I and II) the melanoma cells are only in the epidermis or dermis, possibly reaching a tumor size of up to 5 mm. Thereby, they can be ulcerated, but do not spread to lymph nodes or other body parts. In contrast, in the metastasized stages III and IV, the melanoma is invasive and has formed metastases in lymph nodes or other organs (Balch et al., 2009).

The carcinogenesis of melanoma is a stepwise progression of mutations that drive the transformation of normal melanocytes or nevus cells into a non-metastasized primary tumor, followed by a metastatic melanoma (Miller and Mihm, 2006). Recent studies have identified melanoma-initiating cells, with self-renewal potential, termed as “melanoma stem cells” (Schatton et al., 2008; Boiko et al., 2010; Girouard and Murphy, 2011). However, their presence has controversially been discussed and still is a matter of scientific debate (see, e.g., Ko and Fisher, 2011). The oncogenic transformation of melanocytes can depend on genetic factors, germline predisposition and environmental factors including UV exposure (Ko et al., 2010). For the initiation of the pathogenesis of melanoma, multiple tumor-promoting events in key oncogenic pathways have been described, which are driven by the activation of oncogenes and inactivation of tumor suppressor genes (Ko and Fisher, 2011). Thereby, the “MAPK/ERK” and “PI3K/AKT/mTOR” pathways, which are connected via RAS signaling, have been shown to be centrally involved in melanoma survival, proliferation and tumor progression. In particular, mutations in NRAS, BRAF, c-KIT and PTEN have been identified to play important roles in melanoma development (Tsao et al., 1998; Hocker and Tsao, 2007; Beadling et al., 2008).

Nowadays, the first treatment choice for melanoma is surgery. While non-metastasized melanoma is mainly cured by the removal of the primary tumor, the 5-year survival rate of patients with metastasized melanoma is less than 10 %, due to the aggressiveness of advanced melanoma and existing deficiencies of therapeutic approaches (Kuphal and Bosserhoff, 2009). After surgery, for advanced stages, adjuvant therapies (chemotherapies, radiation and biological therapies including immunotherapy) are mainly used.

To specifically target the underlying melanoma pathways, in the concept of targeted inhibition of mutated kinase oncogenes, several therapeutic agents have been investigated including imatinib, farnesyl transferase inhibitors, RAF and MEK inhibitors and rapamycin (for review see, e.g., Ko and Fisher, 2011). Thereby, targeting only one pathway seems not likely to be clinically efficient. In order to avoid the escape of resistant melanoma cell clones, combinational approaches that target several pathways or a combination with conventional chemotherapies have been performed (see, e.g., McDermott et al., 2008; Kudchadkar, 2010). Since it is known that angiogenesis is crucial for tumor and metastasis growth, also anti-angiogenic therapies (e.g., VEGF ligand-targeting mAb

bevacizumab) have been used for melanoma treatment, however, preferentially in combinational approaches (Hanahan and Folkman, 1996).

In the search for novel treatments, during the last decades, melanoma immunotherapies gained increasing importance. Melanoma is considered as one of the most immunogenic solid tumors, and an ideal candidate to develop immunotherapeutic approaches (Eggermont, 2009). Therefore, numerous early phase immunotherapy clinical trials have been reported, however, so far most of them failed or revealed only low clinical benefit (cf., Jandus et al., 2009; Eggermont, 2009). In advanced metastasized melanoma patients recombinant biologicals have widely been used, including high dose IFNα and IL-2. Thereby, the IFN treatment demonstrated a 10-20 % improvement in relapse-free survival, and the IL-2 treatment revealed durable responses in 10-20 % of the patients (Agarwala and Kirkwood, 1996; Atkins et al., 1999; Tarhini and Agarwala, 2006). Besides the use of cytokine therapies, adoptive T cell transfer approaches have been performed. Thereby, *ex vivo* expanded autologous antigen-specific tumor-reactive T cells, isolated from TILs or patient-derived PB and engineered TCR transgenic human T cells were utilized. As immunologically active effector cells, the antigen-specific T cells were then reinfused into lymphodepleted patients. Thereby, mainly combination therapies are performed with non-myeloablative but lymphodepleting chemotherapy or irradiation with concomitant administration of high dose IL-2, resulting in clinical response rates of 50-70 % (Dudley et al., 2005, 2008; Jandus et al., 2009). Moreover, for melanoma immunotherapy immune checkpoint antagonists were used including CTLA-4 or PD1 blocking mAbs (Jandus et al., 2009; Peggs et al., 2009; Quezada et al., 2010; Ko and Fisher, 2011). In the case of CTLA-4 Ab blockade with ipilimumab, a recent phase III clinical trial with metastatic melanoma patients reported a significant survival benefit in ~1/3 of all patients, indicating a promising treatment option for melanoma (Hodi et al., 2010). Besides the chemotherapeutic drug dacarbazine, aldesleukin (recombinant IL-2), IFN-α2b and pegIFN-α2b recently also ipilimumab has been approved by the Food and Drug Administration (FDA) for melanoma treatment (CenterWatch, 2011; NCI, 2011). Furthermore, different types of anti-melanoma antigen-defined vaccines have been described including dendritic cell-based vaccines, whole cell allogenic tumor vaccines, viral vectors as antigen delivery vehicles, DNA vaccines and peptide-based immunotherapy approaches (Jandus et al., 2009). Nowadays, for melanoma peptide-based vaccines, simultaneous injections of multiple tumor-associated peptides, mainly HLA-A2-restricted, together with immunostimulatory adjuvants (e.g., GM-CSF, IL-2, IL-12) are used. In the last years, numerous melanoma TAAs have been identified. The first evidence of a promising clinical benefit using peptide-based vaccination against melanoma has been shown in a prospective randomized multicentric phase III clinical trial. Thereby, a survival advantage has been shown for peptide vaccine-treated stage IV melanoma patients using $gp100_{209\text{-}217}$ peptide vaccination together with high dose IL-2 (Schwartzentruber et al., 2009). These positive encouraging observations indicate that optimized peptide-based immunotherapy might be a promising future melanoma treatment, to achieve clinically relevant results.

## 5.8. Melanoma tumor-associated antigens

The first melanoma TAAs, specifically expressed by tumor cells, were identified and cloned in the 1990s (van der Bruggen et al., 1991; Rosenberg, 1999). Until today, a large number of characterized MHC class I- and II-restricted epitopes of immunogenic melanoma TAAs have been added (cf., Cancer Immunity, peptide database, last update of January 2011; www.cancer immunity.org). As many antigens presented by tumors can also be expressed by normal tissues, problems can occur during targeting approaches of immunotherapy. For example, side effects such as vitiligo through off-target T cell responses were detected in melanoma trials using melanocyte differentiation antigens as target. Thereby, vitiligo, a depigmentation disorder, is an autoimmune disease of the skin and hair, caused by the destruction of melanocytes (Caspi, 2008).
Summarized, T cell-defined melanoma antigens can be classified on the basis of their expression pattern, and include melanocyte linage/differentiation antigens (e.g., Melan-A/MART-1, gp100/pmel17, TRP2, Tyrosinase, RAB38/NY-Mel-1), oncofetal/cancer-testis antigens that are expressed in germ cells of testis and ovary but silent in normal somatic cells (e.g., Mage-A1, MAGE-C2, GAGE-1, NY-Eso-1), mutational or atypical antigens (e.g., NA17-A) and antigens that are over-expressed in melanoma (e.g., MDM2, MIF, p53).

## 5.9. Dysplastic nevi

Dysplastic nevi are benign melanocytic dysplasias with architectural disorders and cytological atypia (Peter et al., 1992; Elder, 2010). A stepwise transformation of melanocytes to melanoma has been described by the traditional “Clark model of melanoma progression” (Fig. 10; Clark et al., 1984). This model emphasizes the proliferation of melanocytes, followed by the formation of nevi and the subsequent development of dysplasia, hyperplasia, invasion and metastasis (Clark et al., 1984; Miller and Mihm, 2006). Based on the described model, a dysplastic nevus has a malignant potential, and is characterized as an asymmetric pre-malignant lesion with irregular borders that give rise to a melanoma. Currently, most dermatologists emphasize that a dysplastic nevus is not a direct precursor that in every case, unrestricted develop into melanoma. It could be shown that ~26 % of all melanoma arise from nevi, of which 43 % arose from dysplastic nevi. Thus indicates that most cutaneous melanoma arise from normal-appearing skin, mainly in response to molecular events in oncogenic pathways (Bevona et al., 2003; Ko et al., 2010). Therefore, nowadays, dysplastic nevi are realized as lesions that can give rise to melanoma. Since melanoma often can only be clearly distinguished from dysplastic, but benign, lesions through pathological investigations, dysplastic nevi are carefully controlled and often removed by surgery.

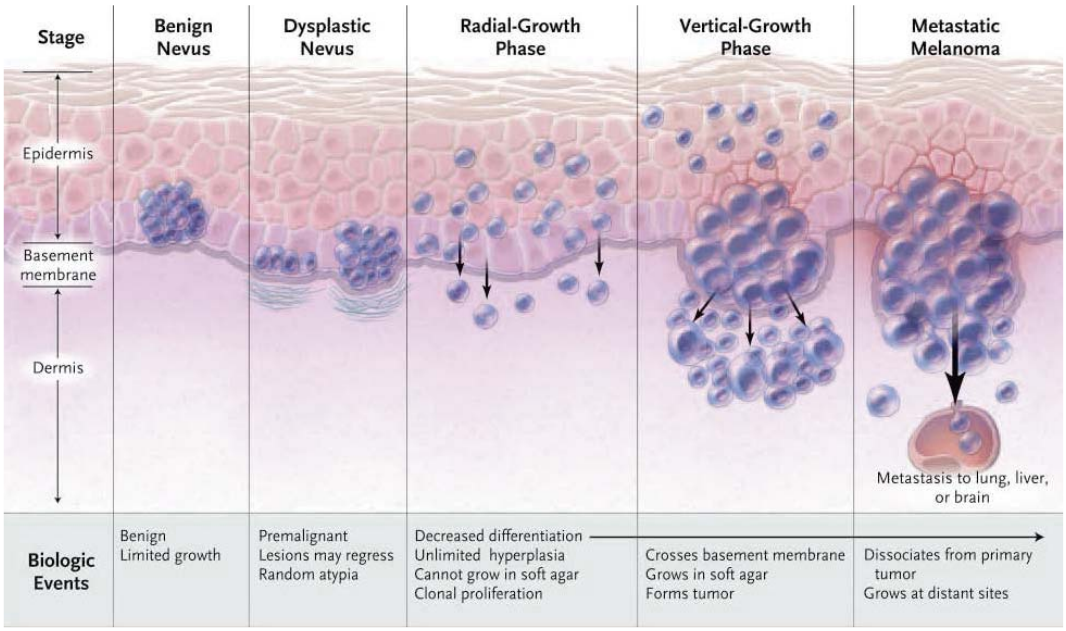


**Figure 10**. **An overview of the Clark model of melanoma progression.** Aberrant proliferation of normal melanocytes leads to the formation of a benign nevus, followed by the formation of a dysplastic nevus (asymmetric with irregular borders). A dysplastic nevus than enters a radial growth phase, followed by a vertical growth through the basement membrane and can become invasive, resulting in a metastasis formation. The figure is taken from Miller and Mihm, 2006.

## 5.10. Cell adhesion molecules

Cell adhesion molecules (CAMs) are predominantly transmembrane glycoproteins, involved in intercellular binding of adjacent cells to each other or to the extracellular matrix (ECM). They play a crucial role in a number of biological processes including homeostasis, embryogenesis, development of neural tissue, inflammation, immune cell transmigration and immune response. Four major groups of CAMs have been described, defined as “cadherins”, “integrins”, “selectins” and the “immunoglobulin (Ig) superfamily” (Pignatelli and Vessey, 1994; for detailed overviews see Behrens and Nelson, 2004; LaFlamme and Kowalczyk, 2008; Nelson and Fuchs, 2010).

The carcinoembryonic antigen-related cell adhesion molecules (CEACAMs, CD66) are highly glycosylated transmembrane proteins of the Ig superfamily and have first been described in 1972 (von Kleist et al., 1972; Mach and Pusztaszeri, 1972; see also Horst and Wagener, 2004). They are involved in cell-cell recognition and modulate cellular processes such as shaping of tissue architecture, neovascularization, angiogenesis, regulation of insulin action, T cell proliferation and have also been described as bacterial and viral pathogen receptors. Moreover, CEACAMs play an important role in tumor-associated mechanisms (see, e.g., Hammarstrom, 1999; Kuespert et al., 2006). Thereby, the expression of CEACAM1 on melanoma cells has shown to be responsible for the inhibition of melanoma-specific T cell responses, leading to impaired T cell functions (Markel et al., 2006).

The L1 cell adhesion molecule (L1CAM, CD171), also a member of the Ig superfamily, was discovered in 1984 (Rathjen and Schachner, 1984), and has an important role in the function of the nervous system and the development of human malignancies. In cancer, L1CAM has been revealed to enhance cell proliferation, invasion, motility, tumor metastasis formation and resistance to chemotherapy (Schaefer and Altevogt, 2010).

Besides CEACAM1, a potential immunosuppressive role of further tumor-expressed CAMs including CEACAM6 and L1CAM might be possible, and has to be addressed in future investigations.

## 5.11. Newcastle disease virus

Moreover, oncolytic virotherapy, for example mediated by Newcastle disease virus (NDV), can be used for cancer treatment. NDV, a paramyxovirus, is in general not infectious for humans (only mild flu-like symptoms, conjunctivitis or laryngitis), but able to cause the highly contagious “Newcastle disease” in birds (Schirrmacher and Fournier, 2009). NDV is enveloped and contains a single-stranded negative-sense RNA genome, coding for six major proteins, i.e., “nucleocapsid protein” (NP), “phosphoprotein” (P), “matrix protein” (M), “fusion protein” (F), “hemagglutinin-neuraminidase protein” (HN) and the “polymerase large protein” (L).

Cassel and Sinkovics introduced NDV into the clinic as an experimental therapeutic oncolytic agent. There, it now is used for more than 50 years (e.g., Cassel and Garrett, 1965; Sinkovics and Horvath, 2000). Thereby, NDV has been used for cancer therapy, because of its safety, cancer-selective replication and oncolytic and immune stimulatory properties (Pecora et al., 2002; Schirrmacher, 2005). The clinical anti-cancer potential of NDV oncolytic virotherapy has been evaluated for oncolysates and whole cell vaccines including the “autologous tumor vaccine modified by infection with NDV” (ATV-NDV) that stimulate the immune system. Additionally, patients have also been infected with lytic NDV (cf., Schirrmacher and von Hoegen, 1993; Schirrmacher and Fournier, 2009). For example, NDV oncolysates were used for the treatment of melanoma in phase I and II clinical trials, and revealed an improved overall survival (Murray et al., 1977; Cassel and Murray, 1992).

After the systemic application, in general, only a fraction of the virus reach the tumor tissue (Bian et al., 2005), therefore, a major problem for oncolytic viral applications is the efficient viral tumor targeting. In this context, the viral transport through “hitchhiking” on blood circulating cells has been shown for retrovirus and vesicular stromatitis virus (Cole et al., 2005; Rooney, 2005; Qiao et al., 2008). If this kind of viral transfer will also be possible for NDV, has to be investigated.

## 5.12. Objectives of the thesis

Besides conventional therapies, immunotherapies are used as a promising and potent option for cancer treatment. Thus, for malignant melanoma various different immunotherapeutic strategies have been investigated, and revealed promising results. In this context, the improved understanding of the regulation of spontaneous tumor-associated antigen (TAA)-reactive autologous T cell responses in cancer patients and the identification of relevant antigens for a therapeutic induction of those responses appears to be crucial for the optimization of future immunotherapies. Moreover, using gene therapy, currently various approaches follow the generation of optimized T cell receptor (TCR) transgenic T cells to prevent the potential generation of hybrid dimer self-reactive TCRs. Therefore, pre-clinical studies, that utilize animal models, have to be conducted to reveal the functionality and safety of the TCR constructs. In order to optimize immune-based cancer treatments, the identification of further mechanisms, responsible for the induction of cancer-directed functional-loss of impaired effector T cells, will also be important. In addition, to increase the treatment efficiency of oncolytic NDV virotherapy, the viral transport to the tumor is needed to be optimized. Therefore, while focusing on four different approaches, the major aim of the presented thesis is to address mechanisms, crucial for the optimization of cancer immune therapeutic interventions.

The first approach will characterize spontaneously induced endogenous TAA-reactive memory T cell responses, and analyze their regulation after tumor or lesion resection in the peripheral blood of melanoma and dysplastic nevi patients. Therefore, various polypeptides specific for melanoma TAAs that contain epitopes for $CD4^+$ and $CD8^+$ T cell recognition will be designed. Thereby, in non-metastasized melanoma patients the spontaneously induced T cell responses will be investigated after tumor resection over time and compared to responses revealed in healthy donors. Additionally, the Treg contribution to the activation status of the pre-existing TAA-reactive T cells will be addressed.

In a second project, the *in vivo* efficiency of human T cells, transduced with previously optimized and functional-expressed TCR constructs, specific for the antigens MDM2 and gp100 will be investigated in a murine xenotransplantation model. Thereby, the TCR constructs were optimized in order to avoid “off-target” reactions, caused by hybrid mispaired TCR chain formation.

The third approach will aim the immunosuppressive importance of the cell adhesion molecules CEACAM6 and L1CAM. In this context, the tumor cell-mediated impact on human TAA-reactive T cell responses and T cell-dependent tumor recognition will be addressed.

In the fourth project, the viral transport of the Newcastle disease virus (NDV) to tumor cells will be optimized. Thereby, human T cells will be investigated for their potential to deliver NDV particles.

# 6. Material

All brand and product names used are registered trademarks of the manufacturers.

## 6.1. Laboratory equipment

| Product | Supplier |
|---|---|
| Autoclip wound clip applier / remover | Becton Dickinson (BD), Heidelberg, Germany |
| Axioplan 2 imaging microscope | Carl Zeiss, Jena, Germany |
| Axiophot 2 microscope / AxioCam HR | Carl Zeiss |
| Axiovert 25 microscope | Carl Zeiss |
| Binocular microscope | Carl Zeiss |
| Biological safety cabinet | Integra Biosciences, Fernwald, Germany |
| Biological safety cabinet | The Baker Company, Sanford, ME, USA |
| Caliper | Bauhaus, Heidelberg |
| Cell culture incubator | Sanyo, Bad Nenndorf, Germany |
| Centrifuge Biofuge fresco | Heraeus, Hanau, Germany |
| Centrifuge Megafuge 2.0R | Heraeus |
| CTL ImmunoSpot S5 UV analyzer | CTL, Bonn, Germany |
| Digital analytical balance | Mettler Toledo, Giessen, Germany |
| Dissecting cutlery | Fine Science Tools, Heidelberg |
| Electroblotting chamber | CTI, Idstein-Taunus, Germany |
| Electrophoresis power supply | Biotec-Fischer, Reiskirchen, Germany |
| Flow cytometer FACS Calibur | BD |
| Flow cytometer FACScan | BD |
| Flow cytometer FACS Canto II | BD |
| Flow sorter Aria 2 | BD |
| Freezer (-20°C) | Liebherr, Ochsenhausen, Germany |
| Freezer (-80°C) | Thermo Fisher Scientific, Karlsruhe, Germany |
| Freezing container Mr. Frosty | Nalgene, Thermo Fisher Scientific |
| Freezing container | Carl Roth, Karlsruhe |
| Fridge (4°C) | Liebherr |
| Gammacell 1000 | Atomic Energy of Canada, Ottawa, ON, Canada |
| Gammatron Cobalt 60 therapy unit | Siemens, Munich, Germany |
| Glass cuvettes | Thermo Fisher Scientific |
| Heatable magnetic stirrer | Heidolph Instruments, Schwabach, Germany |
| Heat block, thermo mixer | Grant Instruments, Cambridgeshire, UK |
| Heat sealer | Perkin-Elmer |
| Ice machine | Hoshizaki, Willich-Muenchheide, Germany |
| Innova 44 incubator / shaker | New Brunswick, Wesseling-Berzdorf, Germany |
| Inoculation loop holder | neoLab, Heidelberg |
| IVIS100 *in vivo* imaging system | Xenogen, Caliper, Mainz, Germany |

| | |
|---|---|
| Leica CM3050 S cryo-microtome | Leica Microsystems, Wetzlar, Germany |
| Leica DM LB2 microscope / DC480 camera | Leica Microsystems |
| Liquid scintillation counter MicroBeta Trilux 1450 | Perkin-Elmer, Ueberlingen, Germany |
| Lumat LB 9507 luminometer | Berthold Technologies, Bad Wildbad, Germany |
| Magnetic particle concentrator | Dynal, Invitrogen, Darmstadt, Germany |
| Micropipettes (2-1000 µl) | Gilson, Middleton, WI, USA |
| Microwave | Bosch, Heidelberg |
| Milli-Q water purification device | Millipore, Eschborn, Germany |
| Multichannel pipettes | Rainin, Mettler Toledo |
| Neubauer hemocytometer | Brand, Wertheim, Germany |
| Novex mini-cell gel chamber | Invitrogen |
| OctoMACS separator | Miltenyi Biotec, Bergisch Gladbach, Germany |
| Owl EasyCast gel electrophoresis system | Nunc, Thermo Fisher Scientific |
| Packard COBRA γ-counter | Perkin-Elmer |
| PCR thermal cycler PTC-100 | MJ Research, Waltham, MA, USA |
| pH meter | WTW, Weilheim, Germany |
| Photometer GeneQuant pro | Amersham Biosciences, Freiburg, Germany |
| Pipetboy | Brand |
| Plate reader | Perkin-Elmer |
| Precision balance (PB602-S/FACT) | Mettler Toledo |
| Quartz cuvettes | Hellma Analytics, Muellheim, Germany |
| Rollers synchronous mixer RM5 | Karl Hecht GmbH, Sondheim, Germany |
| Shandon cytospin 2 cytocentrifuge | Thermo Fisher Scientific |
| Shaver for mice (type 1556) | Moser, Berlin, Germany |
| Table top centrifuge | Heraeus |
| Tomtec Harvester Mach 3 | Perkin-Elmer |
| Ultracentrifuge | Beckman Coulter, Krefeld, Germany |
| UV gel documentation system | Konrad Benda, Wiesloch, Germany |
| Video graphic printer UP-890 CE | Sony, Berlin |
| Vaccu-Pette/96, multiwell pipetter | Bel-Art, Sigma-Aldrich, Munich |
| Vortexer (Reax 2000) | Heidolph Instruments |
| Vacuum pump | neoLab |
| Water bath | Julabo, Seelbach, Germany |
| X-ray film-processor Optimax Typ TR | MS Laborgeraete, Heidelberg |

## 6.2. Consumables

| Product | Supplier |
|---|---|
| Black 96 microwell plate | Nunc |
| Blood lancets | B. Braun, Melsungen, Germany |
| Capillaries, heparinized (32 mm / 9 µl) | Hirschmann Laborgeraete, Eberstadt, Germany |
| Cell culture dishes (Ø 60 x 16, 96 x 21, 146 x 21 mm) | TPP, Trasadingen, Switzerland |
| Cell scraper | Sarstedt, Nuembrecht, Germany |
| Cell strainer (40, 70, 100 µm) | Falcon, BD |
| Conical centrifuge tubes (15, 50 ml) | TPP |
| Cryogenic vials (2 ml) | Corning, VWR, Darmstadt |
| Cryomold adapters, Tissue-Tek | Sakura Finetek, Staufen, Germany |
| Dako Pen | Dako, Hamburg, Germany |
| Disposable needles | BD |
| Disposable scalpel, Feather | PfM, Cologne, Germany |
| Disposable syringes (1, 5, 10, 20 ml) | BD |
| Disposable syringes (50 ml) | Terumo, Eschborn |
| ELISPOT 96 well plate (MAHA S45, clear) | Millipore |
| Erlenmeyer glass flasks | Thermo Fisher Scientific |
| Ficoll tubes - Leucosep (50 ml) | Greiner Bio-one, Frickenhausen, Germany |
| Filter cards/sample chambers for cytospin | Thermo Fisher Scientific |
| Flat-bottom plates (6, 12, 24, 48, 96 well) | Falcon |
| Flat-bottom plates (6, 12, 24, 48, 96 well) | TPP |
| Glass cover slips | R. Langenbrinck, Teningen, Germany |
| Konica-Minolta medical film | Konica-Minolta, Langenhagen, Germany |
| Luminometer tubes (5 ml, 75 x 12 mm) | Sarstedt |
| MACS columns | Miltenyi Biotec |
| Menzel Super Frost Plus object slides | Thermo Fisher Scientific |
| Micro-fine insulin syringe/needle (1 ml) | BD |
| Microtome blades Leica 819 | Leica Microsystems |
| Needles (0.4 mm x 19 mm) | BD |
| Optilux petri dishes (Ø 100 x 20 mm) | Falcon |
| Parafilm | Pechiney Plastic Packaging, Chicago, IL, USA |
| Petri-Seal, adhesive sealing film | Sigma-Aldrich |
| Pipette filter tips (10, 20, 100, 200, 1000 µl) | Starlab, Ahrensburg, Germany |
| Pipette tips (10, 200, 1000 µl) | Starlab |
| Pipette tips (200 µl) | Rainin |
| Plastic membrane bag for 1450 MicroBeta | Perkin-Elmer |
| Plastic serum pipettes, sterile | Greiner Bio-One |
| Poly-prep slides, poly-L-lysine coated | Sigma-Aldrich |

| | |
|---|---|
| Polypropylene tubes (1.3 ml) | Greiner Bio-one |
| Polypropylene round bottom tubes (5 ml) | Falcon |
| Polypropylene round bottom tubes with cap (14 ml) | Falcon |
| Polystyrene tubes (0.6 ml) | Greiner Bio-one |
| Polystyrene round bottom tubes with cap (5 ml) | Falcon |
| Polystyrene round bottom tubes with 35 µm cell strainer cap (5 ml) | Falcon |
| Polyvinylidene difluoride (PVDF) membrane | Millipore |
| Printed Filtermate A for MicroBeta (90 x 120 mm) | Perkin-Elmer |
| Reagent reservoirs, sterile (50 ml) | Corning |
| Round-bottom plate (96 well) | TPP |
| Round-bottom plate (96 well) | Falcon |
| Safe-lock tubes (0.5, 1.5, 2 ml) | Eppendorf, Wesseling-Berzdorf |
| Safe-lock tubes, Biopur (1.5, 2 ml) | Eppendorf |
| Serological pipettes, 5, 10, 25 ml | Falcon |
| S-Monovette 10ml 9NC, trisodium citrate | Sarstedt |
| Soft Ject tuberkulin syringe (1 ml) | Henke Sass Wolf, Tuttlingen, Germany |
| Syringe filter unit (0.22, 0.45 µm) | Millipore |
| Tissue culture flask/filter cap (25, 75, 150 $cm^2$) | TPP |
| Whatman 3MM gel blot paper | Sigma-Aldrich |

## 6.3. Assay kits

| **Product** | **Supplier** |
|---|---|
| Alkaline phosphatase conjugate substrate kit | Bio-Rad, Munich |
| $CD4^+CD25^+$ regulatory T cell isolation kit, human | Miltenyi Biotec |
| DakoCytomation EnVision$^+$ system-HRP (AEC) kit | Dako |
| Dual-luciferase reporter assay system | Promega, Mannheim, Germany |
| Dynal $CD4^+$ isolation kit | Dynal |
| Dynal $CD8^+$ isolation kit | Dynal |
| Dynal T cell negative isolation kit | Dynal |
| Dynabeads untouched human T cell kit | Dynal |
| Endofree plasmid Maxi kit | Qiagen, Hilden, Germany |
| Enhanced chemiluminescence (ECL) detection system | Amersham-Buchler, GE Healthcare, Freiburg |
| QIAprep spin Miniprep kit | Qiagen |
| Venor GeM mycoplasma detection kit | Minerva Biolabs, Berlin |

## 6.4. Chemicals, biological reagents, media, supplements and buffers

All chemicals used for media, buffers and other solutions were obtained from Merck (Darmstadt), Sigma-Aldrich, Roche Diagnostics (Mannheim), Serva (Heidelberg) or Carl Roth. Further reagents are indicated respectively. Double distilled water ($ddH_2O$) was received using a Milli-Q water purification device and autoclaved before use.

### 6.4.1. Chemicals and biological reagents

| Product | Supplier |
|---|---|
| 4',6-diamidino-2-phenylindole (DAPI) | Serva |
| 7-AAD | BD |
| 100 bp DNA Ladder | Invitrogen |
| 100 bp DNA Ladder | New England Biolabs (NEB), Frankfurt, Germany |
| 1 kb DNA Ladder | NEB |
| Acetic acid | Fluka, Sigma-Aldrich |
| Acetone | Sigma-Aldrich |
| Agarose | Invitrogen |
| Ammonium chloride ($NH_4Cl$) | Fluka |
| Ammonium hydroxide solution ($NH_4OH$; 1 M) | Fluka |
| Ampicillin | Sigma-Aldrich |
| Antibody (Ab) diluent | Dako |
| Aqua ad iniectabilia | B. Braun |
| BamHI methyltransferase reaction buffer | NEB |
| Benzonase | Merck |
| Bouin's solution | Sigma-Aldrich |
| Bovine serum albumin (BSA), fraction V | Sigma-Aldrich |
| Bromphenol blue | Merck |
| BSA (100X) | NEB |
| CD4 MicroBeads, human | Miltenyi Biotec |
| Coomassie brilliant blue R-250 | Sigma-Aldrich |
| Deoxyribonuclease I from bovine pancreas (DNase I) | Sigma-Aldrich |
| Dimethyl sulphoxide (DMSO) | Sigma-Aldrich |
| Dithiothreitol (DTT) | Serva |
| Diphteria toxin | Calbiochem, Merck |
| D-luciferin potassium salt | Synchem, Felsberg, Germany |
| Dulbecco`s PBS powder without $Ca^{2+}$, $Mg^{2+}$ (for 10 l) | Biochrom |
| Dynabeads pan mouse IgG | Dynal |
| Dynabeads CD3/CD28 T cell expander, human | Dynal |
| EDTA (1 % in PBS without $Ca^{2+}$, $Mg^{2+}$) | Biochrom |
| Endobulin (human IgG) | Baxter, Unterschleißheim, Germany |
| Ethanol absolute | Sigma-Aldrich |
| Ethidium bromide | Sigma-Aldrich |
| Fixation/permeabilization concentrate | eBioscience, Frankfurt |

| | |
|---|---|
| Fixation/permeabilization diluent | eBioscience |
| Fluoromount-G | Southern Biotech, Biozol, Eching, Germany |
| GeneRuler DNA ladder mix | Fermentas, Thermo Fisher Scientific |
| Geneticin sulfate (G-418) | Gibco, Invitrogen |
| Glacial acetic acid | Sigma-Aldrich |
| Glycerol | Carl Roth |
| Glycine | Gerbu, Gaiberg, Germany |
| Heparin-Natrium (25 000 I.E./5 ml) | B. Braun |
| Hyaluronidase from sheep testes, type V | Sigma-Aldrich |
| Hygromycin B | Invitrogen |
| Isofluran | Baxter |
| Isopentane | Carl Roth |
| Isopentanol | Sigma-Aldrich |
| Isopropanol | Fluka |
| JetPEI transfection reagent | Polyplus-transfection, Peqlab, Erlangen, Germany |
| Ketanest S | Pfizer, Karlsruhe |
| Loading dye solution (6X) | Fermentas |
| Low molecular weight DNA Ladder | NEB |
| Lympholyte-M cell separation centrifugation medium, mouse | Cedarlane, Biozol |
| Matrigel basement membrane matrix, phenol-red free | BD |
| Mayer´s Hematoxylin (Lillie´s modification) | Dako |
| MB Taq DNA polymerase (hot-start) | Minerva Biolabs |
| Methanol | VWR |
| [methyl-$^{3}$H]-Thymidine (5 mCi, 185 MBq) | Perkin-Elmer |
| Milk powder | Carl Roth |
| MTS cell titer 96 aqueous solution | Promega |
| NaCl (sodium chloride) | Sigma-Aldrich |
| $Na_2{}^{51}CrO_4$ (5 mCi, 185 MBq) | Perkin-Elmer |
| NEB reaction buffer 1 and 3 | NEB |
| Norleucine-DL | Sigma-Aldrich |
| Normal serum (chicken, goat, mouse) | Santa Cruz Biotechnology, Heidelberg |
| Normal serum (rat) | eBioscience |
| Paraffin wax pellets | BDH Prolabo, VWR |
| Paraformaldehyde | Merck |
| Permeabilization buffer (10X) | eBioscience |
| Plasmocin | Invivogen, Toulouse, France |
| Polybrene (Hexadimethrine bromide) | Sigma-Aldrich |
| Poly-L-lysine hydrobromide | Sigma-Aldrich |
| Potassium hydrogen carbonate ($KHCO_3$) | Sigma-Aldrich |
| Propidium iodide (PI) | Sigma-Aldrich |
| Protein assay dye reagent concentrate | Bio-Rad |
| Protein marker, broad range (2-212 kDa) | NEB |
| Puromycin | PAA, Pasching, Austria |
| Restriction enzymes (BamHI, HindIII, KpnI, NcoI, PstI) | NEB |

| | |
|---|---|
| Retronectin | Takara Bio, Mobitec, Goettingen, Germany |
| Rompun 2 % | Bayer-Schering Pharma, Leverkusen, Germany |
| SDS | Carl Roth |
| Sodiumhydroxide pellets | Sigma-Aldrich |
| Spitacid | Ecolab, Duesseldorf, Germany |
| Staphylococcal enterotoxin B (SEB) | Sigma-Aldrich |
| Streptavidin-alkaline phosphatase | Mabtech, Hamburg |
| Tissue-Tek | Sakura Finetek |
| TransIT-LT1 transfection reagent | Mirus Bio, MoBiTec, Goettingen |
| Tris(hydroxymethyl)aminomethane | Sigma-Aldrich |
| Tris-glycine 4-20 % gradient gels | Anamed, Gross-Bieberau, Germany |
| Triton X-100 | Fluka |
| Trypan blue solution (0.4 %) | Fluka |
| Trypsin-EDTA (10X) | PAA |
| Tween 20 | Sigma-Aldrich |

### 6.4.2. Media and supplements

| Product | Supplier |
|---|---|
| AB serum, human | PAN Biotech, Aidenbach, Germany |
| Agar | Fluka |
| Biocoll separating solution (density 1.077 g/ml) | Biochrom |
| DMEM high glucose (4.5 g/l), L-Glutamine, sodium pyruvate, sodium bicarbonate (D6429) | Sigma-Aldrich |
| DMEM high glucose (4.5 g/l), without L-Glutamine (E15-009) | PAA |
| DMEM/F-12 (1:1) high glucose (3.2 g/l) without L-Glutamine (21331020) | Gibco |
| D-PBS without $Ca^{2+}$, $MgCl_2$ (D8537; 1X) | Sigma-Aldrich |
| Fetal calf serum (FCS) | Biochrom |
| Hepes (1 M) | PAA |
| L-Glutamine (200 mM) | BioWhittaker, Lonza, Cologne |
| Non-essential amino acids (NEAA; 100X) | BioWhittaker |
| Penicillin/Streptomycin (Pen/Strep; 100X) | PAA |
| RPMI 1640 with L-Glutamine, sodium bicarbonate (R8758) | Sigma-Aldrich |
| RPMI 1640 with Hepes, without L-Glutamine and phosphate | PAN-Biotech |
| S.O.C. medium | Invitrogen |
| Tryptone | Applichem, Darmstadt |
| X-VIVO 20 serum-free medium with L-Glutamine, gentamicin | Lonza |
| Yeast extract | Gerbu |

FCS and AB serum were generally inactivated at 56°C for 30 min and filtered (0.22 µm) sterile before used as media supplements.

- **Dendritic cell medium**

| | |
|---|---|
| X-VIVO 20 | 50 ml |
| Human rGM-CSF | 560 U/ml |
| Human rIL-4 | 50 U/ml |

- **DMEM, 10 % FCS**

| | |
|---|---|
| DMEM with L-Glutamine | 500 ml |
| 10 % FCS | 50 ml |
| Pen/Step | 5 ml |
| Hepes | 5 ml |

- **DMEM, 20 % FCS**

| | |
|---|---|
| DMEM with L-Glutamine | 500 ml |
| 20 % FCS | 100 ml |
| Pen/Step | 5 ml |
| Hepes | 5 ml |

- **DMEM/F-12, 10 % FCS**

| | |
|---|---|
| DMEM/F-12 | 500 ml |
| 10 % FCS | 50 ml |
| Pen/Step | 5 ml |
| Hepes | 5 ml |
| 200 mM L-Glutamine | 5 ml |

- **Freezing medium**

| | |
|---|---|
| 80 % FCS | 40 ml |
| 20 % DMSO | 10 ml |

Freezing medium was routinely filtered (0.22 µm) sterile and 5 ml aliquots in 15 ml tubes were prepared and stored at -20°C until use.

- **LB medium**

| | |
|---|---|
| Tryptone | 10 g |
| Yeast extract | 5 g |
| NaCl | 10 g |
| add dd$H_2O$ to 1 l, pH 7.0, autoclaved | |

- **LB Agar medium for bacterial plates (LB Agar plates)**

| | |
|---|---|
| Tryptone | 10 g |
| Yeast extract | 5 g |
| NaCl | 10 g |
| Agar | 15 g |
| add dd$H_2O$ to 1 l, pH 7.0, autoclaved | |

The homogeneous solution was cooled to ~50°C, ampicillin was added and the Agar medium spilled to Optilux petri dishes and allowed to solidify under sterile conditions. The plates were stored upside down at 4°C for up to 2 weeks until use.

- **Phoenix medium**

| | |
|---|---|
| DMEM with L-Glutamine | 500 ml |
| 10 % FCS | 50 ml |
| NEAA | 5 ml |
| Pen/Step | 5 ml |
| Hepes | 5 ml |

- **Phosphate-free T cell TCR medium**

| | |
|---|---|
| RPMI without L-Glutamine and phosphate | 500 ml |
| 10 % AB Serum | 50 ml |
| Pen/Step | 5 ml |
| 200 mM L-Glutamine | 5 ml |

- **Phosphate-free T cell TCR medium with cytokines**

| | |
|---|---|
| Phosphate-free T cell TCR medium | 50 ml |
| Human rIL-2 | 100 U/ml |
| Human rIL-4 | 3 U/ml |
| Human rIL-7 | 20 ng/ml |
| Human rIL-15 | 20 ng/ml |

- **RPMI medium 10 % FCS**

| | |
|---|---|
| RPMI with L-Glutamine | 500 ml |
| 10 % FCS | 50 ml |
| Pen/Step | 5 ml |
| Hepes | 5 ml |

- **RPMI medium without serum**

| | |
|---|---|
| RPMI with L-Glutamine | 500 ml |
| Pen/Step | 5 ml |
| Hepes | 5 ml |

- **T cell medium**

| | |
|---|---|
| RPMI with L-Glutamine | 500 ml |
| 10 % AB serum | 50 ml |
| Pen/Step | 5 ml |
| Hepes | 5 ml |

- **T cell medium with cytokines**

| | |
|---|---|
| T cell medium | 50 ml |
| Human rIL-2 | 100 U/ml |
| Human rIL-4 | 3 U/ml |

### 6.4.3. Buffers

The following buffers used, were generally freshly prepared and stored at 4°C.

- **ACK lysis buffer for red blood cell lysis**

| | |
|---|---|
| $NH_4Cl$ | 8.29 g |
| $KHCO_3$ | 1 g |
| EDTA | 0.0372 g (0.1 mM) |
| add $ddH_2O$ to 1 l, pH 7.2 - 7.4 | |

- **Bluing reagent for IHC staining**

| | |
|---|---|
| 1 M $NH_4OH$ solution | 18.5 ml |
| add $ddH_2O$ to 500 ml | |

- **BSA blocking buffer for retronectin plate coating (2 % in PBS)**

| | |
|---|---|
| PBS | 50 ml |
| BSA (fraction V) | 1 g |
| Solution was filtered (0.22 µm) sterile. | |

- **Coomassie brilliant blue staining solution**

| | |
|---|---|
| Coomassie brilliant blue R-250 | 0.2 g |
| Isopropanol | 400 ml |
| Acetic acid | 70 ml |
| add $ddH_2O$ to 1 l, pH 7.2 | |

- **Dulbecco`s PBS without $Ca^{2+}$, $Mg^{2+}$ (10X)**

| | |
|---|---|
| Dulbecco`s PBS powder (for 10 l) | |
| add $ddH_2O$ to 1 l, pH 7.2 - 7.4 | |

- **ELISPOT washing buffer (0.25 % Tween in PBS)**

| | |
|---|---|
| PBS | 500 ml |
| Tween 20 | 1.25 ml |

- **ELISPOT 6 % AB serum blocking buffer**

| | |
|---|---|
| RPMI with L-Glutamine | 46 ml |
| 6 % AB serum | 3 ml |
| Pen/Step | 0.5 ml |
| Hepes | 0.5 ml |

- **ELISPOT 10 % AB serum blocking buffer**

| | |
|---|---|
| RPMI with L-Glutamine | 44 ml |
| 10 % AB serum | 5 ml |
| Pen/Step | 0.5 ml |
| Hepes | 0.5 ml |

- **FACS buffer**

| | |
|---|---|
| PBS | 49 ml |
| FCS | 1 ml |

- **Formaldehyde fixation buffer**

| | |
|---|---|
| Paraformaldehyde | 1 g |
| PBS | 100 ml |

- **Laemmli sample buffer (2X)**

| | |
|---|---|
| Tris | 3.6 g (10 mM) |
| DTT | 0.6 g |
| Glycerol | 20 ml |
| SDS | 10 g |
| Bromophenol blue | 0.2 g |
| add $ddH_2O$ to 100 ml, pH 6.8 | |

- **MACS buffer**

| | |
|---|---|
| PBS | 46.827 ml |
| EDTA | 2.923 ml (2 mM) |
| AB serum | 250 µl |

- **Permeabilization buffer for microscopy**

| | |
|---|---|
| PBS | 100 ml |
| Triton X-100 | 0.2 g |

- **PVDF membrane blocking milk buffer**

| | |
|---|---|
| PBS (10X) | 100 ml |
| Milk powder | 50 g |
| Tween 20 | 0.5 g |
| add $ddH_2O$ to 1 l, pH 7.2 - 7.4 | |

- **PVDF membrane destaining buffer**

| | |
|---|---|
| Isopropanol | 400 ml |
| Acetic acid | 70 ml |
| add $ddH_2O$ to 1 l, pH <7.2 | |

- **PVDF membrane washing buffer (PBS-Tween)**

| | |
|---|---|
| PBS (10X) | 100 ml |
| Tween 20 | 0.5 g |
| add $ddH_2O$ to 1 l, pH 7.2 - 7.4 | |

- **SDS-PAGE electrophoresis running buffer (10X)**

| | |
|---|---|
| Tris | 28 g (231 mM) |
| SDS | 20 g |
| Glycine | 144 g |
| add $ddH_2O$ to 1 l, pH 8.8 | |

- **Semi-dry transfer buffer 1**

| | |
|---|---|
| Tris | 36.3 g (300 mM) |
| Isopropanol | 200 ml |
| add $ddH_2O$ to 1 l, pH 10.4 | |

- **Semi-dry transfer buffer 2**

| | |
|---|---|
| Tris | 3.025 g (25 mM) |
| Isopropanol | 200 ml |
| add dd$H_2O$ to 1 l, pH 10.4 | |

- **Semi-dry transfer buffer 3**

| | |
|---|---|
| Tris | 3.025 g (25 mM) |
| Norleucine-DL | 5.24 g |
| add dd$H_2O$ to 1 l, pH 9.4 | |

- **Tris-acetate-EDTA (TAE) buffer (50X)**

| | |
|---|---|
| Tris | 242 g (2 M) |
| Glacial acetic acid | 57.1 ml |
| 0.5 M EDTA | 100 ml |
| add dd$H_2O$ to 1 l, pH 8.5 | |

- **Tumor digestion buffer**

| | |
|---|---|
| PBS | 10 ml |
| Hyaluronidase type V | 0.5 mg/ml |
| DNase I | 0.5 mg/ml |

## 6.5. Antibodies

If not further indicated, the listed Abs react against human epitopes.

### 6.5.1. Flow cytometry

| Specificity | Species | Isotype | Conjugate | Clone | Supplier |
|---|---|---|---|---|---|
| CCR7 | rat | IgG2a | PE | 3D12 | BD |
| CD3 | mouse | IgG2a | FITC | HIT3a | BD |
| CD3 | mouse | IgG1 | PE | UCHT1 | BD |
| CD3 | mouse | IgG2a | PE-Cy5 | HIT3a | BD |
| CD4 | mouse | IgG1 | FITC | RPA-T4 | BD |
| CD4 | mouse | IgG1 | PerCP-Cy5.5 | RPA-T4 | BD |
| CD4 | mouse | IgG1 | APC | RPA-T4 | BD |
| CD8 | mouse | IgG1 | FITC | HIT8a | BD |
| CD8 | mouse | IgG1 | APC-Cy7 | SK1 | BD |
| CD11c | mouse | IgG1 | PE | B-ly6 | BD |
| CD14 | mouse | IgG2a | PE | M5E2 | BD |
| CD25 | mouse | IgG1 | FITC | M-A251 | BD |

| | | | | | |
|---|---|---|---|---|---|
| CD25 | mouse | IgG1 | APC-Cy7 | M-A251 | BD |
| CD27 | mouse | IgG1 | PerCP-Cy5.5 | M-T271 | BD |
| CD45 | mouse | IgG1 | APC | HI30 | BD |
| CD45RO | mouse | IgG2a | PE | UCHL1 | BD |
| CD45RO | mouse | IgG2a | APC | UCHL1 | BD |
| CD62L | mouse | IgG1 | FITC | DREG-56 | BD |
| CD69 | mouse | IgG1 | PE | FN50 | BD |
| CD127 | mouse | IgG1 | PE | HIL-7R-M21 | BD |
| CEACAM1 | mouse | IgG1 | - | GM8G5 | Axxora, Loerrach, Germany |
| CEACAM6 | mouse | IgG1 | - | 9A6 | Axxora |
| CEACAM6 | mouse | IgG1 | FITC | 9A6 | Santa Cruz Biotechnology |
| Fusion (F) protein of NDV | mouse anti NDV | IgG1 | - | Icii | Prof. Dr. V. Schirrmacher, DKFZ |
| Foxp3 | mouse | IgG1 | APC | 236A/E7 | eBioscience |
| HLA-A2 | mouse | IgG2b | - | BB7.2 | Dr. G. Molden-hauer, DKFZ |
| HLA-ABC | mouse | IgG1 | FITC | G46-2.6 | BD |
| HLA-DR | mouse | IgG2a | PE | G46-6 | BD |
| IgG/IgM | goat anti mouse | Ig | FITC | polyclonal | BD |
| IgG | goat anti mouse | Ig, $F(ab')_2$ | FITC | polyclonal | Jackson Immuno Research, Dianova, Hamburg |
| IgM/IgG/ IgA | goat anti mouse | Ig, $F(ab')_2$ | PE | polyclonal | Southern Biotech |
| Isotype control | mouse | IgG1 | FITC | MOPC-21 | BD |
| Isotype control | mouse | IgG1 | PE | MOPC-21 | BD |
| Isotype control | mouse | IgG1 | APC | MOPC-21 | BD |

| | | | | | |
|---|---|---|---|---|---|
| L1CAM | mouse | IgG1 | - | L1-9.3 | Dr. G. Molden-hauer |
| $V_\beta$ 6 TCR (MDM2 TCR) | rat anti mouse | IgG2b | PE | RR4-7 | BD |
| $V_\beta$ 14 TCR (gp100 TCR) | mouse | IgG1 | PE | CAS1.1.3 | Beckman Coulter |

### 6.5.2. Cell culture and ELISPOT

| Specificity | Species | Isotype | Conjugate | Clone | Supplier |
|---|---|---|---|---|---|
| CD3 | mouse | IgG2a | - | Okt3 | Dr. G. Molden-hauer |
| CD19 | mouse | IgG1 | - | HD37 | Dr. G. Molden-hauer |
| CD28 | mouse | IgG2a | - | 9.3 | Dr. G. Molden-hauer |
| CD56 | mouse | IgG1 | - | C218 | Beckman Coulter |
| CEACAM6 | mouse | IgG1 | - | 9A6 | Axxora |
| IFNγ | mouse | IgG1 | - | 1-D1K | Mabtech |
| IFNγ | mouse | IgG1 | biotin | 7-B6-1 | Mabtech |
| Isotype control | mouse | IgG1 | - | DAK-GO1 | Dako |
| L1CAM | mouse | IgG1 | - | L1-9.3 | Dr. G. Molden-hauer |

ELISPOT analyses were performed using streptavidin-alkaline phosphatase.

### 6.5.3. Immunohistochemistry, immunofluorescence and immunoblot

| Specificity | Species | Isotype | Conjugate | Clone | Supplier |
|---|---|---|---|---|---|
| actin | mouse | IgG1 | - | C4 | MP Biomedicals, Illkirch Cedex, France |
| CD45 | mouse | IgG1 | - | HI30 | BD |
| gp100 | mouse | IgG1 | - | HMB45 | Enzo, Loerrach |
| Isotype control | mouse | IgG1 | - | DAK-GO1 | Dako |

| | | | | | |
|---|---|---|---|---|---|
| Keratin 8 | mouse | IgG1 | - | Ks8-17.2 | Progen, Heidelberg |
| Keratin 18 | mouse | IgG1 | - | Ks18.174 | Progen |
| L1CAM | mouse | IgG1 | - | L1-9.3 | Dr. G. Molden-hauer |
| MDM2 | mouse | IgG2b | - | IF2 | Invitrogen |
| MDM2 | mouse | IgG2b | - | IF2 | Calbiochem |
| Melan-A/ MART-1 | mouse | IgG2b | - | M2-7C10 + M2-9E3 | Thermo Fisher Scientific |
| Melan-A/ MART-1 | mouse | IgG1 | - | A103 | Dako |
| NDV | rabbit anti NDV | Ig | - | polyclonal | Prof. Dr. V. Schirrmacher |
| Pan-cytokeratin | mouse | IgG1 | - | C11 | Santa Cruz Biotechnology |
| p53 | mouse | IgG2a | - | Bp53-11 | Progen |
| Tyrosinase | mouse | IgG2a | - | T311 | Invitrogen |
| Vimentin | mouse | IgG2a | - | VIM 3B4 | Progen |

Secondary Abs conjugated with fluorochromes used for immunofluorescence microscopy were directed against species-specific IgGs and had been generated in goat or chicken. Cy3- (Jackson Immuno Research) and Alexa Fluor 488- or Alexa Fluor 594-conjugated (Invitrogen) secondary Abs against mouse and rabbit IgGs were used. Immunoblot analyses were performed using horseradish peroxidase (HRP)-conjugated secondary goat anti mouse IgG/IgM Abs (Jackson Immuno Research).

## 6.6. Multimers/tetramers (HLA-A*0201)

| **Product** | **Supplier** |
|---|---|
| **gp100** (280-288, YLEPGPVTA)-PE-Cy5 [0.43 mg/ml] | Prof. Dr. P. Romero, Ludwig Institute for Cancer Research, Lausanne, Switzerland |
| **MDM2** (81-88, LLGDLFGV)-PE [0.38 mg/ml] | Prof. Dr. P. Romero |

## 6.7. Primers

The primers used for sequencing were produced by Eurofins MWG Operon, Ebersberg, Germany.

| Product | Primer sequence |
|---|---|
| **pBullet-IRES forward** | 5'- tcg ctg gaa agg acc tta c -3' (19 mer) |
| **pBullet-IRES reverse** | 5'- cgg gcc agg tga ata tca aat c -3' (22 mer) |

## 6.8. Peptides

The following peptides were produced by the Peptide Synthesis Facility of the DKFZ (Dr. R. Pipkorn).

| Protein | Amino acid sequence | Peptide |
|---|---|---|
| **GAGE-1** | MSWRGRSTYR PRPRRYVEPP EMIGPMRPEQ FSDEVEPATP EEGEPATQRQ | (1-50) |
| **gp100/pmel17** | SITGSLGPLL DGTATLRLVK RQVPLDCVLY RYGSFSVTLD IVQGIESAEI | (449-498) |
| **MAGE-A1** | PARYEFLWGP RALAETSYVK VLEYVIKVSA RVRFFFPSLR EAALREEEEG | (259-308) |
| **MAGE-C2** | WGPRAHSESI KKKVLEFLAK LNNTVPSSFP SWYKDALKDV EERVQATIDT | (301-350) |
| **MDM2** | KEVLFYLGQY IMTKRLYDEK QQHIVYCSND LLGDLFGVPS FSVKEHRKIY | (51-100) |
| **Melan-A/MART-1** | GHGHSYTTAE EAAGIGILTV ILGVLLLIGC WYCRRRNGYR ALMDKSLHVG | (16-65) |
| **MIF** | LMAFGGSSEP CALCSLHSIG KIGGAQNRSY SKLLCGLLAE RLRISPDRVY | (47-96) |
| **NA17-A** | MVLPDVFIRC VVFCLTVVCW TWVPLRGPSS PGSYRKWMCF SESQVQPTQK | (1-50) |
| **NY-Eso-1** | FTVSGNILTI RLTAADHRQL QLSISSCLQQ LSLLMWITQC FLPVFLAQPP | (126-175) |
| **p53** | TAKSVTCTYS PALNKMFCQL AKTCPVQLWV DSTPPPGTRV RAMAIYKQSQ | (118-167) |
| **RAB38/NY-Mel-1** | ATIGVDFALK VLHWDPETVV RLQLWDIAGQ ERFGNMTRVY YREAM GAFIV | (40-89) |
| **TRP2** | ALPHSAANDP IFVVISNRLL YNATTNILEH VRKEKATKEL PSLHVLVLHS | (381-430) |
| **Tyrosinase** | MLLAVLYCLL WSFQTSAGHF PRACVSSKNL MEKECCPPWS GDRSPCGQLS | (1-50) |
| **gp100** | YLEPGPVTA | (280-288) |
| **HIV-pol** | ILKEPVHGV | (476-484) |
| **MDM2** | LLGDLFGV | (81-88) |
| **p53** | LLGRNSFEV | (264-272) |

## 6.9. Cytokines

| Product | Supplier |
|---|---|
| Human rGM-CSF (Leukine, Sargramostim) | Berlex, Bayer-Schering Pharma |
| Human rIL-2 (Proleukin) | Chiron, Ratingen, Germany |
| Human rIL-4 | Promokine, PromoCell, Heidelberg |
| Human rIL-7 | Promokine |
| Human rIL-15 | Promokine |

## 6.10. Plasmids

| | |
|---|---|
| **pBullet** | MoMuLV retroviral vector with transgene (TCR genes of α or β chain), cytomegalovirus (CMV) promoter |
| **pCOLT-GALV** | packaging helper plasmid for retroviral production, expression of GALV envelope (env) proteins, CMV promoter |
| **pHIT60** | packaging helper plasmid for retroviral production, expression of MuLV gag/pol proteins of retroviral capsid and reverse transcriptase polymerase, CMV promoter |
| **pcDNA3.1-luc-hygro** | coding for firefly luciferase, CMV promoter |

All different pBullet plasmid constructs as well as the packaging helper plasmids pCOLT-GALV and pHIT60 were kindly provided by Dr. R.-H. Voss (Department of Hematology and Oncology, University of Mainz, Mainz). The individual TCR transduction settings using different pBullet plasmid combinations are indicated in the table below (bold letters). The original retroviral pBullet vector was developed and first described by Willemsen et al., 2003. The pcDNA3.1-luc-hygro plasmid was kindly provided by Dr. J. Ni (DKFZ).

| Product | Plasmid maps / informations |
|---|---|
| pBullet_IRESpuro-[NcoI] | Appendix 13.1. |
| pBullet_IRESneo-[NcoI] | Appendix 13.2. |
| ▪ **Mock** | |
| pBullet_Mu Wta TCR MDM2_IRESpuro | Appendix 13.3. |
| pBullet_Mu Wtb TCR MDM2_IRESneo | Appendix 13.4. |
| ▪ **Mu Wt TCR MDM2** | |
| pBullet_Mu Mta TCR MDM2 G85.1caR_IRESpuro | Appendix 13.5. |
| pBullet_Mu Mtb TCR MDM2 R88cbG_IRESneo | Appendix 13.6. |
| ▪ **Mu Mt Arg/Gly TCR MDM2** | |
| pBullet_Hu Wta TCR gp100_IRESpuro | Appendix 13.7. |
| pBullet_Hu Wtb TCR gp100_IRESneo | Appendix 13.8. |
| ▪ **Hu Wt TCR gp100** | |

| | |
|---|---|
| pBullet_Mu Ca T84caC_IRESpuro | Appendix 13.9. |
| pBullet_Hu Chim scTCR gp100 Mu Cb S79cbC_IRESneo<br>▪ **Hu Chim scTCR gp100 MuC$_\beta$ S79C + MuC$_\alpha$ T84C** | Appendix 13.10. |
| pBullet_IRESpuro-[NcoI] | Appendix 13.1. |
| pBullet_eGFP_IRESneo<br>▪ **EGFP** | Appendix 13.11 |
| pCOLT-GALV | Weijtens et al., 1998 |
| pHIT60 | Soneoka et al., 1995 |
| pcDNA3.1-luc-hygro | firefly luciferase fragment of vector pGL3-Basic (Promega) was integrated into pcDNA3.1/Hygro pasmid (Invitrogen) |

## 6.11. Viruses

Strains of the Newcastle disease virus (NDV), a negative-sense single stranded RNA virus, belonging to the viral family of *paramyxoviridae* (Avulavirus) can be differentiated on the basis of their avian (chicken) pathogenicity into strains of high (velogenic), intermediate (mesogenic) and low-to-no (lentogenic) virulence.

| **Product** | **information** |
|---|---|
| **NDV-Ulster** | lentogenic strain, nonlytic, avirulent |
| **NDFL-EGFP** | lentogenic strain, nonlytic, avirulent; recombinant strain expressing the jellyfish EGFP protein, based on the NDV strain LaSota |
| **NDFLtagEGFP** | mesogenic strain, lytic, virulent; recombinant strain expressing the jellyfish EGFP protein, based on the NDV strain LaSota |
| **MTH-68** | mesogenic strain, lytic, virulent |

All different viruses were propagated in embryonated chicken eggs, harvested from the allantoic fluid, purified by ultracentrifugation, resuspended in a PBS/0.1 % EDTA solution and cryopreserved in aliquots at -80°C. The virus amount was quantified by a hemagglutination assay, while 1 hemagglutination unit (HU) was defined as the smallest virus concentration leading to visible sheep erythrocyte agglutination (see also Schirrmacher et al., 1999). The different NDV strains were produced and kindly provided by Prof. Dr. V. Schirrmacher.

## 6.12. Bacteria

| **Product** | **Supplier** |
|---|---|
| Library efficiency DH5α competent cells | Invitrogen |
| One Shot TOP10 competent cells | Invitrogen |

## 6.13. Cell lines

Most cell lines were obtained from the American Type Culture Collection (ATCC; supplier LGC Standards, Luckenwalde, Germany). Further cell line contributors are indicated.

| Cell line | Origin | Supplier | Medium |
|---|---|---|---|
| **BT-474** | human adenocarcinoma, breast | ATCC (HTB-20) | DMEM/F-12, 10 % FCS |
| **C32** | human melanoma, primary, skin | ATCC (CRL-1585) | DMEM, 10 % FCS |
| **Capan-1** | human adenocarcinoma, pancreas | ATCC (HTB-79) | RPMI, 10 % FCS |
| **HCT-15** | human adenocarcinoma, colorectal | ATCC (CCL-225) | DMEM, 10 % FCS |
| **HT-29** | human adenocarcinoma, colorectal | ATCC (HTB-38) | DMEM/F-12, 10 % FCS |
| **IM-9** | human multiple myeloma | ATCC (CCL-159) | RPMI, 10 % FCS |
| **Jurkat (JCD28)** | human T cell leukemia | Tumor bank, DKFZ | RPMI, 10 % FCS |
| **KPL-4** | human adenocarcinoma, breast | Dr. D. Zopf, Bayer Schering Pharma | RPMI, 10 % FCS |
| **KS 22.24** | human adenocarcinoma, breast | Dr. B. Gueckel University of Tuebingen, Tuebingen, Germany | RPMI, 10 % FCS |
| **KS WT** | human adenocarcinoma, breast | Dr. B. Gueckel | RPMI, 10 % FCS |
| **LoVo** | human adenocarcinoma, colorectal | ATCC (CCL-229) | RPMI, 10 % FCS |
| **Malme-3M** | human melanoma, metastasis, lung | ATCC (HTB-64) | DMEM, 20 % FCS |
| **MCF-7** | human adenocarcinoma, breast | ATCC (HTB-22) | DMEM, 10 % FCS |
| **MCF-7 CEACAM6 high** | human adenocarcinoma, breast | C. Pfirschke, personal thesis contribution | DMEM, 10 % FCS |
| **MeWo** | human melanoma, metastasis, lymph node | ATCC (HTB-65) | DMEM, 10 % FCS |
| **MeWo-luc** | human melanoma, metastasis, lymph node | C. Pfirschke, personal thesis contribution | DMEM, 10 % FCS + 100 µg/ml Hygromycin |

| | | | |
|---|---|---|---|
| **Phoenix ampho** | human embryonic kidney | ATCC (SD-3443) | Phoenix medium |
| **RPMI 8226** | human multiple myeloma | ATCC (CCL-155) | RPMI, 10 % FCS |
| **SK-Mel-2** | human melanoma, metastasis, skin | ATCC (HTB-68) | DMEM, 10 % FCS |
| **SK-Mel-23** | human melanoma, metastasis, skin | Prof. Dr. L. Old, Memorial Sloan-Kettering Cancer Center, New York, NY, USA | RPMI, 10 % FCS |
| **SKMM2** | human multiple myeloma | Prof. Dr. H. Goldschmidt, University Hospital Heidelberg, Heidelberg | RPMI, 10 % FCS |
| **T2** | human lymphoblast | ATCC (CRL-1992) | RPMI, 10 % FCS |
| **U266** | human multiple myeloma | ATCC (TIB-196) | RPMI, 10 % FCS |
| **U2OS** | human osteosarcoma | ATCC (HTB-96) | DMEM, 10 % FCS |
| **WM-115** | human melanoma, primary, skin | ATCC (CRL-1675) | DMEM, 10 % FCS |
| **WM-266-4** | human melanoma, metastasis, skin | ATCC (CRL-1676) | DMEM, 10 % FCS |

## 6.14. Mice

The non-obese diabetic (NOD)-severe combined immune-deficient [(SCID); NOD-SCID] mice have impaired T and B lymphocyte development, whereas NOD *scid* gamma (NSG) mice bear a targeted mutation in the gene encoding the IL-2 receptor gamma chain gene (*IL2rg*$^{null}$) and lack mature T cells, B cells, functional natural killer (NK) cells and are deficient in cytokine signaling. For animal experiments 7-9 week old female mice of the two immunodeficient mice strains NOD-SCID (NOD.CB17-*Prkdc*$^{scid}$/NcrCrl) and NSG (NOD.Cg-*Prkdc*$^{scid}$IL2rg$^{tm1Wjl}$/SzJ) were used. The NOD-SCID mice were purchased from Charles River Laboratories (Sulzfeld, Germany) and the NSG mice from the Animal Facility of the DKFZ. All mice were kept under specific pathogen-free conditions in individually ventilated cages (Animal Facility, DKFZ). Food and water were administered “ad libitum” and a day night rhythm of 12 h was ensured. All animal experiments were approved and authorized by the regulatory authorities (Karlsruhe) and performed according to local animal experimental ethics committee guidelines and permissions.

## 6.15. Peripheral blood samples of healthy donors and patients

Leukocyte cell concentrates, also referred to as “Buffy coat” blood samples, of healthy donors were provided from the Blood Donation Center of the University of Heidelberg. Peripheral blood samples of melanoma and dysplastic nevi patients were obtained from the Department of Dermatology, University Hospital Heidelberg. The ethics application form for this study was approved by the ethical committee and the written consent was obtained from all analyzed patients.

## 6.16. Software

| Product | Supplier |
|---|---|
| Adobe Photoshop (CS2) | Adobe Systems, Munich |
| AxioVision LE (4.4) | Carl Zeiss |
| CellQuest Pro (4.02) | BD |
| Clone Manager Professional (9) | Scientific & Education Software, Cary, NC, USA |
| CTL ImmunoSpot Professional (4) | CTL |
| EndNote (X4) | Adept Scientific, Frankfurt |
| FACS Diva software (6) | BD |
| FlowJo (8.8) | Tree Star, Ashland, OR, USA |
| GraphPad Prism (5) | GraphPad Software, LaJolla, CA, USA |
| KS-ELISPOT software (4) | Carl Zeiss |
| Living Image (2.50), Igor Pro (4.09A) | Xenogen |
| Microsoft Office 2007 | Microsoft, Redmond, WA, USA |
| Microsoft Windows 7 | Microsoft |
| SigmaPlot (10.0) | Systat Software, Erkrath, Germany |

# 7. Methods

## 7.1. Cell culture methods

### 7.1.1. Thawing cryopreserved cells

For thawing of cells, growth medium (37°C) was added to frozen cells into cryogenic vials and the content immediately transferred into 15 ml tubes, containing 10 ml growth medium. After one washing and centrifugation step with respective growth medium [1200-1400 rpm, 5 min, room temperature (RT)], the cells were seeded in cell culture flasks in fresh medium and cultured in a cell culture incubator at 37°C, 5 % $CO_2$. The medium was completely renewed after 24 h and the cells cultured until use.

### 7.1.2. Cultivation of adherent and suspension cells

All cell lines were grown in cell culture dishes or flasks and incubated at 37°C, 5 % $CO_2$. For detachment of adherent cells from the culture flask surface, the growth medium was removed and the cell layer carefully washed with warm phosphate buffered saline (PBS). Then 1X Trypsin-ethylenediaminetetraacetic acid (Trypsin-EDTA) solution was added for ~5 min at 37°C, depending on the type of cells. The Trypsin-EDTA solution was inactivated using double amount of fresh culture medium supplemented with fetal calf serum (FCS), followed by a centrifugation step (1200 rpm, 5 min, RT). For sub-cultivation, cells were distributed to new culture plates or flasks in a 1:5 to 1:20 ratio, depending on the cell line.

Suspension cells were usually maintained by the addition or replacement of the required fresh growth medium. In general, the cell lines were passaged 2-3x per week. Permanent cell lines were only used for experiments until they reached a passage number of thirty, afterwards a new vial of cells was thawed. All permanent cell lines were regularly tested for mycoplasma contamination (7.3.14.).

### 7.1.3. Determination of cell number and viability

Viable cells were quantified using a Neubauer hemocytometer. Since Trypan blue can only traverse the damaged plasma membrane of nonviable cells, it was used to distinguish between alive or dead cells. In order to produce a statistically significant count, all four large chamber squares and at least hundred living cells were counted for each sample. The cell number was calculated using the following formula:

$$\text{Cell number} = \left[\frac{\text{total cell count}}{\text{number of counted large squares}}\right] \text{x dilution factor x volume x } 10^4$$

### 7.1.4. Irradiation of cells

For antigen-specific stimulation of T cell receptor (TCR) transgenic T cells, peptid-loaded transporter associated with antigen processing (TAP)-deficient T2 cells were used and autologous peripheral blood mononuclear cells (PBMC) as feeder cells. Peptide-pulsed T2 cells were irradiated with 70 gray (Gy) and PBMC with 35 Gy using the Gamma cell 1000 irradiation device. The cells were irradiated at a concentration of $1x10^6$ cells/ml medium in 15 or 50 ml tubes. To get a homogenous cell suspension, cells were carefully shacked shortly before irradiation.

### 7.1.5. Blockade of cell adhesion molecules on tumor cells

To block carcinoembryonic antigen-related cell adhesion molecule 6 (CEACAM6) or L1 cell adhesion molecule (L1CAM), human tumor cells of lines, e.g., MeWo, KS WT, MCF-7, MCF-7 CEACAM6 high or Capan-1 ($1x10^6$ - $2x10^6$) were incubated with monoclonal antibodies (mAbs) specific for CEACAM6, L1CAM or the isotype control at 37°C for 30 min. Thereby, the cells were resuspended in 200 µl X-VIVO medium and an Ab concentration of 30 µg/ml was used. Afterwards, the cells were centrifuged and the medium discarded, followed by a washing step with X-VIVO medium. The Ab-blocked cells were immediately used for ELISPOT (7.2.10.) or radioactive chromium isotope 51 ($^{51}Cr$) release cytotoxicity (7.2.12.) assays.

### 7.1.6. Fixation of cultured cells

For fixation, on the one hand, the cells were grown on sterile glass cover slips, which had been pre-coated with 0.01 % poly-L-lysine in double distilled water ($ddH_2O$) for 30 min at RT, and washed 2x with PBS (37°C). On the other hand, cells were instead harvested with Trypsin-EDTA (7.1.2.) and single cell suspensions were dispersed to poly-prep slides using a cytospin cytocentrifuge at 500 rpm for 3 min. The cells were then fixed in methanol at -20°C for 5 min followed by incubation in acetone at -20°C for 30 sec. Cover slips and slides were air-dried at RT and immediately used for histological stainings (7.3.15.).

### 7.1.7. Freezing cells

For freezing of cells, PBMC and T cells were resuspended in 500 µl FCS and permanent cell lines in 500 µl growth medium and transferred into cryogenic vials. After addition of 500 µl freezing medium [final dimethyl sulfoxide (DMSO) concentration of 10 %], the vials were placed into a freezing container with isopentanol or a Styrofoam box and transferred immediately to -80°C. After 24 h, the cells were transferred to liquid nitrogen (-196°C), for long time storage.

## 7.2. Immunological methods

### 7.2.1. Peptide synthesis and storage

Lyophilized 50aa synthetic long peptides were solved in Aqua ad iniectabilia containing 10 % DMSO. The lyophilized human leukocyte antigen A2 (HLA-A2)-restricted short peptides were instead solved in pure DMSO. After dissolving, the peptide concentration was controlled via Bradford protein assay (7.3.1.) and optical density (OD) measurement at 280 nm using a photometer (7.3.5.). Aliquots of the peptides were stored at -80°C.

### 7.2.2. Isolation of human PBMC from melanoma and dysplastic nevi patients

For the PBMC isolation, a Ficoll density gradient centrifugation was performed. Therefore, ~40 ml peripheral blood (PB) was removed from each patient using sodium citrate vacutainers (green blood sample tubes). Biocoll separating solution (15.5 ml) was added into Leucosep 50 ml tubes (carrying a porous barrier) and centrifuged for 2 min at 1400 rpm, to allow the separating solution to pass the porous barrier. Beforehand, 20 ml of gently mixed PB was added, each Ficoll tube was loaded with 15 ml Roswell Park Memorial Institute (RPMI) medium supplemented with Hepes and Penicillin/Streptomycin (Pen/Strep). The tubes were then centrifuged at 2000 rpm for 20 min at RT without the centrifuge break, allowing the gradients not to mix. The resulting plasma/separating solution interphase contained the mononuclear cells as shown in Fig. 11.

The cells with a higher density, like granulocytes or erythrocytes were sedimented at the bottom of the Ficoll tube, below the porous barrier. Above the interphase, the plasma was removed and stored at -20°C for further analyses (7.3.17.). The interphase of each patient was collected with plastic serum pipettes and combined in a 50 ml tube. The cells were washed with RPMI, performing a centrifugation step (1400 rpm, 10 min, RT). The cell pellet was then resuspended in 20 ml X-VIVO medium and transferred into tissue treated cell culture dishes (Ø 96 x 21 mm).

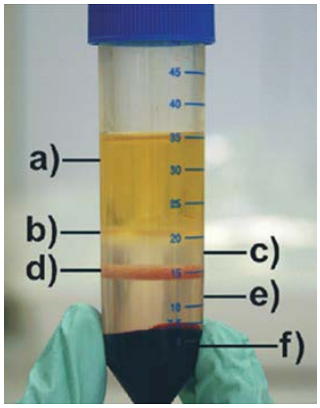


**a)** plasma

**b)** interphase of PBMC

**c)** Biocoll separating solution

**d)** porous barrier

**e)** Biocoll separating solution

**f)** pellet of erythrocytes and granulocytes

**Figure 11. Ficoll centrifugation using Leucosep 50 ml tubes with a porous barrier.** After Ficoll density gradient centrifugation, the sequence of layers occurred as indicated from **a**) - **f**). PBMC (**b**) were used for isolation of autologous T cells and dendritic cells. The plasma (**a**) was stored at -20°C for further investigations. The figure is modified from the Greiner Bio-one Leucosep information sheet.

To allow the adherence of mononuclear cells to the plastic surfaces of the cell culture dishes, an adherence phase was performed at 37°C for 2 h. Since lymphocytes remain in the supernatant, the non-adherent mononuclear cells were carefully removed, centrifuged and resuspended in 20 ml T cell medium supplemented with human recombinant cytokines of interleukin 2 (rIL-2) and rIL-4. Finally, the cells were cultured in non-tissue treated cell culture plates (Optilux, Falcon). In parallel, 20 ml dendritic cell medium supplemented with human recombinant granulocyte macrophage colony-stimulating factor (rGM-CSF) and rIL-4 was added to the adherent cells. In general, in order to mature dendritic cells out of mononuclear cells, autologous dendritic cells and T cells of the same donor were separately cultivated for 7 d. Every 2-3 d half of the medium was replaced with new cytokine-supplemented medium.

### 7.2.3. Isolation of human PBMC from healthy donors

PBMC of healthy donors were isolated performing a Ficoll density gradient centrifugation from leukocyte cell concentrates (Buffy coat). The blood was diluted 1:1 in PBS and added to the Ficoll tubes that contained 15.5 ml Biocoll separating solution below a porous barrier. The tubes were centrifuged at 2000 rpm for 20 min at RT without the centrifuge break. The plasma/separating solution interface was collected with plastic serum pipettes, combined in a 50 ml tube and washed with PBS. The PBMC were counted using Trypan blue and either stored frozen ($5x10^7$ cells / cryogenic vial) for later retroviral TCR transductions (7.3.9.) or directly used as healthy donor controls for ELISPOT (7.2.10.) and flow cytometry (7.2.13.) assays. In the latter case, cells were equally treated as described above (7.2.2.).

### 7.2.4. Generation and enrichment of dendritic cells from human PBMC

GM-CSF and IL-4 promote the differentiation and maturation of monocytes into dendritic cells. After a human rGM-CSF and human rIL-4 cytokine-dependent cultivation phase in X-VIVO medium for 7 d, dendritic cells were enriched via negative magnetic separation using mAb-pre-coupled Dynabeads. Thereby, T cells [cluster of differentiation 3 (CD3)], B cells (CD19) and NK cells (CD56) were depleted. After enrichment, the dendritic cells were bead- and Ab-free.

Prior to dendritic cell isolation, 100 µl X-VIVO medium washed pan mouse IgG Dynabeads per patient were coupled with 4 µg of CD3, CD19 or CD56 mAbs, respectively while incubating on a rotator at 4°C for 30 min. All three fractions were pooled in a 15 ml tube and washed 2x with X-VIVO medium. Thereby, the resuspended beads were placed into the magnetic field of a magnetic particle concentrator for 2 min. The washed beads were then resuspended in 300 µl X-VIVO medium and stored on ice until the cells were prepared for further purification.

Matured dendritic cells that have a plastic cell shape with cellular processes can be removed from the plate by rinsing with X-VIVO medium. After a centrifugation step (1400 rpm, 10 min, RT), the pellet was resuspended in 1 ml X-VIVO medium and transferred to a 15 ml tube. In a next step, 300 µl of the CD3/CD19/CD56 Ab pre-coupled Dynabeads were added to the cells and incubated

on a rotator at 4°C for 30 min. Afterwards, X-VIVO medium was added up to 7 ml and the tube placed into a magnetic particle concentrator for 2 min. The supernatant without beads, that contained the purified dendritic cells, was carefully removed, transferred into a 15 ml tube, centrifuged, counted and immediately used for ELISPOT (7.2.10.) and regulatory T cell (Treg) specificity (7.2.11.) assays.

### 7.2.5. Pulsing of dendritic cells with peptides

Purified dendritic cells were used as antigen-presenting cells in ELISPOT (7.2.10.) and Treg specificity (7.2.11.) assays. For the ELISPOT assay, $1x10^4$ dendritic cells per well were used. They were resuspended in 30 µl X-VIVO medium and directly added to the pre-treated ELISPOT plate. To avoid drying of the plate, already 20 µl X-VIVO medium were provided. To reach a final peptide concentration of 20 µg per $1x10^4$ dendritic cells in 100 µl medium (0.2 µg/µl) per well, polypeptides in a concentration of 20 µg in 50 µl X-VIVO medium were added. To guarantee the functionality of the assay, as positive control, staphylococcal enterotoxin B (SEB) as super antigen, was used in a concentration of 10 µg per $1x10^4$ dendritic cells in 100 µl X-VIVO medium (0.1 µg/µl). Dendritic cells in the presence of peptides were pulsed at 37°C for 18 h, before the T cells were added.

For the Treg specificity assay, $5x10^3$ dendritic cells in 50 µl X-VIVO medium were used per well (96 well round-bottom plate, TPP). Polypeptides in a concentration of 20 µg in 50 µl X-VIVO medium were added (final peptide concentration per well 0.2 µg/µl). The dendritic cells were pulsed with peptides at 37°C for 18 h, before the Treg were added.

### 7.2.6. Pulsing of T2 cells with peptides

To receive a peptide-dependent antigen-specific activation of T cells, TAP-deficient T2 cells were used as antigen-presenting cells, to present HLA-A2-restricted short peptides to TCR transgenic T cells. T2 cells ($1x10^6$) were resuspended in 90 µl growth medium and transferred to a 96 well round-bottom plate (Falcon). To gain a final peptide concentration of 100 µM, 10 µl diluted peptides were added to the cells and incubated at 37°C for 2 h. The peptide-loaded T2 cells were used as target cells in a $^{51}Cr$ release cytotoxicity assay (7.2.12.) and as irradiated antigen-presenting cells (7.1.4.) for the antigen-specific expansion of TCR transgenic T cells (7.3.9.).

### 7.2.7. Isolation of $CD3^+$ T cells from human PBMC

Human $CD3^+$ T cells were purified from PBMC using the “Dynal T cell negative isolation kit” or the “Dynabeads untouched human T cell kit”, according to the manufacturer´s recommendations. These kits deplete B cells, NK cells, monocytes, platelets, dendritic cells, granulocytes and erythrocytes. The purified T cells are bead- and Ab-free. Finally, the negatively isolated T cells were centrifuged, counted and used for ELISPOT (7.2.10.), Treg specificity (7.2.11.) or $^{51}Cr$ release cytotoxicity (7.2.12.) assays.

### 7.2.8. Isolation of $CD4^+CD25^+$ Treg

$CD4^+CD25^+$ Treg were purified from $CD3^+$ T cells using the "$CD4^+CD25^+$ regulatory T cell isolation kit" according to the manufacturer`s protocols. The protocol is a two-step procedure, thereby, in the first step $CD4^+$ T cells were negatively isolated using a T cell Biotin-Ab cocktail and anti-biotin MicroBeads that bind CD8, CD14, CD16, CD19, CD36, CD56, CD123, TCRγ/δ and CD235a positive cells. In the second step, $CD4^+CD25^+$ Treg were positively selected from $CD4^+$ pre-enriched cells using CD25 MicroBeads. The $CD4^+CD25^+$ Treg were used for Treg specificity assays (7.2.11.) and flow cytometry analyses (7.2.13.). The Treg-depleted remaining cells were also used for further investigations including ELISPOT (7.2.10.) and Treg specificity (7.2.11.) assays. Therefore, the eluted magnetic labeled $CD4^-$ cell fraction (mainly $CD8^+$ cells), received during the first protocol step, were recombined with the "flow-through fraction" (cell fraction, not retained in the magnetic field) of $CD4^+CD25^-$ cells from the second protocol step. The $CD8^+$ and $CD4^+CD25^-$ T cells were termed "T cells without Treg".

### 7.2.9. Isolation of $CD4^+$ and $CD8^+$ T cells

$CD4^+$ T cells were purified from $CD3^+$ T cells using "CD4 MicroBeads" according to the manufacturer`s recommendations. The unlabeled cells obtained from the flow-through fraction (for definition see 7.2.8.) were $CD8^+$. $CD4^+$ and $CD8^+$ T cells were used for ELISPOT assay (7.2.10.). For NDV modification experiments (7.3.12.), $CD4^+$ and $CD8^+$ T cell populations were directly isolated from PBMC using the "Dynal $CD4^+$ and $CD8^+$ isolation kits", respectively.

### 7.2.10. Enzyme-linked immunospot assay

The enzyme-linked immunospot also referred as ELISPOT assay is a sensitive single cell assay that allows the analysis of immune responses by counting the number of cytokine-producing, activated antigen-specific T cells in cell material, like PB. Moreover, it provides informations about the frequency of the *ex vivo* analyzed antigen-specific T cell immunity. During the T cell activation cytokines, like interferon γ (IFNγ), are secreted that can be detected in the ELISPOT assay using mAbs. Each spot that develops during the assay represents a single reactive cell. The principle of the IFNγ ELISPOT assay is shown in Fig. 12.

To remove all added cytokines from the medium, 1 d before the purification of dendritic cells and T cells, the medium of both parallel cell cultures was completely removed, centrifuged and the cells resuspended in X-VIVO medium (without cytokines). MultiScreen-HA 96-well ELISPOT plates with a 0.45 µm pore size mixed cellulose esters membrane (mixture of cellulose acetate and cellulose nitrate), were coated with mouse anti-human INFγ mAb (1 µg/100 µl PBS per well) and incubated overnight at 4°C. The supernatant was discarded and the plate washed 3x with 200 µl ELISPOT washing buffer followed by 2 washes with 200 µl PBS per well using a multichannel pipette. To block unspecific binding, the plate was incubated with ELISPOT 10 % AB serum blocking buffer at 37°C for 2 h. Afterwards, the plate was washed 2x with ELISPOT washing buffer

and 2x with PBS, followed by an incubation with ELISPOT 6 % AB serum blocking buffer at 37°C for 30 min. The blocking solution was removed and the plate washed 3x using X-VIVO medium. Then 100 µl X-VIVO medium was added per well to the freshly prepared, Ab coated, washed and blocked ELISPOT plate. The plate was placed to 37°C and prior addition of dendritic cells, the medium was discarded and immediately 20 µl X-VIVO medium added per well to avoid drying of the membrane.

Purified dendritic cells ($1x10^4$ in 30 µl X-VIVO medium; 7.2.4.) were transferred to the prepared ELISPOT plate. During the next step, dendritic cells were pulsed with polypeptides (final peptide concentration per well: 20 µg peptide / $1x10^4$ dendritic cells / 100 µl medium) in the ELISPOT plate (7.2.10.) and incubated at 37°C for 18 h. To assess the background T cell reactivity against endogenous human proteins, human IgG (Endobulin) was used as a control for the tumor-associated antigens (TAAs). To guarantee the functionality of the ELISPOT assay, as positive control, the super antigen SEB was used. Additionally, mono-cultures of unpulsed dendritic cells and T cells served as negative controls. Moreover, each individual setting was tested in triplicates. After peptide-pulsing of dendritic cells overnight, T cells ($5x10^4$ T cells / 100 µl X-VIVO medium / well) were added to the ELISPOT assay at a dendritic cell:T cell ratio of 1:5. Following different T cell subsets were used for the assay:

- $CD3^+$ T cells, termed as “T cells with Treg” (7.2.7.)
- $CD8^+$ and $CD4^+CD25^-$ T cells, termed as “T cells without Treg” (7.2.8.)
- $CD4^+$ T cells (7.2.9.)
- $CD8^+$ T cells (7.2.9.)

The total volume of the ELISPOT assay after dendritic cell, peptide and T cell application was 200 µl / well and assay was incubated at 37°C and 5 % $CO_2$ for 40 h. Afterwards, the plate was washed 4x with 200 µl ELISPOT washing buffer. Remaining cells were lysed, adding 200 µl $ddH_2O$ to each well, followed by further 3 washing steps with ELISPOT washing buffer and 3x with PBS. A biotin-conjugated mouse anti-human INFγ mAb (0.1 µg/100 µl PBS per well) was added and incubated at 37°C for 2 h. This mAb recognize an INFγ epitope that differs from the epitope, recognized by the coating INFγ Ab. During the next steps, the plate was washed 4x with ELISPOT washing buffer and 3x with PBS before 100 µl streptavidin-alkaline phosphatase (1:1000 dilution in PBS) was added and incubated at 37°C for 1.5 h. Afterwards, the plate was washed 5x with ELISPOT washing buffer and 3x with PBS. The membrane-bound INFγ was finally visualized using the “alkaline phosphatase conjugate substrate kit”. A color development reagent containing 5-bromo-4-chloro-3-indoyl phosphate (BCIP) and nitroblue tetrazolium (NBT) yields purple spots at the sides of the antigen-Ab-complexes on the white background. The color reaction was stopped by washing the plate 3x with $ddH_2O$, followed by an incubation with $ddH_2O$ at RT for 10 min. Finally, the supernatant was completely discarded, the bottom of the ELISPOT plate removed and the membrane wrapped in tissue papers and dried for 3 d in the dark. IFNγ spots were automatically quantified using the Axioplan 2 imaging microscope (KS-ELISPOT software) or the CTL ImmunoSpot analyzer (CTL ImmunoSpot software).

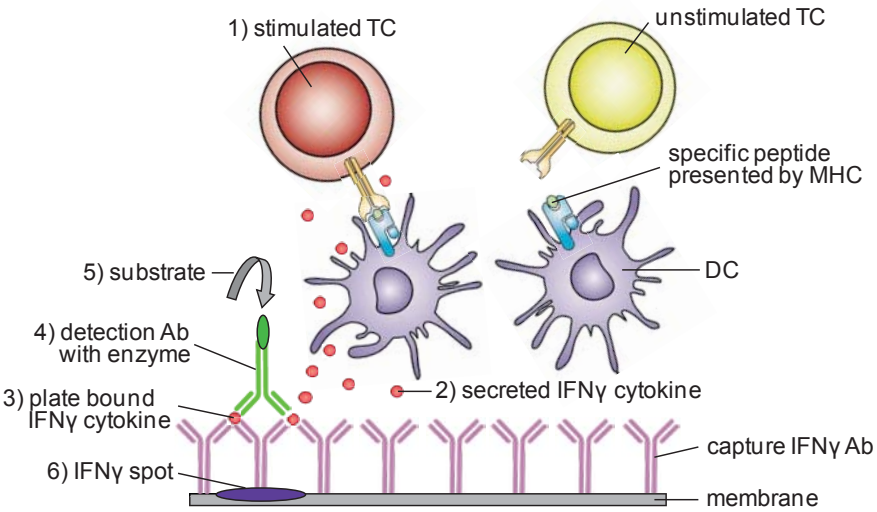


**Figure 12. Scheme of the IFNγ ELISPOT assay.** Autologous dendritic cells (DC) were pulsed with specific 50aa polypeptides or human IgG as control. Autologous TAA-reactive T cells (TC) that were able to respond to the specific presented peptides got stimulated (**1**) and secreted cytokines like IFNγ (**2**). The secreted IFNγ cytokines bound to IFNγ capture Abs on the ELISPOT membrane (**3**). The cytokine-Ab complexes were detected through a biotinylated IFNγ Ab, followed by the incubation with alkaline-phosphatase conjugated streptavidin (**4**). After the addition of substrate (**5**), a colored precipitate formed and appeared as purple spots at the sites of antigen-Ab-complexes on the ELISPOT membrane (**6**). For the generation of the figure, illustrations of cells were used from the *Nature Reviews* journal.

### 7.2.11. Treg specificity assay - [$^3$H] -Thymidine uptake assay

The Treg specificity assay analyzes the suppression of polyclonally activated T cell proliferation by antigen-specific Treg that had been stimulated via antigen-pulsed autologous dendritic cells. The T cell proliferation was detected by an incorporation of [$^3$H]-Thymidine into the nucleic acid of proliferating cells. The more proliferation had occurred in an investigated well, the more [$^3$H]-Thymidine had been incorporated into nucleic acid and could be detected using a liquid scintillation counter. The principle of the Treg specificity assay is shown in Fig. 13.

The enriched dendritic cells ($5x10^3$ in 50 µl X-VIVO medium; 7.2.4.) were transferred into 96 well round-bottom plates (TPP) and polypeptides in a concentration of 20 µg in 50 µl X-VIVO medium were added (final peptide concentration: 20 µg peptide / $5x10^3$ dendritic cells / 100 µl medium) and incubated at 37°C for 18 h. As a control for the TAAs, human IgG was used. Afterwards, $2.5x10^4$ Treg in 50 µl X-VIVO medium (7.2.8.) were added to peptide-pulsed dendritic cells and incubated overnight. Finally, $2.5x10^4$ polyclonally activated $CD8^+$ and $CD4^+CD25^-$ T cells ("T cells without Treg"; 7.2.8.) were transferred in 50 µl X-VIVO medium to the peptide-pulsed dendritic cells and Treg and incubated at 37°C for another 72 h.

Beforehand, $CD8^+$ and $CD4^+CD25^-$ T cells ($1x10^6$ cells / 2 ml X-VIVO medium per well) had been polyclonally activated using a mouse anti-human CD3 mAb (1 µg/ml PBS per well) pre-coated 12 well plate (Falcon) at 37°C for 14 h. The plate was pre-coated with the Ab overnight at 4°C. Afterwards, the Ab was removed and the plate carefully washed 3x with PBS, to remove the unbound Ab, before the T cells were added. After activation, the T cells were removed from the

coated plate, centrifuged (14000 rpm, 10 min, RT), washed 1x with PBS, resuspended in X-VIVO medium, counted and finally applied to the Treg specificity assay (described above). The final volume was 200 µl per well and for each setting a triplicate was analyzed. As controls, unpulsed dendritic cells were cultured with Treg and polyclonally activated T cells. Furthermore, a co-culture of dendritic cells and polyclonally activated T cells in the absence of Treg and a dendritic cells mono-culture was investigated. After cultivation for 72 h, 1 µCi [$^3$H]-Thymidine was added per well and incubated at 37°C for further 24 h. Afterwards, in order to promote complete cell lysis, the plate was frozen at -20°C and thawed 2x at 37°C. Following, the cells were harvested and nucleic acid was captured on a filter membrane. The membrane displayed spots of bound nucleic acids, comprising distinct quantities of incorporated [$^3$H]-Thymidine. Then, the membrane was dried in a microwave at 600 W for 2 min and transferred into a plastic membrane bag. Scintillation fluid (5 ml) was added and the plastic bag sealed. The extent of cell proliferation was measured with a liquid scintillation counter, quantifying the amount of β-radiation on the filter membrane.

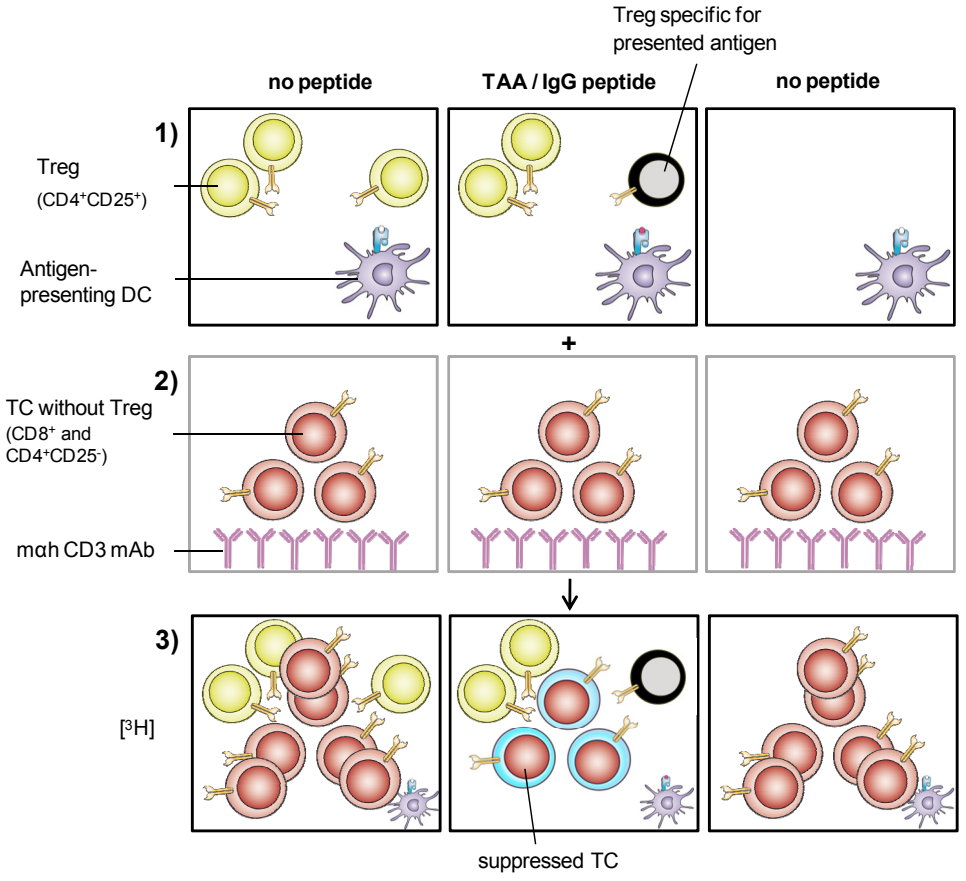


**Figure 13. The principle of the Treg specificity assay. 1**) For the determination of Treg specificity, dendritic cells (DC) were pulsed with 50aa TAA polypeptides or human IgG. As control unpulsed DC were investigated (no peptide). Autologous Treg were added. Treg specific for an antigen, presented by DC, were selectively activated (black compared to yellow Treg cells). **2**) Polyclonally (αCD3 mAb) activated effector T cells without Treg (TC) were transferred to the Treg and peptide-pulsed DC co-culture. **3**) Specifically activated Treg, suppressed the proliferation of effector T cells, measured by [$^3$H]-Thymidin incorporation (turquoise compared to red effector T cells). As control, the proliferation of polyclonally activated effector T cells, without Treg addition was investigated. For the generation of the figure, illustrations of cells were used from the *Nature Reviews* journal.

### 7.2.12. $^{51}$Cr release cytotoxicity assay

The method to analyze cell-dependent cytotoxicity is based on the release of radioactive $^{51}$Cr from dead cells. As target cells, peptide-loaded T2 cells (7.2.6.) or cells from cancer lines including MeWo and KS WT were used. Therefore, dependent on the experiment, 1-5x$10^6$ cells were resuspended in 100 µl growth medium in 5 ml tubes and labeled with 100 µCi radioactive $^{51}$Cr at 37°C for 1.5 h. Thereby, the $^{51}$Cr enters the membrane of the cells, and binds covalently to proteins and accumulates within the cytoplasm of the cells. The used volume of $^{51}$Cr per 5 ml tube depends on the age of the $^{51}$Cr, as indicated below:

- 1$^{st}$ week: 100 µl $^{51}$Cr
- 2$^{nd}$ week: 125 µl $^{51}$Cr
- 3$^{rd}$ week: 150 µl $^{51}$Cr

After 45 min of incubation, the cells were gently shacked. The labeled target cells were washed 3x with the appropriate growth medium to remove the unbound $^{51}$Cr. Then, the cells were counted, resuspended to a final concentration of 3x$10^4$ cells/ml and 100 µl of $^{51}$Cr labeled target cells were co-cultured with cytotoxic effector T cells at 37°C for 4 h.

Beforehand, in parallel, effector T cells had to be transferred to 96 well round-bottom plates (Falcon). Serial T cell dilutions (100:1, 50:1, 25:1, 12.5:1, 6.25:1, 3.125:1, 1.56:1, 0.78:1, 0.39:1) were analyzed in triplicates with a maximum T cell concentration of 3x$10^5$ cells in 100 µl medium (100 effector T cells:1 target cell). The total volume of the assay was 200 µl. As negative control, the spontaneous release of the $^{51}$Cr by the target cells was analyzed using $^{51}$Cr-labeled target cells without effector cells. Moreover, the maximum release of the $^{51}$Cr by the target cells was achieved using $^{51}$Cr-labeled target cells together with 100 µl of 10 % Triton X-100, as detergent, in the appropriate growth medium. The plates were centrifuged (500 rpm, 3 min, RT) and incubated at 37°C for 4 h. Afterwards, the plates were centrifuged again (1000 rpm, 3 min, RT) without the centrifuge brake and 100 µl of the supernatants carefully removed and transferred to polystyrene tubes (0.6 ml). The tubes were sealed with melted paraffin wax pellets and the radioactivity measured in the culture supernatant using the Packard COBRA γ-counter. The higher the amount of $^{51}$Cr released into the culture supernatant (% specific lysis) was, the more target cells have specifically been killed by the effector T cells. The following formula was used to calculate the specific cytotoxicity:

$$\begin{matrix}\text{percent specific lysis} \\ \text{(cpm, counts per min)}\end{matrix} = \left[\frac{(\text{experimental cpm} - \text{spontaneous release cpm})}{(\text{maximum release cpm} - \text{spontaneous release cpm})}\right] \times 100$$

### 7.2.13. Flow cytometry

Flow cytometry or fluorescence activated cell sorting (FACS) is a method that can be used to discriminate cells based to their size, structure, cell surface properties and cellular internal composition. To analyze cells via FACS, they must be labeled with Abs specific for certain cellular

structures. The staining can either be a “direct labeling” using primary Abs linked to fluorescent dyes or an “indirect labeling” using an unlabeled primary Ab followed by a fluorescent-dye labeled secondary Ab. For the investigation of the phenotype of primary cells and cells of permanent culture lines, surface/extracellular and intracellular/intranuclear stainings were performed. In general, all staining procedures were conducted on ice, while protecting the cells from light.

#### 7.2.13.1. Surface/extracellular staining

The immunophenotype and activation status of different cell populations were investigated. Thus, single cell suspensions were produced, counted and defined cell numbers (1-5x$10^5$ cells) transferred into polypropylene tubes (1.3 ml). The cells were then washed with 600 µl FACS buffer using a table centrifuge and the supernatants discarded. Subsequently, cell surface Fc-receptors were blocked, performing an incubation step in 5 % Endobulin in a volume of 50 µl on ice for 15 min. The cells were again washed in FACS buffer and the pellet resuspended in 50 µl of the primary Ab and incubated for 30 min. Unbound Abs were removed, by a washing step with FACS buffer and the pellet was either resuspended in 200 µl FACS buffer (if the primary Ab was direct-fluorochrome labeled) or in 50 µl of a secondary fluorescent-dye labeled Ab. In the latter case, to allow the Ab binding, again incubated for further 30 min, followed by a washing step in FACS buffer and finally also resuspended in 200 µl FACS buffer. Subsequently, the cells were analyzed on a FACScan, FACS Calibur or FACS Canto II flow cytometer using CellQuest Pro and FACS Diva software, respectively. In general, at least 20 000 events were recorded. As control stainings, single stainings of each Ab and unstained cells were investigated.

#### 7.2.13.2. Intracellular/intranuclear staining

In order to stain for regulatory T cells, after a surface/extracellular staining, an intranuclear staining for Foxp3 was added. Therefore, the cells were fixed in 200 µl fixation/permeabilization buffer (eBioscience) on ice for 30 min, centrifuged and permeabilized with 500 µl permeabilization buffer (eBioscience) for 20 min. Afterwards, the cells were centrifuged and blocked in 2 % normal rat serum in a volume of 50 µl for 15 min, followed by the addition of 50 µl Foxp3 Ab, diluted in permeabilization buffer (1:5 dilution). Finally, a washing step with permeabilization buffer was performed, the cells resuspended in 100 µl FACS buffer and analyzed on a FACS Canto II flow cytometer (in general, 50 000 events were recorded).

#### 7.2.13.3. Multimer/tetramer staining

Multimers, of peptide/major histocompatibility complex (MHC) linked with fluorescent dyes, were used as TCR ligands to directly identify and quantify antigen-specific T cells that express a specific TCR on their surface. Based on the receptor specificity, fluorochrome-labeled MHC-peptide tetramers are bound by TCRs on T cells and can be detected and counted using the FACS method. T cells, transduced with TCRs for glycoprotein 100 (gp100) or murine double minute 2

(MDM2; 7.3.9.) were phenotypically analyzed for their antigen-specific TCR expression using gp100 (280-288) and MDM2 (81-88) HLA-A2-restricted tetramers.

In general, a tetramer staining was combined with a staining of T cell surface markers. TCR transgenic T cells ($1x10^5$ cells) were washed with FACS buffer and blocked with 5 % Endobulin for 15 min (see also 7.2.13.1.). Following, the cells were washed and incubated with 0.5 µl tetramer in 50 µl FACS buffer (~4 µg/ml), protected from light at 4°C for 45 min. Then, the cells were washed, incubated with anti-CD8 or anti-CD4 fluorochrome-labeled Abs on ice for 30 min, washed again, centrifuged and the pellet was resuspended in 200 µl FACS buffer. Finally, the stained cells were analyzed on a FACS Calibur flow cytometer (at least 20 000 events were recorded).

#### 7.2.13.4. Detection of nonviable cells in the flow cytometry assay

In general, propidium iodide (PI), a fluorescent molecule that intercalates into double-stranded nucleic acids, is excluded from viable cells but can penetrate cell membranes of dying or dead cells and bind to deoxyribonucleic acid (DNA), resulting in a red fluorescent signal. Therefore, PI was used to exclude dead cells from FACS stained, non-fixed cell populations. The FACS staining was performed as described above (7.2.13.1.). Before starting the measurement on a flow cytometer, 50 µl PI (working stock 5 µg/ml diluted in PBS) were added to the stained cells, resuspended in 200 µl FACS buffer, and incubated for 1 min. The final PI concentration was 1.25 µg/ml.

For the exclusion of nonviable cells from the FACS assays, besides PI, a further nucleic acid dye, 7-aminoactinomycin D (7-AAD) was used. The advantage of 7-AAD is the ability to be used in conjunction with phycoerythrin (PE)- and fluorescein isothiocyanate (FITC)-labeled Abs, with minimal spectral overlap between the 7-AAD, PE and FITC fluorescence emissions. Therefore, before starting the FACS measurement, 5 µl 7-AAD (stock 50 µg/ml) were added to the stained cells, resuspended in 200 µl FACS buffer (final 7-AAD concentration 1.25 µg/ml) and incubated for 10 min.

#### 7.2.13.5. Cell separation by flow cytometry

In order to receive MCF-7 cells that express to a higher percentage CEACAM6, compared to MCF-7 parental cells, a FACS sort for CEACAM6-positive MCF-7 cells was performed. Therefore, single cell suspensions of MCF-7 cells were resuspended at $3x10^5$ cells / per tube. The staining was conducted as described for the surface/extracellular staining (7.2.13.1.), with the exception that the whole procedure was performed in 15 ml centrifuge tubes under sterile conditions in a cell culture hood. The cells were centrifuged (1200 rpm) at 4°C for 5 min. All solutions used, were sterile [FACS buffer, Endobulin, Abs, PI]. As primary Ab, mouse anti-human CEACAM6 Ab and as secondary fluorescent-dye labeled Ab, goat anti-mouse IgG-FITC were used. After the staining, the cells were filtered through a sterile 35 µm cell strainer cap into a 5 ml polystyrene round bottom tube. To label dead cells, prior to sorting, 50 µl PI solution was added to the 200 µl cell suspension. Using the Flow sorter Aria 2, $PI^-CEACAM6^+$ MCF-7 single cells were sorted into FCS-precoated

polystyrene tubes (5 ml) that contained 1 ml growth medium. The sterile cell sort was thankfully performed by Dr. S. Schmitt (Flow Cytometry Unit, DKFZ).

#### 7.2.13.6. Identification of HLA-A2$^+$ blood donors

PB cells of each donor were stained for their surface expression of HLA-A2 using flow cytometry (7.2.13.1.). Therefore, 70 µl of mouse anti-human HLA-A2 Abs and as secondary fluorochrome-labeled Abs, goat anti-mouse IgG-FITC were used. As a positive control, cells of HLA-A2$^+$ lines including T2, MeWo or MCF-7, were stained in parallel.

## 7.3. Molecular biological methods

### 7.3.1. Bradford protein assay

The Bradford protein assay is a method to determine the total protein concentration in a sample solution. Thereby, the absorbance maximum of the dye Coomassie brilliant blue shifts from 465 nm to 595 nm, as bindings to proteins occurs. The increase of absorbance at 595 nm can be used to measure the protein concentration in the solution. For the generation of a standard curve, standardized samples with known BSA concentrations (0.1-1.2 mg/ml) were used. Into a 96 well flat-bottom plate, 100 µl of the standard and the test samples were transferred in duplicates. Afterwards, 100 µl protein assay dye reagent concentrate (1:5 diluted in dd$H_2O$; Bio-Rad) was added to each well and the absorbance measured after 6 min using a plate reader. The protein concentration within the samples was calculated using the linear scale of the resulting standard curve.

### 7.3.2. Transformation of bacteria

Bacterial transformation is a method that enables bacteria to absorb exogenous DNA. Thereby, competent bacteria are used as bacteria that can be transformed naturally or via artificial modification (i.e., chemical methods or electroporation). As competent bacteria, the Escherichia coli (E. coli) strains “Library efficiency DH5α competent cells” and “One Shot TOP10 competent cells” were use and stored in aliquots at -80°C.

Plasmid DNA (10 ng) was transferred into sterile 14 ml polypropylene tubes with caps and placed on ice. As negative transformation control, a tube without plasmid DNA was used. Competent bacteria aliquots were thawed on ice and 100 µl bacteria were added to the plasmid DNA, immediately mixed and incubated on ice for 30 min, to allow the attachment of the DNA to the bacteria. For DNA uptake, a heat shock step at 42°C for 45 sec was performed, followed by incubation on ice for further 2 min. To recover from the heat shock, 900 µl sterile antibiotic-free super optimal broth medium with catabolite repression (S.O.C. medium) was added per tube and

then placed to 37°C in a bacteria incubator for 1 h. During this time the plasmid-encoded antibiotic resistance was accomplished.

Due to the low number of bacteria which contain the plasmid DNA, it was necessary to select for plasmid-containing bacteria, performing an antibiotic selection with ampicillin. In general, E. coli strains are sensitive to antibiotics like ampicillin. However, the plasmids used for transformation comprised ampicillin resistance genes. Thus, when the bacterial transformation is plated to medium containing ampicillin, only bacteria with plasmid DNA have the ability to metabolize ampicillin and form bacterial colonies. Therefore, during the next step, the bacteria transformation approach was plated to Luria Bertani (LB) Agarplates (pre-warmed at 37°C), containing ampicillin (final concentration 100 µg/ml). Different quantities (10 µl, 50 µl, 100 µl, 200 µl) were transferred to individual plates and the bacteria solution was streaked using an inoculation loop. The inoculation loop was sterilized in a flame between the individual plates and allowed to cool down. To absorb the inoculums, the plates were incubated for 5 min, then inverted and further incubated at 37°C overnight. In a final step, individual colonies were picked with a sterile pipette tip to inoculate "bacteria start cultures" for plasmid amplification (7.3.4.). The selection plates with transformed colonies of bacteria were finally closed with Petri-Seal and stored at 4°C.

### 7.3.3. Storage and recovery of bacteria strains

Frozen stocks of all transformed bacteria were produced. Therefore, 150 µl sterile glycerol was transferred to a cryogenic vial (2 ml) and 850 µl bacteria suspension was added, mixed, stored on ice for 30 min and finally transferred to -80°C for long term storage. For recovery, bacteria from frozen stocks were scraped using a sterile pipette tip and transferred to Erlenmeyer flasks containing LB medium and ampicillin. In order to prevent loss in cell viability, during this procedure the frozen stocks were not thawed.

### 7.3.4. Preparation of plasmid DNA from bacteria

"Bacteria start cultures" [5 ml LB medium containing ampicillin (100 µg/ml)] were inoculated with a single colony from a streaked selective bacterial LB plate or material from a frozen bacterial glycerol stock (7.3.3.). The cultures were incubated in 50 ml Erlenmeyer flasks and vigorously shaken at 37°C overnight. The next day, 1 ml of the culture was utilized to isolate plasmid DNA using the "QIAprep spin Miniprep kit" according to the manufacturer´s instructions. Before the Maxi DNA preparation (Maxi Prep) was performed, the accuracy of the plasmid Miniprep DNA was investigated via enzymatic digestion (7.3.7.).

For Maxi DNA preparation, 250 ml LB medium containing ampicillin (100 µg/ml) was inoculated with 500 µl of the bacteria start culture using 1000 ml Erlenmeyer flasks for incubation. The culture was vigorously shaken at 37°C overnight. The next day, the plasmid DNA was purified using the "Endofree plasmid Maxi kit" according to supplier´s instructions. Afterwards, the plasmid DNA was resuspended in endotoxin-free Tris-EDTA (TE) buffer (content of Qiagen kits), diluted 1:10 in

endotoxin-free Aqua ad iniectabilia. A photometer was used to measure the plasmid DNA concentration (7.3.5.). For the retroviral plasmids, the plasmid DNA was adjusted to a final concentration of 0.5 µg/µl. The firefly-luciferase plasmid DNA had a concentration of 1 µg/µl. Before the plasmid DNA was used for experiments, the accuracy of the DNA was analyzed by enzymatic digestion (7.3.7.) and sequencing (7.3.8.).

### 7.3.5. Determination of nucleic acid and protein concentration

The nucleic acid [DNA, total ribonucleic acid (RNA)] and the protein concentration were determined photometrically via measuring the absorbance. Nucleic acids absorb ultraviolet (UV) light with a wave length of 260 nm. Thereby, the optical density at 260 nm ($OD_{260}$) of 1.0 is equivalent with a DNA concentration of 50 µg/ml. In contrast, proteins absorb UV light with an absorption maximum at 280 nm. The optical density at 280 nm ($OD_{280}$) of 1.4 is equivalent with a protein concentration of 1 mg/ml. The ratio of the absorption at 260 and 280 nm ($A_{260/280}$) enables the estimation of a protein contamination in a DNA preparation and can therefore be used as a measure of the sample purity. The ratio should be in a range of 1.8-2.0. The absorption of DNA or protein was normalized against the respective diluents, i.e., Aqua ad iniectabilia, TE buffer or DMSO.

### 7.3.6. Agarose gel electrophoresis

Agarose gel electrophoresis is a method to determine the size of nucleic acid fragments. As DNA is negatively charged, it is forced to migrate through an agarose matrix in response to an electric current and runs from the negatively charged cathode towards the positively charged anode. Thereby, small fragments run faster than larger ones, at a rate proportional to their size. For electophoretic separation of DNA, 1 % agarose gels that can resolve DNA from 0.2-10 kilobase (kb) in length have been used. In some cases, 1.5 % agarose gels were used to separate smaller fragments more precisely.

The agarose was dissolved in 1X Tris-acetate-EDTA (TAE) buffer using a microwave and allowed to cool. Ethidium bromide (stock concentration 10 mg/ml), an UV-fluorescent dye was used for DNA visualization. It was directly added to the melted agarose solution (final concentration 0.2 µg/ml) and gently poured into a gel tray. The gel was allowed to harden and the combs were removed. As running buffer, 1X TAE was added to the electrophoresis chamber and the gel covered with buffer. The gel was then loaded with sample volumes of 5-10 µl resuspended in 6X loading dye solution (10 µl restriction digest, 5 µl polymerase chain reaction (PCR) product, 0.5 µl pure DNA; mixed with 1-2 µl loading dye solution, if required adjusted with Aqua ad iniectabilia). Following DNA molecular weight standard ladders were used: “Low molecular weight ladder”: 25-766 base pairs (bps), “100 bp ladder”: 0.1-1.5 kb, “1 kb ladder”: 0.5-10 kb and “GeneRuler”: 0.1-10 kb. The gel chamber was attached to the electrodes and constant voltages were applied (~80-110 volts for 30-50 min, depending on the gel size). Finally, the gels were examined using an UV gel documentation system.

### 7.3.7. Enzymatic restriction digest of plasmid DNA

The enzymatic digestion of plasmid DNA using restriction enzymes, the restriction endonucleases, is a process of cutting DNA into smaller pieces. Restriction endonucleases recognize specific palindromic sequences and cleave a phosphodiester bond on each strand at the appropriate specific DNA sequence. After digestion with restriction endonucleases, the resulting DNA fragments can be separated by agarose gel electrophoresis (7.3.6.) and their size can be estimated. For optimum activity, each restriction enzyme required specific reaction conditions.

The following procedure of a restriction digestion was generally performed. Thereby, the plasmid DNA (0.5-1 µg) was transferred to safe-look tubes (1.5 ml) and a mixture, containing restriction enzymes and buffers was added (Tab. 1), carefully mixed and incubated at 37°C for 1 h., To prevent nonspecific degradation of the DNA, the tubes were afterwards placed on ice. Finally, to separate the digested fragments, an agarose gel electrophoresis (7.3.6.) was performed. In Fig. 14 a representative gel of an enzymatic restriction digest is shown.

| Constituents | Volume per single reaction |
|---|---|
| plasmid DNA | 0.5 - 1 µg |
| 10X NEB reaction buffer | 2 µl |
| 100X BSA* | 0.2 µl |
| Restriction enzyme | 1 µl |
| Aqua ad iniectabilia | add to 20 µl |

**Table 1. Solutions for the restriction digestion of plasmid DNA.** * BSA was used if required.

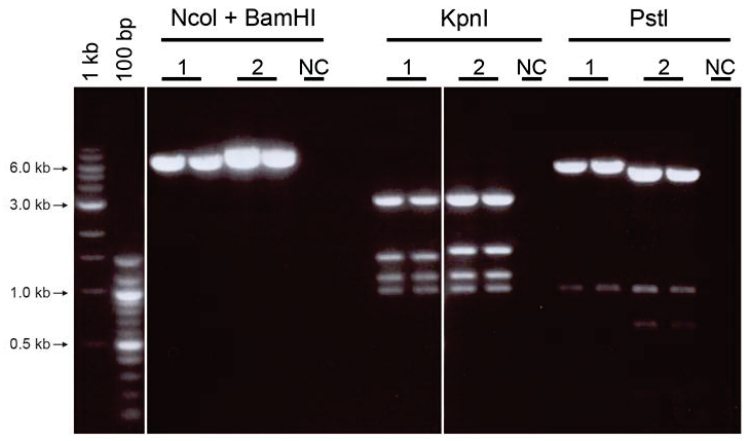


**Figure 14. Representative 1 % agarose gel of an enzymatic restriction digest.** Using the enzymes NcoI, BamHI, KpnI and PstI, a restriction digest of plasmid DNA (**1**) pBullet_IRESpuro-[NcoI] and (**2**) pBullet_IRESneo-[NcoI] was performed and evaluated on an agarose gel. Instead of plasmid DNA, Aqua ad iniectabilia was used for the digest as negative control (**NC**). Since the expected fragments sizes were detected, the plasmids had the correct structure [**NcoI + BamHI**: 7073 bps (**1**) / 7168 bps (**2**); **KpnI**: 3342, 1530, 1013, 1200 bps (**1**) / 3341, 1633, 1006, 1200 bps (**2**); **PstI**: 5881, 1022 bps (**1**) / 5151, 1015, 635 bps (**2**)]. As size markers 100 bp and 1 kb DNA ladders were used.

### 7.3.8. Sequencing

Before the plasmid DNA (7.3.4.) was used for experiments, the sequence accuracy was analyzed by sequencing. Thereby, the nucleotide order of a DNA fragment was analyzed. “Single read sequencing” was performed by GATC Biotech (Konstanz, Germany) using a DNA concentration of 30-70 ng/µl. All sequence specific primers were used at a concentration of 10 pmol/µl.

### 7.3.9. Production of TCR transgenic human T cells

To obtain high affine mono-specific tumor antigen-reactive TCR transgenic T cells, recognizing specific melanoma antigens, human T cells were genetically modified by TCR gene transfer. TCR transgenic T cells could be received, while performing a retroviral transduction of T cells using retrovirus-containing supernatants of transfected Phoenix ampho cells.

#### 7.3.9.1. Transfection of the packaging cell line Phoenix ampho

The cell line Phoenix ampho is an amphotropic system that allows the delivery of genes to dividing cells of most mammalian species, including human cells. Thereby, it can be used for moloney murine leukemia virus (MoMuLV)-derived retrovirus production. The cell line is based on the human embryonic kidney line 293T and has stable integrated expression vectors for retroviral group-specific antigen (gag), retroviral reverse transcriptase polymerase (pol) and amphotropic virus envelope (env) proteins (see also Pear et al., 1997; Swift et al., 2001).

In order to receive Phoenix cells that produce high virus titers, a drug selection of the cells had to be performed before they were used for transfection. The selection was achieved with plasmocin (25 µg/ml) and hygromycin B (312.5 µg/ml) for 6 d. Moreover, plasmocin (25 µg/ml) and diphteria toxin (1 µg/ml) were added from d7 until d14. To maintain and not to reduce the transfection efficiency, during the whole cultivation process, the cells did never reach a higher confluence than ~70 % before they were passaged. Afterwards, the cells were cultured in normal growth medium for one week and multiple aliquots of drug-selected Phoenix ampho cells ($3x10^6$ cells/cryogenic vial) were frozen until used for following transfection experiments.

For starting a retroviral transfection, the drug-selected Phoenix ampho cells were thawed and cultured in growth medium in T75 flasks for 3 d. Subsequently, $1.5x10^6$ cells per flask were plated in 15 ml medium and cultured at 37°C, 5 % $CO_2$. Thereby, one flask for each individual transfection approach was prepared. The medium was completely removed 1 d later, 10 ml fresh growth medium added, and the cells incubated at 37°C for at least 4 h before the transfection was performed. In general, Phoenix cells were transfected with two retroviral pBullet plasmids at the same time. One vector that carried the genes for the TCR α chain (puromycin resistance) and one vector containing genes for the TCR β chain (neomycin resistance). In addition, the Phoenix cells were co-transfected with the helper plasmids pHIT60 (coding for viral gag and pol proteins) and pCOLT-GALV (coding for viral env proteins). As control, cells were transfected with empty retroviral plasmids (mock) without genes for TCR α or TCR β. Furthermore, an enhanced green fluorescent

protein (EGFP) transfection was conducted using the pBullet_eGFP_IRESneo vector together with the empty pBullet_IRESpuro vector. The solutions, used for the transfection (indicated in Tabs. 2 and 3) were prepared in safe-lock tubes (1.5 ml, Biopur) and the final transfection mixture incubated at RT for 20 min. Thereafter, the content of one reaction tube was dropwise added to each Phoenix cell culture flask and placed back into the incubator. The next day, the medium of the transfected Phoenix cells was removed and fresh phosphate- and cytokine-free T cell TCR medium (8.5 ml) added and the cells again incubated at 37°C overnight. On the following day, the transduction of T cells was performed using the retroviral-containing Phoenix cells supernatant (7.3.9.3.). The transfection efficiency of Phoenix cells, transfected with the pBullet-eGFP plasmid, was analyzed via flow cytometry for EGFP staining. Before analysis, the EGFP transfected Phoenix cells were fixed in 1 % formaldehyde fixation buffer at RT for 20 min. Thereby, the revealed EGFP transfection efficiency was always ~99%.

| Constituents | Volume per single reaction |
|---|---|
| pCOLT-GALV (0.5 µg/µl) | 4 µl (2 µg) |
| pHIT60 (0.5 µg/µl) | 13 µl (6.5 µg) |

**Table 2. pCOLT-GALV/pHIT60 plasmid mixture.** The plasmids were purified using the "Endofree plasmid Maxi kit". The plasmid mixture was used for transfection of Phoenix ampho cells (Tab. 3).

| Constituents | Volume per single reaction |
|---|---|
| DMEM without supplements | 900 µl |
| TransIT-LT1 transfection reagent | 60 µl |
| pCOLT-GALV/pHIT60 mixture (Tab. 2) | 17 µl |
| pBullet_IRESpuro - TCR α genes (0.5 µg/µl) | 11.5 µl (5.75 µg) |
| pBullet_IRESneo - TCR β genes (0.5 µg/µl) | 11.5 µl (5.75 µg) |

**Table 3. Solutions for the transfection of Phoenix ampho cells.** The transfection of Phoenix cells was performed using the TransIT-LT1 transfection reagent in Dulbecco's modified Eagle's medium (DMEM) without supplements (PAA).

#### 7.3.9.2. *Coating of cell culture plates with Retronectin*

Retronectin is the recombinant human fibronectin fragment CH-296 that was pre-coated to culture plates (12 well, Falcon). It enhances retroviral mediated gene transduction by co-localizing integrin receptor [very late antigen 4 and 5 (VLA-4, VLA-5)]-positive target cells and virions on the fibronectin fragments. The plates were coated with 1 ml retronectin per well (final concentration 50 µg/ml in PBS) and incubated at 4°C overnight. The Retronectin solution was removed, the wells blocked with 1 ml 2 % BSA (fraction V) in PBS at RT for 30 min followed by a washing step with PBS. Human T cells that should be transduced with retroviral vectors can now be added to the Retronection pre-coated plate (7.3.9.3.).

#### 7.3.9.3. Retroviral transduction of human T cells

Human PBMC from healthy donors (7.2.3.) were thawed, resuspended in phosphate-free T cell TCR medium with cytokines at a concentration of $2x10^6$ cells/ml and transferred to 24 well plates (Falcon). Thereby, a volume of 2 ml/well was used and the medium supplemented with the human cytokines rIL-2, rIL-4, rIL-7 and rIL-15. For T cell activation, the mouse anti-human CD3 mAb (clone Okt3; 20 ng/ml) was added to the medium, and the cells incubated at 37°C for 2 d. Afterwards, pre-activated T cells were centrifuged, counted in Trypan blue, resuspended in phosphate- and cytokine-free T cell TCR medium ($5x10^6$ T cells/500 µl) and transferred to Retronectin pre-coated 12 well plates (7.3.9.2.).

In order to transduce human T cells, supernatants of Phoenix cells, transfected 2 d before with retroviral pBullet plasmids (7.3.9.1.), were used. Therefore, the Phoenix cell supernatants, of each individual transfection approach, were removed and transferred to 15 ml tubes. Immediately, 8.5 ml phosphate- and cytokine-free T cell TCR medium was carefully added to the Phoenix cells and the flasks placed back to 37°C and incubated again overnight. To remove Phoenix cells that may have been transferred to the supernatants, the virus-containing supernatants were centrifuged (1000 rpm, 3 min, RT). Afterwards, 8 ml were carefully removed and transferred to new 15 ml tubes. In the next step, the viral supernatants (4 ml/well) were added together with polybrene (4 µg/ml) and rIL-2 (100 U/ml) to the pre-plated T cells. The content of all wells was carefully mixed using a 1 ml pipette tip, the plates centrifuged (3000 rpm, 60 min, 30°C) without the centrifuge brake and incubated at 37°C overnight. In general, T cells of two different donors were transduced in parallel.

The next day, a second transduction cycle was performed. Therefore, from each well of the 12 well plates, 3.5 ml supernatant were carefully removed and discarded. Fresh virus-containing supernatants of Phoenix cells were prepared (as the day before) and added in a volume of 3.5 ml/well, supplemented with polybrene and rIL-2. The plates were again centrifuged without the centrifuge brake and incubated at 37°C for at least 4 h. After incubation, the T cells were removed from the 12 well plates and the second transduction cycle was completed. Therefore, the T cells were centrifuged (1500 rpm, 5 min, RT) and the supernatant discarded. Afterwards, cells were washed with T cell TCR medium and counted. Finally, T cells were resuspended to a concentration of $0.5x10^6$ cells/ml in phosphate-free T cell TCR medium supplemented with cytokines and Dynabeads CD3/CD28 T cell expander (12.5 µl beads/$1x10^6$ cells; 0.5 beads:1 T cell). In general, 3 d after completed transduction, TCR transgenic T cells could be selected (7.3.9.4.).

#### 7.3.9.4. Drug selection of retrovirally transduced human T cells

In order to receive only T cells that were efficiently transduced with both exogenous TCR chains, a drug selection was performed for one week. To select for the TCR β chain, Geneticin sulfate (G-418) and for the TCR α chain puromycin were used. The transduced T cells were adjusted to a concentration of $0.5x10^6$ cells/ml in phosphate-free T cell TCR medium containing cytokines, and G-418 (final concentration 0.8 mg/ml) was added for 7 d. After 6 d, additionally puromycin (final

concentration 5 µg/ml) was added for 1 d. In order to complete the drug selection, the cells were centrifuged. Beforehand, the CD3/CD28 T cell expander beads were removed in the magnetic field of a magnetic particle concentrator. Subsequently, the cells were counted, resuspended to a concentration of $0.5x10^6$ cells/ml in phosphate-free T cell TCR medium containing cytokines and cultured at 37°C. In order to increase the number of the genetically engineered T cells, the cells were expanded as described in 7.3.9.5..

#### 7.3.9.5. Expansion of retrovirally transduced human T cells

After the G-418/puromycin drug selection (7.3.9.4.), the TCR transduced T cells were expanded either polyclonally using CD3/CD28 T cell expander beads or antigen-specifically using irradiated peptide-loaded T2 cells and irradiated PBMC feeder cells. Thereby, during the whole cultivation time, the medium was partially renewed if necessary and cells were expanded in volume to larger cell culture plates or flasks.

For polyclonal expansion, T cells adjusted to a concentration of $0.5x10^6$ cells/ml were treated with CD3/CD28 T cell expander beads (12.5 µl beads / $1x10^6$ cells; 0.5 beads:1 T cell). The beads were left in culture for approximately two weeks.

For antigen-specific expansion, 1 ml of T cells, adjusted to a concentration of $0.5x10^6$ cells/ml, were transferred to 24 well plates (Falcon). As antigen-presenting cells, irradiated T2 cells, loaded with HLA-A2-restricted short peptides, were added per well ($2x10^5$ / 500 µl). In addition, irradiated PBMC, as feeder cells were used ($2x10^6$ / 500 µl per well). Thereby, the irradiation of the cells was performed as described in 7.1.4., and irradiated cells were centrifuged, counted and resuspended in fresh phosphate-free T cell TCR medium containing cytokines, before they were transferred to the pre-plated T cells. The wells were carefully mixed using a 1 ml pipette tip and incubated at 37°C. In general, between d7-d10 a re-stimulation was carried out using the same protocol as described for the primary stimulation.

#### 7.3.9.6. Specificity of retrovirally transduced human T cells

Before TCR transduced T cells were used for animal experiments (7.4.3.), there specificity was controlled. Therefore, the expression of the variable (V) β chain of the TCR was analyzed performing a flow cytometry surface staining (7.2.13.1.). Thereby, for the gp100 $V_\beta$ staining (mouse anti-human $V_\beta$ 14-PE mAb, clone CAS1.1.3), the protocol was performed exceptional at RT for 30 min. Furthermore, in order to analyze the preferential TCR chain pairing, a tetramer staining (7.2.13.3.) was conducted. In addition, the cytolytic function of the transduced T cells was examined by $^{51}Cr$ release cytotoxicity assay (7.2.12.) using peptide-loaded T2 cells or cells of cancer lines including MeWo and KS WT, as target cells. Moreover, the functional expression of the transduced TCRs was investigated through IFNγ ELISPOT assay (7.2.10.).

### 7.3.10. Stable transfection of MeWo cells with a luciferase expression vector

To construct stable transfected, firefly luciferase-positive cells, cells of the human melanoma line MeWo were transfected with plasmid DNA (pcDNA3.1-luc-hygro) using the cationic polymer transfection reagent jetPEI according to the manufacturer's instructions. The transfection was carried out in 6 well plates (TPP) in DMEM, supplemented with 10 mM Hepes and 10 % FCS, and was performed when the cells had a confluency of 50-60 %. After 48 h, the cells were detached using 1X Trysin-EDTA, distributed to two cell culture dishes (Ø 60 x 16 mm) and cultured in growth medium. The next day, hygromycin B was added to the medium (final concentration 200 µg/ml). The medium was completely renewed after 3 d and hygromycin B was added in general from now on in a final concentration of 100 µg/ml. Every 2 d the medium was changed, until single clones were detectable.

Single clones were then transferred to flat-bottom 96 well plates (TPP), directing a sterile pipette tip to the cell colony followed by the transfer to fresh medium into a single separate well. These clones were expanded until ~90 % confluence was reached and analyzed for *in vitro* luciferase expression (7.3.11.). The luciferase-positive clones were kept in culture and grown to higher cell numbers. Thereby, recurrent testing for stable luciferase gene expression occurred using the "Dual-luciferase reporter assay system" and *in vitro* luciferase imaging on the IVIS100 imaging machine. Finally, the stable transfected cells were used for the engraftment of immunodeficient mice and analyzed through *in vivo* imaging using the IVIS100 imaging system (7.4.4.).

### 7.3.11. *In vitro* luciferase measurement

The luciferase activity of stable transfected MeWo cell clones (7.3.10.) was examined through two different *in vitro* assays. First, single clone cells were analyzed for luciferase expression using the "Dual-luciferase reporter assay system" according to the manufacturer's recommendations. Therefore, the cells (~90 % confluency in 96 well) were lysed using passive lysis buffer. Afterwards, luciferase assay reagent II (50 µl) was added to 5 ml luminometer tubes, followed by the addition of 10 µl cell lysate. Finally, the firefly luciferase activity was measured at the Lumat LB 9507 luminometer.

Second, *in vitro* luciferase imaging on the IVIS100 imaging machine was performed. Therefore, cells of the individual clones were washed in PBS, counted and resuspended in 100 µl PBS. The cell suspension was transferred to black 96 well plates, 100 µl D-luciferin (600 µg/ml) was added per well (final concentration 300 µg/ml) and immediately the luciferase activity measured.

### 7.3.12. Infection of cells with NDV

In order to optimize the viral transport of NDV to tumor cells, various cell types were treated with NDV including MCF-7 cells and human cells of healthy donors (PBMC, $CD3^+$, $CD4^+$, $CD8^+$ T cells). Thereby, nonactivated and activated T cells were used. The activation of human T cells (adjusted to $1x10^6$ cells/ml) was performed in 12 well plates (Falcon) for 20 h using anti-CD3 (clone Okt3)

and anti-CD28 (clone 9.3) Abs (2 µg each/4x$10^6$ cells), or CD3/CD28 T cell expander beads (25 µl beads/1x$10^6$ cells; 1 beads:1 T cell). The T cell activation was analyzed by flow cytometry, measuring CD25 and CD69 expression. The NDV strains NDV-Ulster, NDFL-EGFP, NDFLtagEGFP and MTH-68 were investigated.

#### 7.3.12.1. Virus binding and modification of cells with NDV

For NDV modification, cells were washed with serum- and antibiotic-free growth medium (1200 rpm, 5 min, RT) and counted. Afterwards, 1x$10^7$ cells were incubated with NDV (0.5 HU - 500 HU) in a volume of 1 ml of serum- and antibiotic-free growth medium at 37°C for 1 h. During the incubation, cells were homogenized with a vortexer every 15 min. The cells were then washed 2x in their respective growth medium, counted and cultured in serum containing medium. To investigate the bound virus, cells were directly stained with Abs against NDV (staining of viral fusion (F) protein) and analyzed by flow cytometry (7.2.13.). For the study of viral replication, through F protein staining or intracellular EGFP signal, the infected cells were seeded into cell culture plates and analyzed at later time points.

#### 7.3.12.2. Co-culture of MCF-7 cells with NDV-modified human carrier cells

Human PBMC and T cells (for more information about the different cell types used, see 7.3.12.) were modified with NDV as described above (7.3.12.1.). Afterwards, NDV-modified carrier cells were added to MCF-7 target cells and co-cultured for 3, 6, 9, 20 or 30 h. Thereby, the ratio of tumor cells to NDV-modified carrier cells varied from 1:0.25 - 1:5, and directly infected MCF-7 tumor cells were used as controls. The extent of MCF-7 cell infection by NDV, either direct or indirect via T cell-mediated cross-infection through viral hitchhiking, was analyzed using flow cytometry (7.2.13.) or immunofluorescence microscopy (7.3.15.).

### 7.3.13. Tumor neutralization assay

To analyze the anti-tumor effect of T cell-mediated viral hitchhiking *in vitro*, MCF-7 cells were co-cultured for 2 d with NDV-modified nonactivated or activated T cells. Thereby, various NDV amounts (0.5, 10, 50 HU) and tumor cell to T cell ratios (1:1, 1:2, 1:5) were analyzed.

Before T cells were added, 2x$10^4$ untreated MCF-7 cells were resuspended in 100 µl growth medium, transferred to 96 well plates and allowed to attach for at least 4 h. After modification of T cells with NDV (7.3.12.1.), respective T cell numbers according to the different cell ratios were resuspended in 100 µl medium and added to the pre-plated tumor cells. All experimental approaches were performed in triplicates. Moreover, as controls, directly infected MCF-7 cells and MCF-7 cells without NDV (positive values) were investigated. The total volume was 200 µl/well and the plates were incubated at 37°C for 2 d. Subsequently, the supernatants were removed, the plates carefully washed with PBS and 100 µl RPMI supplemented with 5 % FCS transferred to each well. Afterwards, 20 µl MTS [3-(4,5-dimethylthiazol-2-yl)-5-(3-carboxy-methoxyphenyl)-2-(4-

sulfophenyl)-2H-tetrazolium] solution was added to the MCF-7 cell layer and incubated at 37°C for ~40 min, protected from light. Thereby, viable cells were able to convert the yellow MTS-tetrazol component into the brown-colored formazan product. The reaction was stopped with 20 µl 10 % sodium dodecyl sulfate (SDS) per well, and the color alteration measured with a plate reader at 490 nm. Control wells that only contained medium and MTS solution were used to define the background value. The tumor growth inhibition in percent was calculated using the following formula:

$$\text{percent tumor growth inhibition} = 1 - \left[ \frac{A_{490}\ \text{experimental well} - A_{490}\ \text{background}}{A_{490}\ \text{positive well} - A_{490}\ \text{background}} \right] \times 100$$

### 7.3.14. Testing of cell lines for mycoplasma infection

All cell lines used for experiments were routinely tested for mycoplasma infection using the PCR-based "Venor GeM mycoplasma detection kit" according to the manufacturer's instructions. Additionally, directly before implantation into mice, tumor cells used for animal experiments were tested for mycoplasma infection. Thereby, all cell lines used for investigations in the presented thesis were proven to be mycoplasma free.

The cell supernatants were collected in safe-lock tubes (1.5 ml), heated at 96°C for 5 min and centrifuged (13000 rpm, 5 sec, RT). Afterwards, the supernatants were transferred into new tubes and stored at 4°C for up to 14 d. The mycoplasma detection kit utilizes PCR to detect most common mycoplasma (*M.*) species including *Acholeplasma laidlawii, M. arginini, M. fermentans, M. hominis, M hyorhinis, M. orale, M. pneumoniae, M. salivarium and M. synoviae*. The used primer set is specific to the highly conserved 16S rRNA coding region in the mycoplasma genome. For PCR, 2 µl of the sample supernatants were incubated with 23 µl of the mixture shown in Tab. 4. The PCR program included 1 cycle at 94°C for 2 min, followed by 39 cycles at 94°C, 55°C and 72°C, each step for 30 sec. Thereafter, 5 µl of the PCR product was loaded to a 1.5 % agarose gel (7.3.7.). A representative gel electrophoresis of a mycoplasma PCR is shown in Fig. 15.

Furthermore, besides the mycoplasma PCR, a multiplex cell contamination test (McCT) was performed for the cell lines. The test was carried out by the Genomics and Proteomics Core Facility (Dr. M. Pawlita) at the DKFZ (for further details see Schmitt and Pawlita, 2009).

| Constituents | Volume per single reaction |
|---|---|
| PCR grade water | 15.3 µl |
| 10X reaction buffer | 2.5 µl |
| Primer/nucleotide mix | 2.5 µl |
| Internal control | 2.5 µl |
| Polymerase (5 U/µl) | 0.2 µl |

**Table 4. Mycoplasma PCR mixture.** All components were purchased from Minerva Biolabs.

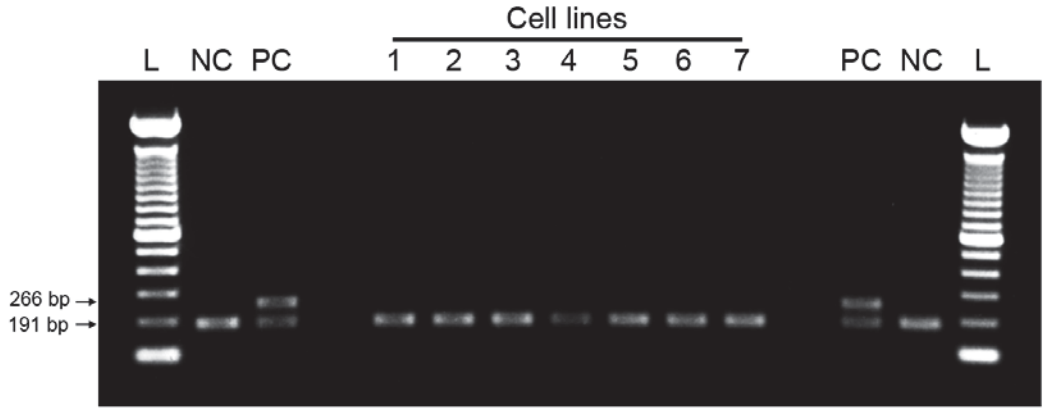


**Figure 15. Representative 1.5 % agarose gel of a mycoplasma PCR**. Internal control DNA, indicating a successfully performed PCR, was used in each sample, resulting in a distinct 191 bp band in every lane. The positive control (**PC**) shows in addition to the internal control band at 191 bp, a band at 266 bp. As negative control (**NC**), instead of sample supernatant, 2 µl PCR grade water was used. All tested human cell lines (**1**: MeWo, **2**: SK-Mel-23, **3**: Capan-1, **4**: IM-9, **5**: MCF-7, **6**: U2OS, **7**: Malme-3M), investigated in the presented PCR, are mycoplasma-free, as no band at 265-274 bp size was detected. As size marker a 100 bp ladder (**L**) was used.

### 7.3.15. Immunohistochemistry and immunofluorescence microscopy

To investigate the presence of several antigens in cell culture and *in situ*, immunohistochemistry (IHC) and immunofluorescence microscopy were performed. Beforehand, the tumors and various organs were removed from mice. The samples were immediately snap-frozen in isopentane, which had been pre-cooled in liquid nitrogen and stored at -80°C. To achieve sections of 5 µm thickness, the frozen samples were placed into cryomold adapters, aligned using Tissue-Tek and sectioned with a Leica cryo-microtome. Afterwards, the sections were transferred to Super Frost Plus object slides, air-dried for a minimum of 1 h, fixed in acetone at -20°C for 10 min and immediately used for histological stainings or stored at -20°C until use. In general, the staining procedures were always performed in wet chambers, and glass cuvettes were used for the washing steps. Primarily, the fixed tissue sections were thawed to RT and a Dako Pen was used to encircle the staining regions. Prior to the immunostaining procedure, all tissue sections were rehydrated in PBS and permeabilized with PBS containing 0.2 % Triton X-100 for 5 min, followed by 3 washing steps in PBS (each 5 min).

For IHC investigations, the "DakoCytomation EnVision$^+$ system-horseradish peroxidase (HRP) - 3-amino-9-ethylcarbazole (AEC) kit" for use with mouse primary Abs was utilized according to the manufacturer's recommendations. This system is a two-step IHC staining technique, based on a HRP-labeled polymer which is conjugated with secondary Abs. After permeabilization the endogenous peroxidase of the sections had to be blocked, followed by rinsing with dd$H_2O$ and 2x in PBS (each step 5 min). The primary mouse anti-human Abs, diluted in Antibody diluent, were added and incubated for 1 h. Afterwards, 3 washing steps in PBS (each 5 min) were carried out and HRP-labeled Polymer-anti-mouse were added for 35 min, followed by 2 further washing steps in PBS. Then, the AEC-substrate chromogen was administered, which resulted in a red-brown-

colored precipitate at the antigen site. The sections were rinsed with $ddH_2O$ and washed 2x in PBS (each 5 min) and 2x in $ddH_2O$ (each 3 min). For nuclear counter stain, the sections were incubated with Mayer´s Hematoxylin for ~1 min, rinsed with $ddH_2O$, placed in bluing reagent (0.037 mol/l ammonia water) for 30 sec and washed 2x in $ddH_2O$ (each step 5 min). Finally, the specimens were aqueously mounted with Fluoromount-G using glass cover slips. The IHC samples were recorded with a Leica DM LB2 microscope which was equipped with a DC480 Leica camera.

For immunofluorescence microscopy, tissue sections or cultured cells, grown on glass cover slips or cytocentrifuged to slides (7.1.6.), were used. The fixed cells or tissue sections were also rehydrated and permeabilized using PBS containing 0.2 % Triton X-100. Furthermore, to avoid unspecific staining of the secondary Ab, the specimens were blocked with PBS containing 5 % serum of the appropriate species for 15 min, followed by 3 washing steps in PBS. The primary Abs were applied at RT for 1 h. Subsequently, 4 washing steps were performed using PBS (5 min each) before the secondary Abs coupled to Cy3, Alexa Fluor 488 or Alexa Fluor 594 were added and incubated at RT for 45 min, protected from light. For staining of the nuclei, 4',6-diamidino-2-phenylindole (DAPI) was used, and incubated together with the secondary Ab. Accordingly, 4 washing steps with PBS (each 5 min), 3x short rinses in $ddH_2O$ and finally dehydration in 100 % ethanol for 1 min were performed. After air-drying, specimens were finally mounted with Fluoromount-G using glass cover slips. The images were recorded with a Zeiss Axiophot 2 microscope, equipped with an AxioCam HR.

### 7.3.16. SDS-polyacrylamide gel electrophoresis and immunoblotting

For the identification of proteins, present in cultured cells, SDS-polyacrylamide gel electrophoresis (SDS-PAGE) followed by immunoblot analysis using specific Abs were performed. The SDS-PAGE is based on the principle that polypeptides can be separated according to their electrophoretic mobility (Weber and Osborn, 1969). Therefore, dithiothreitol (DTT) is used as a reducing agent to destroy disulfide bridges, and SDS to break up the secondary and tertiary structure of proteins and protein-complexes by destroying hydrogen bonds. Thereby, the resulting SDS-modified polypeptide-based chains dissociate and become negatively charged, resulting in the ability to migrate in the electric field in relation to their specific charge and mass.

In general, cells were grown to confluence in tissue culture flasks or dishes and gently washed 2x with PBS (37°C) to remove dead cells and residual medium. Immediately, 1 ml 2X Laemmli sample buffer was added and the cells were scraped off using cell scrapers and transferred to safe-look tubes (1.5 ml). The samples were then incubated with 3 µl benzonase per ml buffer and homogenized by sucking up and down using a 1 ml pipette tip for several times. Thereby, benzonase acts as an unspecific endonuclease which decomposes all kinds of RNA and DNA. Then, the samples were heated at 95°C for 5 min, to denature and SDS-couple the polypeptides, centrifuged (13000 rpm, 3 min, RT) and the supernatants used for subsequent protein separation or stored at -20°C until use.

Accordingly, 10-20 µl of the samples were loaded per slot of a Tris-glycine 4-20 % gradient gel, which had been placed into a gel chamber, filled with 1X SDS-PAGE electrophoresis running buffer. As reference system for the molecular weight of the polypeptides, a broad range 2-212 kilodalton (kDa) protein marker with 13 different polypeptides of known molecular weight was used. The proteins were separated at 20 mA per gel for 1.5-2 h. Afterwards, the polypeptides were transferred from the gel to a polyvinylidene difluoride (PVDF) membrane using a special semi-dry transfer technique (Kyhse-Andersen, 1984). Therefore, Whatman 3MM blotting papers were equilibrated in transfer buffer 1, 2 and 3, respectively, and arranged in the blotting chamber with the PVDF-membrane sheet (rinsed in isopropanol and equilibrated in transfer buffer 2) and the SDS gel (equilibrated in transfer buffer 3). The alignment of the semi-dry blot is shown in Tab. 5 (beginning at the anode). Subsequently, the semi-dry blots run at 130 mA for 1.5 h.

Afterwards, to visualize the polypeptide bands, the resulting PVDF membrane was stained with Coomassie brilliant blue R-250 staining solution. Thereby, background staining was reduced using PVDF membrane destaining buffer for washing. Finally, before immunodetection, the membranes were air-dried. The detection of the polypeptides, bound to the PVDF membrane, was performed using an indirect enzyme immune assay. Background reactions, due to non-specific binding, were reduced through incubation in PBS-Tween buffer containing 5 % milk powder for 30 min. Subsequently, the membranes were incubated with the primary Abs (diluted to appropriate concentrations in PBS-Tween milk buffer) for at least 1 h, washed 3x in PBS-Tween buffer and incubated for further 30 min with HRP-conjugated secondary goat anti-mouse IgG/IgM Abs, followed by several washing steps in PBS. All steps were performed at RT using a shaker.

Finally, for the detection of the secondary Ab, bound to the proteins, the “Enhanced chemi-luminescence (ECL) detection system” was used. Therefore, the membranes were shortly dried and incubated for 1 min in the ECL solution. Thereby, the HRP catalyzed the oxidation of luminol to 3-aminophthalate, which led to the emission of low intensity light at 428 nm, detectable on a Konica-Minolta medical film using a developing machine.

| **cathode** |
|---|
| 6 x Whatman papers in transfer buffer 3 |
| **SDS gel** in transfer buffer 3 |
| **PVDF membrane** in transfer buffer 2 |
| 3 x Whatman papers in transfer buffer 2 |
| 6 x Whatman papers in transfer buffer 1 |
| **anode** |

**Table 5. Semi-dry blot alignment.** Whatman 3MM blotting papers were equilibrated in transfer buffer 1, 2 or 3, the PVDF membrane in transfer buffer 2 and the SDS gel in transfer buffer 3.

### 7.3.17. Detection of autoimmune markers in human plasma

Human plasma was obtained after Ficoll density gradient centrifugation (see also 7.2.2.) of PB from melanoma and dysplastic nevi patients and stored in aliquots at -20°C. The plasma was used to measure the following autoimmune markers: anti-nuclear auto-Abs (ANA), anti-neutrophilic cytoplasmic auto-Abs (ANCA), perinuclear ANCAs (p-ANCA) and the rheumatoid factor. The autoimmune diagnostics was performed by the central laboratory of the Analysis Center of the University Hospital Heidelberg (head: Prof. Dr. P. Nawroth).

## 7.4. Animal methods

### 7.4.1. Anesthesia of mice

To receive a narcosis time of ~30 min, non-obese diabetic-severe combined immune-deficient (NOD-SCID) and NOD *scid* gamma (NSG) mice were anesthetized intraperitoneally (i.p.). Thereby, per mouse up to 30 g body weight, 100 µl Rompun/Ketanest S solution were used (0.4 mg xylazin, 1 mg ketamin per mouse; for composition of solution see Tab. 6.). The anesthetic effect was controlled by checking the plantar reflexes of the mouse. During anesthesia, to avoid hypothermia, mice were kept on a thermal mat and PBS was placed to the eyes to avoid drying. Furthermore, until they woke up, the mice were monitored during the recovery phase. During the *in vivo* imaging, inhalative anesthesia with 2 l/min Isofluran-$O_2$ mixture was performed (7.4.4.).

| Constituents | Volume per 10 ml solution |
|---|---|
| 1X PBS | 4 ml |
| 20 mg/ml Rompun 2 % (xylazin) | 2 ml |
| 25 mg/ml Ketanest S (ketamin) | 4 ml |

**Table 6. Preparation of injection anesthesia solution.** The solution was always sterile freshly prepared prior to each animal experiment and stored at RT until use.

### 7.4.2. Inoculation of tumor cells

The cells of various tumor lines were injected into mice to observe their *in vivo* growth behavior, resulting in a tumor formation. In general, cells of the different lines were collected from tissue culture flasks, and 1 ml of the cell culture supernatants were removed for mycoplasma PCR investigation (7.3.14.).

For intradermal (i.d.) primary and secondary tumor cell inoculation, the cells were centrifuged (1200 rpm, 5 min, RT), washed in PBS, counted, resuspended to a concentration of $2.5x10^6$ cells in 50 µl matrigel basement membrane matrix and transferred to sterile safe-lock tubes (1.5 ml). Since matrigel is only liquid at lower temperatures and becomes solid at higher temperatures, after the addition of matrigel, the cell suspension was kept on ice at all times. Afterwards, the mice were

anesthetized with Rompun/Ketanest S (7.4.1.) and shaved before the resuspended cells ($2.5x10^6$ cells / 50 µl matrigel) were injected i.d. to the right (primary tumor) or the left (secondary tumor) flank using 0.4 mm x 19 mm needles connected to 1 ml syringes. In contrast for tumor irradiation experiments (7.4.5.), tumor cells were applied i.d. to the right hind leg. In general, the tumor growth was measured every 2-3 d using a caliper and the tumor diameters and the tumor volumes (e.g., Schatton et al., 2008) were calculated using the following formulas:

$$\text{Tumor diameter (mm)} = \frac{(\text{length} + \text{width})}{2}$$

$$\text{Tumor volume (mm}^3\text{)} = \left[\frac{\pi}{6}\right] \times 0.5 \times \text{length} \times (\text{width})^2$$

$$\pi = 3.14159$$

In some experiments, the primary tumor was removed and a secondary tumor administered to the opposite flank of the same mice. Therefore, the mice were again anesthetized and shaved around the primary tumor. Since the tumor has been injected i.d., it could be carefully lifted with sterile tweezers and subsequently be removed with sterile scissors. The wound was immediately closed using the autoclip wound clip applier. A second tumor was injected i.d. to the left flank of the same mice 2 d later. After 10 d, the wound clips were removed under anesthesia (7.4.1.).

For subcutaneous (s.c.), intraveneous (i.v.) or i.p. tumor cell inoculations, the tumor cells were centrifuged (1200 rpm, 5 min, RT), washed in PBS and counted. Afterwards, they were resuspended to a concentration of $2.5x10^6$ cells in 100 µl PBS and transferred to sterile safe-look tubes (1.5 ml) and placed on ice. Subsequently, 100 µl of the cells were injected s.c. to the shaved right murine flank or i.p. using appropriate needles and syringes as described above. For i.v. application, 100 µl of the tumor cell suspension was injected into the tail vain using 1 ml Micro-Fine insulin syringes with 0.33 mm x 12.7 mm needles. Prior to cell application, the mouse tail was pre-warmed with a red light lamp to allow the vessel vasodilatation.

### 7.4.3. Adoptive T cell transfer *in vivo*

To investigate whether the tumor growth was controlled by TCR transgenic T cells (7.3.9.), various MDM2 and gp100 TCR transduced human T cell constructs were adoptively transferred to mice, priorily engrafted i.d. with human melanoma cells resuspended in matrigel (7.4.2.). In general, on d7 after primary tumor cell inoculation, the transduced T cells ($2x10^6$ - $5x10^6$ cells) were resuspended in 100 µl PBS and injected i.v. into the tail vain (1 ml Micro-Fine Insulin syringes, 0.33 mm x 12.7 mm needles). Before i.v. injection, a vasodilatation of the mouse tail was performed as described (7.4.2.). As control settings, mock transduced T cells (empty retroviral plasmid without genes for TCR α or β chains, used for T cell transduction), and PBS without T cells were injected.

### 7.4.4. *In vivo* imaging of luciferase expression

The IVIS100 imaging system was used for bioluminescence imaging *in vivo* to repeatedly investigate the tumor growth of stably transfected firefly luciferase-positive tumor cells (7.3.10.) in mice. Therefore, D-luciferin was used as substrate for the firefly luciferase. This enzyme catalyzes the oxygenation of D-luciferin using ATP and molecular oxygen to oxyluciferin, a highly unstable singlet-excited compound, which emits light upon relaxation to its ground state.

The lyophilized D-luciferin powder was solved in PBS, filtered sterile (0.22 µm syringe filter unit) and stored in 1 ml aliquots at -80°C. The *in vivo* imaging of shaved mice was performed 5 min after i.p. injection of the D-luciferin solution and up to five mice could be analyzed in parallel. Thereby, the injected volume of D-luciferin was dependent on the body weight of the mice (cf., Tab. 7). During the whole imaging process, the mice received inhalative anesthesia of an Isofluran/$O_2$ mixture (2 l/min). The bioluminescence signal was quantified in units of photons/second/square centimeter/steradian (p/sec/cm$^2$/sr). In general, the mice were imaged 2x per week, investigating different exposure times (1, 10, 20, 30, 60, 120 and 300 sec).

| Weight of mice [g] | D-luciferin (30 mg/ml) [µl] |
|---|---|
| 17.5 - 18.5 | 90 |
| 18.5 - 19.5 | 95 |
| 19.5 - 20.5 | 100 |
| 20.5 - 21.5 | 105 |
| 21.5 - 22.5 | 110 |
| 22.5 - 23.5 | 115 |
| 23.5 - 24.5 | 120 |
| 24.5 - 25.5 | 125 |
| 25.5 - 26.5 | 130 |
| 26.5 - 27.5 | 135 |
| 27.5 - 28.5 | 140 |
| 28.5 - 29.5 | 145 |
| 29.5 - 30.5 | 150 |

**Table 7. D-luciferin volume for mice injection.** D-luciferin was constituted in PBS at a stock concentration of 30 mg/ml. Depending on the murine body weight, respective volumes were injected.

### 7.4.5. Irradiation of mice

To investigate a combinational treatment approach, consisting of local low dose tumor irradiation and adoptive immunotherapy with TCR transgenic T cells, mice were locally irradiated at the tumor injection side, in general, 6 d after i.d. tumor application to the right hind leg (7.4.2.). An irradiation with 2 Gy was performed using the Gammatron Cobalt 60 therapy unit. Therefore, the mice were fixed in a special rack that only allowed the irradiation of the tumor (see also Fig. 66). The local low dose irradiation was kindly performed by A. Tietz-Dalfuß (Clinical Cooperation Unit Radiation Oncology, DKFZ).

### 7.4.6. Preparation of single cell suspensions from murine organs

To analyze the presence of previously i.v. injected TCR transgenic T cells, single cell suspensions were produced from PB and tumors of tumor-bearing mice.

#### 7.4.6.1. Cell suspensions from PB

Murine PB samples were obtained from the retro-orbital venous plexus of mice using heparinized capillaries or from the submandibular vein using blood lancets. Thereby, if the blood was taken from the venous plexus behind the eye, the mice received inhalative anesthesia with Isofluran. In general, ~200 µl PB were removed per mouse and immediately mixed with 100 µl heparin, to prevent clotting and placed on ice until treated with 10 ml ACK lysis buffer at RT for 10 min, to obtain red blood cell lysis. The reaction was stopped using PBS supplemented with 5 % FCS.

Afterwards, the cells were centrifuged (1500 rpm, 5 min, 4°C), washed with FACS buffer and used for flow cytometry analysis to stain for human T cells, which had before been adoptively transferred to mice (7.3.9.; 7.4.3.). FACS staining was performed as described in 7.2.13., with the exception that 5 % Endobulin together with 5 % hybridoma supernatant 2.4G2 in PBS (anti-CD16/CD32; kindly provided by Dr. J. Ni) were used for initial blocking of the surface Fc-receptors.

#### 7.4.6.2. Cell suspensions from tumors

The tumors applied i.d., were either surgically removed (see 7.4.2.), keeping the mice alive, or the mice were sacrificed by cervical dislocation before tumor removal. The weights of the individual tumors were measured with a digital analytical balance. Afterwards, the tumors were stored frozen to use for later IHC stainings (7.3.15.) or single cell suspensions were immediately prepared for FACS analysis. For the latter, the tumors were cut into small pieces (~8 mm), treated in 50 ml tubes with tumor digestion buffer (10 ml/tumor; containing hyaluronidase and DNase I) and incubated at 37°C for 30 min while permanent shaking. Single cell suspensions were obtained by mincing the digested tumors through 70 µm-pore cell strainers, followed by a washing and centrifugation step in PBS (1600 rpm, 10 min, 4°C). The cells were subsequently resuspended in 7 ml PBS and filtered through 40 µm-pore cell strainers. The cell suspension was then loaded to 6 ml Lympholyte-M solution in 15 ml tubes, followed by a density gradient centrifugation (1500 g, 26 min, 22°C, decelerated brake). After the centrifugation step, the PBMC layer was removed, washed with FACS buffer and used for flow cytometry (7.2.13.) to stain for human T cells (7.4.3.). The FACS protocol was used with the modification of Fc-receptor blocking (see 7.4.6.1.).

### 7.4.7. Staining of lung metastases

To control metastases formation after tumor cell injection *in vivo*, lungs from tumor bearing mice were removed and stained in Bouin's solution containing picrinic acid at RT for 72 h. In Bouin's solution, normal tissues become a brown color while metastases stain yellow. Therefore, at the lung surface, the metastatic nodules could be analyzed.

## 7.5. Statistical analysis

Differences between the test groups were analyzed using the nonparametric unpaired two-tailed "Student t test" and differences were considered to be significant on the basis of the 95 % confidence interval. The calculated p values indicate, whether a statistical significant difference between the test groups exist. Following p values display significant differences: * p value ≤ 0.05, ** p value ≤ 0.01 and *** p value ≤ 0.001. In contrast, p values > 0.05 and < 0.1 were not considered to be statistically significant but indicated a trend. If not indicated differently, the experimental data were expressed as Mean ± standard error of the mean (SEM).

The tumor volume and diameter of various TCR transgenic T cell adoptively transferred mice, from independent experiments, were combined and analyzed against the PBS and mock treated reference control groups over time using the linear regression model with mixed effects (fixed: baseline, treatment, day; random: individual animal, individual experiment). Thereby, the calculation of statistical differences of tumor growth behavior over time, between the individual treated murine groups, was kindly performed by A. Benner (Statistics for Translational Oncology, Division of Biostatistics, DKFZ).

# 8. Results

## 8.1. Characterization of human spontaneous tumor antigen-reactive T cell responses

Spontaneously induced human tumor antigen-reactive memory T cell responses of melanoma patients were investigated by short-term co-culture experiments of patient-derived autologous dendritic cells and T cells. The reactivation of T cells was performed using dendritic cells, loaded with synthetic 50 amino acids (aa) long polypeptides and analyzed through T cell-dependent IFNγ secretion, measured by a short-term ELISPOT assay.

### 8.1.1. Generation of 50aa polypeptides of melanoma tumor-associated antigens

According to their capacity to contain different epitopes that can be presented in the context of MHC class I and class II molecules, synthetic polypeptides with a length of 50aa were generated. Thereby, polypeptides for the following 13 selected melanoma tumor-associated antigens (TAAs) were constructed: GAGE-1, gp100/pmel17, MAGE-A1, MAGE-C2, MDM2, Melan-A/MART-1, MIF, NA17-A, NY-ESO-1, p53, RAB38/NY-Mel-1, TRP2 and Tyrosinase (see also, Tab. 8, NCBI GenBank accession numbers are indicated therein).

The polypeptide sequences were chosen to cover at least one known HLA-A2-(HLA-A*0201) restricted epitope, which had been described in the literature (cf., Tab. 8). Besides these known epitopes, further putative MHC class I and class II epitopes were contained in the peptide sequences, presented through alleles frequently occurring in the human population. These were identified by the help of HLA peptide binding epitope prediction algorithms using the two databases “Syfpeithi” (www.syfpeithi.de; Rammensee et al., 1999) and “Bimas” (www-bimas.cit.nih.gov; Parker et al., 1994). According to the Syfpeithi database, for all 50aa polypeptides, a selection of possible epitopes, presented on MHC class II and class I, with exception of HLA-A2, were predicted and are listed in Appendix 13.12.. Only the top-scoring 2 % of all predicted peptides are shown, because only they should contain the naturally presented epitopes. A reliability of at least 80 % for predicted MHC class I epitopes can be expected. In comparison, since the pocket binding behavior of MHC class II is more variable, the predicted MHC class II motifs have a reliability of ~50 % (Rammensee et al., 1999). Besides the known HLA-A2-restricted epitopes, in all designed 50aa polypeptides, further predicted HLA-A2-restricted epitopes were present (see Appendix 13.13.). To investigate the specificity of the generated 50aa sequences of all polypeptides, a GenBank alignment of the protein sequences were performed using the NCBI Blast database (www.ncbi.nlm.nih.gov/BLAST/Blast.cgi). For all polypeptide sequences, a complete and specific alignment was obtained with the corresponding protein sequence of the respective antigen.

| Tumor antigen | HLA-A*0201 epitope | | Reference | 50aa polypeptide | |
|---|---|---|---|---|---|
| **GAGE-1** (AAA82744)* | YRPRPRRYV | 9-17 | *** van den Eynde et al., 1995 and Syfpeithi prediction | MSWRGRSTYR PRPRRYVEPP EMIGPMRPEQ FSDEVEPATP EEGEPATQRQ | 1-50 |
| **gp100/pmel17** (AAC60634)* | LLDGTATLRL<br>VLYRYGSFSV | 457-466<br>476-485 | Kawakami et al., 1994a<br>Kawakami et al., 1995 | SITGSLGPLL DGTATLRLVK RQVPLDCVLY RYGSFSVTLD IVQGIESAEI | 449-498 |
| **MAGE-A1** (NP_004979)* | KVLEYVIKV | 278-286 | Ottaviani et al., 2005<br>Pascolo et al., 2001 | PARYEFLWGP RALAETSYVK VLEYVIKVSA RVRFFFPSLR EAALREEEEG | 259-308 |
| **MAGE-C2** (AAF07211)* | ALKDVEERV | 336-344 | Ma et al., 2004 | WGPRAHSESI KKKVLEFLAK LNNTVPSSFP SWYKDALKDV EERVQATIDT | 301-350 |
| **MDM2** (AAL40178)* | LLGDLFGV<br>VLFYLGQY | 81-88<br>53-60 | Stanislawski et al., 2001<br>Asai et al., 2002 | KEVLFYLGQY IMTKRLYDEK QQHIVYCSND LLGDLFGVPS FSVKEHRKIY | 51-100 |
| **Melan-A/MART-1** (NP_005502)* | EAAGIGILTV<br>AAGIGILTV<br>ILTVILGVL | 26-35<br>27-35<br>32-40 | Kawakami et al., 1994b<br>Kawakami et al., 1994b<br>Castelli et al., 1995 | GHGHSYTTAE EAAGIGILTV ILGVLLLIGC WYCRRRNGYR ALMDKSLHVG | 16-65 |
| **MIF** (CAG30406)* | LLCGLLAER<br>LLCGLLAERL | 79-87<br>79-88 | *** Cha et al., 2007<br>and Syfpeithi prediction | LMAFGGSSEP CALCSLHSIG KIGGAQNRSY SKLLCGLLAE RLRISPDRVY | 47-96 |
| **NA17-A** (X91652)** | VLPDVFIRC<br>VLPDVFIRCV | 2-10<br>2-11 | Guilloux et al., 1996<br>Fonteneau et al., 1997 | MVLPDVFIRC VVFCLTVVCW TWVPLRGPSS PGSYRKWMCF SESQVQPTQK | 1-50 |
| **NY-ESO-1** (CAA05908)* | SLLMWITQC | 157-165 | Jaeger et al., 1998 | FTVSGNILTI RLTAADHRQL QLSISSCLQQ LSLLMWITQC FLPVFLAQPP | 126-175 |
| **p53** (BAC16799)* | STPPPGTRV | 149-157 | Theobald et al., 1995 | TAKSVTCTYS PALNKMFCQL AKTCPVQLWV DSTPPPGTRV RAMAIYKQSQ | 118-167 |
| **RAB38/NY-Mel-1** (NP_071732)* | VLHWDPETV | 50-58 | Walton et al., 2006 | ATIGVDFALK VLHWDPETVV RLQLWDIAGQ ERFGNMTRVY YREAMGAFIV | 40-89 |
| **TRP2** (ABI73976)* | ATTNILEHV<br>NATTNILEHV | 403-411<br>402-411 | Khong and Rosenberg, 2002 | ALPHSAANDP IFVVISNRLL YNATTNILEH VRKEKATKEL PSLHVLVLHS | 381-430 |
| **Tyrosinase** (AAK00805)* | MLLAVLYCL<br>CLLWSFQTSA | 1-9<br>8-17 | Woelfel et al., 1994<br>Riley et al., 2001 | MLLAVLYCLL WSFQTSAGHF PRACVSSKNL MEKECCPPWS GDRSPCGQLS | 1-50 |

**Table 8. Melanoma TAAs and sequences of the generated 50aa polypeptides.** HLA-A2-(HLA-A*0201) restricted epitopes of melanoma TAAs as described in the literature are listed, respectively. The 50aa polypeptide sequences for the 13 individual antigens are indicated. The respective HLA-A2-restricted epitopes, as described in the literature, are demonstrated in red letters in the context of the polypeptide sequence. * NCBI GenBank accession number; ** NCBI GenBank accession number, a part of an intron sequence was used; *** epitope was selected according to informations from the indicated research paper in combination with an epitope prediction, performed using the Syfpeithi database.

The HLA-A2-restricted epitope for the NA17-A antigen, is a atypical peptide, encoded by an intron sequence of the N-acetyl glucosaminyl-transferase V gene (GnT-V). The NA17-A antigen was derived from a patient (NA17) with cutaneous melanoma metastases (Pandolfino et al., 1992). A promoter within the intron of NA17-A is specifically activated in melanoma cells, resulting in the production of an intron-coated mRNA (Guilloux et al., 1996). Therefore, the 50aa polypeptide for NA17-A was constructed, based on intron and exon sequences as shown in Fig. 16. Besides the described HLA-A2-restricted epitopes, the generated 50aa polypeptide contains further predicted MHC class I (including HLA-A2) and MHC class II epitopes (Appendix 13.12. and 13.13.).

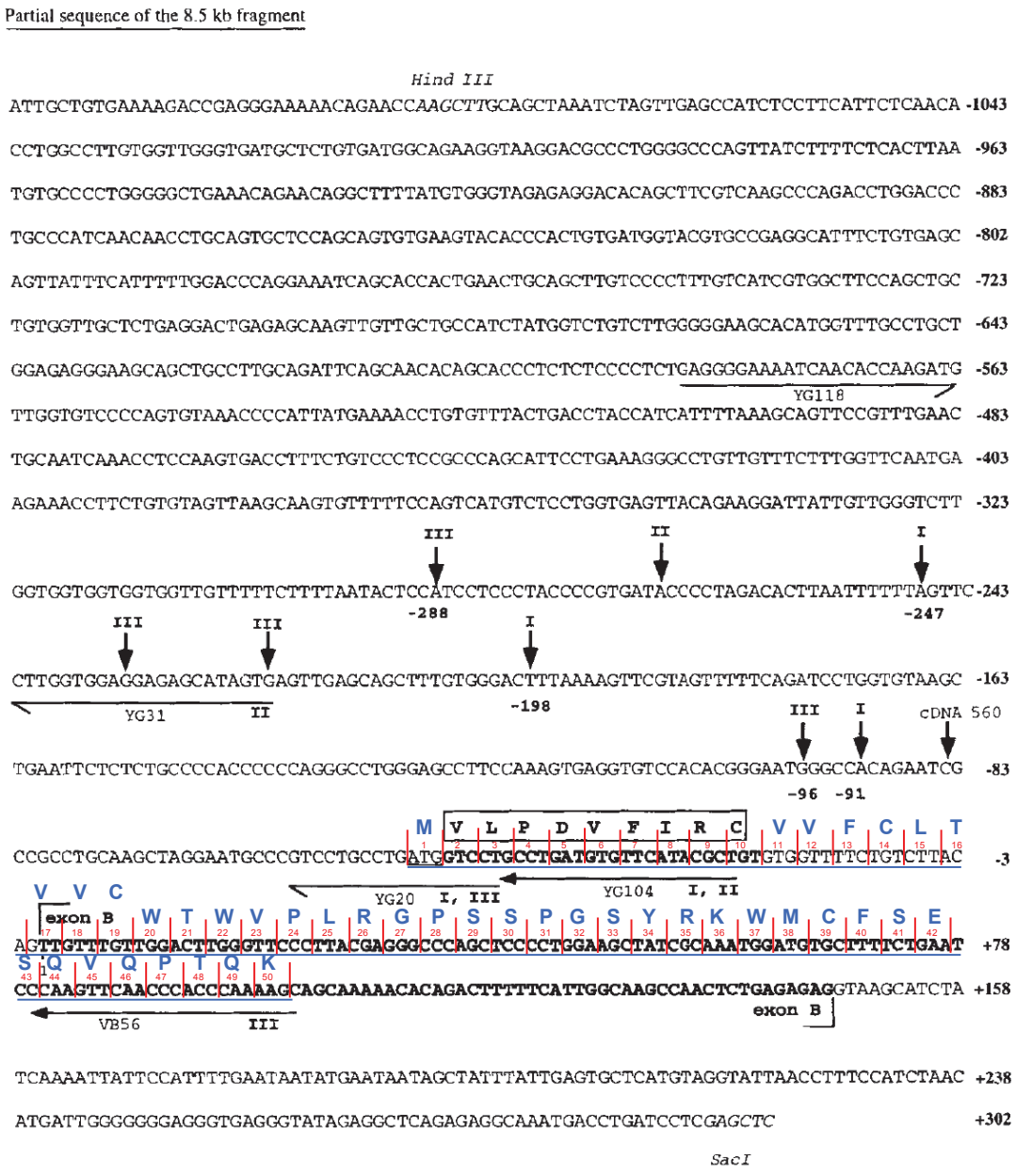


**Figure 16. Generation of the 50aa polypeptide for NA17-A.** The HLA-A2-restricted epitope VLPDVFIRC from the human GnT-V gen is encoded by an intron sequence. Specifically in melanoma cells, a cryptic promoter within the intron is activated. A synthetic 50aa polypeptide was generated surrounding the HLA-A2-restricted epitope (blue underlined sequence). The figure is modified from Guilloux et al., 1996.

### 8.1.2. Patient cohorts used for investigations

The analysis for the presence of spontaneously induced tumor antigen-reactive memory T cell responses was investigated using peripheral blood (PB) samples of 3 patients with dysplastic nevi (DPN), 38 patients with non-metastasized and 8 patients with metastasized malignant melanoma (MM; Tab. 9). As control group, healthy donor PB samples were examined. The main group of patients was diagnosed as non-metastasized melanoma stage IA (cf., Tab. 9). The tumor in these patients is less than 1 mm in diameter and the covering skin layer is not ulcerated. During this stage the melanoma is only located in the skin and there is no sign that it has spread to lymph nodes or other parts of the body.

For the investigation of spontaneously induced tumor antigen-reactive memory T cell responses, PB was taken after resection of the primary tumor from all 38 non-metastasized melanoma patients (stages I and II; Tab. 9). Representative images of a dysplastic nevus and a melanoma stage IA are shown in Fig. 17.

| | | number of patients | |
|---|---|---|---|
| **dysplastic nevus** | | | **3 patients** |
| | | | |
| **non-metastasized melanoma** | | | **38 patients** |
| **melanoma *in situ*** | 0 | - | |
| **stage I** | IA | 24 | |
| | IB | 5 | |
| **stage II** | IIA | 5 | |
| | IIB | 2 | |
| | IIC | 2 | |
| **metastasized melanoma** | | | **8 patients** |
| **stage III** | IIIA | 2 | |
| | IIIB | 1 | |
| | IIIC | - | |
| **stage IV** | IV | 5 | |

**Table 9. Summary of the patient cohorts used.** The PB of 3 patients with dysplastic nevi lesion, 38 non-metastasized as well as 8 metastasized melanoma patients were analyzed for the presence of spontaneously induced tumor antigen-reactive memory T cell responses. The numbers of patients for the different melanoma stages are shown, respectively.

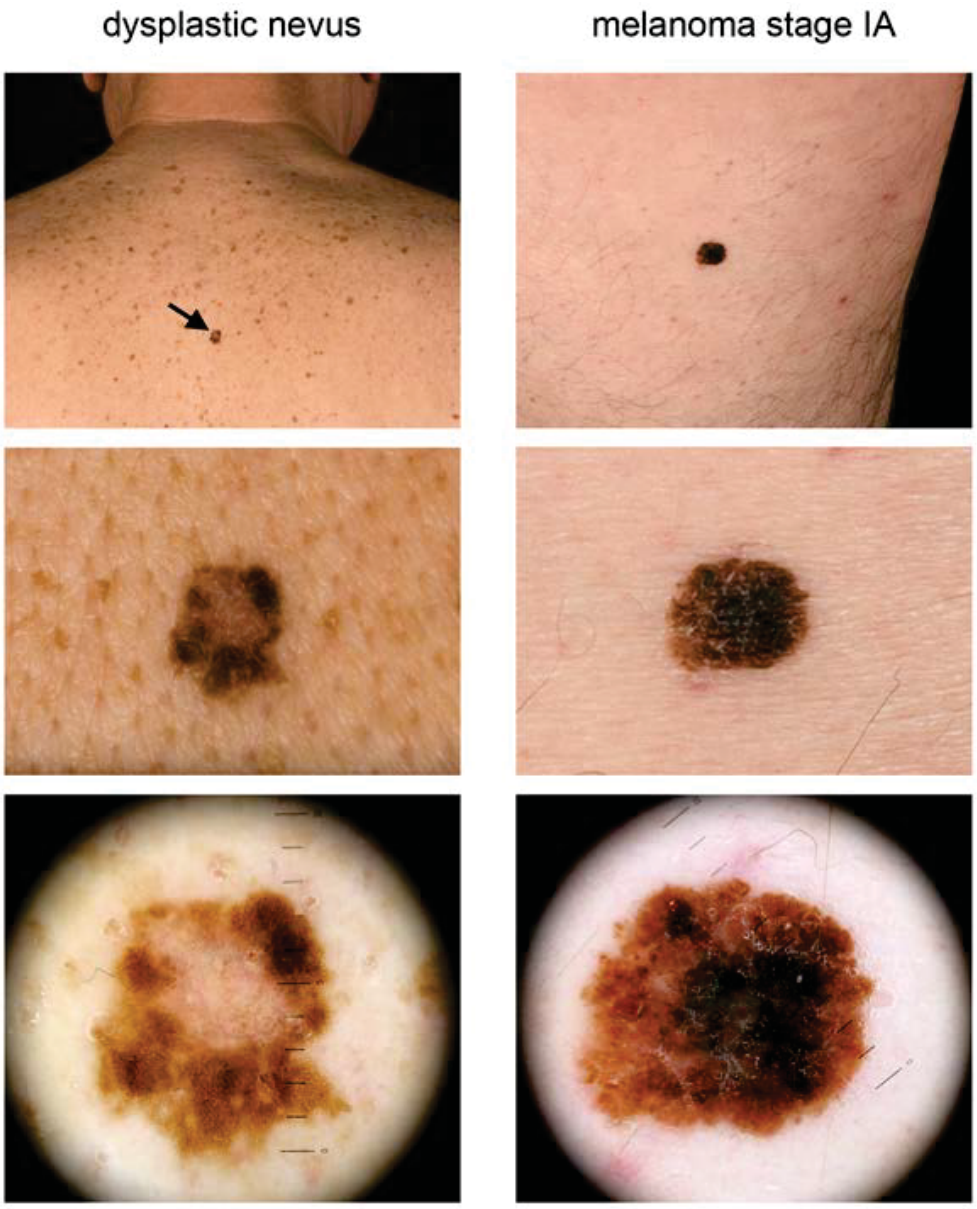


**Figure 17. Representative images of patients, suffering from a dysplastic nevi lesion (left column) or a non-metastasized melanoma stage IA (right column).** Survey micrographs present a dysplastic nevus on the back of patient # 64 (indicated by arrow) and a melanoma stage IA on the thigh of patient # 62. In the middle lane, higher magnifications are shown, whereas in the lower images, a dermatoscope was used for detailed visualization. The pictures were kindly provided from Dr. C. Gebhardt, Department of Dermatology, University Hospital Heidelberg.

### 8.1.3. Tumor antigen-reactive T cell responses to polypeptides in melanoma patients

The presence of spontaneously induced tumor antigen-reactive memory T cells was analyzed in the 38 non-metastasized (stages I, II) and the 8 metastasized melanoma patients (stages III, IV; cf., Tab. 9), performing an *ex vivo* short-term IFNγ ELISPOT assay. For this, $1x10^4$ mature PB-derived dendritic cells were pulsed with the generated 50aa polypeptides of melanoma TAAs for 18 h. The cells were co-cultured with $5x10^4$ autologous PB T cells for 40 h. During this short-term T cell activation, the cytokine IFNγ, produced by reactivated memory T cells, is bound through plate-coupled anti-IFNγ antibodies (Abs). This results in spot formation on the membrane of the IFNγ

ELISPOT assays. Therefore, the secretion of IFNγ was used to analyze, whether pre-existing tumor antigen-reactive memory T cells were present in the PB of melanoma patients upon reactivation.

Representative wells of an ELISPOT plate, showing specific IFNγ spot formation and the associated graph, are displayed in Fig. 18. As control settings, a co-culture of dendritic cells pulsed with human IgG together with autologous T cells as well as single cultures of T cells and dendritic cells were performed. To guarantee the functionality of the performed assay, the bacterial super antigen staphylococcal enterotoxin B (SEB) was used as positive control. In addition, representative IFNγ ELISPOT results of individual non-metastasized melanoma patients are indicated in Figs. 18 and 19. In the presented ELISPOT assay, which was performed with T cells and dendritic cells of patient # 16 significantly increased tumor antigen-reactive T cell responses were shown against the 50aa polypeptides p53 and TRP2, compared to the human IgG control (Fig. 19A). In contrast, however, patient # 5 and # 36 revealed polyvalent T cell responses against all tested polypeptides (Figs. 18B and 19B).

The cumulative data of 38 non-metastasized as well as 8 metastasized melanoma patients showed that spontaneously induced tumor antigen-reactive T cell responses were detected in 76.3 % of all analyzed non-metastasized and in 62.5 % of all metastasized melanoma patients (Fig. 20). In comparison to the IgG control, in all of these samples, the T cell responses were significantly increased against at least one of the tested polypeptides. If patient-derived T cells responded to the generated polypeptides, then they mainly responded against four or more antigens at the same time and therefore, showed a polyvalent T cell response (Fig. 21). For this analysis of response rates, only assays in which at least four 50aa polypeptides of melanoma TAAs could be tested in parallel, were counted.

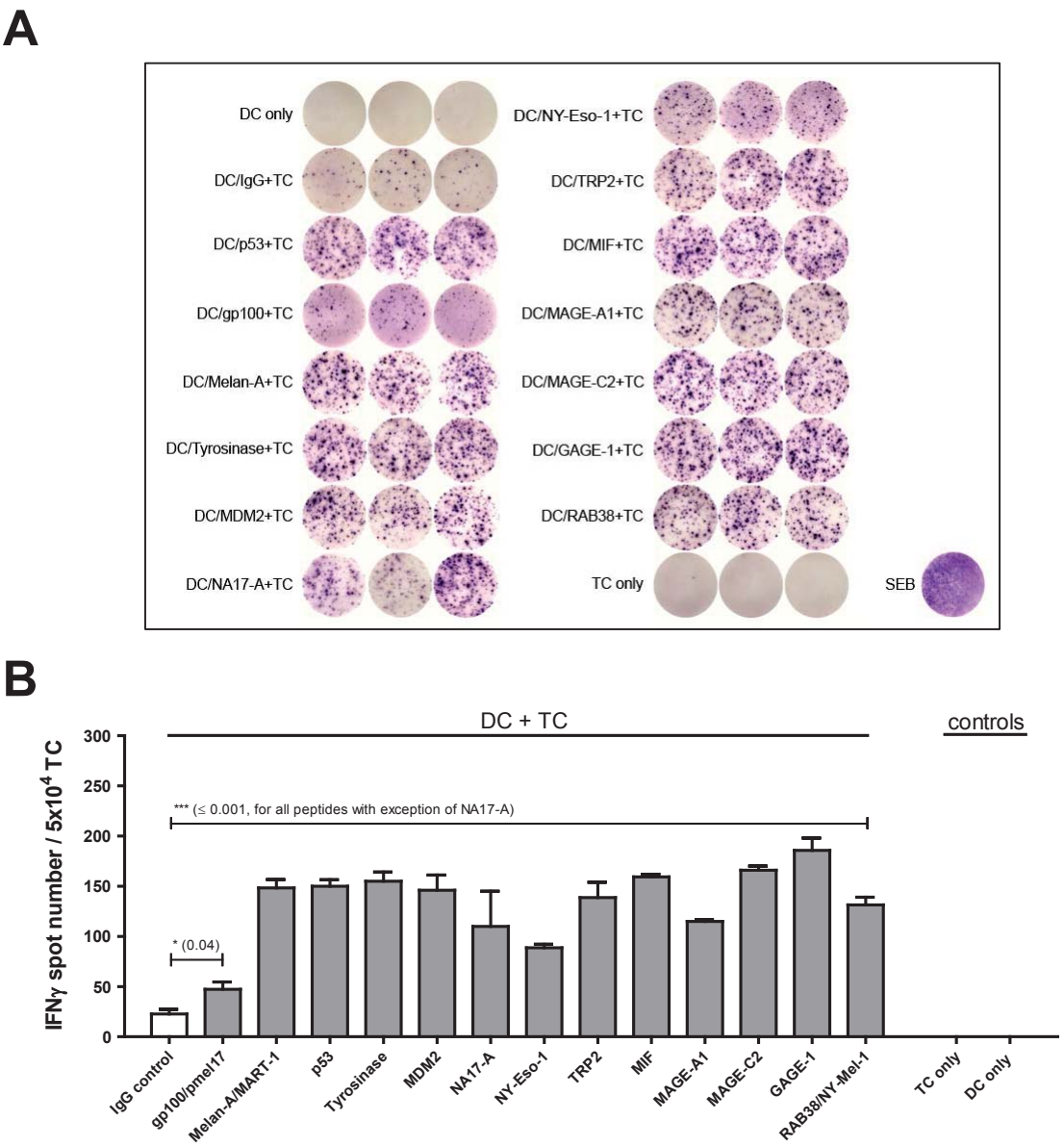


**Figure 18. Representative IFNγ ELISPOT wells of a non-metastasized stage IIC melanoma patient.** Tumor antigen-reactive memory T cell responses against the polypeptides (gp100/ pmel17, Melan-A/MART-1, p53, Tyrosinase, MDM2, NA17-A, NY-Eso-1, TRP2, MIF, MAGE-A1, MAGE-C2, GAGE-1, RAB38/NY-Mel-1) were present in the PB of melanoma patient # 36. As endogenous negative control, a co-culture of dendritic cells loaded with human IgG peptide together with T cells was performed. Additionally, single cultures of dendritic cells and T cells were accomplished as negative controls and a co-culture of SEB pulsed dendritic cells together with T cells were investigated as positive control. **A**) An image of representative ELISPOT wells is shown. **B**) Resulting graph of the spots indicated in A. For statistical analysis, an unpaired two-tailed t test was performed. Significant increased p values were compared to human IgG control: gp100/pmel17 (0.04), Melan-A/MART-1 (0.0001), p53 (0.00009), Tyrosinase (0.0002), MDM2 (0.001), NY-Eso-1 (0.0003), TRP2 (0.001), MIF (0.00001), MAGE-A1 (0.00004), MAGE-C2 (0.00002), GAGE-1 (0.0002), RAB38/NY-Mel-1 (0.0002). DC, dendritic cells; Mean ± SEM; TC, T cells; * p value ≤ 0.05; *** p value ≤ 0.001

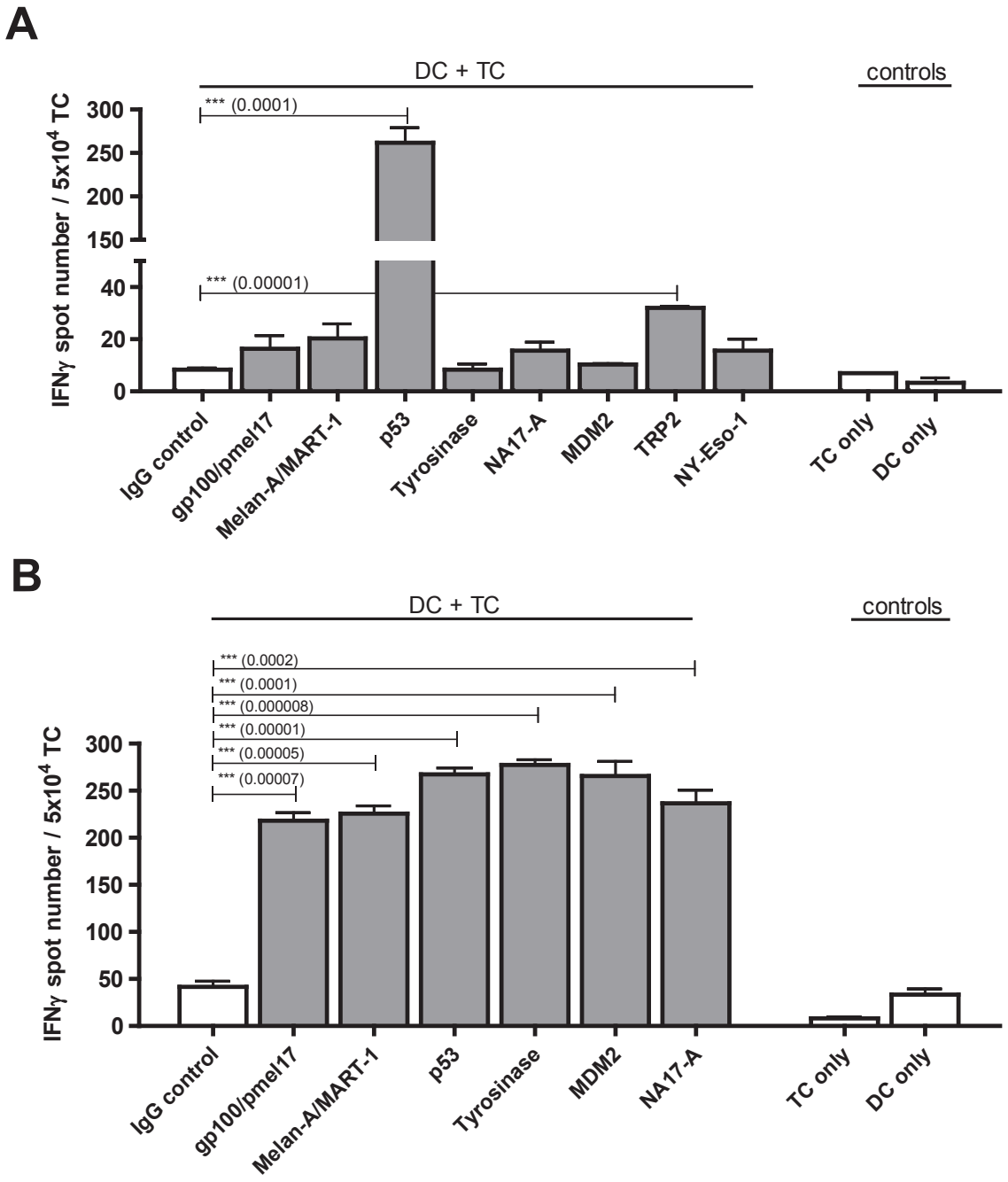


**Figure 19. Representative IFNγ ELISPOT results of two non-metastasized stage IA melanoma patients.** Spontaneously induced tumor antigen-reactive memory T cell responses were detected against polypeptides, derived from melanoma TAAs. **A**) Melanoma patient # 16 showed significant increased spontaneous T cell responses against the polypeptides p53 and TRP2, compared to the human IgG control. **B**) Polyvalent significantly increased T cell responses were detected in melanoma patient # 5, against all investigated polypeptides (gp100/pmel17, Melan-A/MART-1, p53, Tyrosinase, MDM2, NA17-A), compared to human IgG T cell responses. Single cultures of T cells and dendritic cell were accomplished as controls. For statistical analysis, an unpaired two-tailed t test was performed. DC, dendritic cells; Mean ± SEM; TC, T cells; *** p value ≤ 0.001

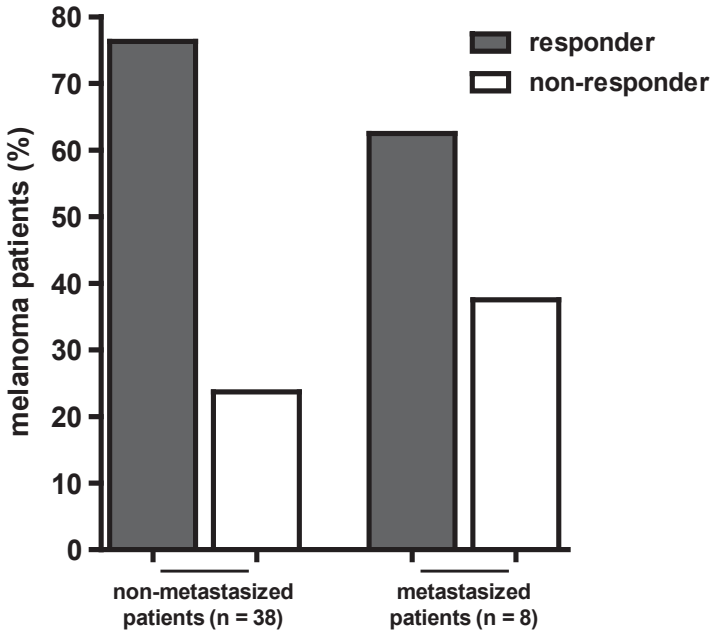


**Figure 20. Proportion of melanoma patients with spontaneously induced tumor antigen-reactive T cell responses.** Tumor antigen-reactive memory T cells occurred in non-metastasized and metastasized melanoma stages. Responder, significant increased number of IFNγ spots by T cells, in response to at least one TAA polypeptide/dendritic cell setting compared to control human IgG peptide/dendritic cell approach. For non-responder, no significantly increased T cell responses were detected. n, number of patients

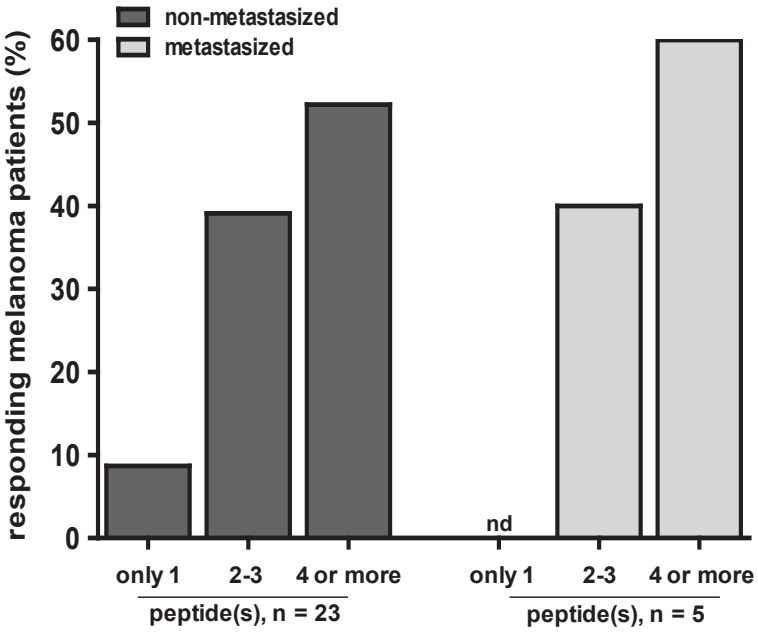


**Figure 21. Number of recognized 50aa polypeptides of melanoma TAAs per responding melanoma patients.** In the majority, when analyzed responders of non-metastasized and metastasized melanoma stages, TAA-reactive T cell responses were found in parallel, against four or more polypeptides. Only the samples, where at least four peptides could be tested have been analyzed. n, number of patients; nd, not detectable

### 8.1.4. Tumor antigen-reactive T cell responses to polypeptides in dysplastic nevi patients

A dysplastic nevus is a lesion that can give rise to malignant melanoma. Therefore, patients with dysplastic nevi, as a kind of a pre-malignant cohort, were also examined for the presence of spontaneously induced tumor antigen-reactive memory T cell responses in the PB. After the resection of the dysplastic nevi lesion, IFNγ ELISPOT assays were performed using autologous T cells and dendritic cells. For T cell reactivation, the dendritic cells were pulsed with the 50aa polypeptides of melanoma TAAs. Two patients were investigated and both showed significantly increased T cell responses against the tested polypeptides (exemplarily depicted for patient # 53 in Fig. 22).

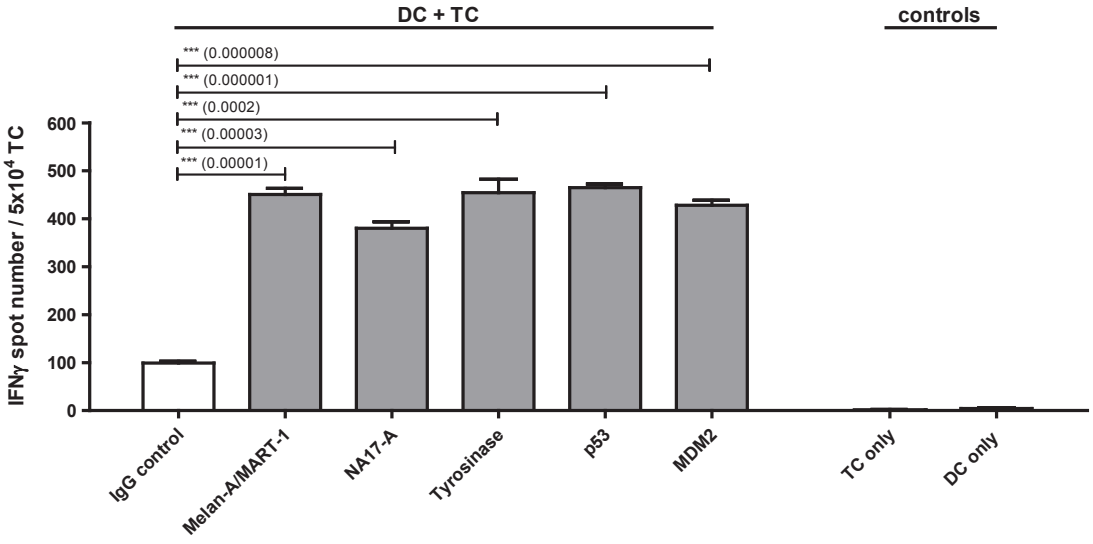


**Figure 22. Representative IFNγ ELISPOT result of a patient with a dysplastic nevi lesion.** In patient # 53, polyvalent significantly increased tumor antigen-reactive T cell responses were detected against all investigated polypeptides (Melan-A/MART-1, NA17-A, Tyrosinase, p53, MDM2), after the resection of the dysplastic nevus. In comparison, single cultures of T cells and dendritic cell were performed as controls. For statistical analysis, an unpaired two-tailed t test was performed. DC, dendritic cells; Mean ± SEM; TC, T cells; *** p value ≤ 0.001

### 8.1.5. HLA-unrestricted $CD4^+$ and $CD8^+$ T cell responses to polypeptides

The 50aa polypeptides were constructed to cover at least one known HLA-A2-restricted epitope (Tab. 8). Predicted by database analysis, other putative MHC class I and class II epitopes were covered in addition. In order to test, whether $HLA\text{-}A2^-$ patient-derived T cells were able to recognize the polypeptides, the patient samples were separated according to their expression of HLA-A2 into $HLA\text{-}A2^+$ and $HLA\text{-}A2^-$ samples. The HLA-A2 expression was assessed by flow cytometry and is representatively shown in Fig. 23A. To guarantee the function of the cellular surface staining, a $HLA\text{-}A2^+$ cell line was always co-stained in parallel as positive control.

The cumulative data of 20 $HLA\text{-}A2^+$ and 18 $HLA\text{-}A2^-$ non-metastasized as well as 4 $HLA\text{-}A2^+$ and 4 $HLA\text{-}A2^-$ metastasized melanoma patients showed that $HLA\text{-}A2^-$ and $HLA\text{-}A2^+$ patient-

derived T cells can specifically recognize the polypeptides, in a similar manner (Fig. 23B). In 70 % of all analyzed HLA-A2$^+$ and in 83.3 % of all HLA-A2$^-$ non-metastasized melanoma patients, significantly increased tumor antigen-reactive memory T cell responses were detected against at least one of the tested polypeptides, in comparison to the IgG control. HLA-A2$^+$ T cells, derived from metastasized patients recognized the polypeptides in 50 % and HLA-A2$^-$ T cells in 75 % of all performed ELISPOT assays (Fig. 23B).

The HLA-A2 expression was also investigated in 2 dysplastic nevi patients, after the resection of the lesion. Both patients-derived T cells specifically recognized the polypeptides, whereas one patient was HLA-A2$^+$ and the other HLA-A2$^-$. The T cell response of the HLA-A2$^-$ dysplastic nevi patient # 53 is shown in Fig. 22.

In general, peptides are presented to CD8$^+$ T cells by MHC class I molecules like HLA-A2, whereas CD4$^+$ T cells need the presentation through MHC class II, for peptide recognition. As shown in Appendix 13.12., the generated polypeptides contained predicted MHC class II-restricted epitopes that could theoretically be recognized by CD4$^+$ T cells. In order to investigate, whether CD4$^+$ T cells of malignant melanoma patients were able to respond to these polypeptides, CD4$^+$ T cells were separated from CD8$^+$ T cells using CD4 MicroBeads. The obtained purity of CD4$^+$ isolated T cells was >99% (Fig. 24A). Performing IFNγ ELISPOT assays, CD4$^+$ as well as CD8$^+$ T cells of the same patient significantly recognized the tested melanoma 50aa polypeptides (Figs. 24C and D). The cumulative data of 2 non-metastasized melanoma patients (in total 15 individual performed tests) showed that after primary tumor resection the frequency of TAA-reactive memory T cells among CD4$^+$ and CD8$^+$ T cells was comparable (Fig. 24B). In the HLA-A2$^+$ patient # 52, strong CD8$^+$ T cell responses against the tumor antigens Melan-A/MART-1 and p53 were observed, indicating the presence of well defined HLA-A2-restricted epitopes, presented by the generated melanoma polypeptides. In addition, CD4$^+$ T cells of the same patient also revealed increased responses against both polypeptides (Fig. 24C). The analysis of the HLA-A2$^-$ patient # 58 indicated that besides HLA-A2 further MHC class I-restricted epitopes were present in the polypeptide sequences. This is exemplarily shown by significant increased CD8$^+$ T cell responses against the polypeptide for Tyrosinase (Fig. 24D). In the same patient, spontaneously induced tumor antigen-reactive memory CD4$^+$ T cell responses were present and revealed strong IFNγ production in response to almost all investigated polypeptides. This observation also indicated the predicted presence of MHC class II-restricted epitopes that were efficiently presented to T cells.

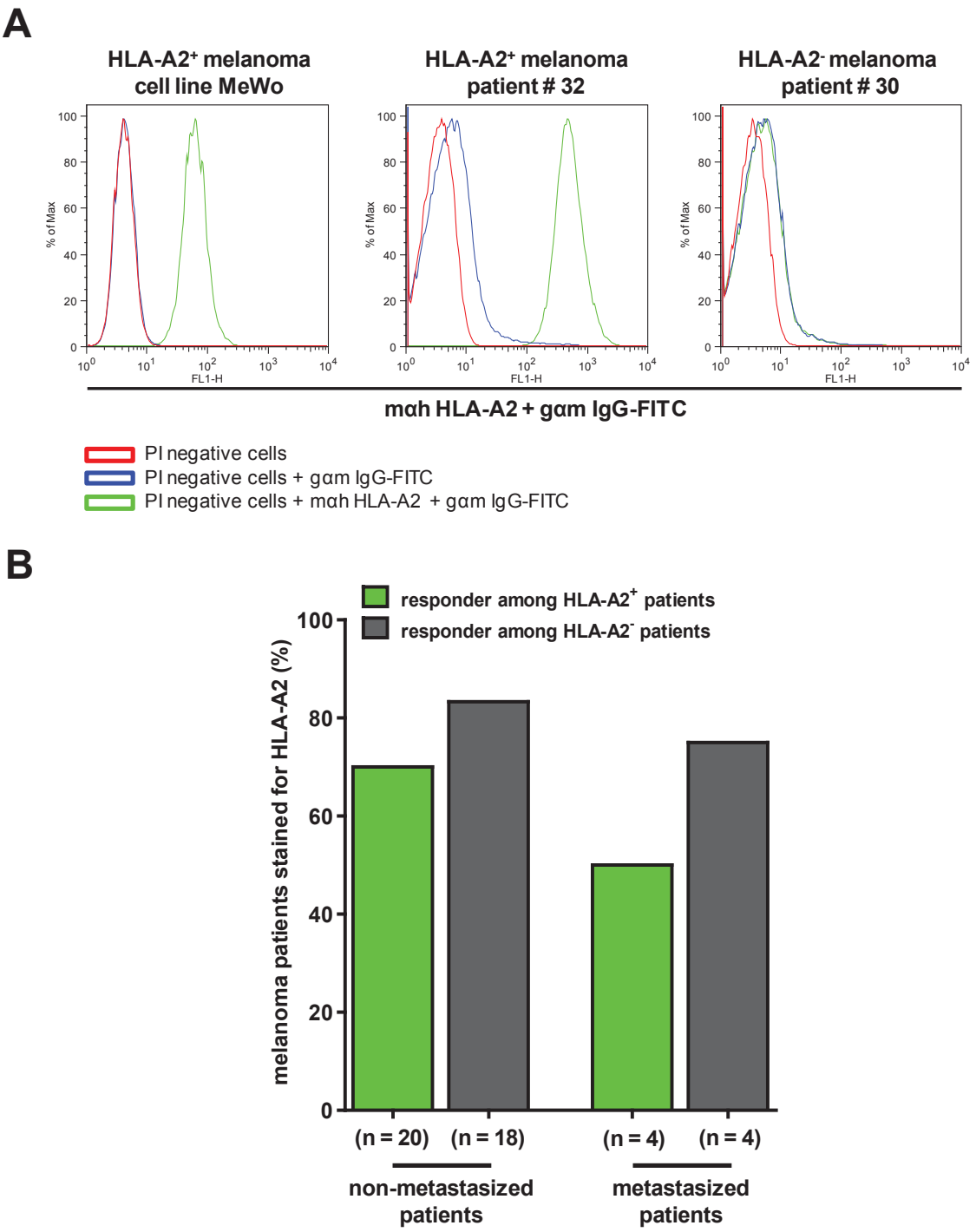


**Figure 23. Proportion of HLA-A2$^+$ and HLA-A2$^-$ melanoma patients with spontaneously induced tumor antigen-reactive T cell responses.** The 50aa polypeptides were recognized by HLA-A2$^+$ and HLA-A2$^-$ T cells of non-metastasized and metastasized melanoma patients. **A**) HLA-A2 flow cytometry staining was used to separate melanoma patient derived cells, concerning to their HLA-A2 expression into HLA-A2$^+$ and HLA-A2$^-$ cohorts. **B**) T cells of HLA-A2$^+$ and HLA-A2$^-$ patients recognized the polypeptides to a similar extent. Responder, significantly increased number of IFNγ spots by T cells, in response to at least one TAA peptide/dendritic cell setting compared to control human IgG peptide/dendritic cell setting. n, number of patients

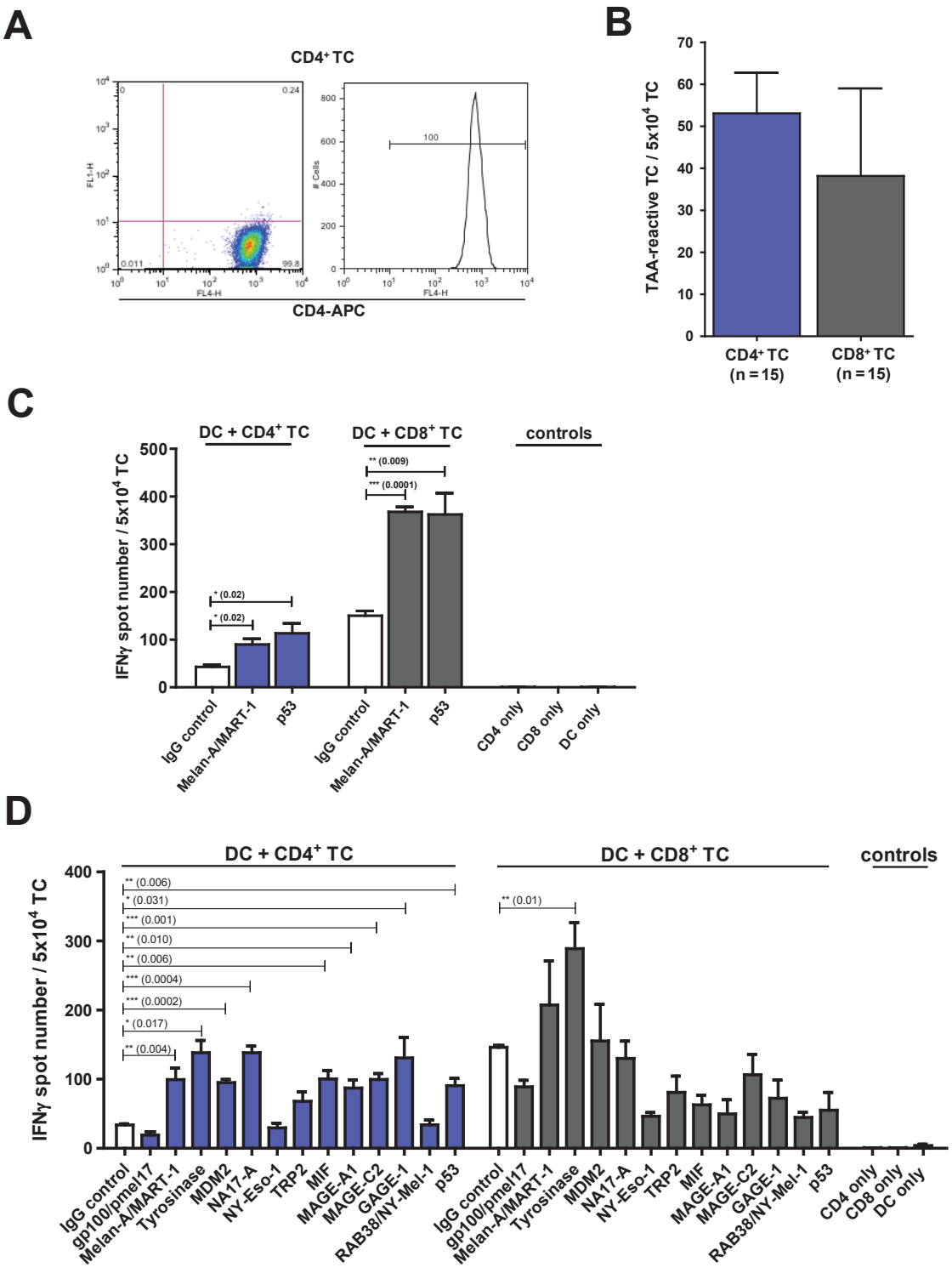


**Figure 24. The 50aa polypeptides are significantly recognized by CD4$^+$ and CD8$^+$ T cells of the same melanoma patients. A**) The purity of CD4$^+$ T cells, isolated with CD4 MicroBeads, was investigated by flow cytometry staining. Dead cells were excluded via 7AAD (left, dot plot; right, histogram). **B**) Frequency of TAA-reactive T cells among CD4$^+$ and CD8$^+$ T cells. **C**) CD4 and CD8 T cell responses of HLA-A2$^+$ patient # 52 (stage IA). **D**) CD4 and CD8 T cell responses of HLA-A2$^-$ patient # 58 (stage IA). For statistical analysis, an unpaired two-tailed t test was performed. DC, dendritic cells; Mean ± SEM; n, number of tests; TC, T cells; * p value ≤ 0.05; ** p value ≤ 0.01; *** p value ≤ 0.001

### 8.1.6. T cell responses to the 13 individual polypeptides in non-metastasized melanoma patients

The T cell responses against the 13 individual 50aa melanoma polypeptides were investigated in a cohort of 36 non-metastasized melanoma patients after primary tumor resection (36 out of 38 patients, since 2 were used for the $CD4^+$ and $CD8^+$ T cell investigation; cf., 8.1.5). In summary, high T cell reactivities were detected against all tested polypeptides. The highest responses were received for Melan-A/MART-1 (63.9 %), Tyrosinase (61.5 %) and NA17-A (41.4 %), followed by MDM2 (39.1 %), p53 (38.2 %), MAGE-C2 (36.4 %), MAGE-A1 (31.3 %), NY-Eso-1 (31.3 %), RAB38/NY-Mel-1 (30.8 %) and GAGE-1 (30.8 %). Even the lowest T cell responses against gp100/pmel17 (23.8 %), MIF (21.4 %) and TRP2 (21.1 %) were above 20 % response rate (Figs. 25A and B).

For all of the examined polypeptides, frequencies of TAA-reactive T cells were analyzed in addition. For instance, within $5x10^4$ $CD3^+$ T cells, ~69 Melan-A/MART-1 and 73 Tyrosinase-reactive T cells as well as 51 NA17-A and 55 MDM2- reactive T cells were detected (Fig. 25C). After short-term reactivation for 40 h using the polypeptides, the percentage of TAA-reactive memory T cells in the PB of non-metastasized melanoma patients, after primary tumor resection was 0.15 % for Tyrosinase (highest frequency) to 0.03 % for TRP2 (lowest frequency). The combined percentages of TAA-reactive T cell among total $CD3^+$ T cells in response to all 13 investigated melanoma polypeptides was 1.09 % (Fig. 25C).

### 8.1.7. T cell frequencies after primary tumor resection in non-metastasized melanoma patients over time

To investigate how the frequencies of TAA-reactive memory T cells behave after primary tumor resection over time, different time points (0-15 d, 16-30 d, 31-45 d, 46-60 d, >60 d) after tumor resection were analyzed for the presence of spontaneously induced tumor antigen-reactive memory T cells (Figs. 26A and B). Thereby, the T cell reactivities were measured using short-term IFNγ ELISPOT assays.

In summary, the general frequency of TAA-reactive T cells was strongly increased after primary tumor resection over time. Shortly after tumor resection (0-15 d), a mean frequency of 26 TAA-reactive T cells per $5x10^4$ total $CD3^+$ TC was detected. The highest frequency (mean 132 TAA-reactive T cells per $5x10^4$ total $CD3^+$ TC) was observed 46-60 d after tumor resection. This demonstrates a strong increase in TAA-reactive T cell frequency in the PB of non-metastasized melanoma patients over time (Figs. 26A and B). At later time points, the tumor antigen-reactive memory T cell frequency decreased to a baseline level (>60 d, mean 21 TAA-reactive T cells per $5x10^4$ total $CD3^+$ T cells; Figs. 26A and B).

Moreover, the individual frequencies of Melan-A/MART-1, Tyrosinase, NA17-A and p53 reactive T cells after tumor resection over time are shown in Figs. 27A-D. All four specificities of TAA-reactive T cells (Figs. 27A-D) showed a similar pattern than the cumulative data of all T cell

frequencies (Fig. 26). The Melan-A/MART-1, Tyrosinase as well as NA17-A and p53 memory T cell frequencies were significantly increased after tumor resection over time, while the strongest increase was detected for Tyrosinase specific T cells (Figs. 27A-D).

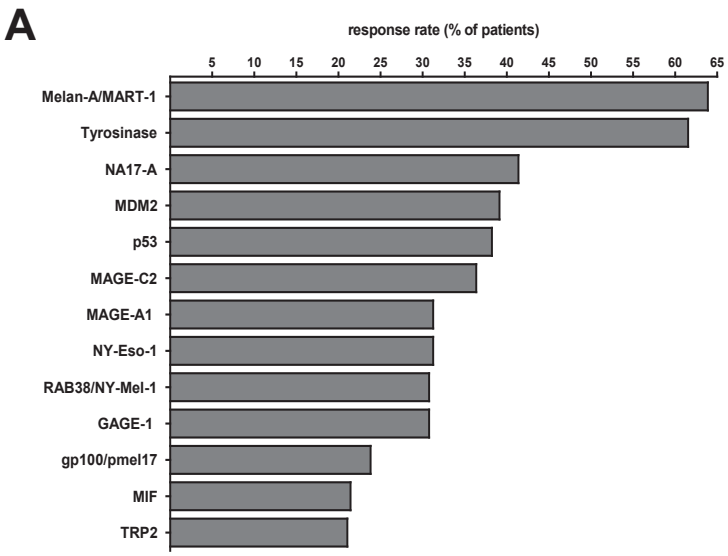


**B**

| 50aa polypeptides | number of patients tested | significant increased TC responses |
|---|---|---|
| Melan-A/MART-1 | 36 | 23 |
| Tyrosinase | 26 | 16 |
| NA17-A | 29 | 12 |
| MDM2 | 23 | 9 |
| p53 | 34 | 13 |
| MAGE-C2 | 11 | 4 |
| MAGE-A1 | 16 | 5 |
| NY-Eso-1 | 16 | 5 |
| RAB38/NY-Mel-1 | 13 | 4 |
| GAGE-1 | 13 | 4 |
| gp100/pmel17 | 21 | 5 |
| MIF | 14 | 3 |
| TRP2 | 19 | 4 |

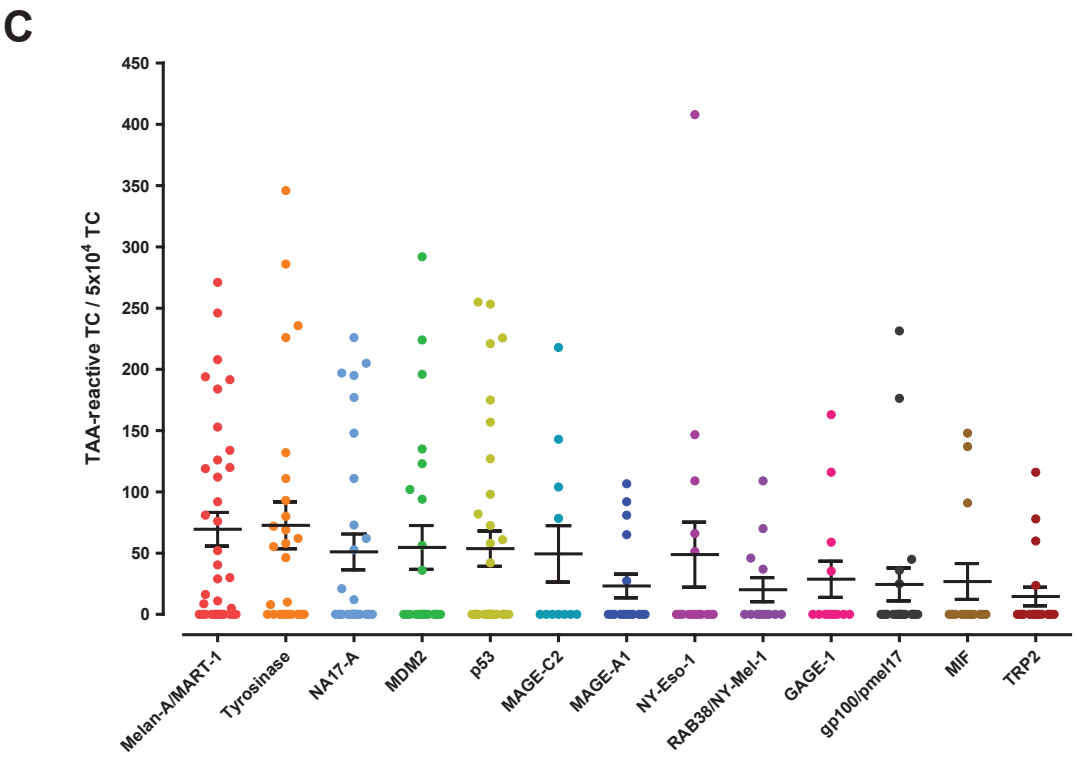


**Figure 25. Recognition of the 13 individual polypeptides by T cells of non-metastasized melanoma patients after primary tumor resection. A**) Response rate of 36 melanoma patients to the 13 investigated polypeptides. **B**) Overview on the tested polypeptides, regarding the numbers of patients studied. Moreover, the numbers of patients are indicated, for those significant increased T cell responses were detected. **C**) Frequency of TAA-reactive T cells against individual polypeptides. Mean ± SEM; TC, T cells

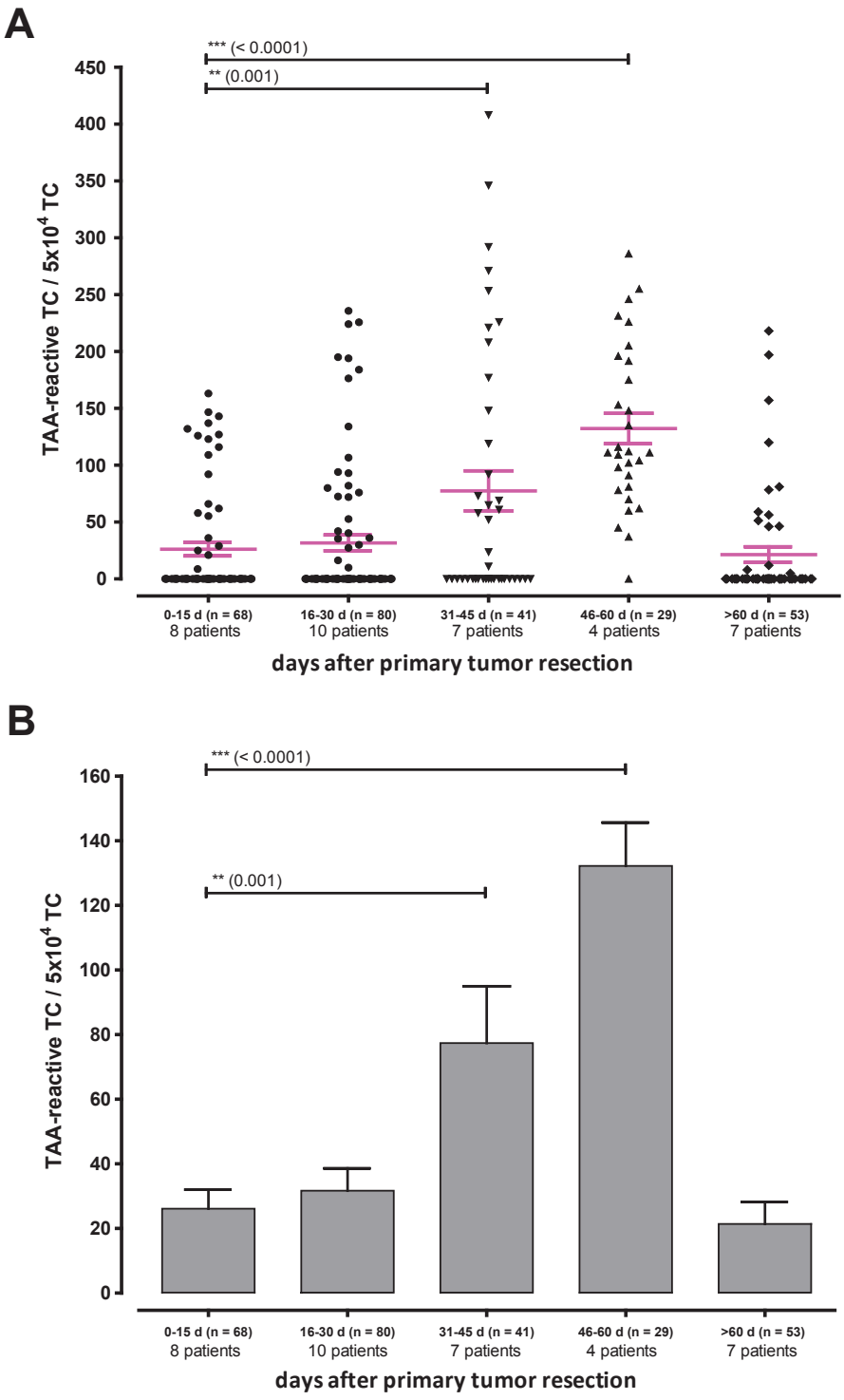


**Figure 26. Frequency of spontaneously induced tumor antigen-reactive memory T cells in non-metastasized melanoma patients after primary tumor resection over time.** The cumulative data of T cell frequencies in response to the 50aa polypeptides after primary tumor resection over time are presented. For the analysis, only the significant increased individual T cell frequencies per investigated polypeptides in comparison to the human IgG control were used. **A**) The scatter plot shows the increase of TAA-reactive memory T cells investigated in 36 non-metastasized melanoma patients after tumor resection over time, up to d60. **B**) The column bar graph indicates the same data as shown in A. For statistical analysis, an unpaired two-tailed t test was performed. Mean ± SEM; n, number of tests; TC, T cells; ** p value ≤ 0.01; *** p value ≤ 0.001

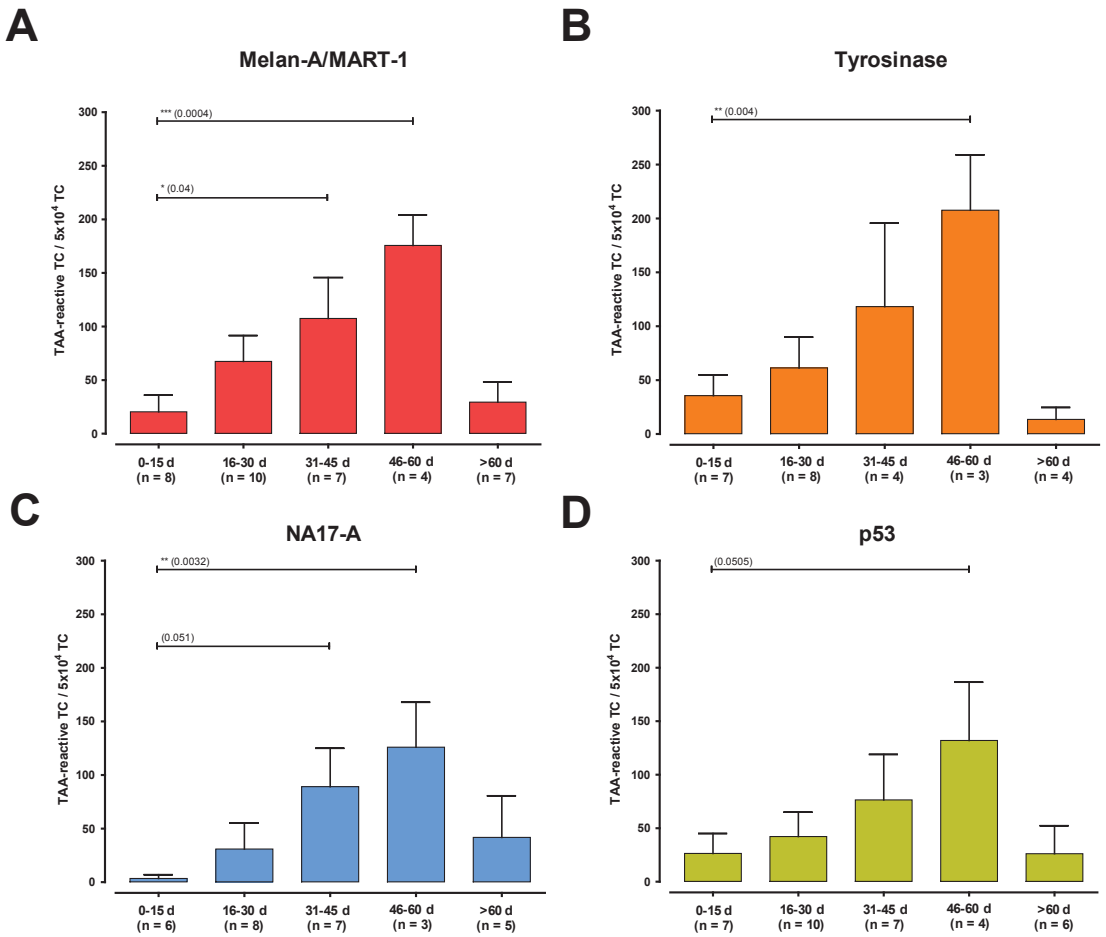


**Figure 27. Frequency of Melan-A/MART-1, Tyrosinase, NA17-A and p53 tumor antigen-reactive T cells in non-metastasized melanoma patients after primary tumor resection over time.** The graphs show the increase of TAA-reactive T cells, specific for **A**) Melan-A/MART-1, **B**) Tyrosinase, **C**) NA17-A and **D**) p53, investigated in the PB of non-metastasized melanoma patients after tumor resection over time. The individual T cell frequencies per analyzed polypeptides are indicated in response to the IgG control. For statistical analysis, an unpaired two-tailed t test was performed. Mean ± SEM; n, number of patients; TC, T cells; * p value ≤ 0.05; ** p value ≤ 0.01; *** p value ≤ 0.001

### 8.1.8. Analysis of the alteration of T cell responses and plasma autoimmune markers in response to the surgical removal of a lesion

In the case, that a skin lesion was suspected to be a skin cancer, a total removal of the lesion (excisional skin biopsy) was performed by dermatologists and diagnosed by pathologists. During the primary surgical removal, the incision was performed elliptical or eye-shaped narrow around the lesion. The wound was then sutured with stitches. Representative images of a surgical removal of a skin lesion - dysplastic nevi - are shown in Fig. 28. In general, the intervention performed to remove a dysplastic nevus or a non-metastasized melanoma indicates a minimal invasive surgery. It is narrowly defined and has only low removal risks including scar formation and redness.


**Figure 28. Representative images of a surgical dysplastic nevi removal.** Micrographs show a dysplastic nevi lesion (indicated by arrow) before (**A**) and after (**B**) the surgical removal, on the back of a patient. Two weeks later, the stitches were taken out (**C**).

To analyze, whether the revealed increase of TAA-reactive memory T cell responses after resection over time, occurred as an unspecific response or side effect to the surgical intervention, blood samples of the same patients were investigated before and after the surgical removal of a lesion. The repeated analysis of the same patient, before and after resection, demonstrated that TAA-reactive T cell responses specifically increased, while unspecific responses against control IgG did not comparably alter over time (Figs. 29A and B). Furthermore, if an unspecific T cell response, caused by the surgical resection, had taken place, an increase in IFNγ spot numbers would had to be expected up to 13 d after resection. The IFNγ spot numbers by T cells (specific against TAAs and unspecific against IgG) were not elevated, 13 d after resection, compared to the obtained IFNγ spot numbers of T cells before the intervention (Fig. 29A).

In addition, autoimmune markers were investigated in the plasma of patients before and after resection. Therefore, the anti-nuclear (ANA) and anti-neutrophilic cytoplasmic auto-Abs (ANCA) as well as the rheumatoid factor were analyzed. In the case of a positive ANCA analysis, an additional test for perinuclear ANCAs (p-ANCA) was performed, against myeloperoxidase (MPO) a target antigen of the p-ANCAs. In summary, comparing the values of autoimmune markers before and after tumor resection, in none of the tested dysplastic nevi as well as non-metastasized melanoma patients, a considerable increase of any autoimmune marker could be detected (Tab. 10).

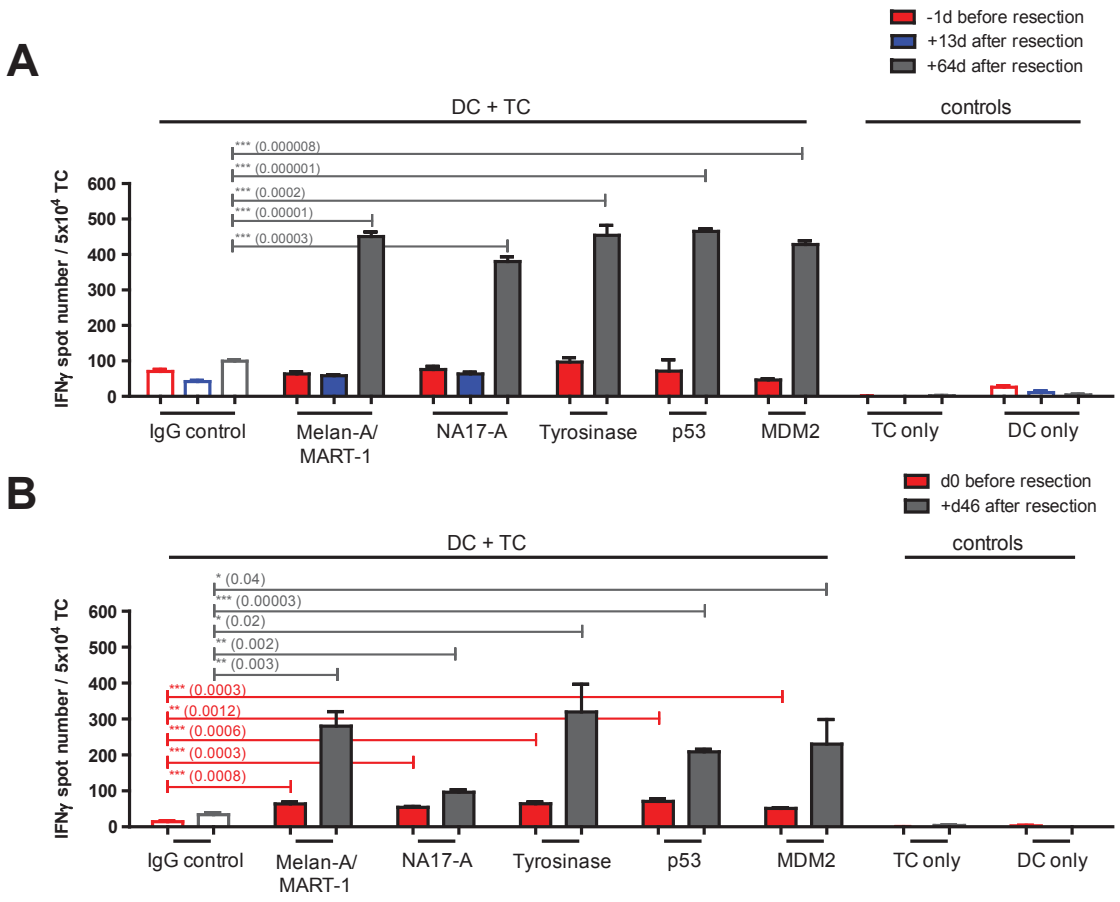


**Figure 29. TAA- and IgG-reactive T cell responses before and after surgical resection.** **A**) Significantly increased tumor antigen-reactive T cell responses developed after the resection, compared to spot numbers before resection in the PB of dysplastic nevi patient # 53. The IFNγ spot numbers of TAA-reactive T cells were strongly increased, 64 d but not 13 d, after resection. T cell responses against the endogenous control antigen (human IgG) were not comparably altered. **B**) Melanoma patient # 57 showed, before and after resection, increased T cell responses against all tested 50aa polypeptides. Thereby, the TAA-reactive T cell frequencies strongly further increased after resection, while T cell responses against IgG were not altered in a comparable attitude. For statistical analysis, an unpaired two-tailed t test was performed. DC, dendritic cells; Mean ± SEM; TC, T cells; * p value ≤ 0.05; ** p value ≤ 0.01; *** p value ≤ 0.001

| *reference range:* | *1:80 titer* | *<1:10 titer* | *<9.0 U/ml* | *<25 IU/ml* |
|---|---|---|---|---|

| patient | time between primary resection (d0) and PB collection | anti-nuclear Ab (ANA) | anti-neutrophilic cytoplasmic Ab (ANCA) | perinuclear anti-neutrophilic cytoplasmic Ab (p-ANCA, MPO) | rheumatoid factor |
|---|---|---|---|---|---|
| 1 (DPN) | **d-1** | 1:40 | **1:32** | <9.0 | <7.0 |
| | **d13** | negative | **1:10** | <9.0 | 13.0 |
| | **d64** | 1:40 | **1:32** | <9.0 | 10.3 |
| 2 (DPN) | **d-1** | **1:320** | negative | n.d. | 9.7 |
| | **d57** | **1:160** | negative | n.d. | 7.7 |
| 3 (MM) | **d0,** direct before resection | **1:160** | negative | n.d. | **25.9** |
| | **d46** | **1:160** | negative | n.d. | **38.6** |
| 4 (MM) | **d0,** direct before resection | negative | negative | n.d. | < 7.0 |
| | **d45** | negative | negative | n.d. | 8.7 |
| 5 (MM) | **d-1** | negative | negative | n.d. | **48.8** |
| | **d40** | negative | negative | n.d. | **42.6** |

**Table 10. Investigation of plasma autoimmune markers.** The plasma of 2 dysplastic nevi patients (DPN) and 3 patients with non-metastasized melanoma (MM) were analyzed for the alteration of autoimmune markers. The auto-Abs ANA, ANCA, p-ANCA and the rheumatoid factor were investigated, before and after surgical resection of the respective lesion. The reference ranges of the respective markers are indicated in the headline of the table. Values out of the reference range are labeled in green bold numbers. Ab, antibody; MPO, myeloperoxidase; n.d., not determined

### 8.1.9. Analysis of a Treg-dependent control of spontaneous T cell responses

It has been shown that tumor-directed T cell responses can be affected by regulatory T cells (Treg; cf., Wang et al., 2004; Bonertz et al., 2009). Therefore, in a next step, a potential role of Treg in controlling spontaneously induced tumor antigen-reactive memory T cell responses, in the PB of patients with dysplastic nevi or non-metastasized melanoma, was analyzed.

In order to detect Treg, an intracellular/intranuclear flow cytometry staining for $CD3^+CD4^+CD25^+$ $Foxp3^+$ T cells was performed. Representative dot plots thereof are shown in Fig. 30A. The percentage of Treg in the PB of non-metastasized melanoma patients after primary tumor resection was comparable to the Treg percentage, in healthy donors (Fig. 30B; median: melanoma 5.0, healthy donor 4.6). Furthermore, to investigate a potential contribution of Treg in controlling spontaneously induced tumor antigen-reactive memory T cell responses, Treg were depleted from the $CD3^+CD4^+$ T cell fraction using $\alpha$CD25-magnetic beads. The depletion of Treg was performed as shown in Fig. 31. Using this protocol, revealed by flow cytometry, the percentage of $CD25^+Foxp3^+$Treg in the $CD3^+CD4^+$ T cell population was strongly reduced. Representative data of melanoma patient # 31 showed a reduction of the Treg percentage from 4.66 to 0.89 % (Fig. 31).

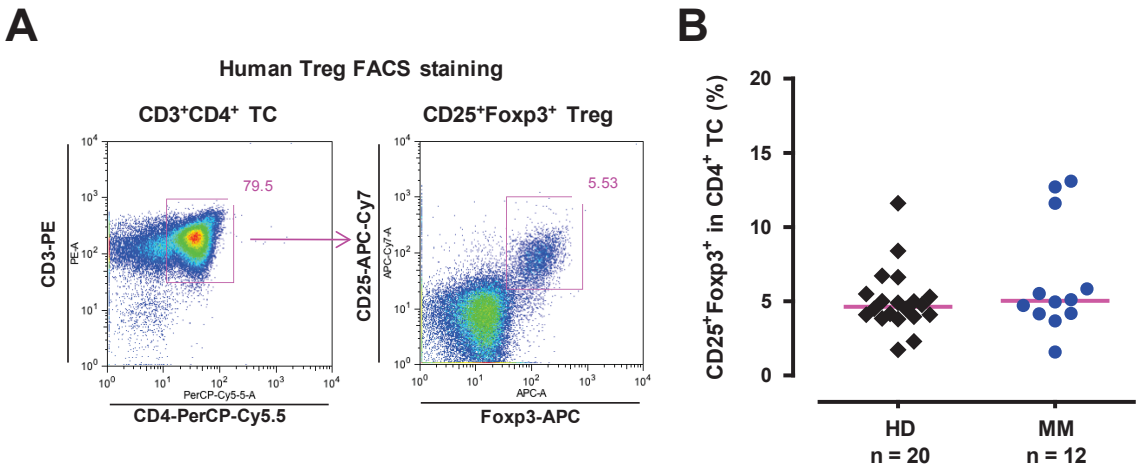


**Figure 30. Percentage of Treg in the PB of healthy donors and non-metastasized melanoma patients after primary tumor resection.** The percentage of Treg was determined by flow cytometry staining. **A**) Representative FACS dot plots of melanoma patient # 29 are presented. Treg were gated on the basis of $CD3^+CD4^+$ cells (left plot, indicated by quadrant) using Abs against CD25 and Foxp3 (right plot, indicated by quadrant). The numbers in the dot plots, indicate the percentage of the respective cell populations. **B**) Cumulative percentage of Treg in the PB of 20 healthy donors (HD) and 12 non-metastasized melanoma patients (MM), after tumor resection. Some of the Treg numbers of HD, used for cumulative calculation, were kindly provided by Dr. Y. Ge, Unit of Translational Immunology, DKFZ. n, number of HD or MM patients respectively; TC, T cells

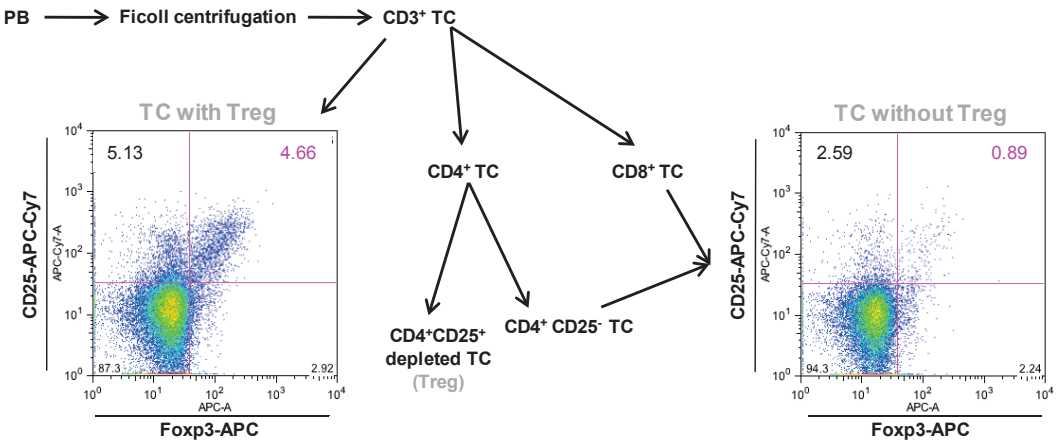


**Figure 31. Depletion of Treg.** After ficoll gradient centrifugation, $CD3^+$ T cells were negatively isolated. One part, was directly used (TC with Treg) and from the second part, $CD4^+$ and $CD8^+$ T cells were isolated. $CD25^+$ cells were depleted from the $CD4^+$ fraction ($CD4^+CD25^+$ Treg). Finally, $CD8^+$ T cells were recombined with $CD4^+CD25^-$ T cells (TC without Treg). The T cell fractions were stained for the presence of $CD3^+CD4^+CD25^+Foxp3^+$ Treg by flow cytometry. The numbers in the dot plots indicate the percentage of the respective cell population. Representative data of non-metastasized melanoma patient # 31 are shown. TC, T cells

In some of the non-metastasized melanoma patients, the depletion of $CD4^+CD25^+$ Treg, from the T cell fraction, resulted in a strong increase of TAA-reactive T cell responses, compared to non-Treg depleted cell populations. For example, in melanoma patient # 9 increased TAA-reactive memory T cell responses against Melan-A/MART-1, p53 and Tyrosinase were only detectable, after the Treg depletion (Fig. 32). This finding was observed for ~16 % of the investigated patient samples. Thereby, preferentially Melan-A/MART-1, p53 and Tyrosinase-reactive T cell responses were shown to be suppressed by Treg.

However, in regard to the cumulative data of 36 non-metastasized melanoma patients after primary tumor resection, the frequency of spontaneously induced tumor antigen-reactive memory T cells was not further increased after Treg depletion (Fig. 33). The same finding was observed for the cumulative data of all 13 individual 50aa polypeptides (Fig. 34). Thereby, compared to the respective total $CD3^+$ non-Treg depleted cell fractions, the cumulative T cell frequencies for all tested polypeptides were not further increased after Treg depletion (Fig. 34). In addition, Treg depletion did not led to a further increase of cumulative TAA-reactive T cell frequencies at any time point, analyzed after tumor resection (Fig. 35). Without Treg depletion, in comparison to healthy donors, the cumulative frequencies of TAA-reactive memory T cells were strongly elevated in the PB of non-metastasized melanoma patients after resection of the tumor (Fig. 33).

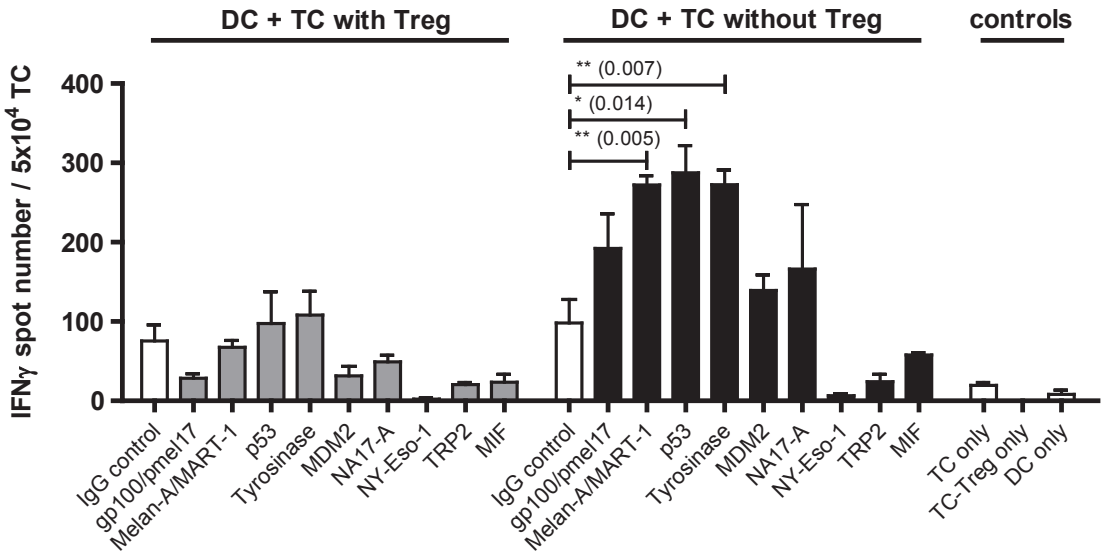


**Figure 32. Representative IFNγ ELISPOT result of a non-metastasized stage IA melanoma patient analyzing T cells with and without Treg.** Increased tumor antigen-reactive T cell responses against 50aa polypeptides could only be detected after Treg depletion from the investigated T cell subset of melanoma patient # 9. As controls, single cultures of dendritic cells (DC only) as well as T cells with Treg (TC only) and T cells without Treg (TC-Treg only) were investigated. For statistical analysis, an unpaired two-tailed t test was performed. DC, dendritic cells; Mean ± SEM; TC, T cells; * p value ≤ 0.05; ** p value ≤ 0.01

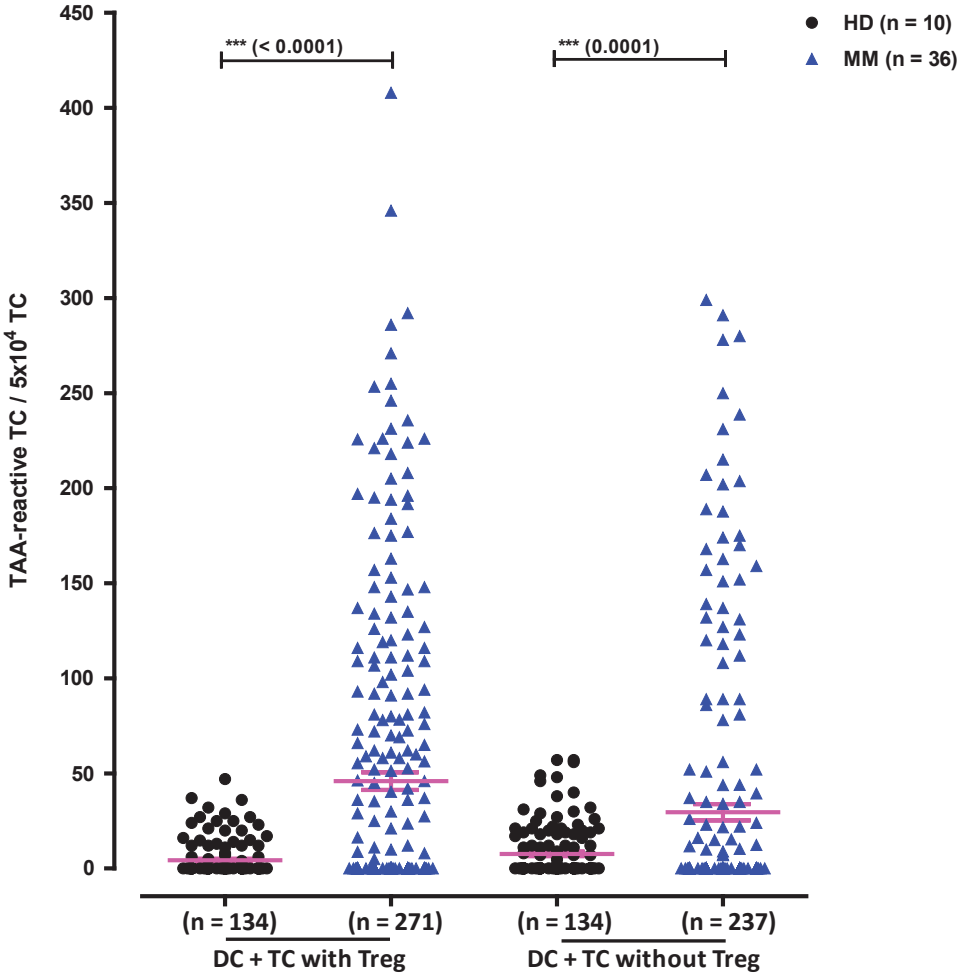


**Figure 33. Frequency of TAA-reactive T cells with and without Treg depletion in healthy donors and non-metastasized melanoma patients.** Cumulative data of TAA-reactive memory T cell frequencies against the 13 individual polypeptides. The T cell frequencies were analyzed without depleting Treg (TC with Treg) as well as with Treg depletion (TC without Treg). The cells of 36 non-metastasized melanoma patients (MM) as well as 10 healthy donors (HD) were investigated. For statistical analysis, an unpaired two-tailed t test was performed. DC, dendritic cells; Mean ± SEM; n, number of tests; TC, T cells; *** p value ≤ 0.001

In subsequent experiments, the influence of a tumor or pre-malignant lesion on the nature of spontaneously induced tumor antigen-reactive memory T cell responses was addressed. Therefore, dysplastic nevi and non-metastasized melanoma patients were analyzed for TAA-reactive T cell responses before and after surgical resection. Before tumor resection, increased TAA-reactive T cell responses were present, without depletion of Treg, in melanoma patient # 57 (Fig. 36). Treg depletion, only marginally increased the tumor-reactive T cell frequencies. After tumor resection, the tumor antigen-reactive T cell responses were strongly elevated and a Treg depletion did not led to a further increase (Fig. 36). The cumulative data of 3 dysplastic nevi as well as 2 non-metastasized melanoma patients showed that TAA-reactive memory T cell responses, against the 50aa polypeptides, were already present before resection. Moreover, at this time, a depletion of Treg did not led to a significant increase of the T cell frequencies. Compared to healthy donors, the T cell frequencies of both patient cohorts were clearly elevated (Fig. 37). After surgical

resection, TAA-reactive memory T cell frequencies were shown to be increased, compared to the frequencies, measured before resection. Whereas, an additional increase of T cell frequencies in response to Treg depletion was not observed (Fig. 37).

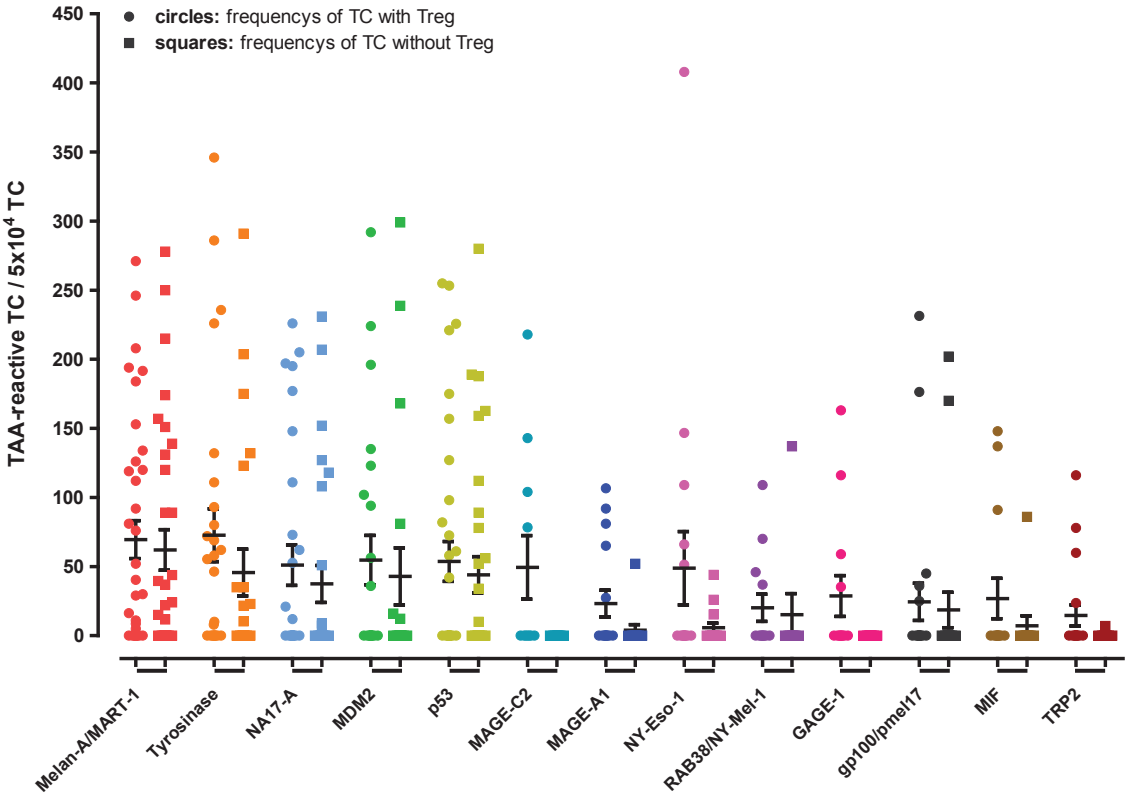


**Figure 34. Recognition of the 13 individual polypeptides by T cells of non-metastasized melanoma patients with and without Treg depletion.** Autologous dendritic cells were pulsed with melanoma polypeptides and a co-culture with autologous T cells was performed. Thereby, T cell fractions with (circles) and without Treg (squares) were analyzed in parallel. The cumulative data of 36 non-metastasized melanoma patients is displayed and only significantly increased T cell responses are shown, compared to the human IgG control. The frequencies of TAA-reactive memory T cells for the individual polypeptides are not elevated after depletion of Treg. TC, T cells

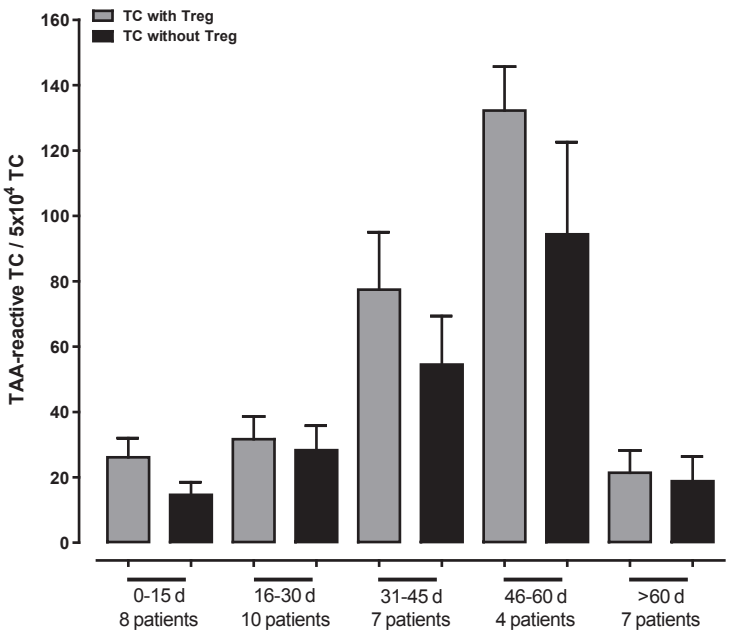


**Figure 35. Frequency of spontaneously induced TAA-reactive T cells with and without Treg depletion, in non-metastasized melanoma patients after primary tumor resection, over time.** The frequency of TAA-reactive memory T cells is increased, after primary tumor resection up to d60, in 36 non-metastasized melanoma patients (gray columns). The depletion of Treg did not further increase the frequency of tumor-reactive memory T cells (black columns). The TAA-reactive T cell frequencies represent the cumulative data, from the T cell frequencies, against the 13 individual 50aa melanoma polypeptides. For the cumulative analysis, the significant increased individual T cell frequencies per analyzed peptides in response to the human IgG control were used. TC, T cells

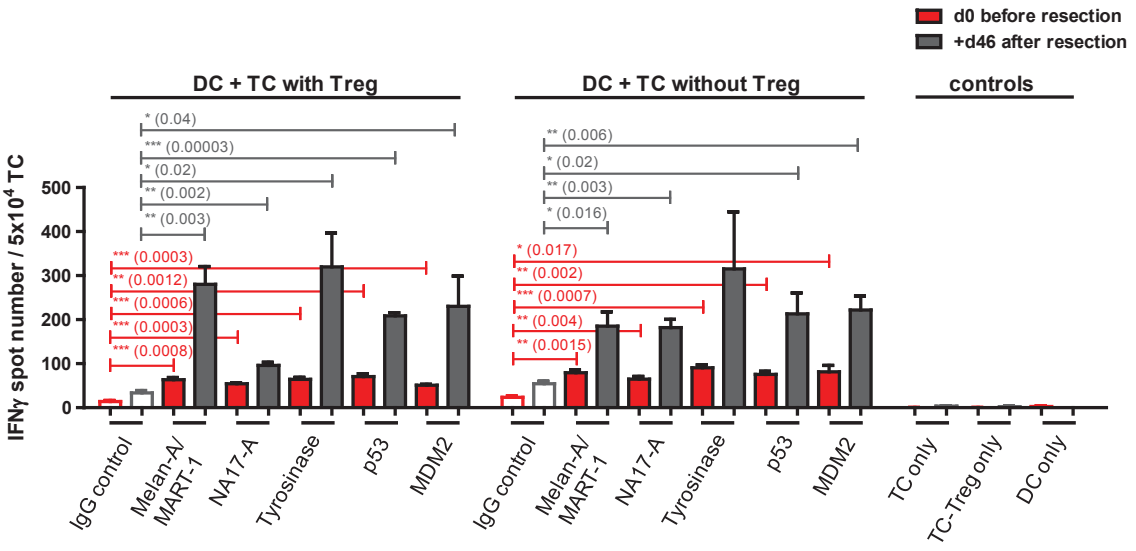


**Figure 36. TAA-reactive T cell responses with and without Treg depletion before and after surgical resection.** In melanoma patient # 57 the T cell responses were marginal elevated in IFNγ spot numbers after Treg depletion, before but not after resection of the primary tumor. As controls, single cultures of dendritic cells (DC only) as well as T cells with Treg (TC only) and T cells without Treg (TC-Treg only) were investigated. For statistical analysis, an unpaired two-tailed t test was performed. DC, dendritic cells; Mean ± SEM; TC, T cells; * p value ≤ 0.05; ** p value ≤ 0.01; *** p value ≤ 0.00

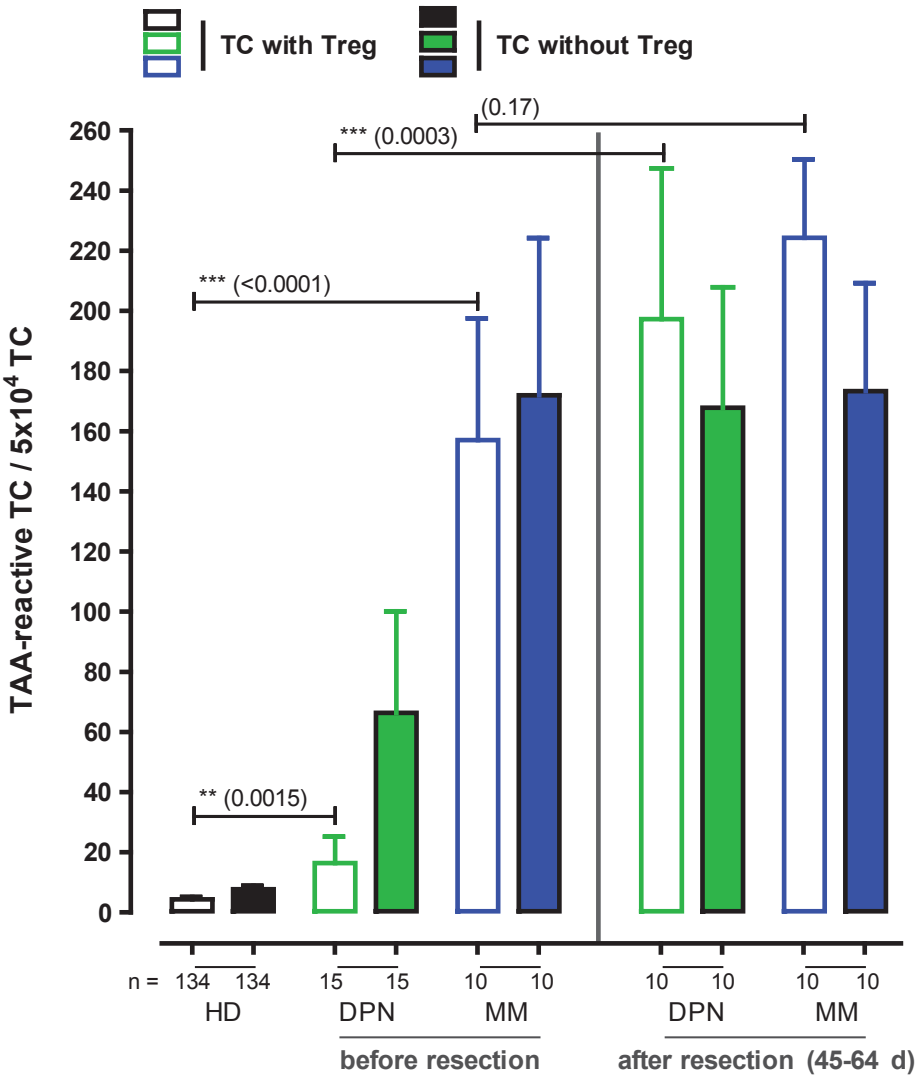


**Figure 37. Frequency of TAA-reactive T cells with and without Treg depletion, in dysplastic nevi and non-metastasized melanoma patients, before and after surgical resection.** The IFNγ ELISPOT data of 3 dysplastic nevi (DPN) and 2 non-metastasized melanoma (MM) patients, before and after resection is shown. Moreover, the data of 10 healthy donors (HD) are depicted. Before the resection of the lesion, the frequency of TAA-reactive memory T cells was clearly elevated in DPN or MM, compared to HD. The depletion of Treg did not significantly increase the T cell frequency in both patient cohorts. The blood of the same patients was investigated for a second time on d45, d46, d57 or d64. After surgical resection, the tumor-specific T cell frequencies were increased, compared to the obtained responses, before resection. A depletion of Treg had no additional impact. The TAA-reactive memory T cell frequencies represent the cumulative data, from the individual T cell frequencies against the 50aa melanoma polypeptides Melan-A/MART-1, NA17-A, Tyrosinase, p53 and MDM2. For the cumulative analysis, the significant increased individual T cell frequencies per analyzed peptides, compared to the human IgG control were used. For statistical analysis, an unpaired two-tailed t test was performed. Mean ± SEM; n, number of tests; TC, T cells; ** p value ≤ 0.01; *** p value ≤ 0.001

### 8.1.10. Antigen-specific Treg in melanoma and dysplastic nevi patients

A Treg specificity assay on the basis of a [$^3$H]-Thymidine uptake was performed to investigate whether $CD4^+CD25^+$ Treg, that were depleted (see, e.g., 8.1.9.) from the $CD3^+CD4^+$ T cell fraction, contained antigen-specific Treg. The percentage of $CD3^+CD4^+CD25^+Foxp3^+$ Treg in the depleted cell fraction was determined by flow cytometry. A representative staining of melanoma patient # 43 showed that the depleted cell population consisted of pure $CD3^+CD4^+$ T cells of which more than 60 % revealed a $CD25^+Foxp3^+$ Treg phenotype (Fig. 38).

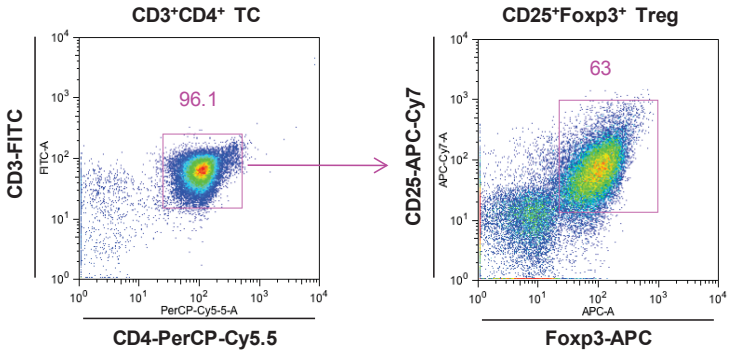


**Figure 38. Percentage of $CD4^+CD25^+Foxp3^+$ Treg in the $CD4^+CD25^+$ depleted T cell fraction.** The percentage of Treg was determined by flow cytometry staining. Representative FACS dot plots of melanoma patient # 43 are presented. The left plot shows the gating strategy for $CD3^+CD4^+$ T cells (indicated by quadrant). Treg were gated on the basis of $CD3^+CD4^+$ cells using Abs against CD25 and Foxp3 (right plot). The quadrant in the right plot indicates the population of $CD4^+CD25^+Foxp3^+$ Treg among $CD3^+$ T cells from the $CD4^+CD25^+$ depleted cell fraction (cf., Fig. 31). The numbers in the dot plots indicate the percentage, of the respective cell population. TC, T cells

To test, whether in dysplastic nevi or non-metastasized melanoma patients the depleted $CD4^+CD25^+$ cell fractions contained antigen-specific Treg, depleted cells were antigen-specifically activated. Therefore, autologous dendritic cells were pulsed with polypeptides of melanoma TAAs or human IgG. Afterwards, CD3 polyclonally activated autologous T cells, depleted from Treg (TC without Treg) were added and the T cell proliferation was examined. Thereby, the T cell proliferation in the context of peptide-stimulated Treg was analyzed, compared to the total T cell proliferation obtained from the co-culture of dendritic cells with polyclonally activated Treg-depleted T cells (Figs. 39A-C; DC + aTC). Before resection of the lesion, for both cohorts, the T cell proliferation was significantly controlled by peptide-stimulated Treg, either TAA-specific (Melan-A/MART-1, Tyrosinase, p53, MDM2) or TAA-unspecific (human IgG, unpulsed dendritic cells). Moreover, compared to the unpulsed dendritic cell setting, antigen-specific Treg were detected for Melan-A/MART-1, Tyrosinase, p53 and human IgG (Figs. 39A-C; no polypeptide).

After resection, the T cell proliferation was no longer controlled in comparison to the unpulsed dendritic cell setting. Compared to the total T cell proliferation, measured in the co-culture of dendritic cells with polyclonally activated Treg-depleted T cells, a Treg-dependent control of T cell proliferation was only marginally detected for p53 and human IgG, (Fig. 39). However, in none of the performed Treg specificity assays, specific Treg for NA17-A were detected (Figs. 39A-C).

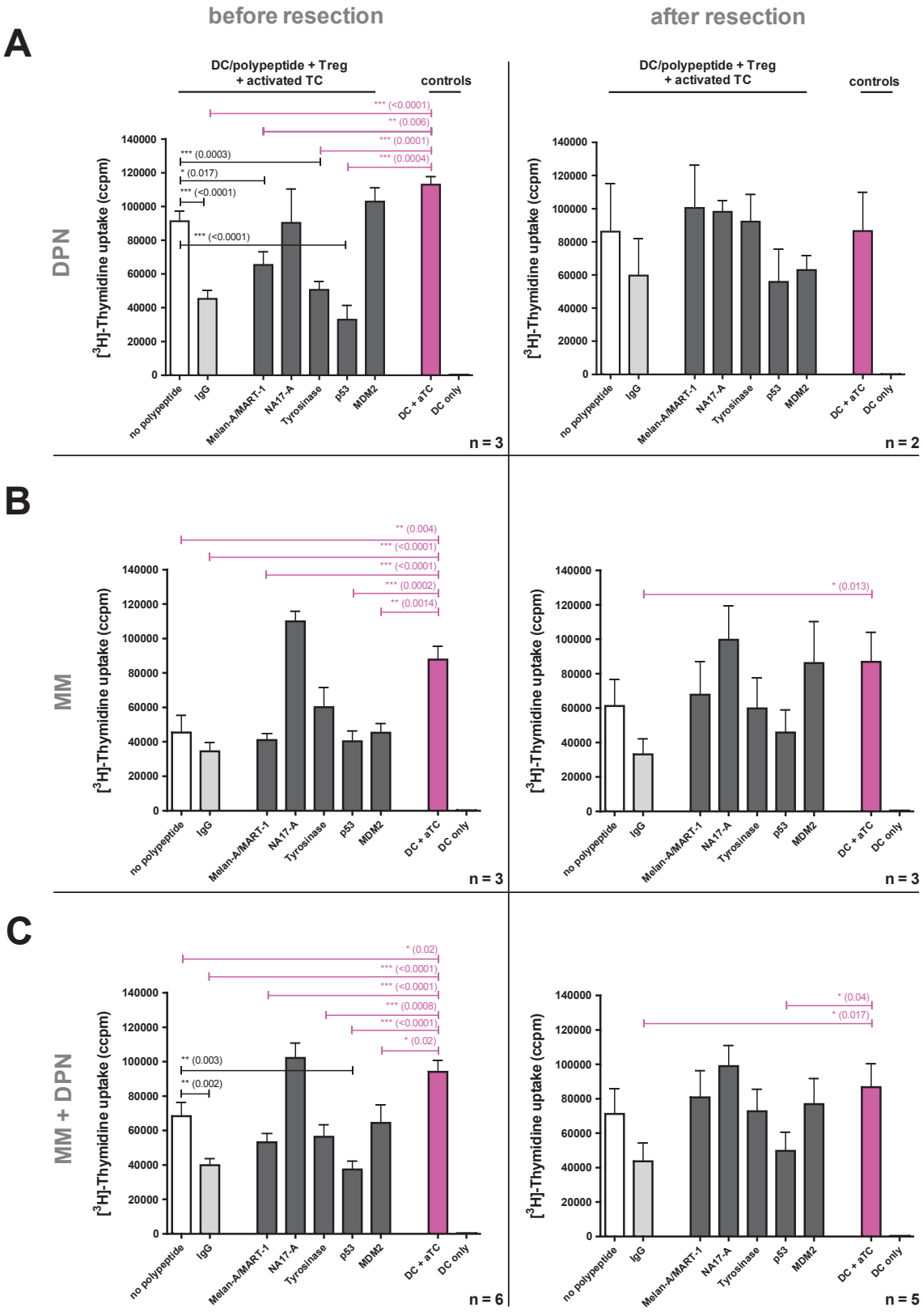


**Figure 39. Control of T cell proliferation by TAA or IgG-specific Treg.** The detailed figure legend is presented on the next page.

←

**Figure 39. Control of T cell proliferation by TAA or IgG-specific Treg.** The proliferation of polyclonally activated Treg-depleted T cells was analyzed in the context of $CD4^+CD25^+$ Treg in dysplastic nevi (DPN; **A**) and non-metastasized melanoma (MM; **B**) patients, before (left column) and after (right column) surgical resection. Treg were stimulated with 50aa polypeptides (dark gray bars) or human IgG (light gray bars), loaded to autologous dendritic cells. **C**) Combined T cell proliferations of DPN and MM patients are shown. The reduction in T cell proliferation, calculated compared to the total proliferation (magenta bars; DC + aTC; magenta p values) and to an unpulsed dendritic cell approach (white bars; DC/no polypeptide + Treg + aTC; black p values). For statistical analysis, an unpaired two-tailed t test was performed. aTC, αCD3-polyclonal activated T cells; DC, dendritic cell; Mean ± SEM; n, number of tests; TC, T cells; * p value ≤ 0.05; ** p value ≤ 0.01; *** p value ≤ 0.001

### 8.1.11. Analysis of T cell co-depletion during Treg depletion

After depletion of $CD4^+CD25^+$ Treg from the $CD3^+$ T cell fraction of non-metastasized melanoma patients, the cumulative data showed that frequencies of TAA-reactive T cells were not increased. Moreover, the depletion led to a reduction of tumor antigen-reactive T cell frequencies (see also, Figs. 33-35). In addition, after Treg depletion, the $CD4^+CD25^+Foxp3^-$ T cell fraction was reduced from 5.13 % to 2.59 %, as exemplarily shown for melanoma patient # 31 (Fig. 31).

To investigate whether conventional T cells were co-depleted during Treg depletion, the depleted cell fractions were analyzed by flow cytometry using Abs specific for CD3, CD4, CD25, Foxp3 and CD127. Effector and memory T cells express CD127 whereas $Foxp3^+$ Treg are negative (cf., Liu et al., 2006). The FACS staining revealed that $CD4^+CD127^+Foxp3^-$ cells (Fig. 40; exemplarily ~22 % for melanoma patient # 43) were co-depleted besides $CD4^+CD25^+Foxp3^+$ Treg (Fig. 40; exemplarily ~64 % for melanoma patient # 43). This observation was representative for six individual samples, of investigated $CD4^+CD25^+$ Treg-depleted fractions of independent patients.

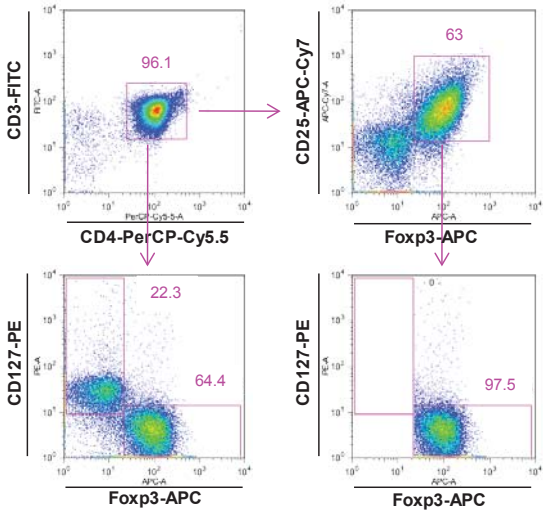


**Figure 40. Co-depletion of $CD4^+CD127^+Foxp3^-$ T cells during Treg depletion.** The percentage of Treg and T cells was determined in the depleted cell fraction by flow cytometry. Representative dot plots of melanoma patient # 43 are presented. The upper left plot shows the gating for $CD3^+CD4^+$ T cells (quadrant). Treg were gated on the basis of $CD3^+CD4^+$ cells using Abs specific for CD25 and Foxp3 (upper right plot). The gated Treg population is negative for CD127 (lower right plot). The lower left plot indicates $CD127^+Foxp3^-$ conventional T cells and $CD127^-Foxp3^+$ Treg. The numbers indicate the percentage of the respective cell populations. Approximately 64 % $Foxp3^+$ Treg and 22 % conventional $CD127^+$ T cells were present in the depleted cell fraction.

### 8.1.12. Summary on spontaneous human tumor antigen-reactive T cell responses

Spontaneously induced tumor antigen-reactive T cells occur in the PB of non-metastasized and metastasized melanoma as well as dysplastic nevi patients. TAA-reactive T cell responses against the 13 generated 50aa melanoma polypeptides (GAGE-1, gp100/pmel17, MAGE-A1, MAGE-C2, MDM2, Melan-A/MART-1, MIF, NA17-A, NY-ESO-1, p53, RAB38/NY-Mel-1, TRP2, Tyrosinase) were detected in the majority of non-metastasized and metastasized melanoma patients. Compared to healthy donors, the observed TAA-reactive memory T cell frequencies were strongly increased in melanoma and dysplastic nevi patients. Thereby, the responses after surgical resection in both cohorts were elevated. The TAA-recognition pattern of melanoma T cells was highly polyvalent and independent of the patients HLA-type. HLA-$A2^+$ and HLA-$A2^-$ patients recognized the polypeptides, that cover MHC class I- and II-restricted epitopes, in a similar manner. Furthermore, $CD4^+$ and $CD8^+$ T cells of the same patient responded to the designed polypeptides. Frequencies of TAA-reactive T cells of non-metastasized melanoma patients strongly increased after primary tumor resection over time. The percentage of $Foxp3^+$ Treg in the PB of non-metastasized melanoma patients after tumor resection was comparable to the Treg percentage observed in healthy donors. In some patients, a depletion of Treg resulted in an increase of TAA-reactive T cell frequencies. Moreover, antigen-specific Treg for Melan-A/MART-1, p53, Tyrosinase and MDM2 have been detected in the PB of melanoma and dysplastic nevi patients. Finally, the cumulative data of the melanoma cohort revealed that a Treg depletion did not led to an additional increase of tumor-reactive T cell frequencies.

## 8.2. *In vivo* efficiency of optimized TCR transgenic human T cells in a xenotransplantation model

Human T cells equipped with tumor antigen-reactive T cell receptors (TCRs) for the antigens MDM2 or gp100 have been optimized *in vitro*, in order to avoid hybrid TCR formation of exogenously introduced and endogenous TCR αβ chains. Those hybrid TCRs have unknown specificities and thus could potentially result in autoimmune reactions.

Therefore, the group of Dr. R.-H. Voss developed different strategies to avoid the formation of hybrid TCRs while favoring preferential pairing of introduced chains. In a cooperation project, during this PhD thesis, those optimized TCR transgenic T cells with specificities for MDM2 or gp100 were investigated under *in vivo* conditions, concerning their ability to control tumor growth.

### 8.2.1. The establishment of the human melanoma murine xenotransplantation model

Since the human TCR transgenic T cells were generated to specifically recognize the antigens MDM2 or gp100, human $MDM2^+$ and $gp100^+$ cell lines, have to be used as target lines for the xenotransplantation model. Therefore, several human primary and metastasized melanoma-derived cell lines were investigated beforehand, concerning their specific tumor antigen expression. The origins of the seven different melanoma cell lines analyzed are indicated in Tab. 11.

To examine the presence of selected tumor antigens (gp100, Melan-A/MART-1, MDM2, p53, Tyrosinase and L1CAM), for all cell lines SDS-PAGE followed by immunoblot analyses were performed. Thereby, the equal amounts of proteins of the respective cell lines were demonstrated by the presence of actin. Summarized, the cell lines Malme-3M, MeWo and SK-Mel-23 comprised all tumor markers investigated (Fig. 41). As control, the human osteosarcoma cell line U2OS and the human breast-adenocarcinoma line MCF-7 were examined. Both cell lines revealed to be negative for the melanoma TAAs gp100 and Melan-A/MART-1. The developmental origin of the melanoma cell lines was controlled by analyzing the intermediate-sized filaments vimentin (for mesenchymal-derived origin) and the keratins 8 and 18 (for epithelial-derived origin). While all melanoma cell lines were positive for vimentin and negative for the keratins 8 and 18, the MCF-7 cells were keratin-positive and vimentin-negative. However, due to some subclones, the osteosarcoma line U2OS revealed both, vimentin and also minor amounts of the keratins 8 and 18-positive cells (Fig. 41).

In addition, since the TCRs used for T cell transduction only recognize peptides presented by HLA-A2 molecules, the HLA-A2 expression of the melanoma cell lines was analyzed by flow cytometry. The cell lines Malme-3M, MeWo, SK-Mel-23 and WM-266-4 were $HLA\text{-}A2^+$, whereas WM-115 revealed to be $HLA\text{-}A2^-$ (Fig. 42). Here, the presence of HLA-A2 for the cell lines C32 and SK-Mel-2 was not analyzed in detail. However, their HLA-A2 expression has well been described in the literature. C32 cells were shown to be $HLA\text{-}A2^+$ (Butler et al., 2007) and SK-Mel-2 cells to be $HLA\text{-}A2^-$ (von Bergwelt-Baildon et al., 2002).

| Human melanoma cell lines | Origin |
|---|---|
| **Malme-3M** | metastasis, lung |
| **C32** | primary melanoma, skin |
| **WM-115** | primary melanoma, skin |
| **WM-266-4** | metastasis, skin |
| **MeWo** | metastasis, lymph node |
| **SK-Mel-23** | metastasis, skin |
| **SK-Mel-2** | metastasis, skin |

**Table 11. Origins of the human melanoma cell culture lines analyzed.** The two melanoma cell lines C32 and WM-115 are derived from primary melanoma whereas Malme-3M, WM-266-4, MeWo, SK-Mel-23 and SK-Mel-2 cells are derived from melanoma metastasis (see also Bean et al., 1975; Carey et al., 1976; Lang et al., 2001; Schmitt et al., 2007).

In order to investigate the engraftment and tumor formation of human melanoma cell lines in NOD-SCID mice *in vivo*, the cell lines Malme-3M, MeWo and SK-Mel-23 were selected. On the one hand, all three cell lines were HLA-A2$^+$, on the other hand, they expressed the complete panel of selected tumor antigens investigated, in particular MDM2 and gp100, the target antigens of the TCR transgenic T cells. Therefore, the cells of the respective lines ($2.5x10^6$ cells resuspended in 50 µl matrigel) were administered intradermally (i.d.) to the right murine flank. The tumor growth was then investigated using a caliper over time up to d50. As control approach, in parallel, 50 µl matrigel without cells was examined. The matrigel degraded *in vivo* and did not increase in volume over time. From d20 on, no further matrigel could be measured (Fig. 43).

However, the cell lines MeWo and SK-Mel-23 showed a strong tumor growth over time whereas the tumor formation of the slowly growing Malme-3M cells did not measurable increase (Fig. 43). SK-Mel-23 cells grew aggressively, since 2 mice from this group died ahead of time by d31 and d44, respectively. In contrast, the tumor formation that resulted from the MeWo cells strongly increased over time, without premature decrease of mice (Fig. 43). On d50, all remaining mice were sacrificed by cervical dislocation and visually investigated for potential metastases formation. In addition, the tumor and the lung of each mouse were removed for further investigations. The determined weights of the MeWo and SK-Mel-23 tumors were strongly increased compared to the Malme-3M tumors (insert in Fig. 43). Furthermore, no metastases formation could be visually detected for mice that received MeWo or Malme-3M cells, whereas inguinal tumor-draining lymph node metastases were detected in both remaining mice that had received SK-Mel-23 cells (Fig. 44). Using picrinic acid containing Bouin´s solution, in none of the mice in which Malme-3M, MeWo or SK-Mel-23 cells had been injected, lung metastases could be observed.

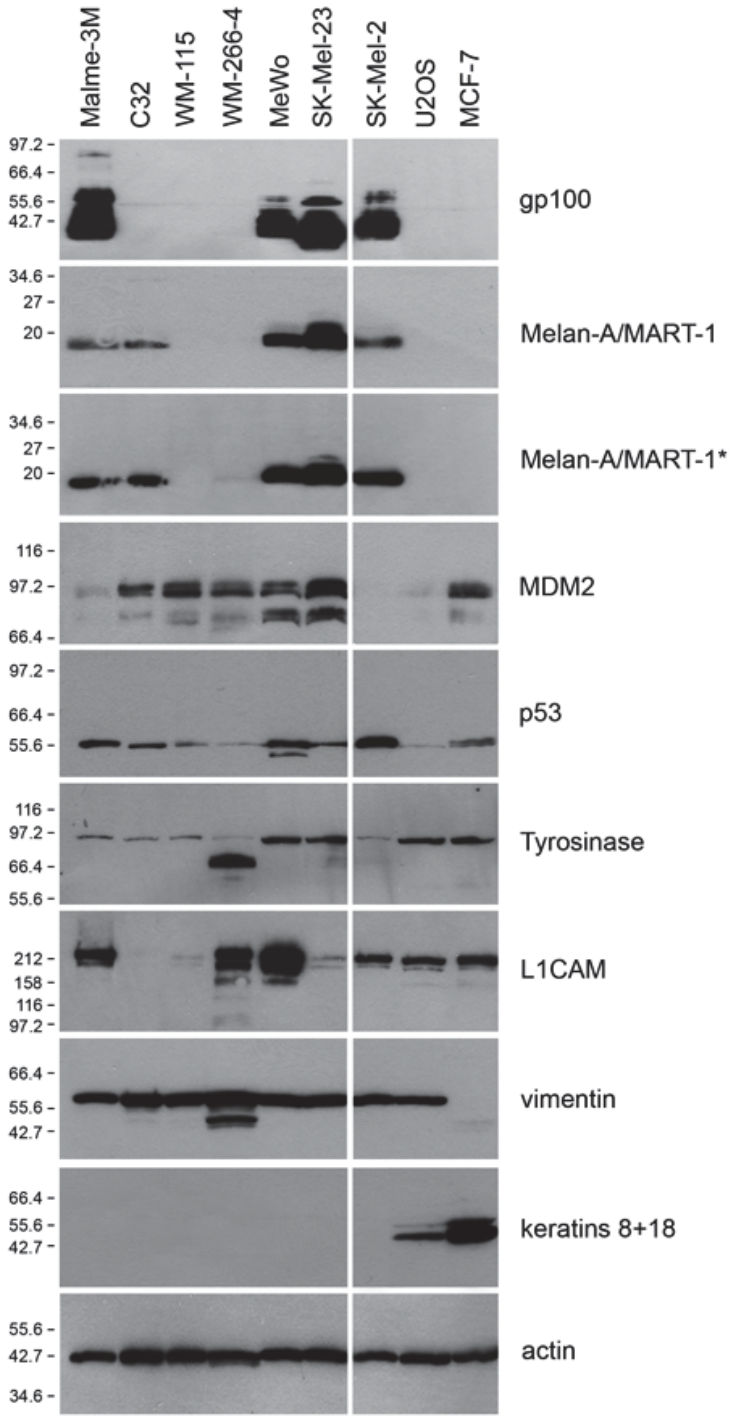


**Figure 41. Protein immunoblot detection of various human melanoma cell lines.** Equal amounts of total proteins from seven melanoma lines (Malme-3M, C32, WM-115, WM-266-4, MeWo, SK-Mel-23, SK-Mel-2) were examined, in comparison to human osteosarcoma (U2OS) and human breast-adenocarcinoma cells (MCF-7). PVDF-membranes were probed with Abs specific for tumor antigens (gp100, Melan-A/MART-1, MDM2, p53, Tyrosinase, L1CAM), intermediate-sized filaments (vimentin, keratins 8+18) and actin. Tumor antigen gp100 is present in Malme-3M, MeWo, SK-Mel-23 and SK-Mel-2, whereas Melan-A/MART-1 is additionally expressed in C32 cells. Varying amounts of MDM2, p53, Tyrosinase and L1CAM are present in all cells. However, MDM2 is lacking in SK-Mel-2 and L1CAM in C32 cells. Note also the positivity of vimentin in all cells, except of MCF-7, which are instead positive for keratins 8 and 18. Molecular weight markers in kDa are indicated on the left margin. For Melan-A/MART-1 two different Ab clones were used (Thermo Fisher Scientific: Melan-A/MART-1; Dako: Melan-A/MART-1*).

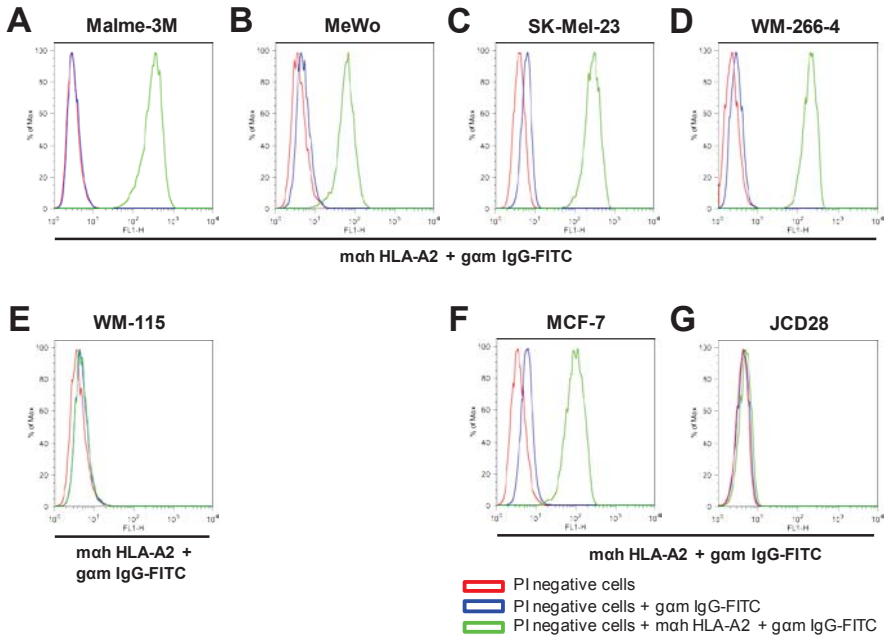


**Figure 42. Flow cytometry analysis of the HLA-A2 presence in various human melanoma cell lines.** The cells of the lines Malme-3M (**A**), MeWo (**B**), SK-Mel-23 (**C**) and WM-266-4 (**D**) were analyzed using flow cytometry and revealed to be HLA-A2$^{+}$ whereas WM-115 cells (**E**) were HLA-A2$^{-}$. As positive control cells of the line MCF-7 (**F**) and as negative control cells of the human T cell leukemia line Jurkat, over-expressing CD28, (JCD28; **G**) were used.

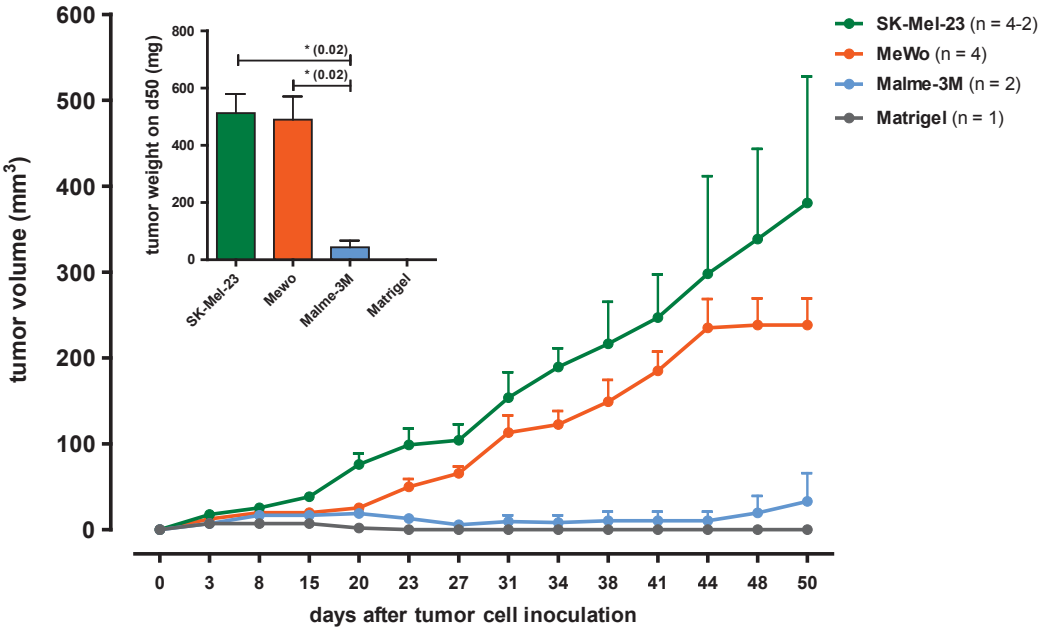


**Figure 43. Engraftment and tumor formation of human melanoma cell lines *in vivo* after i.d. injection into NOD-SCID mice.** Resuspended in 50 µl matrigel, 2.5x10$^{6}$ cells of the melanoma lines SK-Mel-23 (green), MeWo (orange) or Malme-3M (blue) were injected i.d. onto the right flank of NOD-SCID mice. The tumor growth was measured over time up to d50. As control setting, matrigel without cells (grey) was examined. In contrast to Malme-3M cells, a tumor formation over time was detected for MeWo and SK-Mel-23 cells. The insert, in the upper left corner, indicates the tumor weight, resulted from the respective melanoma cells, after tumor removal on d50. For statistical analysis, an unpaired two-tailed t test was performed. Mean ± SEM; n, number of mice; * p value ≤ 0.05

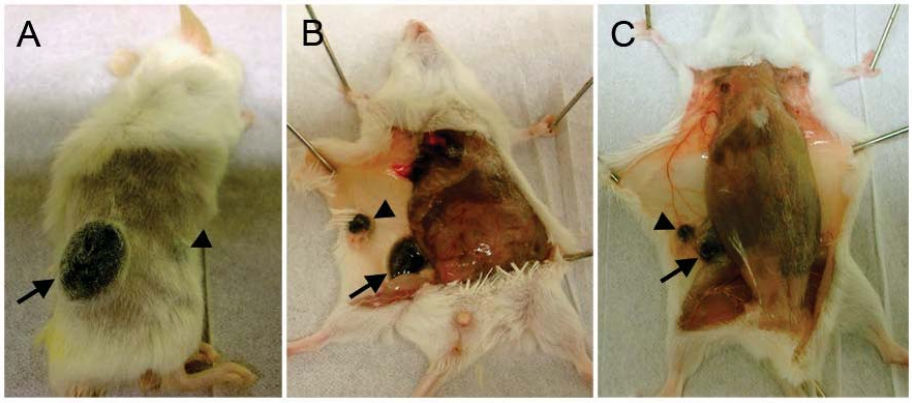


**Figure 44. Lymph node metastases formation of SK-Mel-23 cells in NOD-SCID mice.** SK-Mel-23 tumor-bearing NOD-SCID mice, after i.d. tumor cell injection, were sacrificed on d50 and showed metastases in the inguinal tumor-draining lymph nodes. The primary formed tumor and the lymph node metastasis of one mouse are depicted before (**A**) and after (**B**) opening of the abdominal skin. In **C**), the SK-Mel-23 tumor and lymph node metastasis of a second mouse is shown. The primary tumors are indicated by arrows, the inguinal tumor-draining lymph node metastasis by arrowheads.

For subsequent experiments, as tumor target cell line for the murine xenotransplantation model, the MeWo cell line has been selected, since cells of this line displayed a reproducible engraftment and tumor formation in NOD-SCID mice *in vivo* over time, without leading to the death of the mice. Moreover, the MeWo cells were shown to be positive for MDM2, gp100 and HLA-A2. To verify the presence of MDM2 and gp100 on MeWo cells, as shown by immunoblot investigations (cf., Fig. 41), immunofluorescence microscopy was performed. These stainings also showed that MeWo cells were positive for MDM2 and gp100 (Fig. 45). The cell lines MCF-7 and U2OS were used for control stainings. Thereby, MCF-7 cells were positive for MDM2 and negative for gp100 whereas U2OS cells were generally negative for both markers. However, the U2OS cell line revealed some distinct cell clones that were positive for MDM2 (Fig. 45).

To investigate, how the different approaches of MeWo cell administration influence the tumor formation *in vivo*, $2.5x10^6$ MeWo cells were resuspended in PBS and injected either intraperitoneally (i.p.), intravenously (i.v.) or subcutaneously (s.c.). Between d35 and d42 after cell inoculation, the mice were sacrificed by cervical dislocation and examined for tumor metastases formation. NOD-SCID mice that received MeWo cells i.p. developed metastases throughout the entire abdominal cavity, preferentially in the lymph nodes, the spleen and the intestine as well as showed pleural effusions, hemorrhagic ascites and organ fusions (left column in Fig. 46). Moreover, when MeWo cells were injected i.v., metastases could be detected particularly in the lung and in the intestine (right column in Fig. 46). Lung metastases, that developed after i.v. injection, were stained with Bouin`s solution and are exemplarily shown in Fig. 47B. Furthermore, the administration of tumor cells s.c., did not lead to visible metastases formation. But, compared to i.d. application, the tumor formation in mice that received the cells s.c. was not defined as clearly as in the i.d. injection setting. This would most likely complicate a reliable measurement of the tumor with a caliper. Therefore, for subsequent experiments of the murine xenotransplantation model, the MeWo cells were i.d. injected.

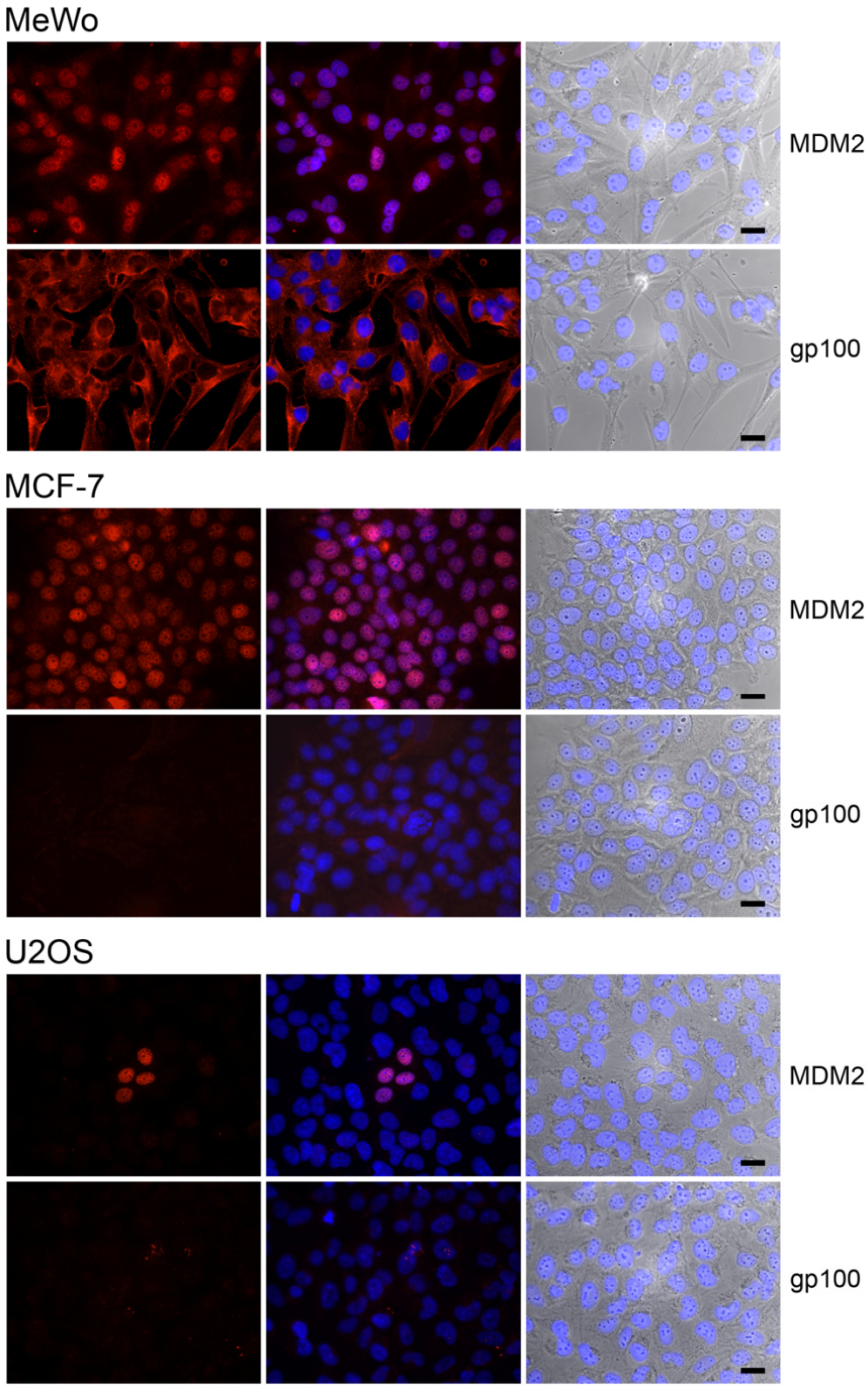


**Figure 45. Immunofluorescence microscopy of MDM2 and gp100 in MeWo cells.** Immunofluorescense microscopical images of MeWo, MCF-7 and U2OS cells are presented. MeWo cells show a strong nuclear staining of MDM2 and gp100 in the cytoplasm (both in red). MCF-7 cells revealed positive for MDM2 and negative for gp100. U2OS cells do not express MDM2 and gp100. However, some single cell clones were MDM2-positive. DAPI (blue) was used to show the cell nuclei and the phase contrast picture to present the cell morphology. Bars represent 20 µm.

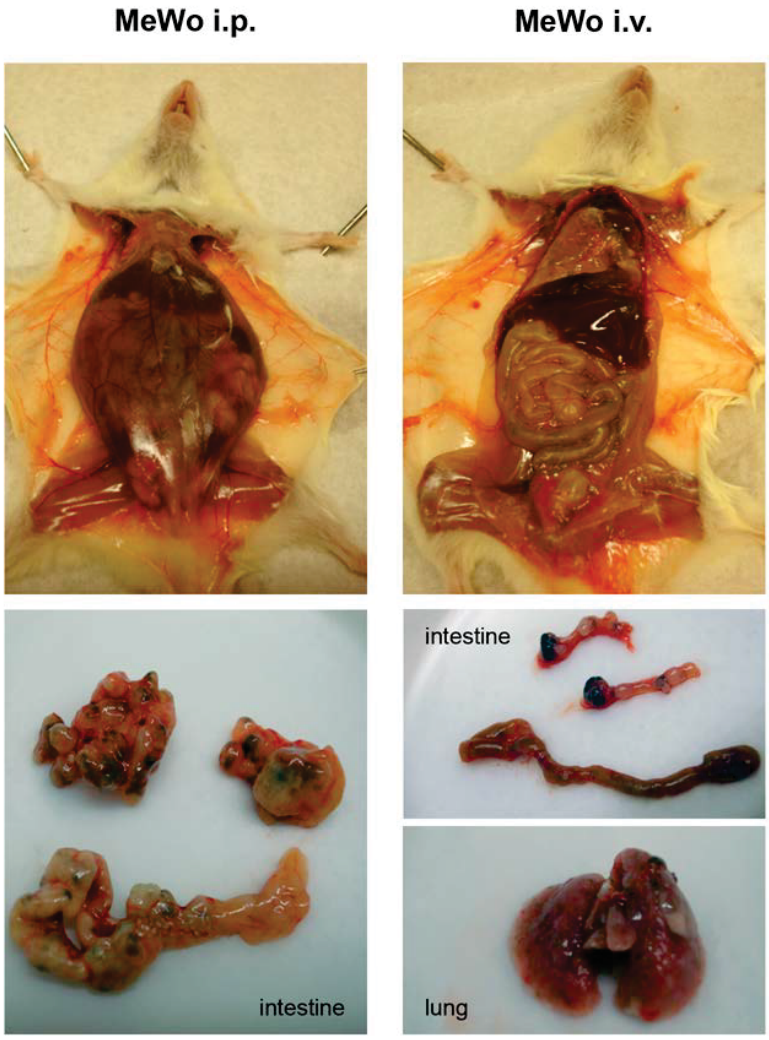


**Figure 46. Metastases formation of MeWo cells after *in vivo* i.p. or i.v. cell injection.** Representative pictures of mice that received 2.5x10$^6$ MeWo cells, resuspended in PBS i.p. (left column) or i.v. (right column). The presented i.p. treated mouse was sacrificed on d42 and the i.v. treated mouse on d36 after MeWo cell injection. The lower micrographs show metastasized murine organs of the respective mice, including intestine and lung.

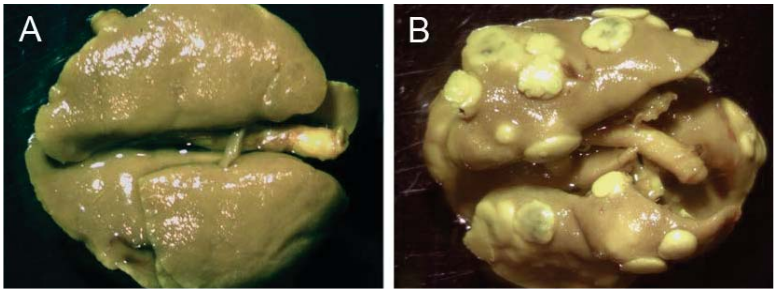


**Figure 47. Lung metastases staining with Bouin`s solution. A**) Lung without metastases formation. The mouse received MeWo cells i.d. and was sacrificed on d38 after tumor cell injection, followed by an examination of the lung for metastases. **B**) Lung with metastases formation. The used mouse received MeWo cells i.v. and was prepared on d35 after injection, before the lung was analyzed for metastases.

### 8.2.2. The production of optimized MDM2 or gp100 TCR transgenic human T cells

TCR transgenic T cells with specificities for MDM2 or gp100 were applied for adoptive transfer experiments using the murine xenotransplantation model. In order to avoid hybrid TCR formation between exogenous and endogenous TCRs, the TCR constructs, used for T cell transduction, were optimized by the group of Dr. R.-H. Voss.

The MDM2 (81-88)-specific TCR, is a mouse-derived TCR originally generated in a partially humanized HLA-A2.1 transgenic mouse model (Stanislawski et al., 2001). The α and β genes have been isolated from murine MDM2 specific T cell clones and were cloned into a retroviral vector system. Using these retroviral plasmids, human T cells can be transduced with the MDM2 TCR genes. To promote TCR chain pairing of the introduced MDM2 TCRs, reciprocally mutant TCRs have been generated. Therefore, a pair of interacting amino acid residues, located in the core MDM2 TCR C-domain interface, Gly-85.1$C_\alpha$ and Arg-88$C_\beta$, was reciprocally replaced in order to swap the steric and electrostatic relationship (reciprocal mutation $C_\alpha$-Arg/$C_\beta$-Gly; for further details see Voss et al., 2008). Moreover, the molecular design of the $C_{\alpha\beta}$ interface was further optimized by changing the side chain volume, charge and H-bonding. One of the most promising constructs revealed through functional *in vitro* investigations, appeared to be the reciprocal mutation $C_\alpha$-Lys/$C_\beta$-Gly. Moreover, to prove antigen-specific recognition of MDM2 TCR transduced T cells *in vivo*, further constructs with mutations in the CDR3 region of the TCR β chain were developed (Dr. R.-H. Voss). The mutations sustained the TCR surface expression, but abolished the avidity of the TCR. All MDM2 TCR constructs, investigated concerning their *in vivo* tumor growth control, are summarized in Fig. 48.

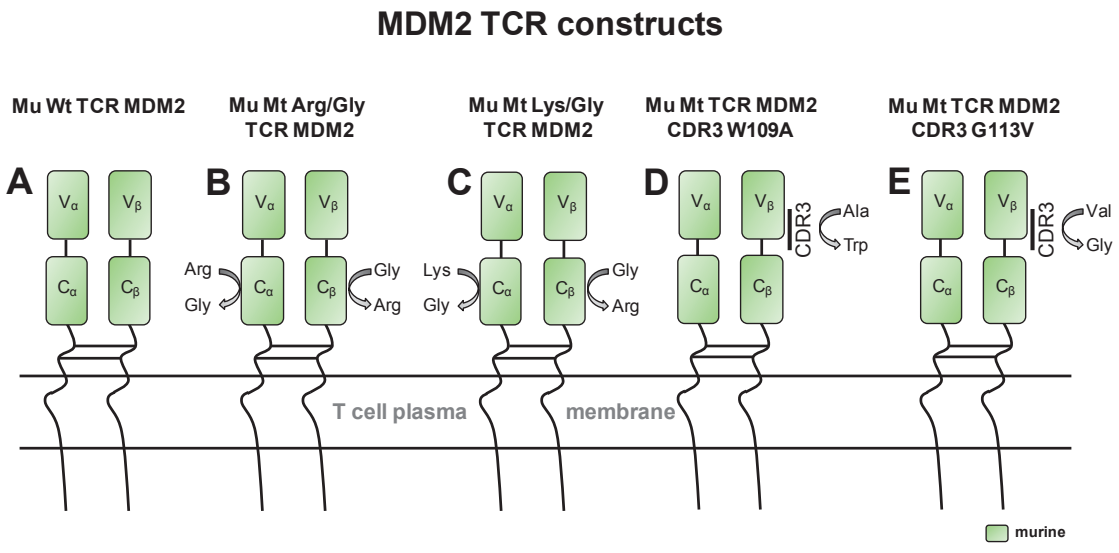


**Figure 48. MDM2 TCR constructs used for retroviral transduction of human T cells. A**) The murine dc Wt MDM2 TCR sustains in the core C-domain interface the Gly-85.1$C_\alpha$ and Arg-88$C_\beta$ pair of interacting aa residues. **B**) and **C**) In order to favor chain pairing of introduced TCRs, two optimized reciprocally mutated MDM2 TCR constructs were analyzed (**B**, Gly-85.1$C_\alpha$-Arg/Arg-88$C_\beta$-Gly; **C**, Gly-85.1$C_\alpha$-Lys/Arg-88$C_\beta$-Gly). **D**) and **E**) Two control MDM2 TCR constructs with aa mutations in the CDR3 region of the TCR β chain, sustained TCR surface expression but with abolished avidity (**D**, CDR3 mutation Trp-109$C_\beta$-Ala; **E**, CDR3 mutation Gly-113$C_\beta$-Val).

Performing a different strategy, compared to the optimized MDM2 TCRs, the human A2.1-restricted gp100 (280-288)-specific dc TCR (Schaft et al., 2003) was also modified in order to avoid hybrid dimer TCR formation. Therefore, a 3-domain single chain (sc) TCR was constructed connecting the variable α ($V_\alpha$) domain to the TCR β chain (Voss et al., 2010). Moreover, to increase the stable expression on the cell surface, the sc construct was further optimized by providing the missing constant α ($C_\alpha$) domain. A truncated TCR α chain, consisting of the signal peptide and the $C_\alpha$ domain was generated and co-expressed. To additionally increase the chain pairing, an artificial disulfide bond was introduced between $C_\alpha$ and $C_\beta$. Furthermore, since it could be shown that introduced murine TCR constructs are functional in human T cells and even more efficiently expressed (Sommermeyer et al., 2006), chimeric TCRs were generated for gp100, replacing the human $C_\alpha$ and $C_\beta$ domains by constant murine domains.

Using the retroviral pBullet vector system, the optimized gp100 constructs were introduced into human T cells, as mentioned for the MDM2 TCR constructs. All gp100 TCR constructs that were investigated are presented in Fig. 49..

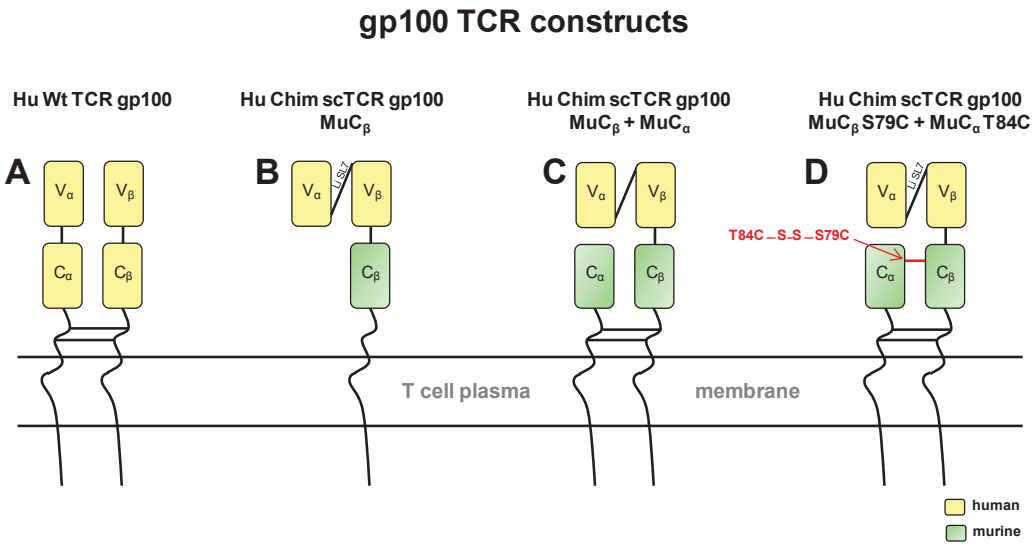


**Figure 49. gp100 TCR constructs used for retroviral transduction of human T cells.** The human dc Wt TCR gp100 (**A**) and 3 scTCR gp100 constructs (**B**-**D**) were analyzed. The scTCR was constructed by connecting the variable $V_\alpha$ domain to the TCR β chain (**B**-**D**). To provide the missing $C_\alpha$ domain, a truncated TCR α was co-expressed (**C**-**D**). To further increase the interchain binding, an artificial disulfide bond (indicated in red) was integrated between the $C_\alpha$ and $C_\beta$ (**D**). All scTCR constructs are chimeric molecules, since their C domains are of murine and their V domains of human origin (**B**-**D**).

In order to investigate the ability to control tumor growth, the optimized MDM2 or gp100 TCR transduced T cells were analyzed during this thesis in the murine melanoma xenotransplantation model *in vivo*. Therefore, the utilized TCR transgenic T cells were either produced by Dr. R.-H. Voss or single handedly (cf., 6.10. for further informations about the used constructs and 7.3.9. about the TCR transgenic T cell generation procedure). Beforehand, using flow cytometry, ELISPOT and $^{51}Cr$ release assays, all Wt and optimized MDM2 or gp100 TCR constructs were tested for their functional expression on the human transgenic T cells.

The majority of the transgenic PBMCs showed a phenotype of $CD3^+$ T cells, which were preferentially $CD8^+$ (Fig. 50). During *in vitro* cell expansion, the $CD4^+$ / $CD8^+$ T cell ratio shifted towards $CD8^+$ cells, however, also $CD4^+$ transduced T cells remained in the cultures (Fig. 50). Using a retroviral EGFP carrying reporter plasmid, the retroviral transduction efficiency was controlled. Shortly after transduction, only a marginal percentage of cells were EGFP-positive (Fig. 51A). In contrast, after drug selection and cell expansion, the EGFP positivity of the transduced cells was >97% (Fig. 51B).

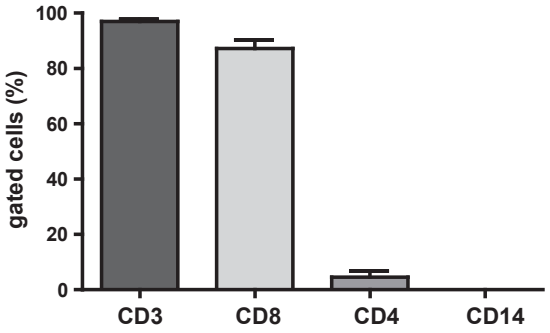


**Figure 50. Representative FACS staining of cell subsets after TCR transduction, drug selection and expansion of human bulk PBMCs.** To investigate the transgenic cell phenotype, the cells were analyzed by flow cytometry after TCR transduction, drug selection and expansion using direct labeled Abs (CD3-PE, CD8-FITC, CD4-FITC, CD14-PE). The transduced cells were mainly $CD3^+$ T cells, whereas more $CD8^+$ than $CD4^+$ T cells and no $CD14^+$ monocytes could be detected. Representative cumulative data of 4 PBMC transduction approaches are indicated. Mean ± SEM

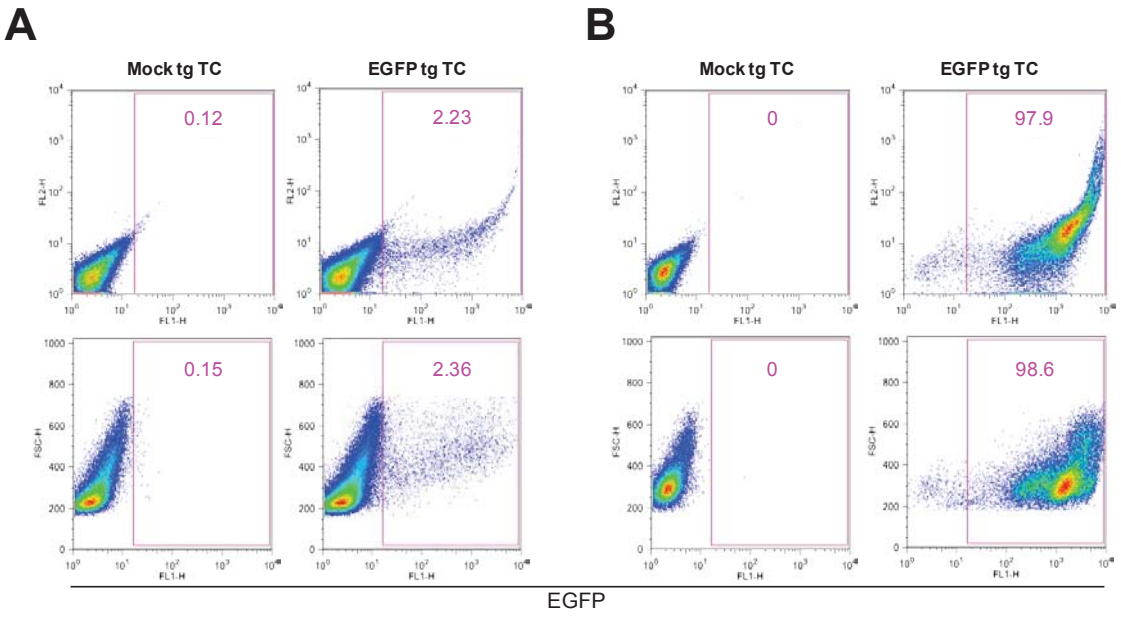


**Figure 51. Retroviral transduction efficiency of EGFP transgenic T cells.** EGFP transduced T cells, before (**A**) and after (**B**) drug selection and cell expansion, compared to Mock transgenic (tg) T cells. The upper dot plot panel indicates the EGFP-positive cells against the 2nd channel (FL2-H). The lower panel shows the same EGFP data blotted against the forward scatter (FSC-H). The magenta numbers in the dot plots indicate the percentage of EGFP-positive cells. Shortly after transduction ~2 % of the T cells were EGFP-positive, while after drug selection and expansion the EGFP positivity was >97 %. TC, T cells

In addition, the expression of the transduced TCRs on the cell surface was investigated by flow cytometry and tetramer staining for the $V_\beta$ chains. Representative flow cytometry data of MDM2 and gp100 transgenic T cells are shown in Fig. 52. Almost all human MDM2 TCR transduced T cells were positive for the $V_\beta$ 6 subfamily domain of this receptor and bound MDM2 tetramers (Fig. 52A). Moreover, human gp100 TCR transduced T cells were positive for the $V_\beta$ 14 subfamily domain and bound gp100 tetramers (Fig. 52B).

Analyzed by $^{51}$Cr release assays, the transduced MDM2 and gp100 transgenic T cells showed a cytolytic function. The transduced T cells were able to specific lyse T2 target cells, loaded with the associated peptides (Figs. 53A and B). Mu Wt TCR MDM2 and Mu Mt Arg/Gly TCR MDM2 transduced T cells efficiently recognized MDM2 peptide-loaded T2 cells, showing an equivalent cytolytic activity, while T2 cells loaded with irrelevant gp100 peptide were not recognized (Fig. 53A). Furthermore, Hu Wt TCR gp100 and Hu Chim scTCR gp100 $MuC_\beta$ S79C + $MuC_\alpha$ T84C transduced T cells efficiently and comparably recognized gp100 peptide-loaded T2 cells. In contrast, T2 cells loaded with irrelevant MDM2, p53 or HIV-pol peptides were not recognized by Hu Chim scTCR gp100 $MuC_\beta$ S79C + $MuC_\alpha$ T84C transduced T cells (Fig. 53B). Compared to Wt TCR MDM2 or gp100 transduced T cells, optimized MDM2 and gp100 TCR transduced T cells showed an equivalent cytolytic activity (Figs. 53A and B). Moreover, the lysis of gp100, MDM2, p53 or HIV-pol peptide-loaded T2 cells was not observed by Mock transduced T cells (Fig. 53B).

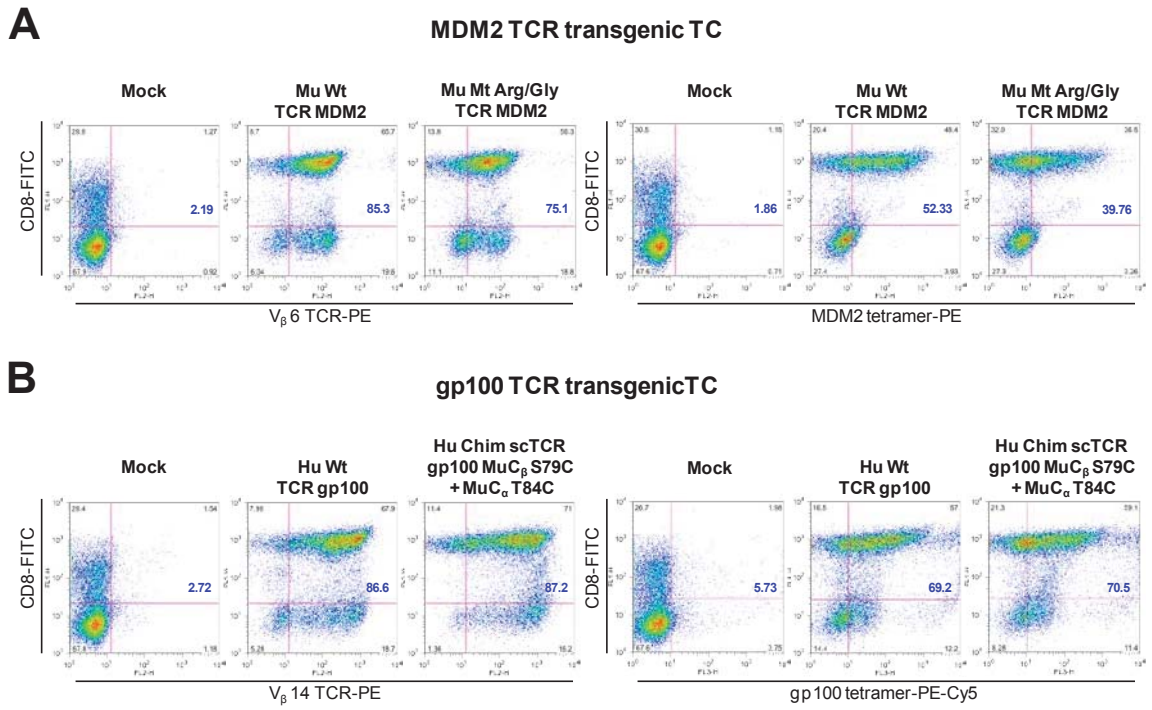


**Figure 52. Expression and tetramer avidity of MDM2 or gp100 TCRs on human T cells.** **A**) Mock, Mu Wt TCR MDM2 and Mu Mt Arg/Gly TCR MDM2 transduced human T cells were tested for $V_\beta$ 6 expression and for binding of tetrameric MDM2 (81-88)-A2.1 complexes by flow cytometry. **B**) Mock, Hu Wt TCR gp100 and Hu Chim scTCR gp100 $MuC_\beta$ S79C + $MuC_\alpha$ T84C transduced human T cells were investigated for $V_\beta$ 14 expression and tetramer gp100 (280-288)-A2.1 binding. The blue numbers depict the combined percentages of positive cells, among all $CD8^+$ and $CD8^-$ cells concerning $V_\beta$ staining or tetramer binding.

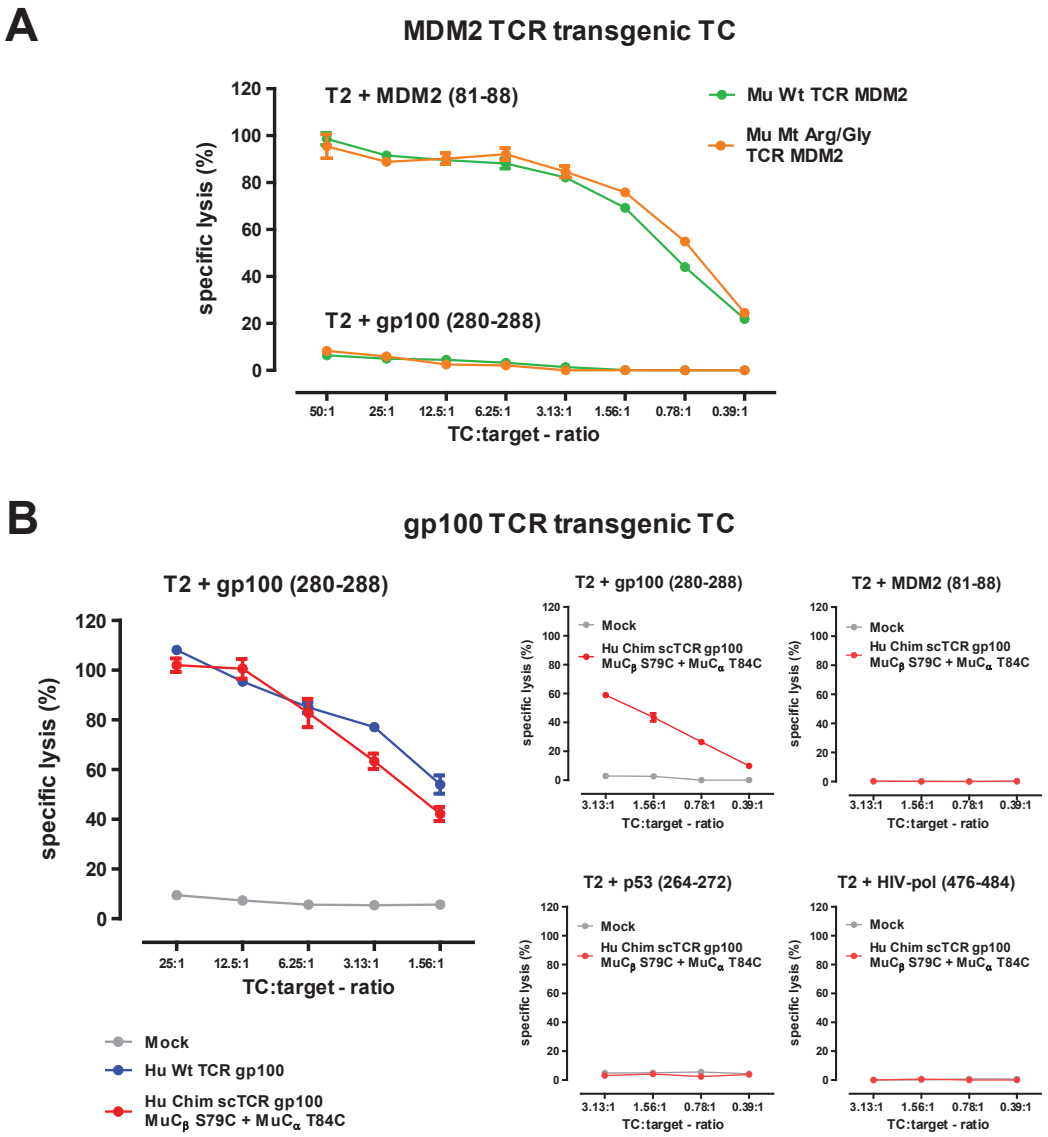


**Figure 53. Cytolytic effector functions of MDM2 or gp100 TCR transduced human T cells.** **A**) Cytotoxicity of human T cells transduced with MDM2 TCR constructs towards MDM2 peptide-pulsed T2 cells at the indicated T cell:target cell ratios. As control setting, T2 cells pulsed with the irrelevant gp100 peptide were analyzed. **B**) Cytotoxicity of human T cells transduced with gp100 TCR constructs towards gp100 peptide-pulsed T2 cells at the indicated T cell:target cell ratios. As control settings T2 cells pulsed with the irrelevant MDM2, p53 or HIV-pol peptides were investigated. TC, T cells

The phenotype of Hu Chim scTCR gp100 $MuC_{\beta}$ S79C + $MuC_{\alpha}$ T84C transduced T cells was investigated by flow cytometry, at the time point of i.v. injection. These transduced T cells revealed to be $CCR7^{-}CD45RO^{+}CD62L^{-}$ and thus showed an effector memory-like phenotype, whereas more than 35 % of the cells were $CD27^{+}$ (Fig. 54). In order to investigate their potential to control tumor growth, various TCR transduced T cells were tested *in vivo* in immunodeficient mice, priorily engrafted with melanoma cells of line MeWo. After tumor growth onset, the transduced T cells were i.v. injected. The precise time schedule of the utilized murine xenotransplantation model is shown in Fig. 55.

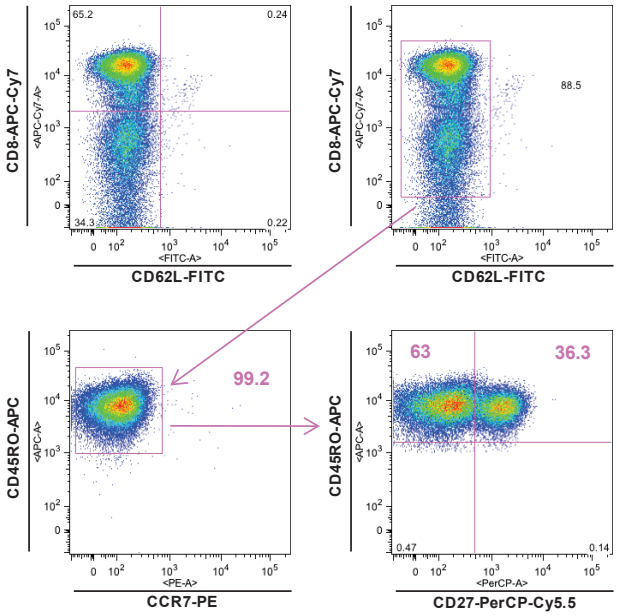


**Figure 54. Representative flow cytometry staining of TCR transduced T cells used at i.v. injection.** The phenotype of Hu Chim scTCR gp100 $MuC_{\beta}$ S79C + $MuC_{\alpha}$ T84C transduced T cells was analyzed by flow cytometry. The upper plots show that the transduced cells are $CD62L^{-}$. The lower left plot indicates the gated population, shown in the upper right plot and demonstrates the expression of CD45RO and CCR7. The transduced T cells revealed an effector memory phenotype ($CCR7^{-}CD45RO^{+}CD62L^{-}$). More than 35 % of these cells were $CD27^{+}$ (lower right plot), that indicates functional effector memory T cells. The numbers in the dot plots show the percentage of the respective cell populations.

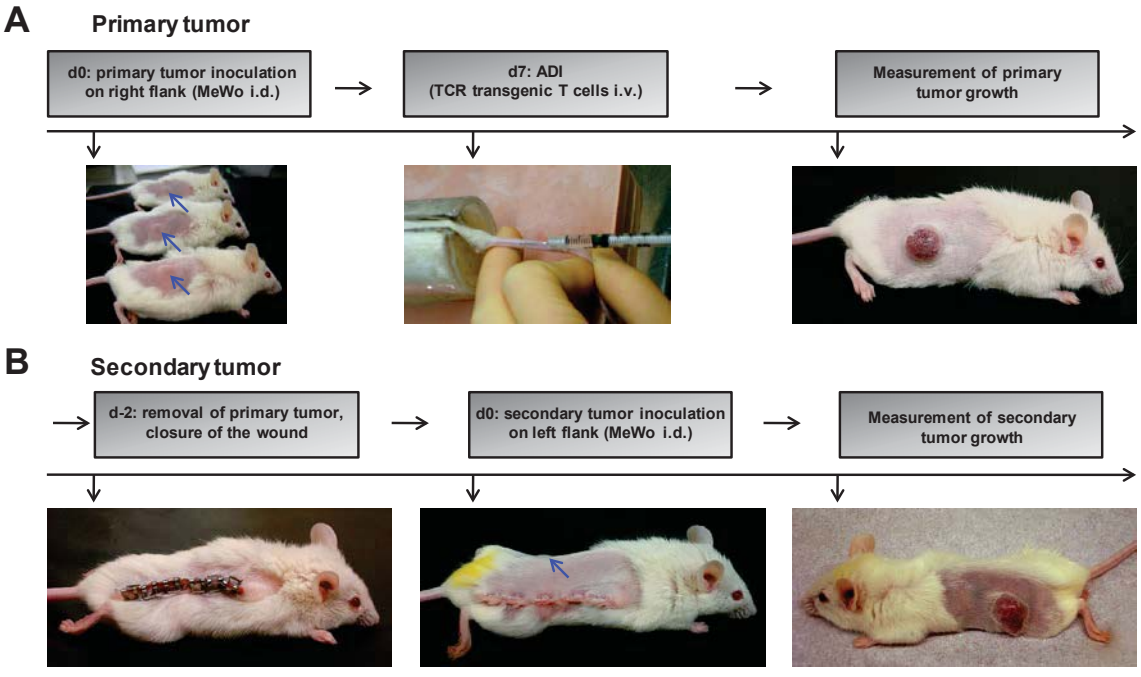


**Figure 55. Experimental setting of the murine xenotransplantation model. A**) Application of the primary tumor: Mice were engrafted i.d. with cells of the line MeWo (blue arrows), resuspended in 50 µl matrigel on d0. TCR transgenic T cells were adoptively transferred i.v. on d7 and the tumor growth was measured over time. **B**) Application of the secondary tumor: In some mice the primary tumor was removed and the wound closed. Two days later a secondary tumor (blue arrow) was injected to the left flank of the same mice and the tumor growth also analyzed over time.

### 8.2.3. Human melanoma growth in mice treated with MDM2 TCR transgenic T cells

The established murine xenotransplantation model was then used, to determine the ability of human T cells, transduced with various MDM2 (81-88)-specific TCRs, to control tumor growth of HLA-A2$^+$MDM2$^+$ MeWo cells in NOD-SCID mice. Therefore, 2.5x10$^6$ cells of the human melanoma cell line were injected on the right flank. Seven days later, the mice were treated with MDM2 TCR transgenic T cells (mean 1.8x10$^6$ cells). Thereby, up to three independent adoptive transfer experiments with those T cells were performed using 40 individual mice in total.

The cumulative data of the independent approaches are shown in Fig. 56. Mice that received PBS or Mock transduced T cells revealed a continuous tumor growth over time, comparable to mice that were treated with control MDM2 TCR transduced T cells. Those TCR constructs were expressed but showed a reduced TCR avidity, caused by mutations in the CDR3 region of the TCR β chain. Therefore, the TCRs were restricted in MDM2 epitope recognition, which resulted in an uncontrolled continuous tumor growth over time (Fig. 56A). In contrast, compared to the control approaches, mice that were treated with high avidity MDM2 TCR specific T cells, showed a melanoma tumor growth control over time (Fig. 56A). In summary, the control of melanoma growth was emerged for all specific MDM2 TCR constructs. Wt TCR MDM2 and both optimized mutant TCR constructs led to a comparable controlled tumor growth whereas the strongest control was received using optimized Mu Mt Arg/Gly TCR MDM2 transgenic T cells. Thereby, the tumor growth was reduced compared to Mock, PBS, Mu Mt TCR MDM2 CDR3 W109A and G113V treated mice (Fig. 56B). Furthermore, the tumor growth of Mu Wt TCR MDM2 processed animals was decreased in comparison with the mice that received the TCR CDR3 W109A construct (Fig. 56B).

Moreover, the ability of MDM2 TCR transgenic T cells to control tumor growth over time could be demonstrated more precisely, comparing the combined tumor growth of mice that either received MDM2 TCR specific T cells (Mu Wt TCR MDM2, Mu Mt Arg/Gly TCR MDM2, Mu Mt Lys/Gly TCR MDM2) or control approaches (Mock, Mu Mt TCR MDM2 CDR3 W109A, Mu Mt TCR MDM2 CDR3 G113V, PBS). Thereby, mice adoptively treated with MDM2 TCR specific T cells indicated a strongly reduced tumor growth over time (Fig. 57).

### 8.2.4. Human melanoma growth in mice treated with gp100 TCR transgenic T cells

Using the established xenotransplantation model, human T cells transduced with various gp100 (280-288)-specific TCR constructs were investigated, concerning their ability to control tumor growth *in vivo* (cf., Voss et al., 2010). Therefore, 2.5x10$^6$ cells of the human HLA-A2$^+$gp100$^+$ MeWo line were injected on the right flank, followed by adoptive T cell transfer of gp100 TCR transgenic T cells (mean 2.4x10$^6$ cells), 7 d later. The primary tumor growth was investigated in up to five independent adoptive transfer experiments, including 108 individual mice. The cumulative data of the independent experiments are presented in Fig. 58.

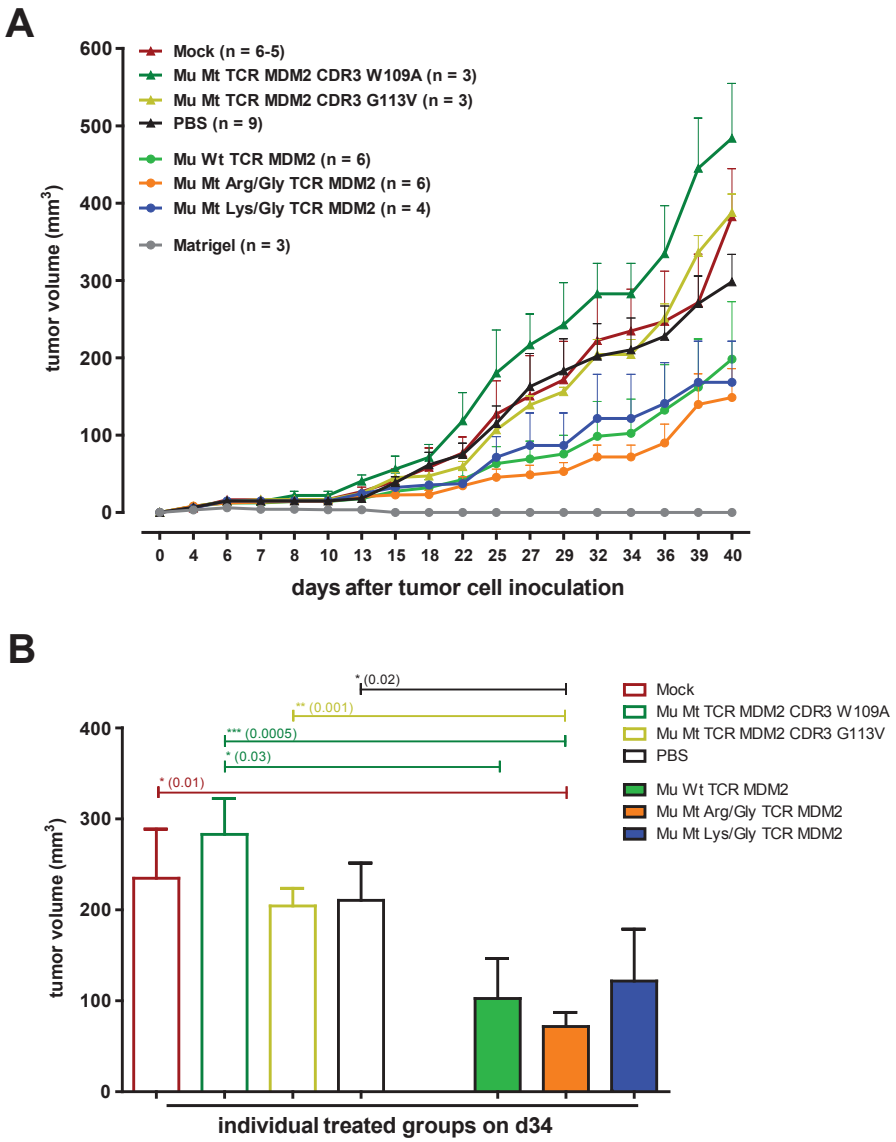


**Figure 56. Melanoma growth in NOD-SCID mice treated with MDM2 TCR transgenic T cells.** **A**) The MeWo growth in individual mice from up to three independent experiments is indicated over time. Matrigel inoculation without tumor cells was analyzed as control. The mice were treated with specific MDM2 TCR transduced T cells or with control approaches on d7. **B**) Statistical analysis of tumor growth on d34. Numbers of mice, investigated per group: Mock n = 5, Mu Wt TCR MDM2 CDR3 W109A n = 3, Mu Wt TCR MDM2 CDR3 G113V n = 3, PBS n = 9, Mu Wt TCR MDM2 n = 6, Mu Mt Arg/Gly TCR MDM2 n = 6, Mu Mt Lys/Gly TCR MDM2 n = 4). For statistical analysis, an unpaired two-tailed t test was performed. Mean ± SEM; n, number of individual mice; * p value ≤ 0.05; ** p value ≤ 0.01; *** p value ≤ 0.001

The tumor volumes of mice treated with Mock transduced T cells or PBS, continuously increased over time (Fig. 58A). Moreover, adoptive transfer of T cells bearing Hu Wt TCR gp100 led to a moderate, but not significant reduction in primary tumor growth over time, indicating a trend of growth control (Fig. 58A). The Hu Chim scTCR gp100 $MuC_{\beta}$ construct did not led to a decrease in tumor volume, compared to PBS or Mock control groups. However, compared to mice treated with PBS, optimized scTCR gp100 constructs that co-expressed a $C_{\alpha}$ domain showed a significantly reduced tumor growth over time. Thereby, the strongest control was received using the

Cys-modified Hu Chim scTCR gp100 $MuC_{\beta}$ S79C + $MuC_{\alpha}$ T84C construct that sustained an additional disulfide bond between the $C_{\alpha}$ and $C_{\beta}$ (Fig. 58B). In this context, a reduction in the tumor volume for individual mice at d25 could be shown for the Cys-modified Hu Chim scTCR gp100 construct compared to PBS and unmodified scTCR (Fig. 58B).

In order to investigate, if transferred TCR transgenic T cells circulate or latently reside in memory niches of secondary lymphatic organs and can be provided for an antigen-specific recall response, mice were engrafted with a secondary tumor without additional T cell application (Fig. 55B). The growth of the secondary tumor was investigated in up to three independent animal experiments, which included in total 61 mice. Thereby, compared to Mock transduced T cell and PBS treated mice, both optimized scTCR gp100 transduced T cell constructs (Hu Chim scTCR gp100 $MuC_{\beta}$ + $MuC_{\alpha}$, Hu Chim scTCR gp100 $MuC_{\beta}$ S79C + $MuC_{\alpha}$ T84C) revealed a strongly reduced secondary tumor growth over time, indicating a memory T cell response of the optimized scTCR gp100 transduced T cells (Fig. 59B). Moreover, the secondary tumor sizes at d25 were significantly reduced in these treated murine cohorts. In contrast, the growth of the secondary tumors in mice originally treated with the un-optimized three domain scTCR or the dc Wt gp100 constructs, were not controlled over time (Fig. 59). Summarized, the revealed differences in tumor growth control were more pronounced in the course of the secondary than the primary tumor immune response, although mice received the gp100 TCR transduced T cells only once, at the beginning (d7) of the consecutive experiments.

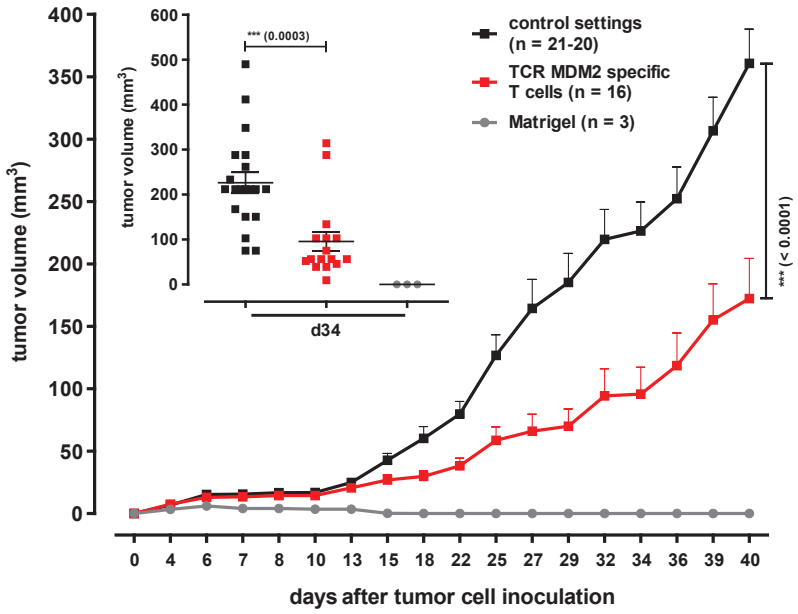


**Figure 57. Combined melanoma growth in NOD-SCID mice treated with MDM2 TCR specific T cell or control approaches.** The MeWo growth, from three independent experiments, in mice that either received MDM2 TCR specific T cells (red: Mu Wt TCR MDM2, Mu Mt Arg/Gly TCR MDM2, Mu Mt Lys/Gly TCR MDM2) or control approaches (black: Mock, Mu Mt TCR MDM2 CDR3 W109A, Mu Mt TCR MDM2 CDR3 G113V, PBS) are indicated. Compared to mice of control groups, significant tumor growth regression is shown for animals, treated with specific MDM2 TCR constructs. For statistical analysis, an unpaired two-tailed t test was performed. Mean ± SEM; n, number of individual mice; *** p value ≤ 0.001

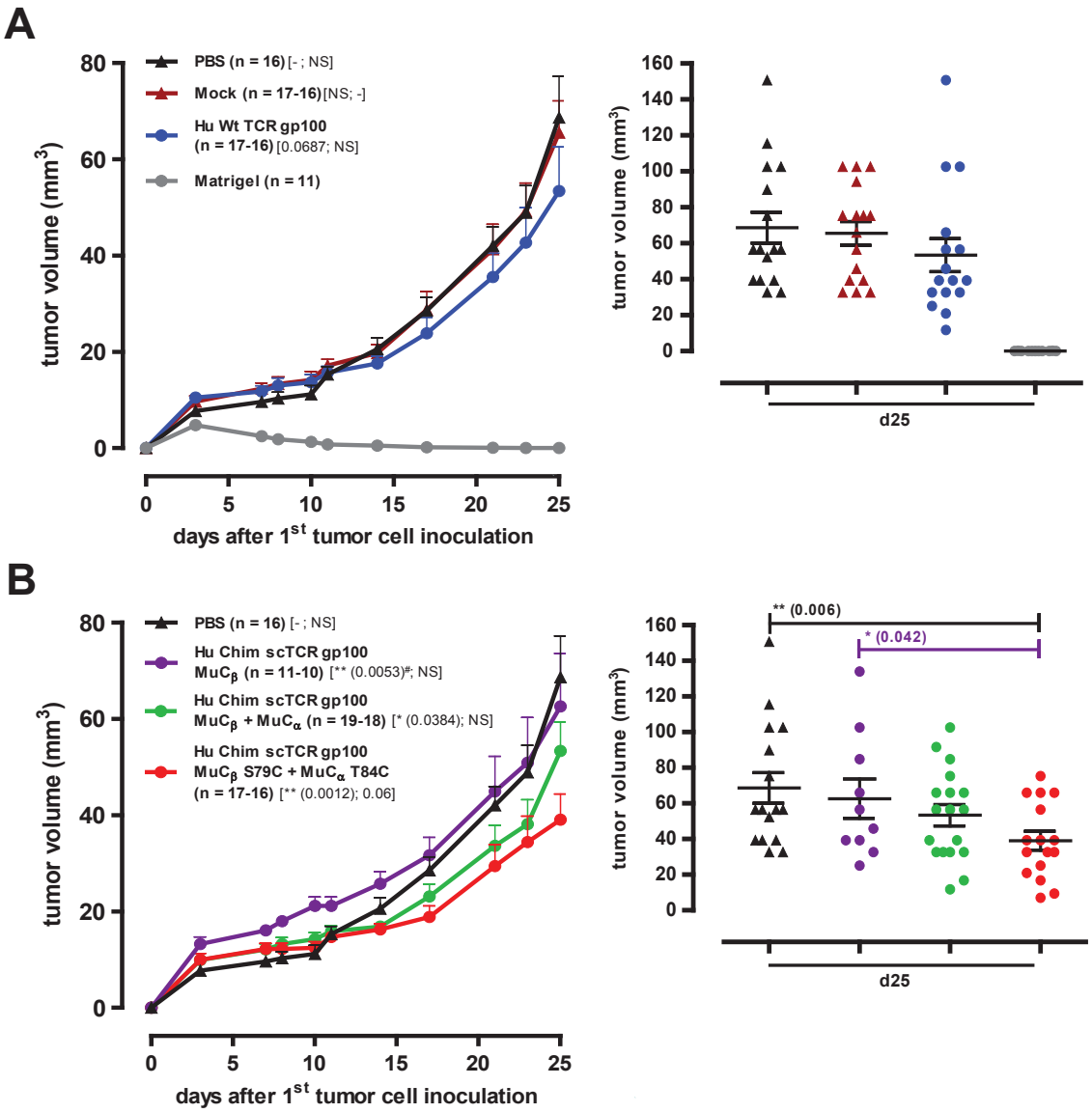


**Figure 58. Primary melanoma growth in NOD-SCID mice treated with gp100 TCR transgenic T cells.** NOD-SCID mice were i.d. engrafted with MeWo cells at the right flank and adoptively transferred i.v. with gp100 TCR transduced T cells on d7 after tumor cell injection. The effect of adoptive immunotherapy (ADI) on primary tumor growth over time is indicated. **A**) Tumor growth of mice treated with PBS, Mock or Hu Wt TCR gp100 transduced human T cells. As control Matrigel without tumor cells was i.d. inoculated. **B**) Tumor growth of mice treated with PBS, Hu Chim scTCR gp100 $MuC_{\beta}$, Hu Chim scTCR gp100 $MuC_{\beta}$ + $MuC_{\alpha}$ or Hu Chim scTCR gp100 $MuC_{\beta}$ S79C + $MuC_{\alpha}$ T84C transduced human T cells. The cumulative Mean ± SEM of up to five independent animal experiments is presented. P values in brackets indicate the statistical significant differences in tumor progression over time, calculated by the linear regression model with mixed effects against [PBS; Mock]. The graphs on the right side indicate the tumor volume of individual mice after primary tumor cell inoculation on d25. For statistical analysis, an unpaired two-tailed t test was performed. Mean ± SEM; n, number of individual mice; NS, not significant; #, significant higher compared to PBS control; * p value ≤ 0.05; ** p value ≤ 0.01

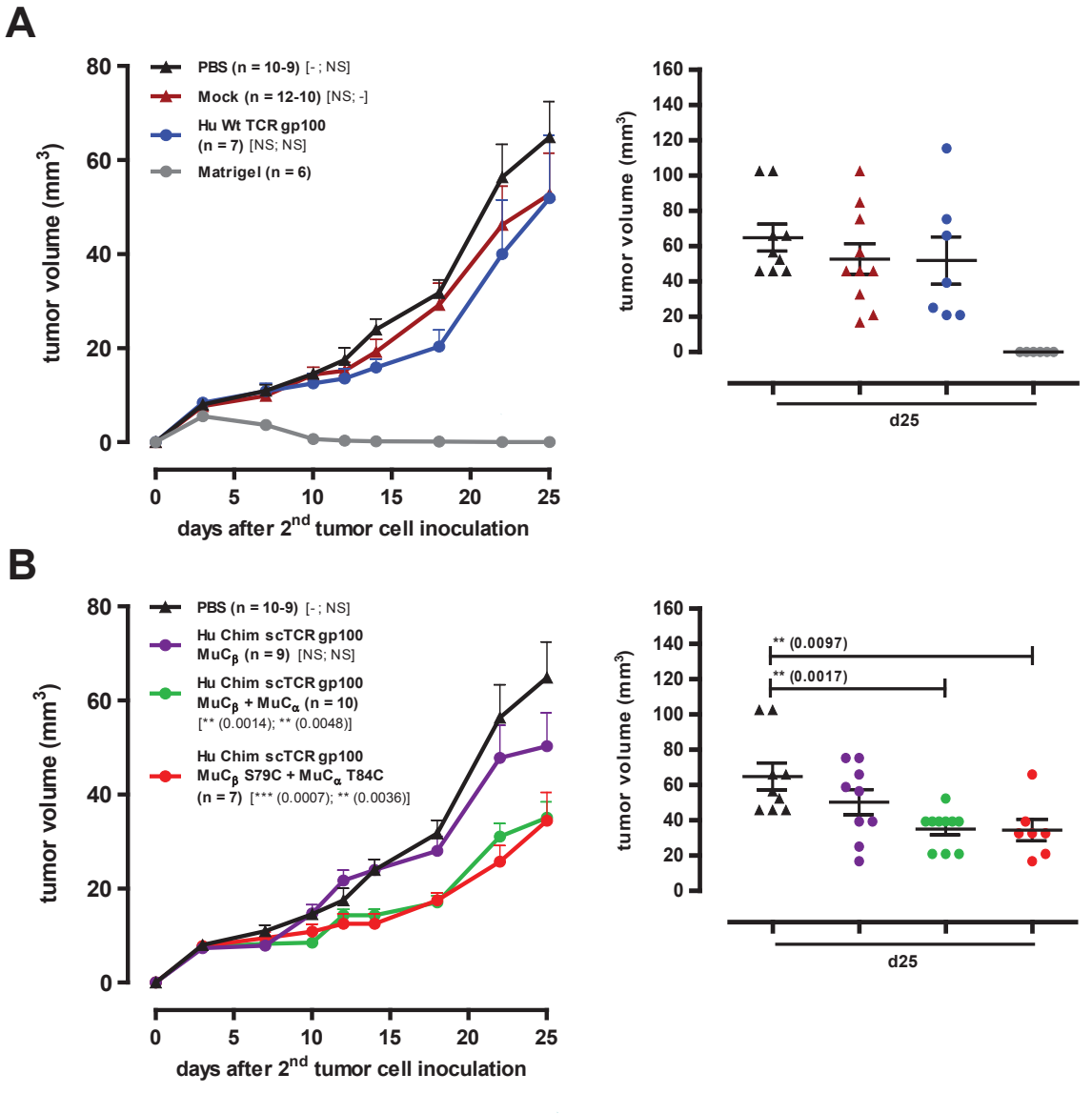


**Figure 59. Secondary melanoma growth in NOD-SCID mice treated with gp100 TCR transgenic T cells.** Primary i.d. applied tumors of NOD-SCID mice, previously treated with gp100 TCR transduced T cells were removed from the right flank and a secondary MeWo tumor was injected to the left flank of the same mice 2 d later (reset to d0). No further adoptive immunotherapy (ADI) with gp100 TCR transgenic T cells was performed. The secondary tumor growth over time under the effect of a long-term T cell response is indicated. **A**) Tumor growth in mice treated with PBS, Mock or Hu Wt TCR gp100 transduced human T cells. As control Matrigel without tumor cells was inoculated. **B**) Tumor growth of mice treated with PBS, Hu Chim scTCR gp100 $MuC_{\beta}$, Hu Chim scTCR gp100 $MuC_{\beta}$ + $MuC_{\alpha}$ or Hu Chim scTCR gp100 $MuC_{\beta}$ S79C + $MuC_{\alpha}$ T84C transduced human T cells. Curves show the cumulative Mean ± SEM of up to three independent animal experiments. P values in brackets indicate the statistical significant differences in tumor progression over time calculated by the linear regression model with mixed effects against [PBS; Mock]. The graphs on the right side indicate the secondary tumor volume of individual mice on d25. For statistical analysis, an unpaired two-tailed t test was performed. Mean ± SEM; n, number of individual mice; NS, not significant; ** p value ≤ 0.01

### 8.2.5. Generation of a stable firefly luciferase transfected MeWo cell line for optimization of the xenotransplantation model

To further investigate the tumor growth, a second measuring system was established. This approach aimed to verify the data of the melanoma growth control by TCR transgenic T cells, described in the previous sections that were obtained using a caliper for tumor growth measurement. In order to confirm the received results, a bioluminescence-based *in vivo* imaging of luciferase-positive tumor cells was established.

Therefore, human melanoma cells of line MeWo were transfected with the pcDNA3.1-luc-hygro vector that contained the firefly luciferase gene under control of a cytomegalovirus (CMV) promoter. The stable transfection was achieved by performing a selection with hygromycin. Afterwards, the firefly luciferase expression on single MeWo clones was analyzed by the *in vitro* luciferase measurement using the firefly luciferase reporter assay. The resulting 34 hygromycin resistant single clones of MeWo-luc were analyzed for firefly luciferase expression in the period of 28 to 41 d post transfection (Fig. 60).

After 4 independent experimental analyzes, of *in vitro* luciferase activity, the 10 hygromycin resistant MeWo-luc clones (11, 27, 29, 34, 36, 39, 44, 45, 49, 54) that revealed the strongest luciferase signal were additionally analyzed for luciferase expression. Therefore, an *in vitro* luciferase imaging was performed, in the period of 52 to 77 d post transfection. In three independent experiments, only the MeWo-luc clones 11, 34 and 36 revealed a stable and reproducible expression of luciferase over time (Figs. 61A-D). Thereby, different cell numbers of the individual clones were examined and revealed that the measured luciferase expression signals correlated with the cell numbers of the analyzed clones. At least $1x10^4$ MeWo-luc cells were required, to receive a luciferase signal that was clearly above the background signal, obtained from cells of the parental MeWo line (Fig. 61).

In order to use the luciferase-positive MeWo clones as potential tumor target cells for the murine xenotransplantation model for following applications, the expression of the MDM2 and gp100 antigens were analyzed by fluorescence microscopy. In this context, all three MeWo-luc lines (clones 11, 34 and 36) revealed positive for MDM2 and gp100 (Fig. 62). Furthermore, to analyze their *in vivo* growth behavior and bioluminescence signal, the MeWo-luc clones 11, 34 and 36 were applied to NOD-SCID mice. Each of the cell lines were i.d. injected in numbers of $2.5x10^6$ cells, resuspended in 50 µl matrigel, to the right flank of NOD-SCID mice. The mice were imaged using the IVIS100 imaging machine. Moreover, the tumor growth was additionally measured using a caliper. All three luciferase cell lines showed a tumor formation *in vivo* that was comparable to the tumor growth of the parental MeWo cells, with exception of cells from the line MeWo-luc 36 that showed a reduced growth behavior (Figs. 63A and B).

Furthermore, only for cells of the MeWo-luc 11 line, a successful tumor formation through *in vivo* imaging was revealed. This was characterized by increased bioluminescence signals over time, in contrast to the other MeWo-luc clones (Figs. 63C and D). The luciferase signals of MeWo-luc 34 and 36 increased up to d7. At this time point they were clearly above the background signal of the

negative controls and comparable to the signal of clone MeWo-luc 11. But in contrast to clone 11, they did not further increase during the following time course (Fig. 63C). Since generally, the tumors of the MeWo-luc 34 and 36 clones grew normally *in vivo*, both clones seemed to be strongly dependent on an ongoing selection by hygromycin, to keep a stable luciferase expression (Figs. 63A-D). In contrast to the *in vitro* cell cultivation, hygromycin was not added to the mice *in vivo*. Moreover, a treatment with matrigel or the application of cells from the parental MeWo line did not exceed the background luciferase value of an untreated mouse (Fig. 63C).

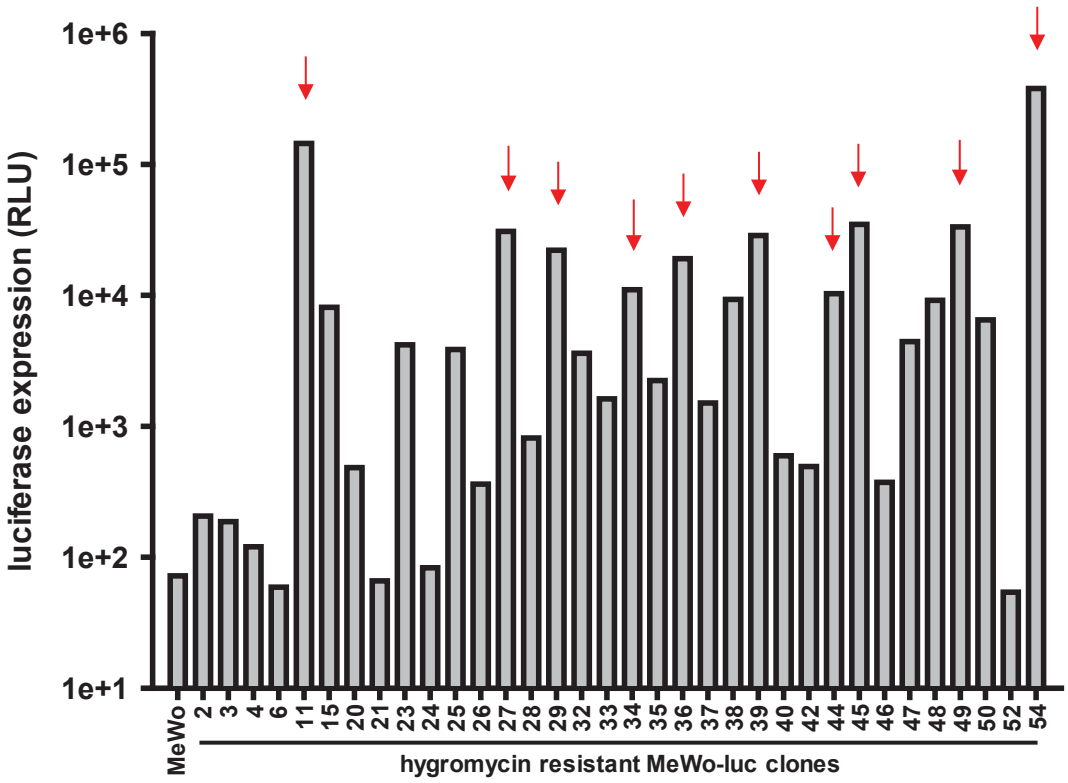


**Figure 60. Generation of firefly luciferase expressing MeWo cell clones.** Cells of the human melanoma line MeWo were transfected with the pcDNA3.1-luc-hygro vector and single clones were selected by hygromycin addition. Thereby, 34 hygromycin resistant single clones of MeWo-luc were obtained and analyzed for *in vitro* firefly luciferase activity, indicated by relative light units (RLU) using the firefly luciferase reporter assay. The 10 MeWo-luc clones, indicated by red arrows were further investigated by *in vitro* luciferase imaging using the IVIS100 imaging machine.

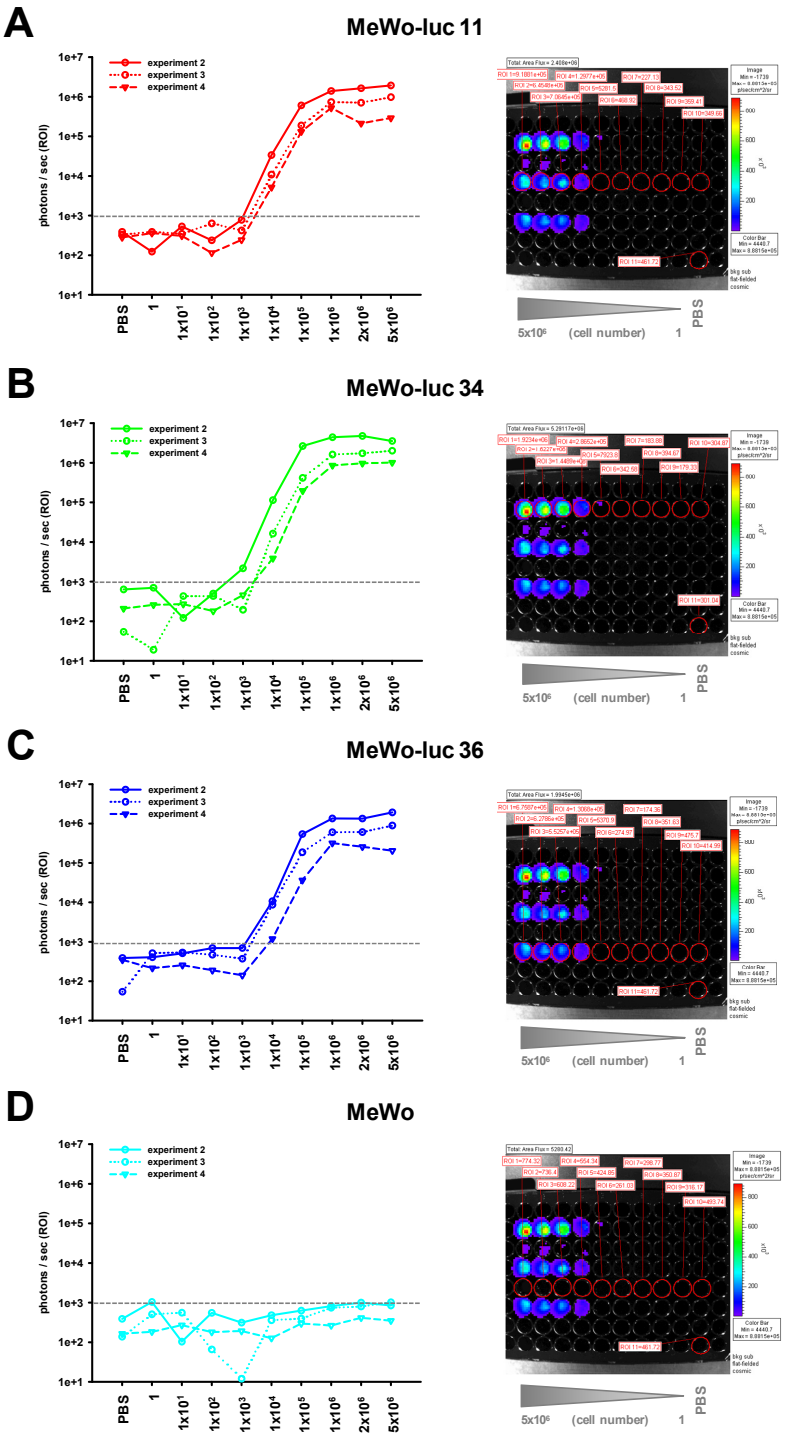


**Figure 61. Verification of firefly luciferase expression in stable transfected MeWo-luc clones.** The stable transfected MeWo-luc clones 11 (**A**), 34 (**B**) and 36 (**C**) were investigated for firefly luciferase expression through *in vitro* luciferase imaging using the IVIS100 imaging system. To investigate the background signal (indicated by dashed line), cells of the parental MeWo line were examined (**D**). Various numbers of cells (1, $1x10^1$, $1x10^2$, $1x10^3$, $1x10^4$, $1x10^5$, $1x10^6$, $2x10^6$, $5x10^6$) of each clone or the parental line were analyzed, in three independent experiments, between d52 to d77 after transfection. As negative control, PBS without any cells was analyzed. The micrographs on the right side show a representative *in vitro* measured plate (exposure time of 300 sec). Thereby, the MeWo-luc clones or the parental line are highlighted by red circles, indicating the calculated region of interest (ROI), which is presented by the respective cumulative data in the graphs on the left side. The bioluminescent signal of the calculated ROI is indicated as p/sec/cm$^2$/sr.

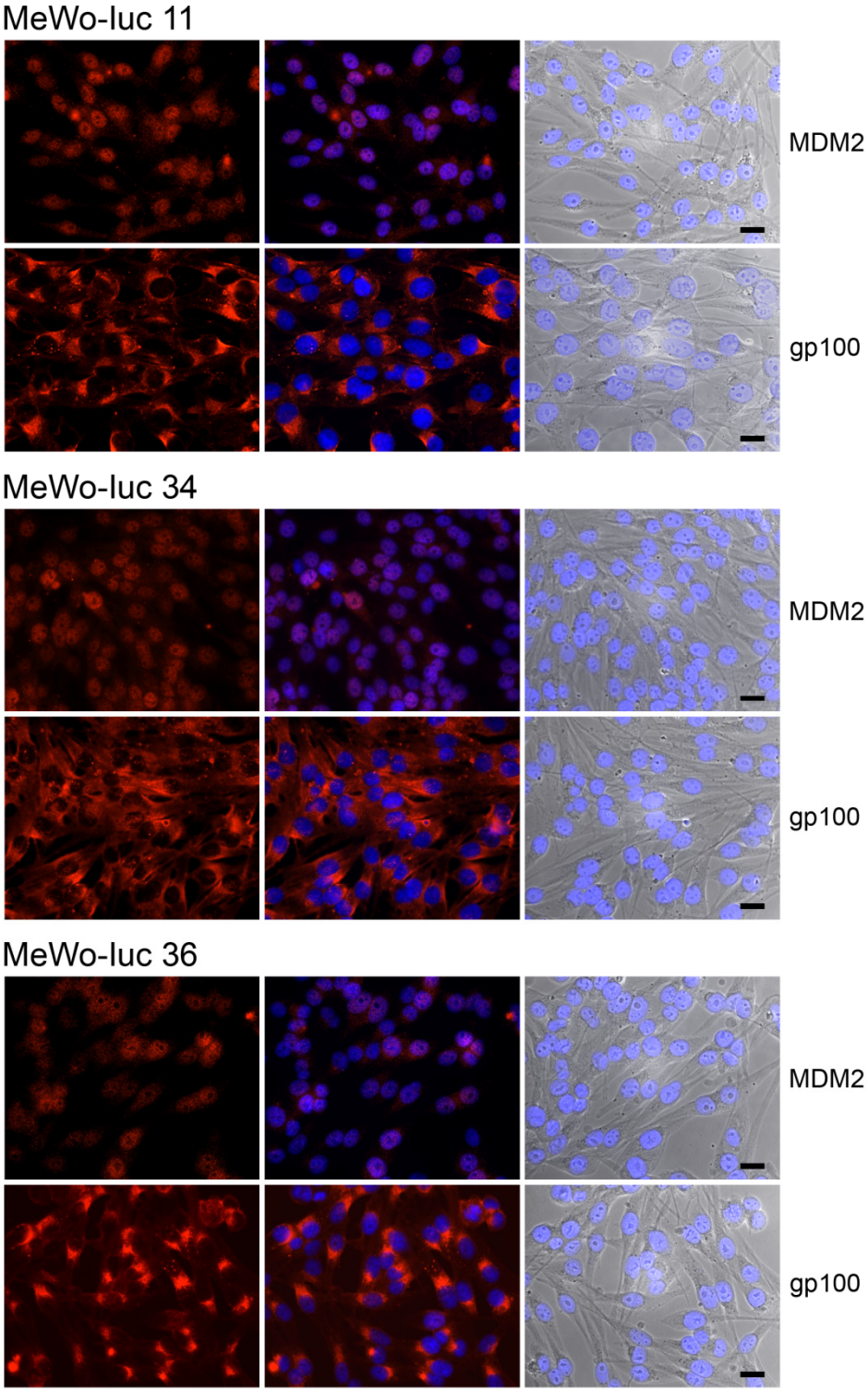


**Figure 62. Immunofluorescence microscopy showing MDM2 and gp100 in selected human melanoma MeWo-luciferase expressing cell clones.** Immunofluorescence microscopy images of MeWo-luc 11, 34 and 36 cells show a strong expression of MDM2 and gp100 (both in red). DAPI (blue) was used to indicate the cell nuclei and the phase contrast image to present the cell morphology. Bars represent 20 µm.

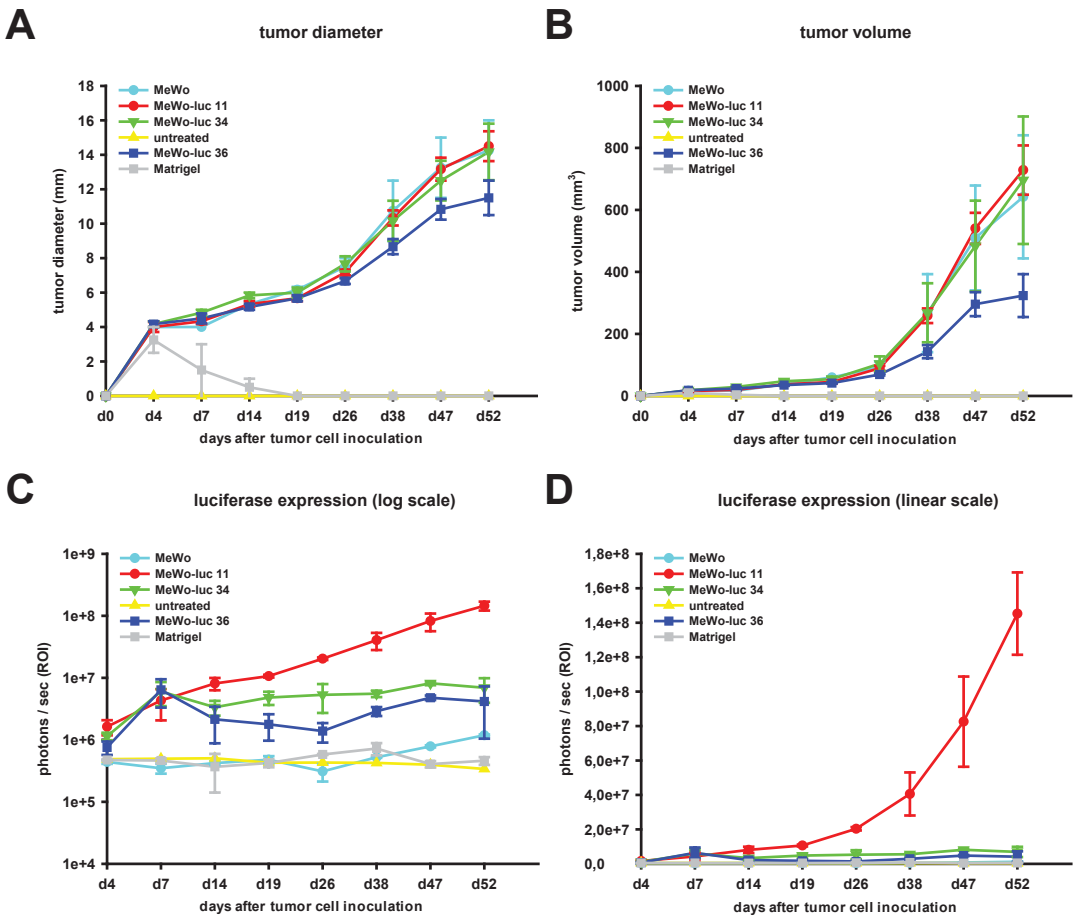


**Figure 63. *In vivo* imaging of tumor formation of the selected MeWo-luc clones 11, 34 and 36.** Local i.d. tumor formation in NOD-SCID mice of stable transfected cells of MeWo-luc clones 11, 34 and 36 (3 mice/group). Cells ($2.5x10^6$) were injected on d0, followed by *in vivo* imaging and tumor measurement. The growth of the luciferase transfected lines were compared to the parental cell line (3 mice). As negative controls, mice injected only with matrigel (2 mice) or entirely untreated (1 mouse) were used. The tumor size-measurement data are indicated as tumor diameter (**A**) and tumor volume (**B**). The bioluminescent luciferase expression (exposure time of 120 sec) is shown in log (**C**) and linear scale (**D**). The calculated ROI is indicated as p/sec/cm$^2$/sr.

Since the MeWo-luc 11 line revealed a stable expression of luciferase, going along with an increased tumor formation over time after a continuous cultivation for more than four months, also in the absence of hygromycin, these cells were used as tumor target line for the murine xenotransplantation model (Fig. 64A). Moreover, cells of this line did not metastasize to murine organs when i.d. injected and only the tumor showed a specific luciferase signal. In mice that received the cells 52 d beforehand, no luciferase signal was detectable in the spleen, lung, liver, intestine, stomach or kidneys (Fig. 64B). In addition, using flow cytometry, the MeWo-luc 11 cells were proven to be HLA-A2$^+$ (Fig. 64C). In summary, these cells were suitable for an i.d. *in vivo* tumor formation, followed by ADI with TCR transgenic T cells.

Therefore, MeWo-luc 11 cells ($2.5x10^6$) were injected i.d. to the right flank of NSG mice and 7 d later, treated with gp100 TCR transgenic T cells ($5x10^6$). The tumor growth was analyzed using a caliper and by detection of the bioluminescence signal of MeWo-luc 11 cells. Compared to NOD-

SCID mice, which lack endogenous T and B cells, in NSG mice also NK cells are absent. They additionally reveal a higher level of engraftment of human cells. The luciferase signal and the measured tumor volume, of PBS treated mice, increased continuously from d4 to d56 (Figs. 65A and B). Compared to PBS treated mice, adoptive transfer of T cells bearing Hu Wt TCR gp100 or Hu Chim scTCR gp100 $MuC_{\beta}$ S79C + $MuC_{\alpha}$ T84C constructs led to a strongly reduced luciferase signal and tumor volume (Figs. 65A and B). Moreover, beforehand transferred human T cells revealed to be $CD3^{+}$ (Fig. 50) and $CD45^{+}$ (data not shown), could be detected in the PB of adoptively treated mice on d12 (Figs. 65C and D).

The MeWo-luc 11 cells, as target line for the xenotransplantation model, verified the treatment results obtained for the adoptive immunotherapy with TCR transgenic T cells. Thereby, the tumor growth was controlled, measured with a caliper and analyzed through luciferase bioluminescence imaging. In these optimized model, Hu Wt TCR gp100 transduced T cells revealed a tumor growth control comparable to Hu Chim scTCR gp100 $MuC_{\beta}$ S79C + $MuC_{\alpha}$ T84C modified cells, explainable by the use of twice as high amounts of transferred T cells, compared to the previous setting (cf., 8.2.4) and the use of NSG mice as model organisms.

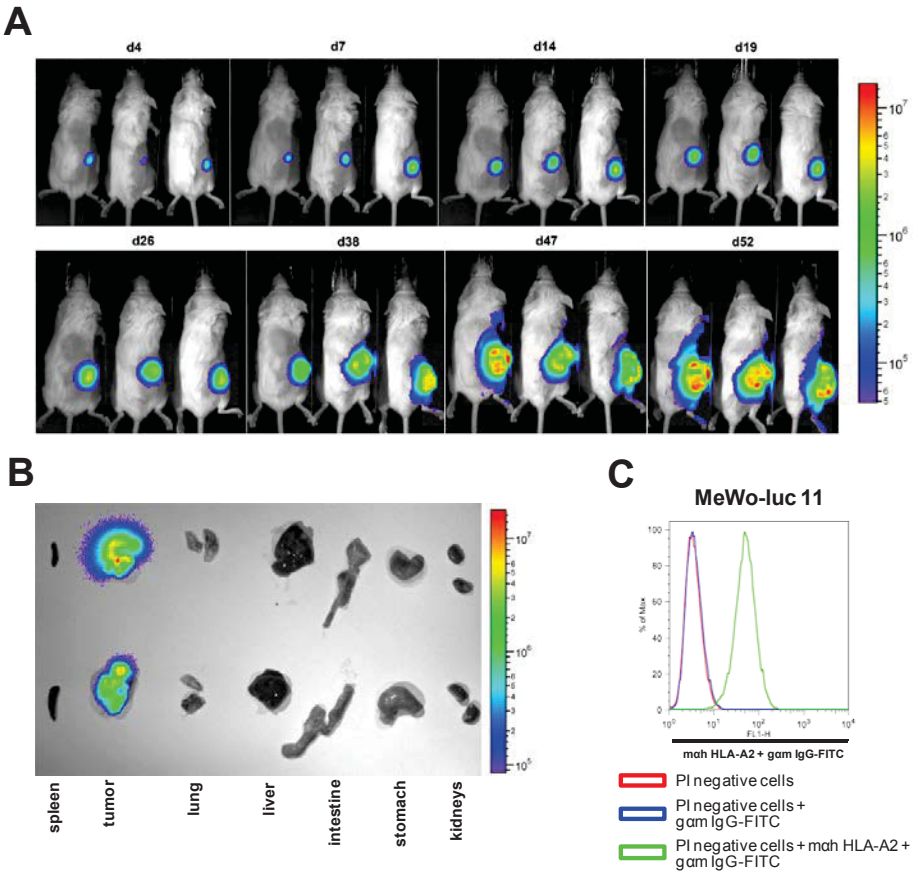


**Figure 64. *In vivo* imaging of tumor formation and analysis of HLA-A2 expression of MeWo-luc 11 cells. A**) Stable transfected MeWo-luc 11 cells ($2.5x10^{6}$) were i.d. injected to three NOD-SCID mice on d0. The tumor formation was followed over time using the IVIS100 imaging system (exposure time of 120 sec). **B**) The mice were sacrificed on d52 and the organs imaged for metastases (exposure time of 60 sec). Representative organs of two MeWo-luc 11 tumor-bearing mice are presented. **C**) Using flow cytometry, MeWo-luc 11 cells were $HLA\text{-}A2^{+}$.

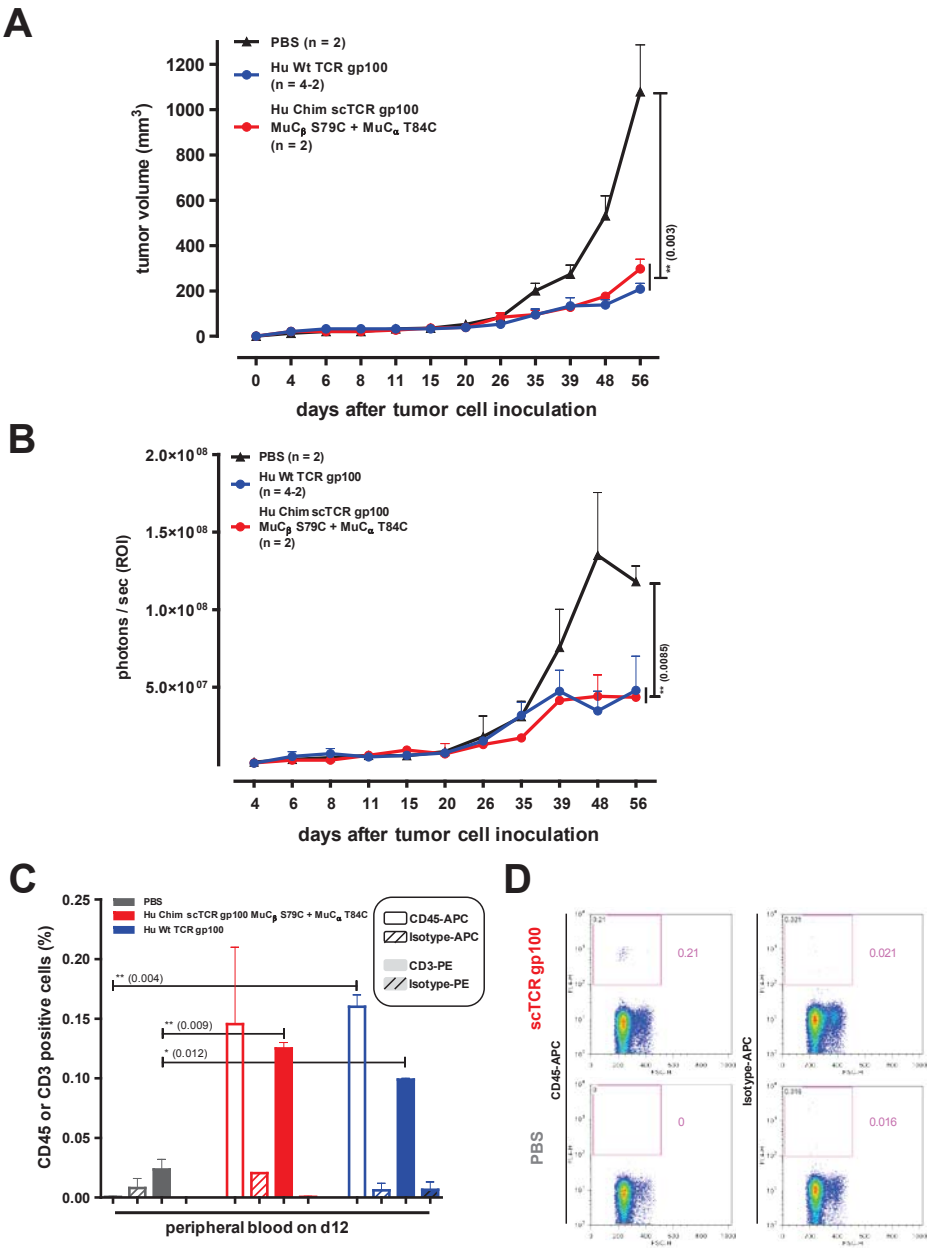


**Figure 65. *In vivo* imaging of MeWo-luc 11 tumor growth in NSG mice treated with gp100 TCR transgenic T cells.** NSG mice were engrafted with MeWo-luc 11 cells ($2.5x10^6$ cells) to the right flank on d0 and adoptively transferred with gp100 TCR transduced T cells (Hu Wt TCR gp100, Hu Chim scTCR gp100 $MuC_\beta$ S79C + $MuC_\alpha$ T84C) on d7 ($5x10^6$ cells). The effect of ADI on tumor growth over time is indicated, measured using a caliper (**A**) and by detection of the luciferase bioluminescence signal of MeWo-luc 11 cells (exposure time of 120 sec; calculated ROI is indicated as p/sec/$cm^2$/sr; **B**). The statistical differences between the groups on d56 are indicated. **C**) The PB of mice (2 mice/group) was analyzed by flow cytometry for $CD45^+$ or $CD3^+$ human T cells on d12. **D**) Representative FACS dot plots (left column: staining with CD45-APC Ab; right column: Isotype-APC Ab control) of PB samples of a tumor-bearing mouse treated with scTCR gp100 (Hu Chim scTCR gp100 $MuC_\beta$ S79C + $MuC_\alpha$ T84C) transgenic human T cells (upper panel) and of a tumor-bearing mouse treated with PBS (lower panel). Dead cells were excluded by 7AAD. The magenta numbers in the dot plots indicate the percentage of positive stained cells. For statistical analysis, an unpaired two-tailed t test was performed. Mean ± SEM; n, number of individual mice; * p value ≤ 0.05; ** p value ≤ 0.01

### 8.2.6. Combinational treatment of adoptive human T cell therapy and local low dose tumor irradiation for optimization of the xenotransplantation model

For the RIP1-Tag5 mouse model of spontaneous insulinomas it has been shown that murine T cell infiltration into the tumor was increased while combining a local low dose tumor irradiation with an adoptive T cell therapy (Ganss et al., 2002; Seibel, 2010). Therefore, to further optimize the xenotransplantation model, before injection of the TCR transgenic T cells, a local low dose tumor irradiation was performed.

In order to irradiate the tumor and not other organs of the mice, the treatment protocol of the animal model had to be modified (cf., Fig. 66). The MeWo cells were i.d. injected to the right murine hind leg of NSG mice. That allowed the irradiation of the tumor-bearing leg without hitting other organs at the same time. A local low dose tumor irradiation with 2 Gy was performed on d6 after tumor cell injection. The adoptive T cell transfer with Hu Chim scTCR gp100 $MuC_{\beta}$ S79C + $MuC_{\alpha}$ T84C modified human T cells occurred on d7 and the tumor growth was measured over time.

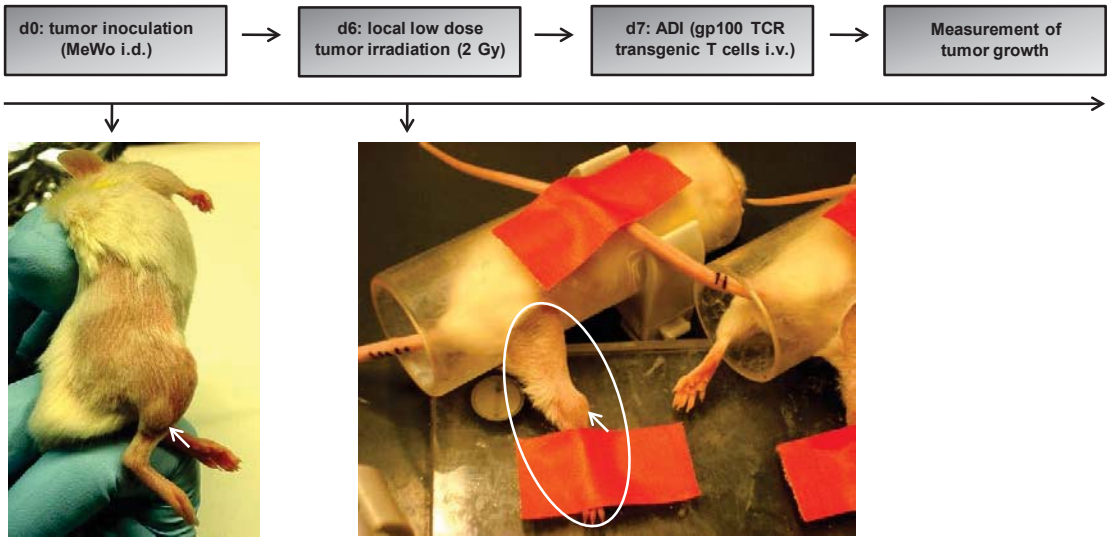


**Figure 66. Experimental setting of the xenotransplantation model with combinational treatment of local low dose tumor irradiation and ADI.** NSG mice were engrafted i.d. on the right hind leg with cells of the line MeWo on d0 (white arrows). A local low dose tumor irradiation (2 Gy) was performed on d6. The area of irradiation is indicated by the white-bordered circuit (right image). TCR transgenic T cells were transferred i.v. on d7 and the tumor growth measured over time.

Two independent murine experiments with combinational treatment of tumor irradiation and ADI were performed, including 21 individual NSG mice. Thereby, the two established tumor measurement methods were used. In the first experiment, MeWo cells ($2.5x10^6$ cells) were injected, followed by the local low dose tumor irradiation on d6 and the transfer of Hu Chim scTCR gp100 $MuC_{\beta}$ S79C + $MuC_{\alpha}$ T84C transduced human T cells ($2.5x10^6$ cells) on d7, d8 and d9. Summarized, already without additional T cell transfer, the local low dose irradiation of the tumor influenced the tumor growth *in vivo* and led to a slower growth compared to the non-irradiated PBS

treated control mice (Figs. 67A and B). However, compared to the PBS treated groups, the combinational approach of local low dose irradiation and adoptive transfer was able to further strongly control the tumor growth over time (Figs. 67A and B). The transferred human T cells could be detected in the PB of adoptively treated mice on d13, after tumor cell injection (Fig. 67C). Compared to PBS treated mice, increased amounts of human $CD45^+$ cells were found in the PB of the adoptively transferred animals. Thereby, in the PB of the tumor irradiated mice, the percentage of these $CD45^+$ cells was slightly, but not significantly, increased compared to adoptively treated non-irradiated animals (Figs. 67C and D).

In the second combinational treatment experiment, MeWo-luc 11 cells were again injected to the right hind leg of NSG mice. The local low dose tumor irradiation was performed on d7, followed by the transfer of Hu Chim scTCR gp100 $MuC_\beta$ S79C + $MuC_\alpha$ T84C transduced human T cells ($5x10^6$ cells) on d8. In summary, both methods for analysis of tumor growth using caliper and bioluminescence signal detection, revealed comparable and reproducible results. It could be shown that the tumor was best controlled in mice that received a combinational treatment (Figs. 68A-D). In addition, this experiment confirmed the observation that the local low dose tumor irradiation alone already slowed the tumor growth (Figs. 67A and B, 68A and B). However, compared to irradiated tumor-bearing mice treated with PBS, it could be confirmed that a combinational treatment with tumor irradiation and ADI using gp100 TCR modified T cells led to an additional reduction in tumor growth, indicted by reduced luciferase signal and measured tumor volume (Figs. 68C and D). Moreover, the luciferase signal and the caliper-measured tumor volume of tumor-bearing mice treated with PBS increased continuously from d3 to d23 (Figs. 68A and B). As shown for the previous experiments, the adoptively transferred T cells were successfully detected in the PB by flow cytometry staining for human $CD45^+$ cells on d14 (data not shown).

→

**Figure 67. Melanoma growth in NSG mice treated with local low dose tumor irradiation and gp100 TCR transgenic T cells.** NSG mice were engrafted with MeWo cells ($2.5x10^6$ cells) at the right hind leg on d0. The tumor was locally irradiated with 2 Gy on d6 and the mice were adoptively transferred with Hu Chim scTCR gp100 $MuC_\beta$ S79C + $MuC_\alpha$ T84C transduced T cells on d7, d8 and d9 (each $2.5x10^6$ cells). The effect of ADI and local low dose tumor irradiation on the tumor growth is indicated and was measured by a caliper (**A**). The statistical differences between the groups on d50 (**A**) and d31 (**B**) are shown. **C**) Using flow cytometry, the PB of mice (3 mice/group) was analyzed for human $CD45^+$ cells on d13. **D**) Representative FACS dot plots (left column: staining with CD45-APC Ab, right column: Isotype-APC Ab control) of PB samples of a tumor-bearing mouse, locally irradiated with 2 Gy and treated with scTCR gp100 TCR transgenic human T cells (upper panel) and of an equally treated mouse injected with PBS (lower panel). Dead cells were excluded by 7AAD. The magenta numbers in the dot plots indicate the percentage of positive stained cells. For statistical analysis, an unpaired two-tailed t test was performed. Mean ± SEM; n, number of individual mice; * p value ≤ 0.05; ** p value ≤ 0.01

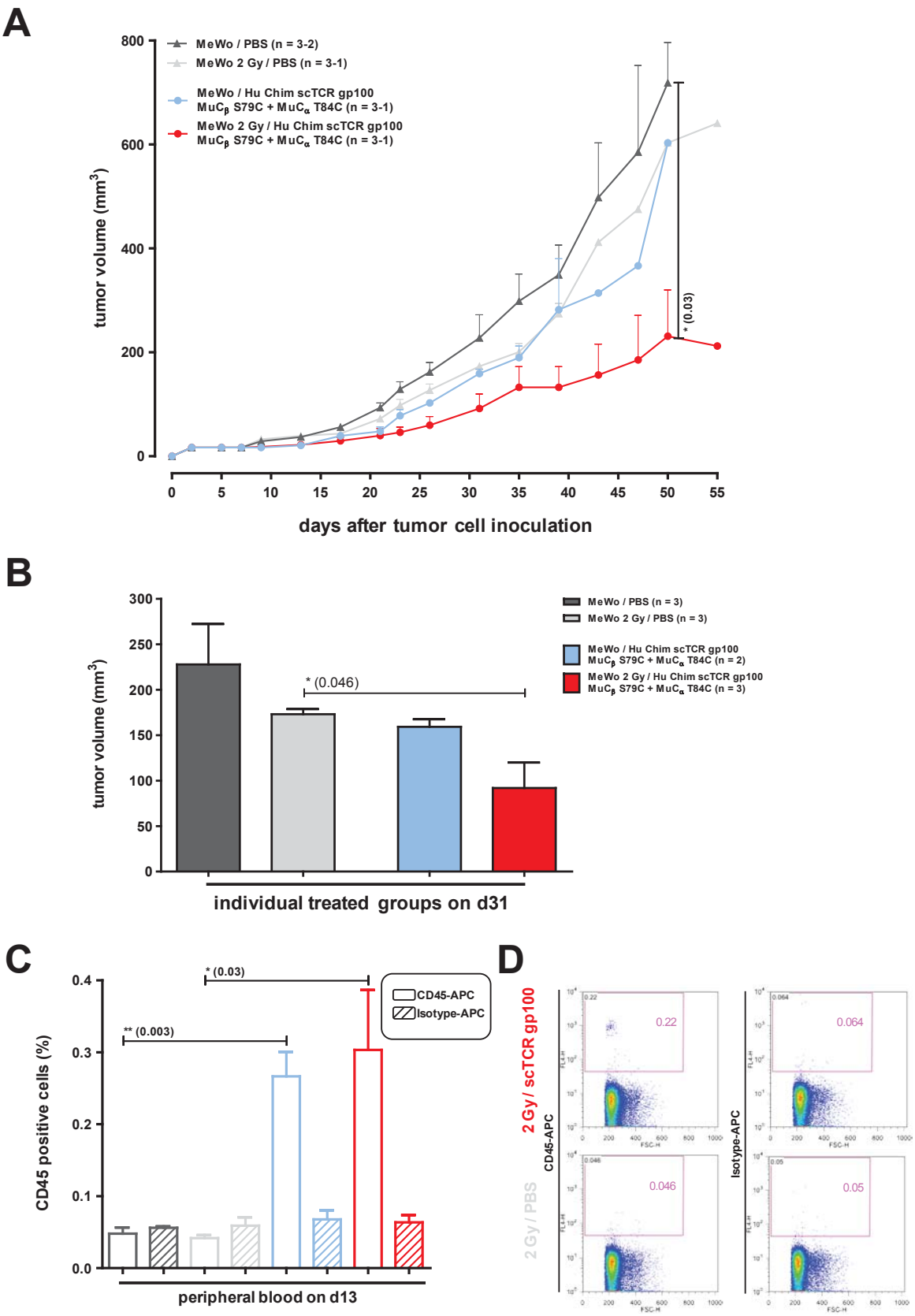


**Figure 67. Melanoma tumor growth in NSG mice treated with local low dose tumor irradiation and gp100 TCR transgenic T cells.** The detailed figure legend is presented on the previous page.

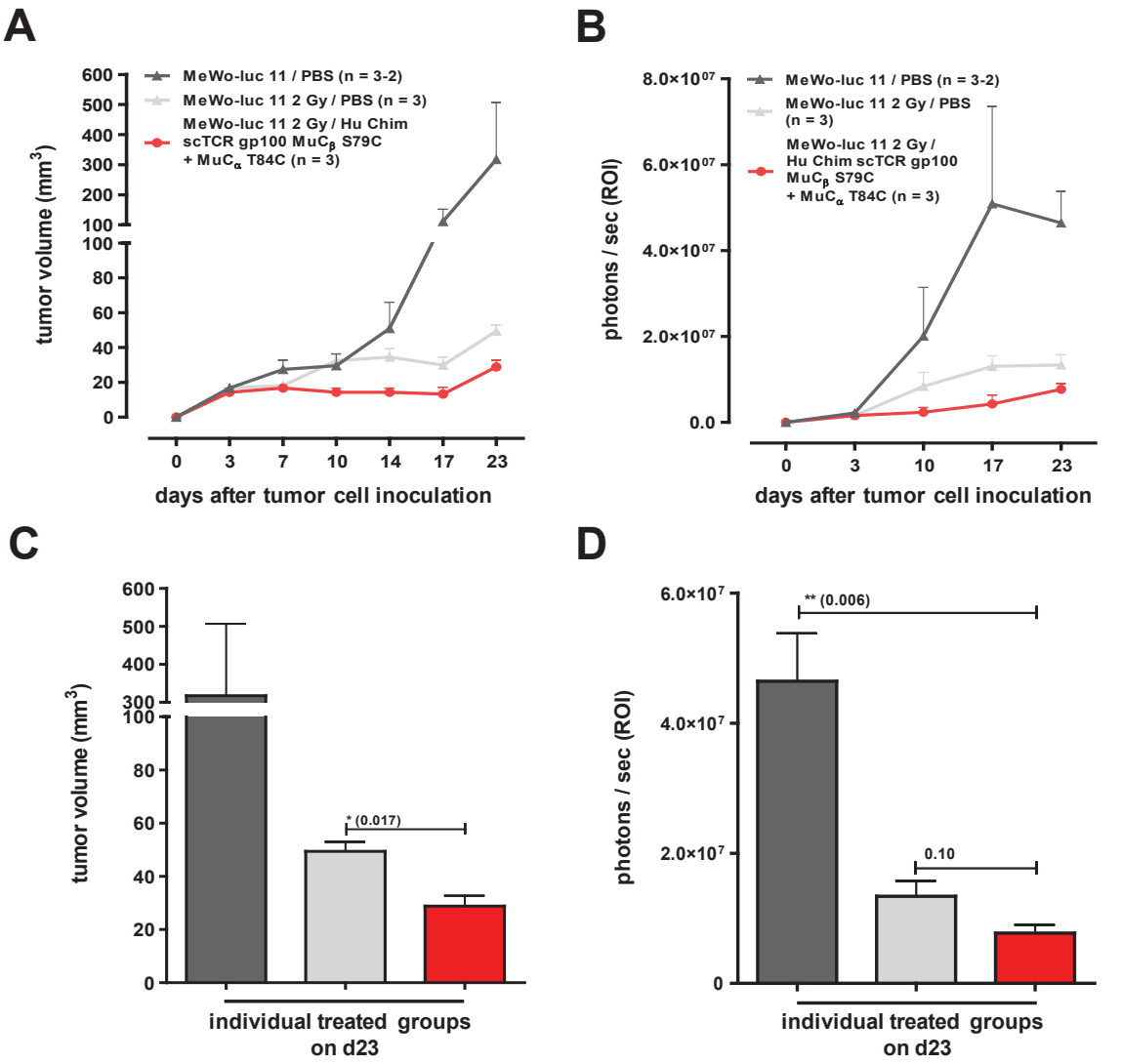


**Figure 68. MeWo-luc 11 tumor growth in NSG mice treated with local low dose tumor irradiation and gp100 TCR transgenic T cells.** NSG mice were engrafted with MeWo-luc 11 cells ($2.5x10^6$ cells) at the right hind leg on d0. The tumor was locally irradiated with 2 Gy on d7 and the mice were adoptively transferred with Hu Chim scTCR gp100 $MuC_\beta$ S79C + $MuC_\alpha$ T84C transduced T cells on d8 ($5x10^6$ cells). The effect of ADI and local low dose tumor irradiation on the tumor growth is indicated and was measured using a caliper (**A**) and by detection of the bioluminescence signal of luciferase-positive MeWo-luc 11 cells using the IVIS100 imaging system (exposure time of 60 sec; calculated ROI is indicated as p/sec/$cm^2$/sr; **B**). The statistical differences between the groups measured by caliper (**C**) or *in vivo* luciferase imaging (**D**) on d23 are shown (black: MeWo-luc 11 / PBS n = 2, gray: MeWo-luc 11 2 Gy / PBS n = 3, red: MeWo-luc 11 2 Gy / Hu Chim scTCR gp100 $MuC_\beta$ S79C + $MuC_\alpha$ T84C transduced T cells n = 3). For statistical analysis, an unpaired two-tailed t test was performed. Mean ± SEM; n, number of individual mice; * p value ≤ 0.05; ** p value ≤ 0.01

Furthermore, the obtained tumors of the combinational treatment experiment were investigated for infiltrated human T cells. Using immunohistochemistry, human $CD45^+$ cells were detected in locally irradiated tumors of adoptively transferred mice. Compared to mice only treated with T cells, were no human $CD45^+$ cells could be detected, the number of revealed $CD45^+$ cells was increased in tumors of mice that received a combinational treatment (Fig. 69). Representative stainings of tumor sections from a mouse that received a combinational treatment are shown in Fig. 70. To ensure the human CD45 Ab specificity, human spleen tissue was tested in parallel. In contrast, the human spleen tissue as expected was negative for gp100 stainings (data not shown).

In addition, flow cytometry analysis was performed to detect human $CD45^+$ cells in the removed tumors. Thereby, no specifically stained $CD45^+$ cells were detected, probably due to the many lost or dead cells caused by digestion or mechanical procedures during the single cell preparation that was needed to perform subsequent stainings.

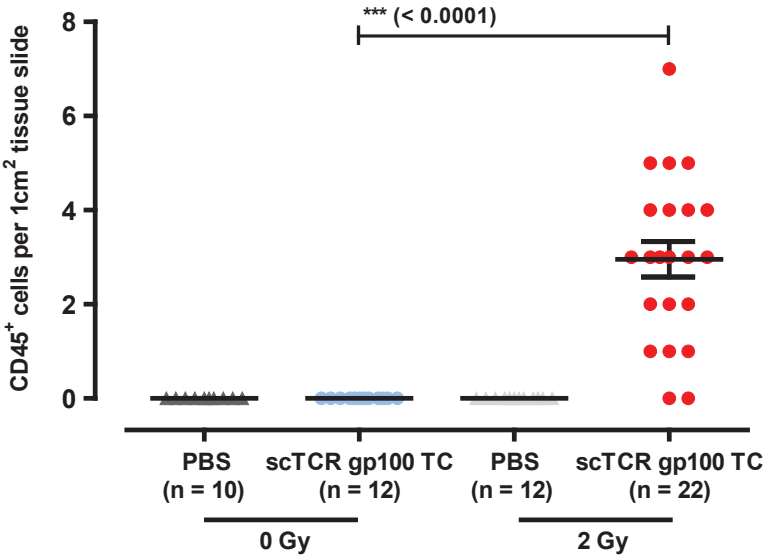


**Figure 69. Cumulative detection of human $CD45^+$ cells in MeWo tumors by immunohistochemistry.** Mice were injected with MeWo cells ($2.5x10^6$ cells), followed by combinational treatment with local low dose irradiation (2 Gy) and ADI using Hu Chim scTCR gp100 $MuC_\beta$ S79C + $MuC_\alpha$ T84C transduced T cells ($5x10^6$ cells). As control, mice were treated with PBS instead of T cells and without local low dose tumor irradiation (0 Gy). The tumors of the respective treated murine groups were removed (between d22-d24 after tumor cell injection) and immediately snap-frozen. The cumulative data of several tumor tissue sections, stained with human CD45 Abs are indicated. The $CD45^+$ stained cells were counted and calculated per tumor area using the following formula for calculation of elliptical areas π x a x b (π = 3.14159). Compared to the other groups, mice treated with the combinational approach showed an increased tumor infiltration of $CD45^+$ cells. n = number of tissue slides; TC, T cells

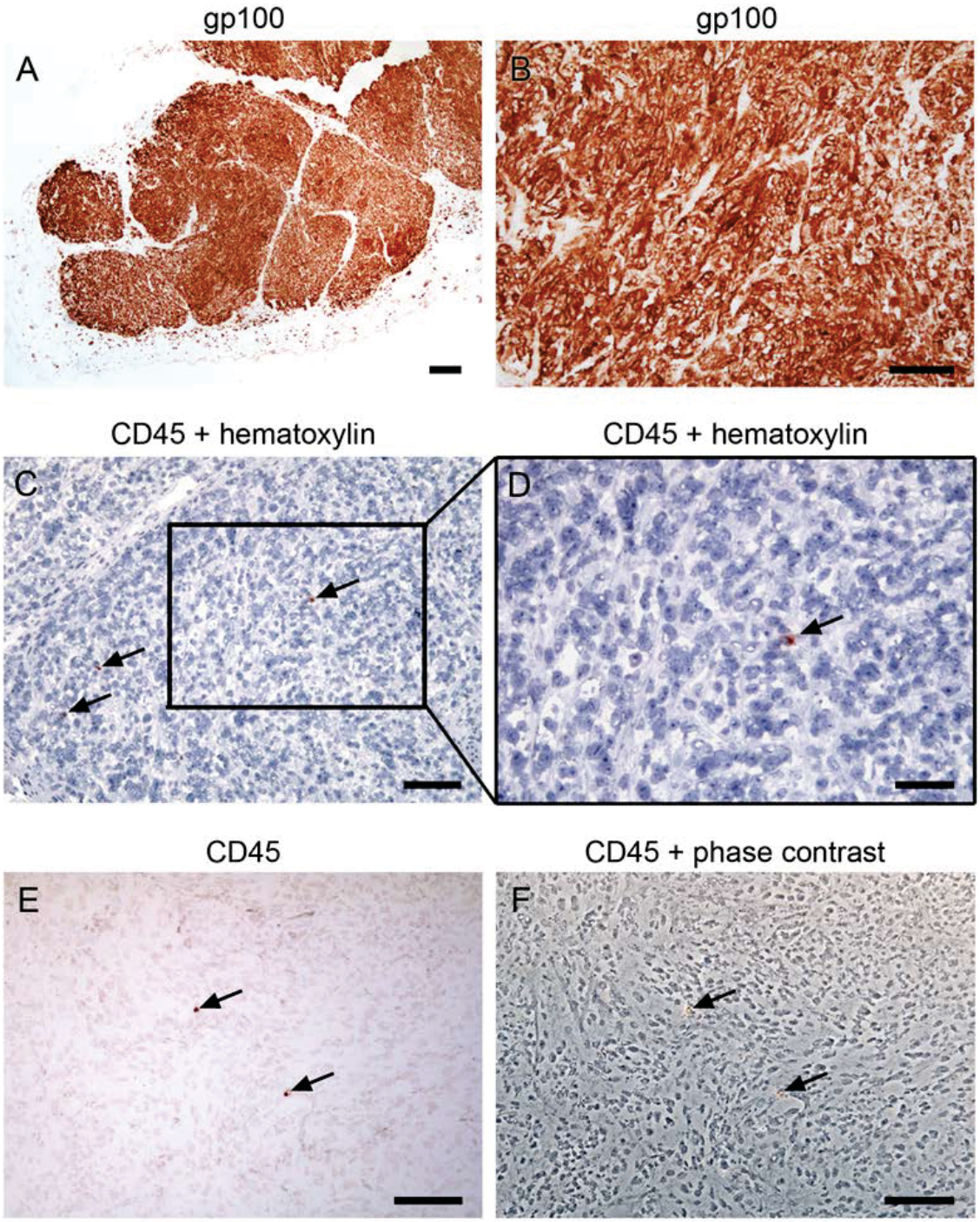


**Figure 70. Immunohistochemical stainings of MeWo tumor sections of a combinational therapy treated mouse.** The NSG mouse was injected with MeWo-luc 11 cells ($2.5x10^6$ cells), followed by therapy with local low dose tumor irradiation (2 Gy) and ADI using Hu Chim scTCR gp100 $MuC_\beta$ S79C + $MuC_\alpha$ T84C transduced T cells ($5x10^6$ cells). The tumor was removed on d24 after tumor cell injection and immediately snap-frozen. Microscopically images of representative tumor sections are presented, showing strong expression of gp100 (red-brown (**A** and **B**) and human $CD45^+$ cells (red-brown), indicated by black arrows (**C-F**). **D**) The magnification of the boxed area presented in **C** is depicted. A nuclear counter stain was performed with Hematoxylin (blue; **C** and **D**). To present the cell morphology, the phase contrast is indicated in image **F**. Bars represent 200 µm (**A**), 100 µm (**B**, **C**, **E**, **F**) and 50 µm (**D**).

### 8.2.7. Summary on the *in vivo* efficiency of optimized TCR transgenic human T cells

TCRs with specificities for MDM2 or gp100, optimized to avoid hybrid dimer formation between exogenous and endogenous TCR chains, were analyzed. The various optimized TCR constructs were transduced into human T cells using retroviral pBullet vectors and shown to be stable and functional expressed by the T cells *in vitro*. In order to investigate the impact of the adoptively transferred, optimized TCR transgenic T cells *in vivo*, a murine xenotransplantation model was established using immunodeficient NOD-SCID or NSG mice. As tumor target line, cells of the HLA-$A2^{+}MDM2^{+}gp100^{+}$ human melanoma line MeWo were i.d. applied.

Human T cells equipped with specifically optimized TCRs for the antigens MDM2 or gp100 were thereby able to strongly control the tumor growth *in vivo*. The tumor growth was analyzed in a large and statistically reliable scale, measured using a caliper and verified by bioluminescence *in vivo* imaging of the stable transfected MeWo-luc 11 line. It could be shown that the effect of tumor growth control by TCR modified T cells was increased using higher numbers of transferred cells.

The transduced T cells revealed an effector memory-like phenotype ($CCR7^{-}CD45RO^{+}CD62L^{-}$), containing cells positive for CD27, a marker that promotes long-term survival and persistence of functional effector memory T cells *in vivo*. Moreover, without further T cell injection, a secondary tumor growth was strongly reduced in the originally adoptively transferred animals, showing a memory T cell response of the transduced T cells. Finally, a combinational treatment of local low dose tumor irradiation of 2 Gy together with an adoptive therapy of gp100 TCR transduced T cells, further controlled the tumor growth *in vivo*.

## 8.3. Further strategies to influence human tumor cell growth

Besides tumor antigen-specific TCR transgenic T cells for tumor growth control, further strategies to target tumor cells and influence the tumor growth behavior were addressed in the presented thesis. On the one hand, the impact of the carcinoembryonic antigen-related cell adhesion molecule 6 (CEACAM6) and L1 cell adhesion molecule (L1CAM) was investigated in the context of T cell-mediated tumor recognition. On the other hand, the viral targeting of oncolytic Newcastle disease virus (NDV) to tumor cells was addressed using human T cells as transfer vehicles to deliver the viral particles in a “hitchhiking”-like process.

### 8.3.1. CEACAM6 expression and impact of CEACAM6 inhibition on human tumor cells

The presence of the cell adhesion molecule CEACAM6 on the surface of tumor cells was analyzed by flow cytometry using a panel of various human tumor cells of breast, colorectal and pancreatic adenocarcinomas as well as multiple myeloma and melanoma lines. Repeated stainings revealed that CEACAM6 was strongly expressed by cells of the breast adenocarcinoma lines BT-474, KS WT, KS 22.24 and KPL-4 (Fig. 71A), cells of the colorectal lines HT-29 and LoVo (Fig. 71B) and cells of the pancreatic adenocarcinoma line Capan-1 (Fig. 71C). Besides the carcinoma lines, in general, CEACAM6 was not present in the multiple myeloma (SKMM2, U266) and melanoma (MeWo) cell lines (Figs. 71D and E). However, compared to the staining controls, cells of the multiple myeloma line RPMI 8226 showed a marginal CEACAM6 presence (Fig. 71D).

In order to test, whether an inhibition of CEACAM6 on tumor cells can influence the tumor cell recognition by human T cells, CEACAM6 was blocked using a CEACAM6-specific Ab. Thereby, as readout system, the short-term IFNγ ELISPOT assay was used. Therefore, a co-culture of Capan-1 cells ($1x10^4$ cells) and pancreatic adenocarcinoma patient-derived PB T cells ($5x10^4$ cells) was performed for 40 h. Compared to untreated Capan-1 cells, after Ab blockade of CEACAM6 on tumor cells, a strongly increased IFNγ production was revealed by patient-derived T cells. In contrast to the measured T cell responses against CEACAM6 Ab blocked tumor cells, an isotype Ab used for tumor cell blocking, resulted in a significantly lower T cell-mediated IFNγ production (Fig. 72).

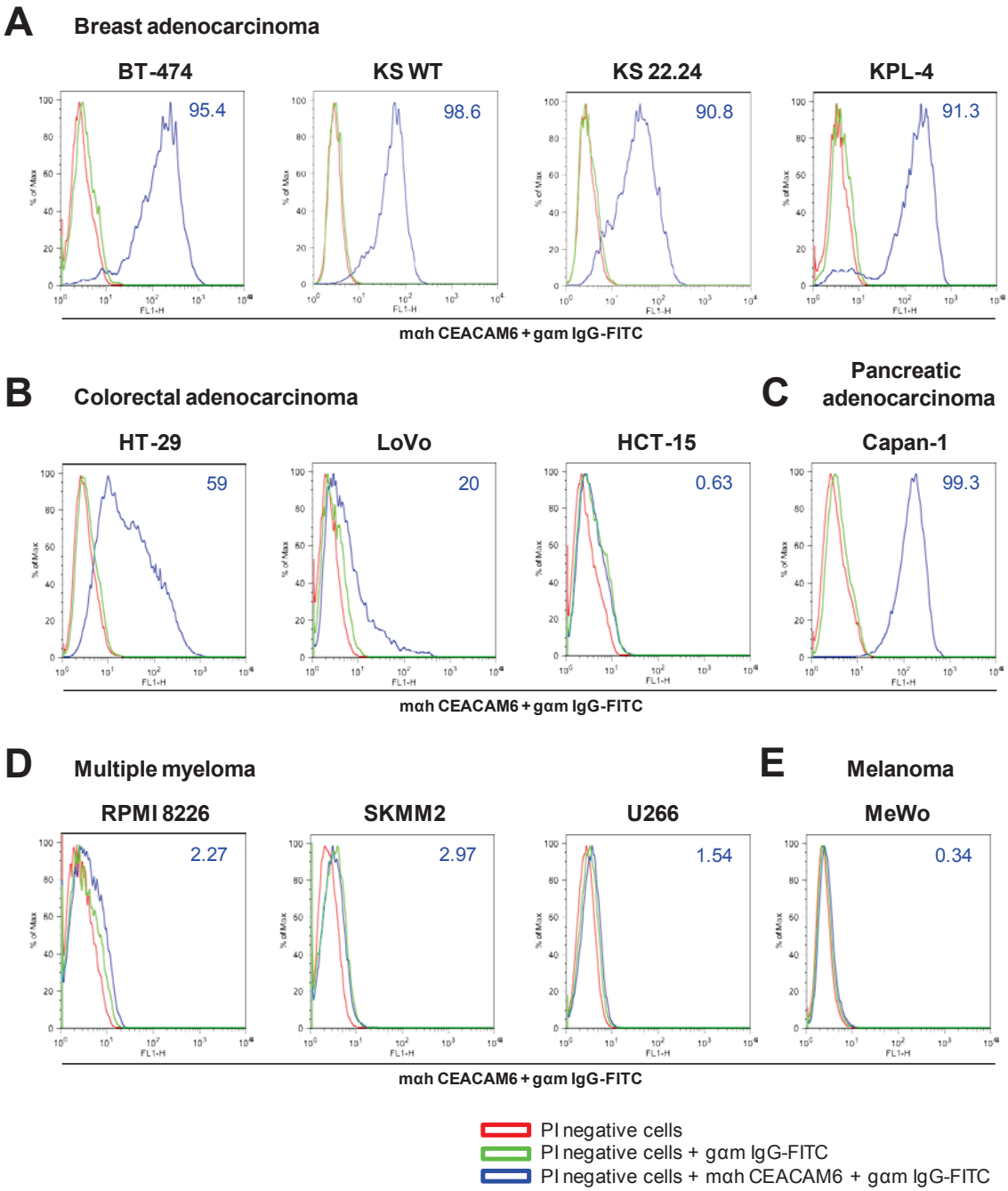


**Figure 71. Flow cytometry analysis of CEACAM6 in various human tumor cell lines.** The breast adenocarcinoma cell lines BT-474, KS WT, KS 22.24, KPL-4 (**A**), colorectal adenocarcinoma cell lines HT-29 and LoVo (**B**) as well as the pancreatic adenocarcinoma cell line Capan-1 (**C**) were positive for CEACAM6. Compared to the control stainings, the multiple myeloma line RPMI 8226 was marginal positive (**D**) and the colorectal adenocarcinoma line HCT-15 (**B**), the multiple myeloma lines SKMM2 and U266 (**D**) as well as the melanoma line MeWo (**E**) revealed to be CEACAM6-negative. Dead cells were excluded by PI. The blue numbers in the dot plots indicate the percentage of CEACAM6-positive cells.

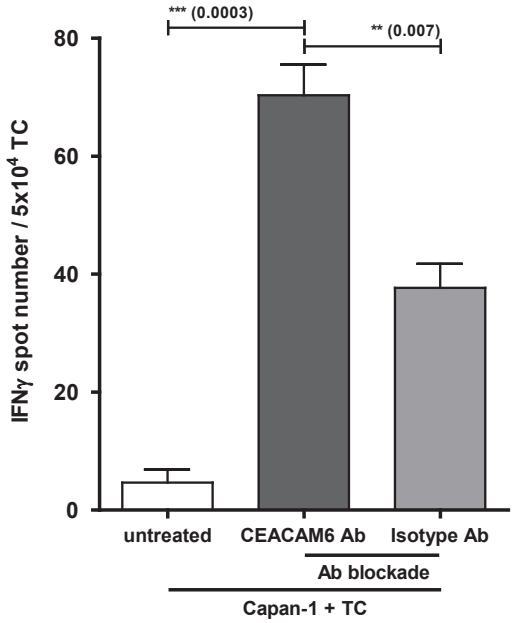


**Figure 72. IFNγ ELISPOT on human T cell responses against CEACAM6-inhibited Capan-1 tumor cells.** Spontaneously induced tumor antigen-reactive memory T cell responses were detected against cells of the human pancreatic adenocarcinoma line Capan-1. $CD3^+$ T cells were negatively isolated from the PB of a patient suffering from a pancreatic adenocarcinoma (obtained from the Department of General, Visceral and Transplantation Surgery, University Hospital Heidelberg). A short-term IFNγ ELISPOT assay using a 1:5 ratio of Capan-1 cells ($1x10^4$) to T cells ($5x10^4$) was performed in triplicates for 40 h. The impact of tumor-expressed CEACAM6 on T cell responses was investigated through CEACAM6 inhibition on Capan-1 cells using CEACAM6 specific Ab for the blockade as well as isotype Ab as control. Compared to untreated or isotype blocked tumor cells, the CEACAM6 blockade on Capan-1 cells led to a strong increase in IFNγ allogenic T cell responses. For statistical analysis, an unpaired two-tailed t test was performed. Mean ± SEM; TC, T cells; Ab, antibody; ** p value ≤ 0.01; *** p value ≤ 0.001

To prove the observation of a CEACAM6-mediated T cell inhibition, a novel cell line was generated. Therefore, the $HLA\text{-}A2^+$ breast adenocarcinoma line MCF-7 was selected, since cells of this line revealed an intermediate CEACAM6 positivity of ~20 % (Fig. 73A). Compared to the parental cell line, the novel isolated line showed an elevated CEACAM6 presence. Thereby, CEACAM6-positive MCF-7 cells were received through flow cytometry based cell sorting. The gating strategy used for the cell sorting is shown in Fig. 73. After sorting, more than 90 % of the MCF-7 cells were positive for CEACAM6 (Fig. 73B). In order to expand these CEACAM6 high expressing MCF-7 cells, to obtain adequate cell numbers, they were cultured *in vitro*. Using flow cytometry, the CEACAM6 level was repeatedly analyzed and revealed that more than 50 % of the cultured cells expressed CEACAM6. Thus, compared to the parental MCF-7 line, the sorted cells indicated an increase of ~30 % in CEACAM6 expression (Fig. 74).

In order to investigate, whether a 30 % elevated CEACAM6 expression on tumor cells influenced the function of human T cells, CEACAM6 was blocked on the tumor cells using a CEACAM6-specific Ab. A short-term IFNγ ELISPOT assay was performed using cells of the respective MCF-7 lines ($1x10^4$ cells of parental and CEACAM6 high) together with breast adenocarcinoma patient-derived PB T cells ($5x10^4$ cells). Spontaneously induced tumor antigen-reactive memory T cell responses were detected against cells of both MCF-7 lines. However,

compared to untreated or isotype controls, a strongly increased IFNγ production by patient-derived T cells could only be detected for MCF-7 CEACAM6 high cells, after CEACAM6 Ab blockade (Fig. 75). A blockade of CEACAM6 on cells of the parental MCF-7 line did not led to an increase in IFNγ secretion by T cells (Fig. 75).

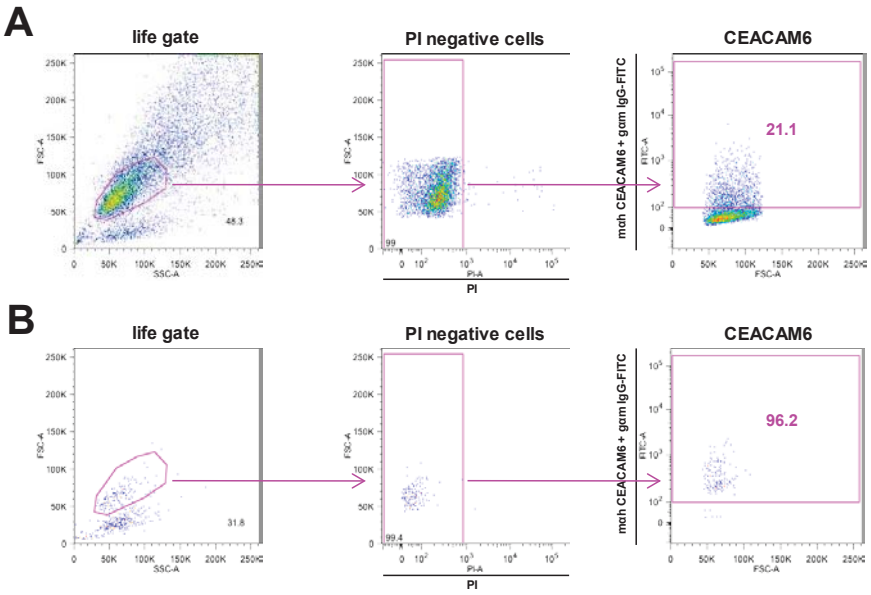


**Figure 73. Gating strategy to isolate CEACAM6-positive MCF-7 cells by flow cytometry sorting. A**) As shown by flow cytometry, ~20 % of the MCF-7 cells expressed CEACAM6. **B**) To increase this percentage, a FACS-based cell sorting for CEACAM6-positive cells was performed and resulted in a cell population of more than 90 % CEACAM6-positive MCF-7 cells. Dead cells were excluded by PI. The numbers in the dot plots indicate the percentage of positive stained cells.

In addition to the cell lines Capan-1 and MCF-7, cells of the line KS WT were investigated as tumor target line. KS WT cells were shown to be HLA-A2$^+$ by flow cytometry (Fig. 76A). Moreover, using immunofluorescence microscopy, the tumor cells revealed to be positive for MDM2 (data not shown). Therefore, cells of this HLA-A2$^+$MDM2$^+$CEACAM6$^+$ line were used as target for Mu Wt TCR MDM2 transgenic human T cells (cf., Fig. 48). Using a IFNγ ELISPOT assay (tumor cells to T cells ratio1:5), compared to IFNγ spot numbers by T cells cultured with untreated tumor cells, the IFNγ production by investigated T cells was increased in the co-culture with CEACAM6 Ab-blocked KS WT cells (Fig. 76B). The maximum IFNγ T cell response of the transgenic cells was obtained using T2 cells loaded with the corresponding MDM2 (81-88) peptide (Fig. 76B). Furthermore, using the $^{51}$Cr release cytotoxicity assay, the impact of tumor-expressed CEACAM6 on the tumor-directed cytolytic function of MDM2 TCR transgenic T cells was addressed. Compared to the lysis of unmodified tumor cells, the specific lysis of CEACAM6 Ab-blocked KS WT cells by TCR MDM2 modified T cells was significantly increased (Fig. 76C). Thereby, cells of the MDM2 peptide-loaded line T2, showed the maximum cytolytic potential of the TCR transduced T cells (Fig. 76C). Summarized, these data demonstrate that MDM2 TCR transduced T cells were able to specifically lyse tumor target cells of line KS WT, in accordance with an increased T cell-dependent IFNγ production as long as CEACAM6 was specifically blocked on the respective tumor target cells.

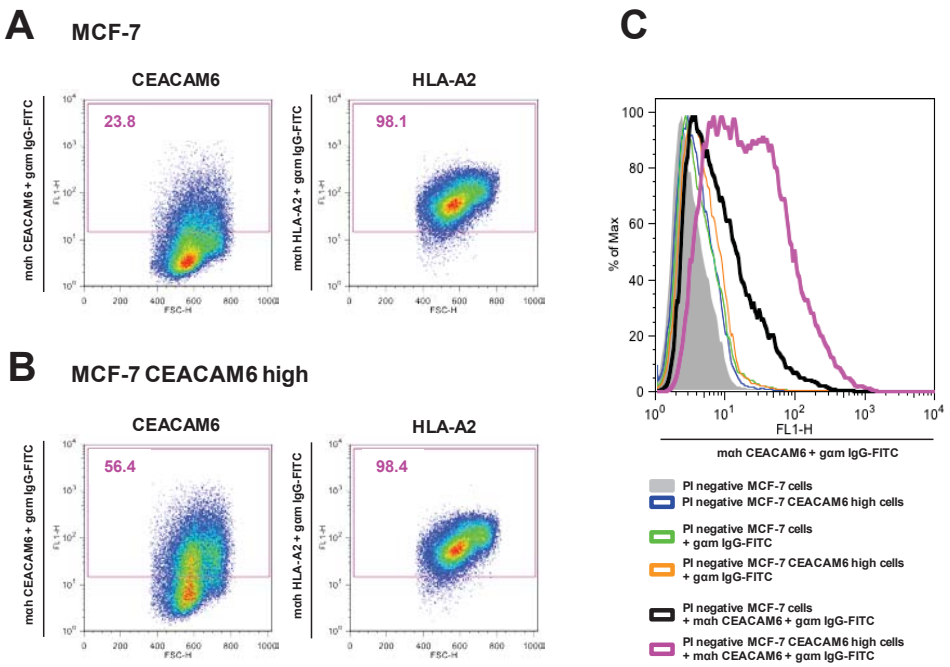


**Figure 74. CEACAM6 expression on cells of the sorted MCF-7 CEACAM6 high cell line.** **A**) The percentage of CEACAM6 expression on HLA-A2$^+$ MCF-7 cells was ~20 %. **B**) After cell expansion, ~50 % of the CEACAM6-sorted HLA-A2$^+$ MCF-7 cells expressed CEACAM6. **C**) Overlay of FACS histograms of the individual stainings. Compared to cells of the parental line, sorted cells showed an elevated CEACAM6 level. Dead cells were excluded by PI. The magenta numbers in the dot plots indicate the percentage of positive stained cells.

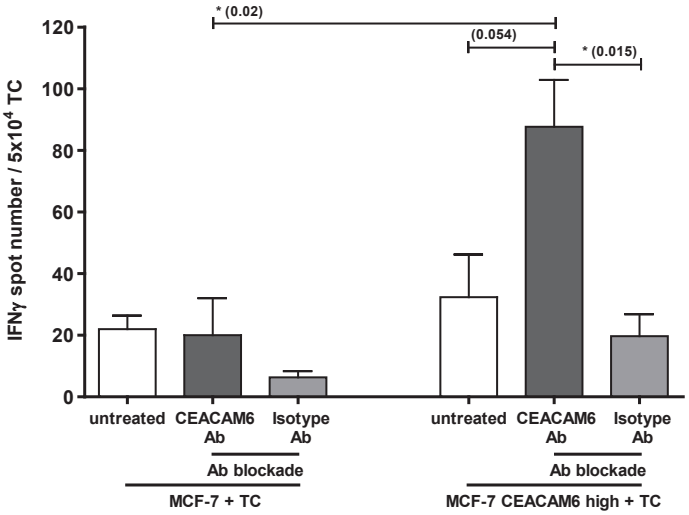


**Figure 75. IFNγ ELISPOT on human T cell responses against CEACAM6-inhibited MCF-7 CEACAM6 high cells.** Spontaneously induced tumor antigen-reactive memory T cell responses were detected against MCF-7 and MCF-7 CEACAM6 high cells. CD3$^+$ T cells were negatively isolated from the PB of a patient, suffering from breast adenocarcinoma (received from the Gynecological Department, University Hospital Heidelberg). A short-term IFNγ ELISPOT assay using a 1:5 ratio of respective MCF-7 cells (1x10$^4$) to T cells (5x10$^4$) was performed in triplicates for 40 h. The impact of tumor-expressed CEACAM6 on T cell responses was investigated through CEACAM6 inhibition using specific Abs as well as isotype Ab as control. Compared to untreated or isotype blocked cells and MCF-7 parental cells, the blockade of CEACAM6 on MCF-7 CEACAM6 high cells led to a strong increase in IFNγ allogenic T cell responses. For statistical analysis, an unpaired two-tailed t test was performed. Mean ± SEM; TC, T cells; * p value ≤ 0.05

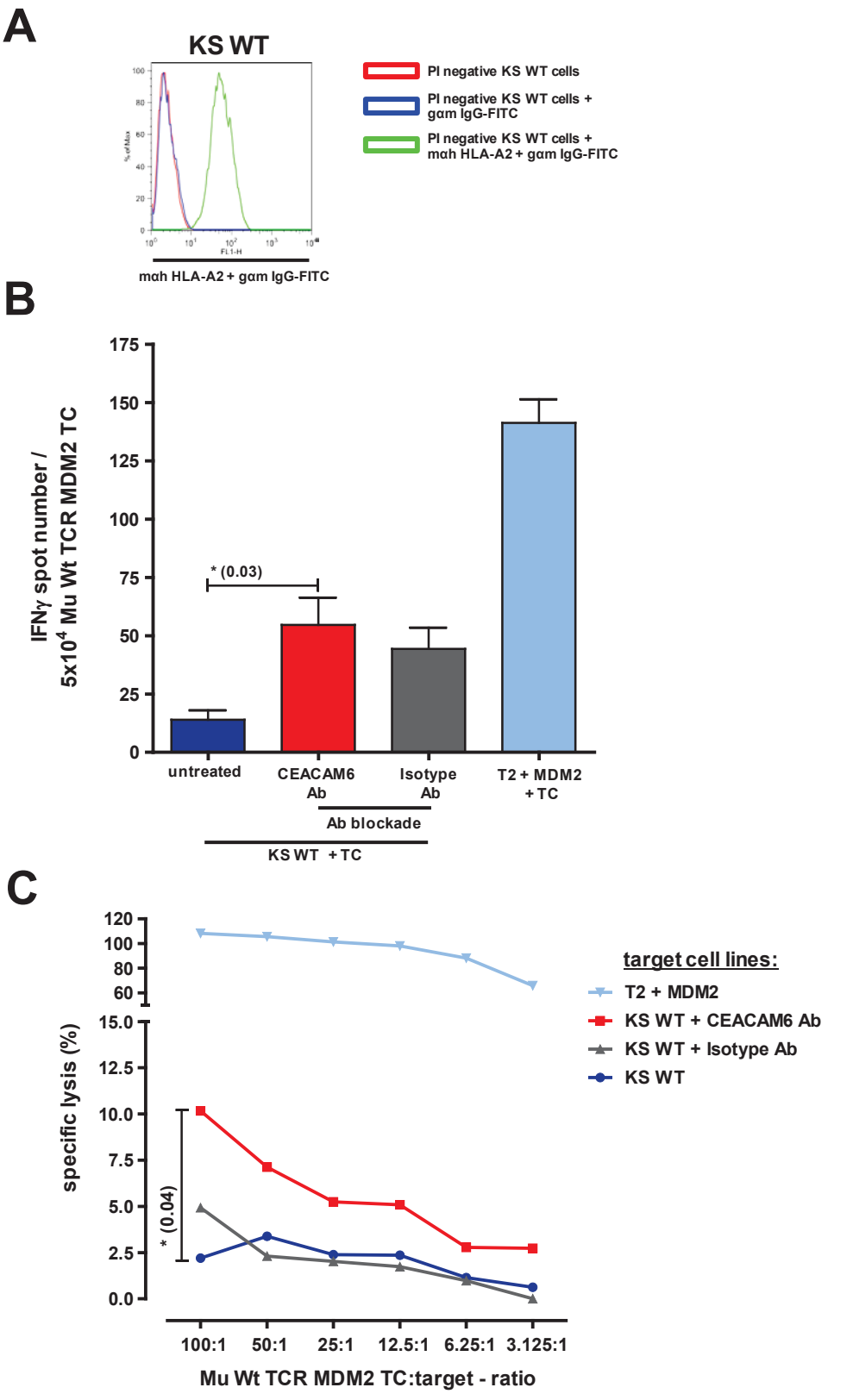


**Figure 76. Functional human T cell responses against KS WT tumor cells through blockade of tumor-expresses CEACAM6.** The detailed figure legend is presented on the next page.

←

**Figure 76. Functional human T cell responses against KS WT tumor cells through blockade of tumor-expresses CEACAM6.** MDM2 antigen-reactive T cell responses were detected against cells of the breast adenocarcinoma line KS WT. **A**) Using flow cytometry, the KS WT cells revealed to be HLA-A2$^+$. Dead cells were excluded by PI. **B**) A short-term IFNγ ELISPOT assay using a 1:5 ratio of KS WT cells (1x10$^4$) to Mu Wt TCR MDM2 transgenic T cells (5x10$^4$) was performed in triplicates for 40 h. The impact of tumor-expressed CEACAM6 on T cell responses was investigated through CEACAM6 inhibition on KS WT cells. Moreover, to analyze the maximum IFNγ T cell response, T2 cells loaded with the specific MDM2 (81-88) peptide, were used. Compared to untreated cells, the blockade of CEACAM6 on KS WT cells led to an increase of IFNγ T cell responses. **C**) Cytotoxicity of human T cells transduced with Mu Wt TCR MDM2 towards KS WT cells and MDM2 peptide-pulsed T2 cells are shown. The used T cell:target cell ratios are indicated. The impact of tumor-expressed CEACAM6 on cytolytic effector functions of MDM2 TCR transgenic T cells was analyzed through CEACAM6 inhibition on KS WT cells. Thereby, in general, CEACAM6-specific Abs for the blockade and isotype Abs were used as control. Compared to untreated tumor cells, the blockade of CEACAM6 on KS WT cells resulted in an increased percentage of specific tumor cell lysis by T cells. For statistical analysis, an unpaired two-tailed t test was performed. Mean ± SEM; TC, T cells; * p value ≤ 0.05

### 8.3.2. Analysis of L1CAM inhibition on human melanoma cells

Since the blockade of the molecule CEACAM6 on tumor cells revealed an increase in T cell function, a further cell adhesion molecule, L1CAM, was additionally investigated concerning the specified effect.

Cells of the melanoma line MeWo were used as tumor target line, since these cells strongly expressed L1CAM, as shown by immunoblot analysis (cf., Fig. 41) and verified by FACS staining (Fig. 77A). Besides the intense L1CAM presence using flow cytometry, MeWo cells were shown to be positive for CEACAM1 (~50 % positivity, data not shown) but negative for CEACAM6 (Fig. 71E).

In order to investigate, whether a specific blockade of L1CAM on MeWo cells resulted in an increased cytolytic function of antigen-specific T cells against tumor cells, a $^{51}$Cr release cytotoxicity assay was performed. Therefore, as effector cells, Hu Chim scTCR gp100 MuC$_\beta$ S79C + MuC$_\alpha$ T84C transduced T cells (cf., Fig. 49) and as target cells, cells of the HLA-A2$^+$gp100$^+$L1CAM$^+$ MeWo line were used. In summary, compared to untreated or isotype Ab-blocked MeWo target cells, the specific Ab-mediated blockade of L1CAM on MeWo cells led to a significant increase in T cell-mediated cytotoxicity (Fig. 77B). Moreover, using gp100 peptide-loaded cells of the line T2, the maximum cytolytic potential of the gp100 TCR transduced T cells could be shown (Fig. 77B).

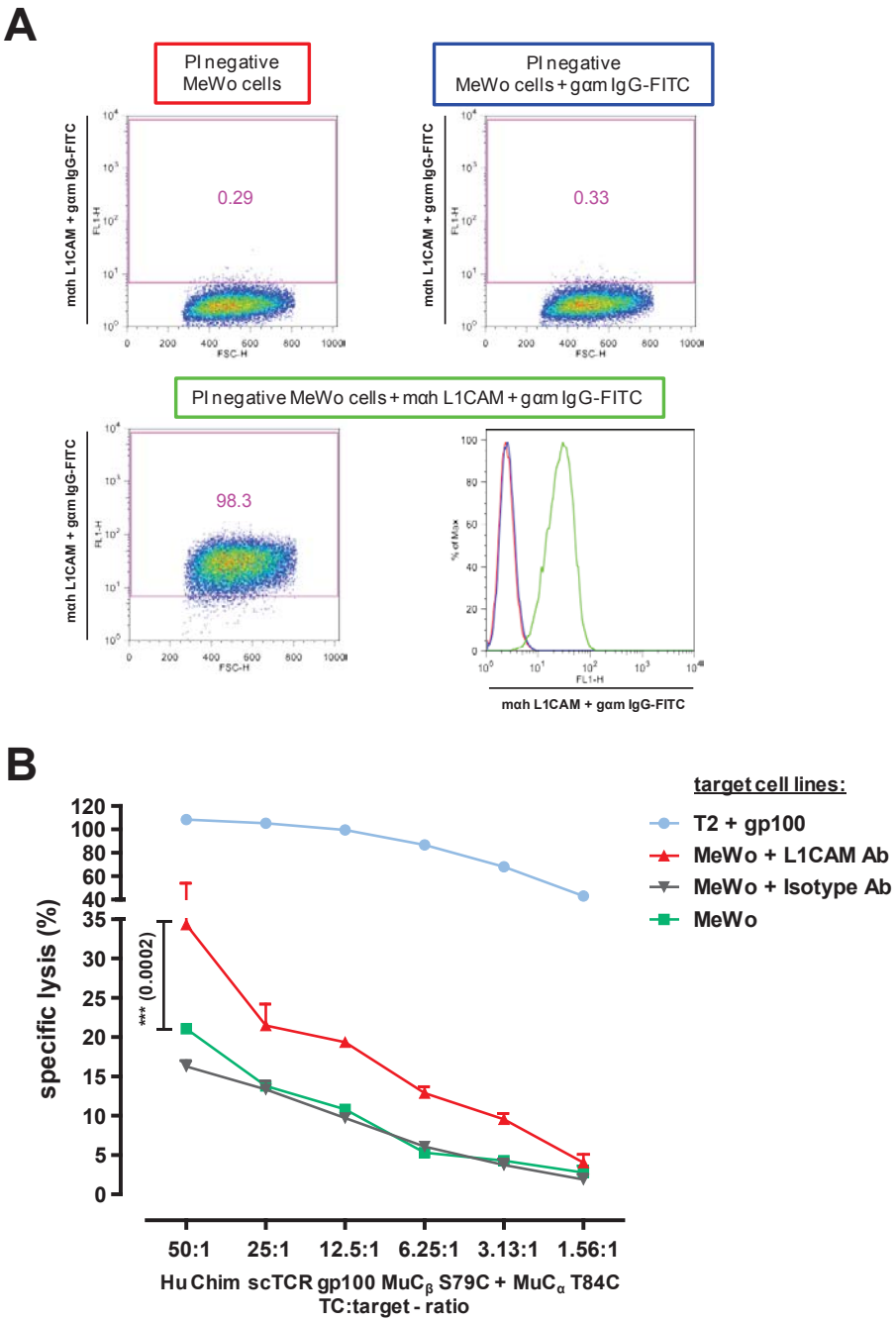


**Figure 77. Functional human T cell responses against MeWo cells through blockade of tumor-expressed L1CAM.** Gp100 antigen-reactive T cell responses were detected against cells of the melanoma line MeWo. **A**) Using flow cytometry, the MeWo cells revealed to be positive for L1CAM. Dead cells were excluded by PI. The magenta numbers in the dot plots indicate the percentage of positive L1CAM MeWo cells. **B**) The cytotoxicity of human T cells, transduced with the Hu Chim scTCR gp100 $MuC_{\beta}$ S79C + $MuC_{\alpha}$ T84C construct, towards MeWo cells and gp100 (280-288) peptide-pulsed T2 cells is shown. The used T cell:target cell ratios are presented. The impact of L1CAM on the cytolytic effector function of gp100 TCR transduced T cell was investigated through L1CAM inhibition on MeWo cells using L1CAM specific Abs for the blockade as well as isotype Ab as control. Compared to untreated tumor cells, the blockade of L1CAM on MeWo cells increased the percentage of specific tumor cell lysis by T cells. For statistical analysis, an unpaired two-tailed t test was performed. Mean ± SEM; TC, T cells; *** p value ≤ 0.001

### 8.3.3. Human tumor cell infection and growth inhibition by Newcastle disease virus transferred on human T cells

In order to test, whether human T cells can be loaded with NDV and used as transport vehicles to transfer the loaded viral particles to tumor cells, PB-derived T cells from healthy donors were modified with the virus. Therefore, T cells were incubated with increased amounts of hemagglutination units (HU) of the lentogenic strain NDV-Ulster or the virulent mesogenic strain MTH-68. Using flow cytometry-based surface staining for the viral fusion (F) protein, the binding of NDV to human T cells was analyzed after an adsorption step of 1 h and 20 h. For both NDV strains, a dose-dependent increase of viral antigens at the cell surface was detected (Figs. 78A and B). Thereby, the percentage of cells that sustained viral antigens was comparable at both time points analyzed (Figs. 78A and B). Investigating the EGFP protein by flow cytometry, the cytoplasmic viral expression in T cells could be addressed after 20 h of infection with the recombinant lentogenic NDV strain NDFL-EGFP. Besides non-activated T cells, also CD3/CD28 activated T cells and MCF-7 cells were modified with NDFL-EGFP and analyzed for EGFP expression. All three cell types showed an EGFP signal in more than 60 % of the cells (Fig. 78C). However, the mean fluorescent intensity of the individual tested groups was different. Compared to non-activated T cells, MCF-7 tumor cells and activated T cells showed a high mean fluorescent intensity (cf., Pfirschke and Schirrmacher, 2009). Moreover, using quantitative real-time PCR, the cytoplasmic viral RNA for the NDV matrix (M) gene was analyzed 20 h after NDFL-EGFP modification. Thereby, the highest amount of the viral M gene was shown for activated T cells, while non-activated T cells expressed much lower and MCF-7 tumor cells intermediate amounts (cf., Pfirschke and Schirrmacher, 2009).

To test, whether NDV can replicate in the different cell types used and produce viable progeny virus, the lytic mesogenic NDV strain NDFLtagEGFP was used for cell modification. After 2 d, the cell culture supernatants of the three infected cell types were carefully removed and tested for the presence of infectious progeny virus. Therefore, MCF-7 cells were used as target for viral modification by NDV particles contained in the supernatant. While supernatants of infected MCF-7 tumor cells contained infectious virus particles, supernatants of non-activated and activated T cells did not contain infectious NDV (Fig. 79).

Correspondingly to analyze whether NDV-modified human T cells can transfer NDV to human tumor cells, an *in vitro* co-incubation of both cell types was performed. Therefore, the virus (NDV strain NDFL-EGFP, 50 HU) was loaded to PBMCs, “non T cells” (PBMCs after removal of T cells), non-activated and activated T cells as well as of $CD4^+$ and $CD8^+$ T cell subsets. The NDV transfer to MCF-7 cells was investigated after a co-culture period of 20 h. Therefore, a flow cytometry-based analysis of EGFP-positive cells was performed while gating on MCF-7 tumor cells. After co-incubation with NDV-modified T cells, ~25 to 40 % of MCF-7 cells were EGFP-positive, depending on the cell ratios used (Figs. 80A-C). In contrast, after co-culture with PBMCs or non T cells only ~12 % of the tumor cells were infected (Fig. 80A). The direct infection of MCF-7 cells revealed an EGFP signal in ~75 % of the cells (Figs. 80A-C).

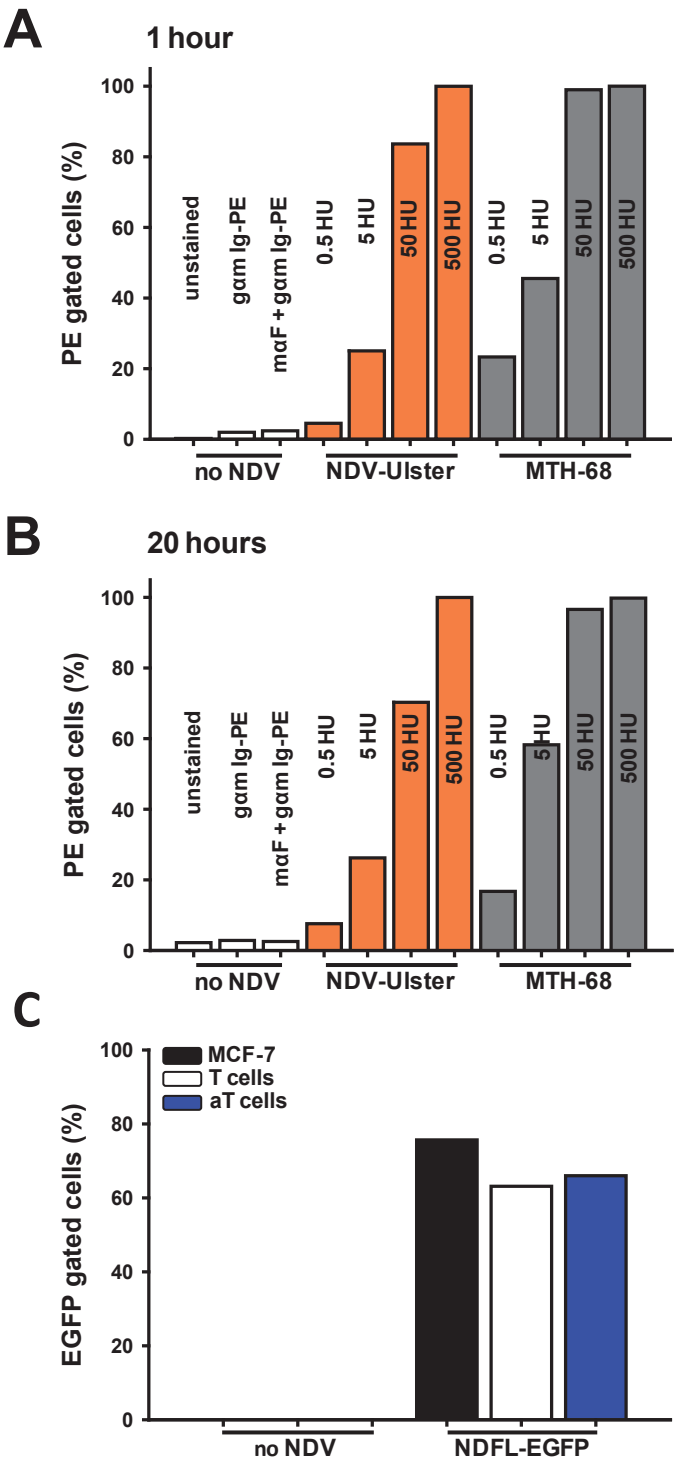


**Figure 78. Modification of human T cells with NDV.** The binding of NDV to human T cells was analyzed 1 h (**A**) and 20 h (**B**) after treatment with different amounts of the NDV strains, NDV-Ulster or MTH-68. Using flow cytometry, the T cells were stained for surface expression of the viral F protein and the percentage of positive cells is indicated. **C**) T cells, activated T cells (aT cells) and MCF-7 cells were modified with the NDV strain NDFL-EGFP using a dose of 50 HU. A flow cytometry analysis for cytoplasmic viral EGFP was performed after 20 h of viral treatment and the percentage of EGFP-positive cells is indicated. These data show an efficient modification of human T cells by NDV. As controls, cells without NDV modification were investigated. In each case representative data from one of two experiments are shown.

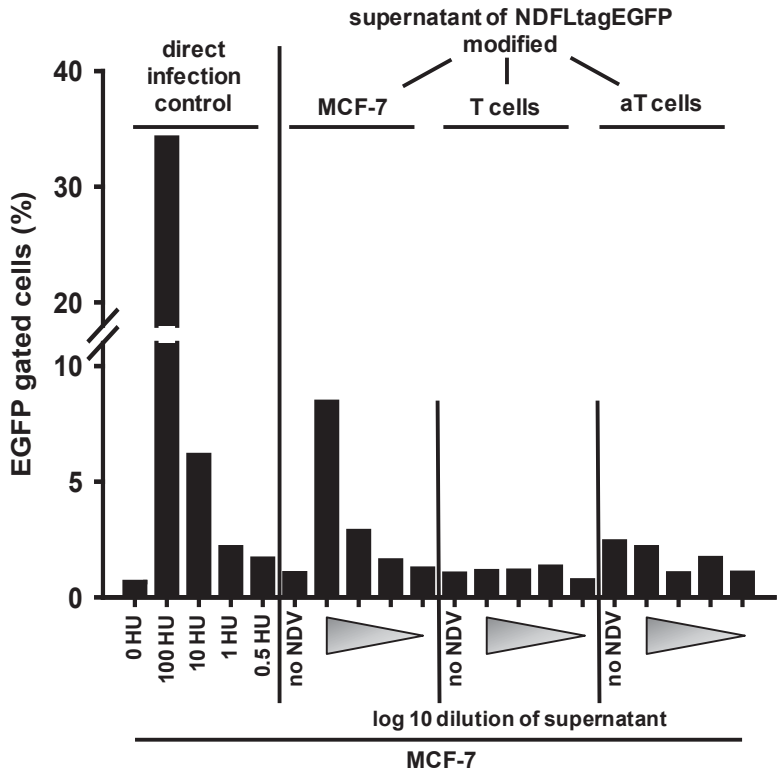


**Figure 79. Analysis of the formation of infectious progeny virus in T cells, activated T cells and MCF-7 tumor cells.** T cells, activated T cells (aT cells) and MCF-7 tumor cells were separately modified with 10 HU of the multicyclic NDV strain, NDFLtagEGFP for 2 d. The supernatants of the NDFLtagEGFP-modified cells were transferred to untreated MCF-7 tumor cells and tested in log 10 dilutions. The MCF-7 cells were analyzed for EGFP expression by flow cytometry, 20 h later. Thereby, progeny virus was only revealed in the supernatants of MCF-7 cells, but not of NDV-modified T cells. As control, MCF-7 samples without supernatants of NDV-modified cells (no NDV; 0 HU) and direct infection controls of MCF-7 cells using different NDFLtagEGFP viral amounts, were investigated.

Since activated T cells could be more efficiently modified with NDV than non-activated T cells, indicated by increased viral mRNA and EGFP protein expression without production of infectious progeny virus (Figs. 78C, 79 and Pfirschke and Schirrmacher, 2009), viral hitchhiking mediated by activated T cells was analyzed. Thereby, compared to non-activated T cells, a higher transfer of NDV to tumor target cells was revealed (Fig. 80B). Moreover, certain subsets of T cells as $CD3^+$ and purified $CD4^+$ and $CD8^+$ T cells were analyzed, concerning their capacity to transfer NDV. All investigated subsets were similarly active in conducting the transfer of NDV (Fig. 80C).

Furthermore, kinetic experiments were performed, to investigate whether direct infection of tumor cells and infection via hitchhiking of NDV-modified T cells take a different time course. Thereby, the time course of MCF-7 cell infection through hitchhiking on NDV-modified T cells compared to direct virus infection of MCF-7 cells is indicated in Figs. 81A and B. By the mean fluorescent intensity of the EGFP signal of MCF-7-infected cells, it could be shown that the direct infection route took ~10 h, while the T cell-mediated hitchhiking-based infection lasted ~20 h (Fig. 81B).

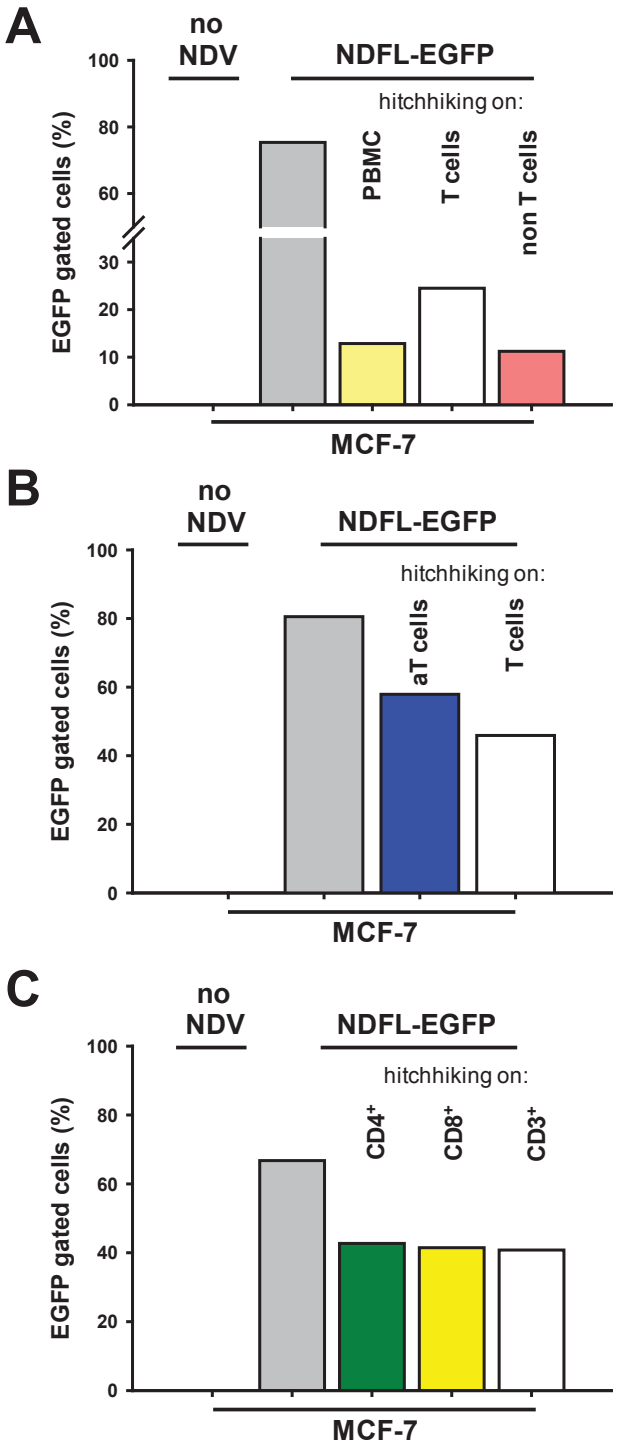


**Figure 80. Transfer of NDV from human T cells via hitchhiking to human tumor target cells.** Flow cytometry analysis showing PBMC, T cells, non T cells (PBMC depleted of T cells) (**A**) and activated T cells (aT cells) compared to non-activated T cells (**B**) as well as $CD3^+$, $CD4^+$ and $CD8^+$ T cells (**C**) which were modified with 50 HU of the NDV strain NDFL-EGFP for 1 h. Following, the NDV-modified cells were co-cultured with untreated MCF-7 tumor cells for 20 h using a tumor cell to T cell ratio of 1:4 (**A**), 1:2 (**B**) or 1:5 (**C**), respectively. As controls, MCF-7 cells without NDV (no NDV) and directly modified with NDV (grey bars), were used. The EGFP signal was analyzed by flow cytometry after a co-culture of 20 h. In accordance to the positive virus modification setting, the specific MCF-7 infection by NDV, transferred via hitchhiking on various human T cell populations could be shown (**A**-**C**). Representative data from one of two experiments are shown.

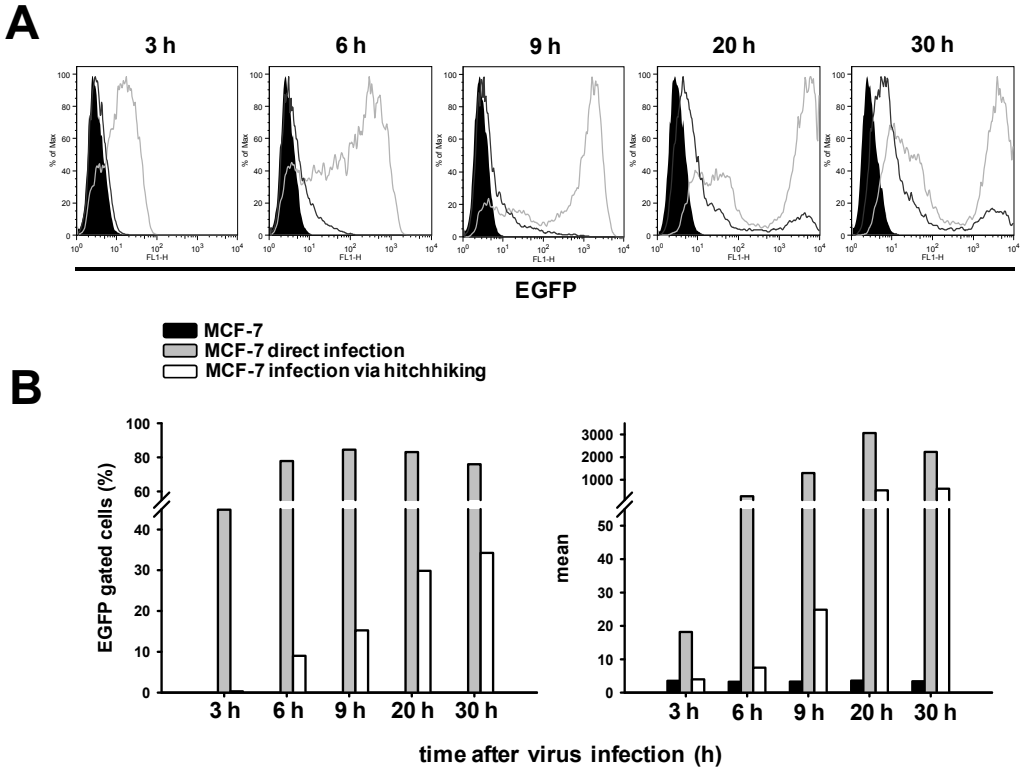


**Figure 81. Kinetic of the T cell-mediated NDV hitchhiking to human tumor target cells.** Using flow cytometry, the time-course of the hitchhiking process of NDV (50 HU NDFL-EGFP) on human T cells was analyzed after 3, 6, 9, 20 and 30 h of co-culture with MCF-7 tumor cells using a tumor cell to T cell ratio of 1:5. **A**) Representative flow cytometry-based histograms present the respective EGFP signals over time. **B**) Graphs indicate the percentage of EGFP-positive cells (left) and the mean of the EGFP positivity (right). Representative data from one of two experiments are shown.

In a next approach, to visualize MCF-7 tumor cell infection by NDV, transferred through hitchhiking on T cells, immunofluorescence microscopy stainings were performed. Therefore, NDV-Ulster (50 HU) was loaded to T cells and co-cultured with MCF-7 cells for 20 h. After washing off the non-adherent cells, the remaining cells were converted to slides. Co-localizations of MCF-7 tumor cells, positive for cytokeratin and NDV, were revealed for the direct infection setting and the hitchhiking approach (Figs. 82A and B).

Moreover, the impact of the used tumor cell to T cell ratios for the hitchhiking approach was examined. A transfer of NDV to MCF-7 cells was clearly detectable using a 1:1 tumor cell to T cell ratio, however, the most effective results were obtained at a 1:5 ratio (Fig. 83A). Furthermore, the dependence of the hitchhiking efficiency on the used virus dose was investigated using different NDV doses for the T cells modification. Thereby, compared to the efficiency with 50 HU of NDV, an increased T cell-dependent hitchhiking of NDV to MCF-7 cells could be observed when a dose of 500 HU was used for T cell modification (Fig. 83B).

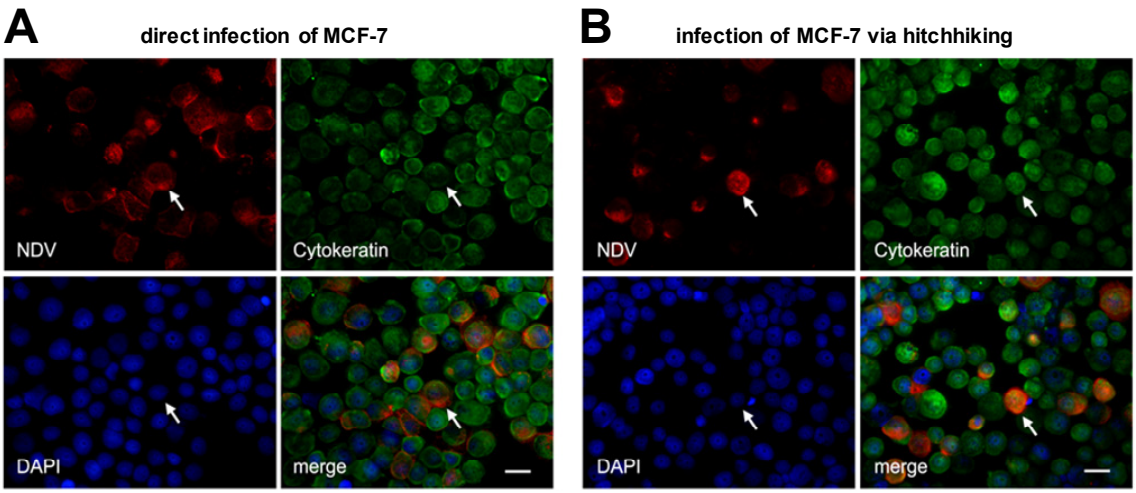


**Figure 82. Immunofluorescence microscopy of NDV-infected MCF-7 cells.** Immunofluorescence microscopical images are presented of direct NDV-infected MCF-7 cells (**A**) and MCF-7 cells infected via hitchhiking of NDV, through NDV-modified T cells using a tumor cell to T cell ratio of 1:5 (**B**). The NDV-Ulster strain (50 HU) was used for investigation. After 20 h cultivation, the MCF-7 cells were dispersed to slides using a cytospin cytocentrifuge and analyzed for virus presence by immunofluorescence microscopy. Cytokeratin stainings were used to visualize the MCF-7 tumor cells (green) and NDV stainings to indicate the virus (red). Indicated by white arrows, the merged pictures exemplarily present NDV-positive MCF-7 tumor cells, resulted from direct NDV infection (**A**) or through hitchhiking-mediated NDV infection (**B**). DAPI (blue) was used to show the cell nuclei. Bars represent 20 µm.

To analyze the tumor growth control by T cell-mediated hitchhiking of NDV *in vitro*, a tumor neutralization assay (TNA) was performed. Therefore, tumor cell monolayers were co-cultured with NDV-loaded T cells for 2 d and the anti-tumor activity, indicated as tumor growth inhibition of NDV, was measured by uptake of 3-(4,5-dimethylthiazol-2-yl)-5-(3-carboxy-methoxyphenyl)-2-(4-sulfophenyl)-2H-tetrazolium solution (MTS) through the remaining viable tumor cells. Thus, non-activated T cells and activated T cells were loaded with different doses of NDV-Ulster or MTH-68. Different tumor cell to T cell ratios were investigated and a tumor growth inhibition of 50 % was observed at a 1:5 ratio, when non-activated T cells were loaded with 10 HU of MTH-68 (Fig. 84A). A similar effect was seen, when 10 HU MTH-68 were directly used for infection. The less virulent strain NDV-Ulster, as expected, revealed less anti-tumor activity after both, direct and hitchhiking-mediated viral infection (Fig. 84A).

Furthermore, elevated anti-tumor activities were observed when activated T cells, instead of non-activated T cells, were used as NDV transfer vehicles. A tumor growth inhibition of 50 % could be shown when activated T cells, without NDV modification, were co-cultures with MCF-7 cells in a tumor cell to T cell ratio of 1:5 (Fig. 84B). Only slightly higher anti-tumor effects were measurable, if activated T cells were loaded with NDV-Ulster, while much stronger anti-tumor activity was examined with MTH-68 modified activated T cells (Fig. 84B). Finally, using this combination of activated T cells and virulent NDV strain MTH-68, the measured tumor growth inhibition was higher than observed for the direct infection of MCF-7 tumor cells with respective amounts of MTH-68 (Fig. 84B).

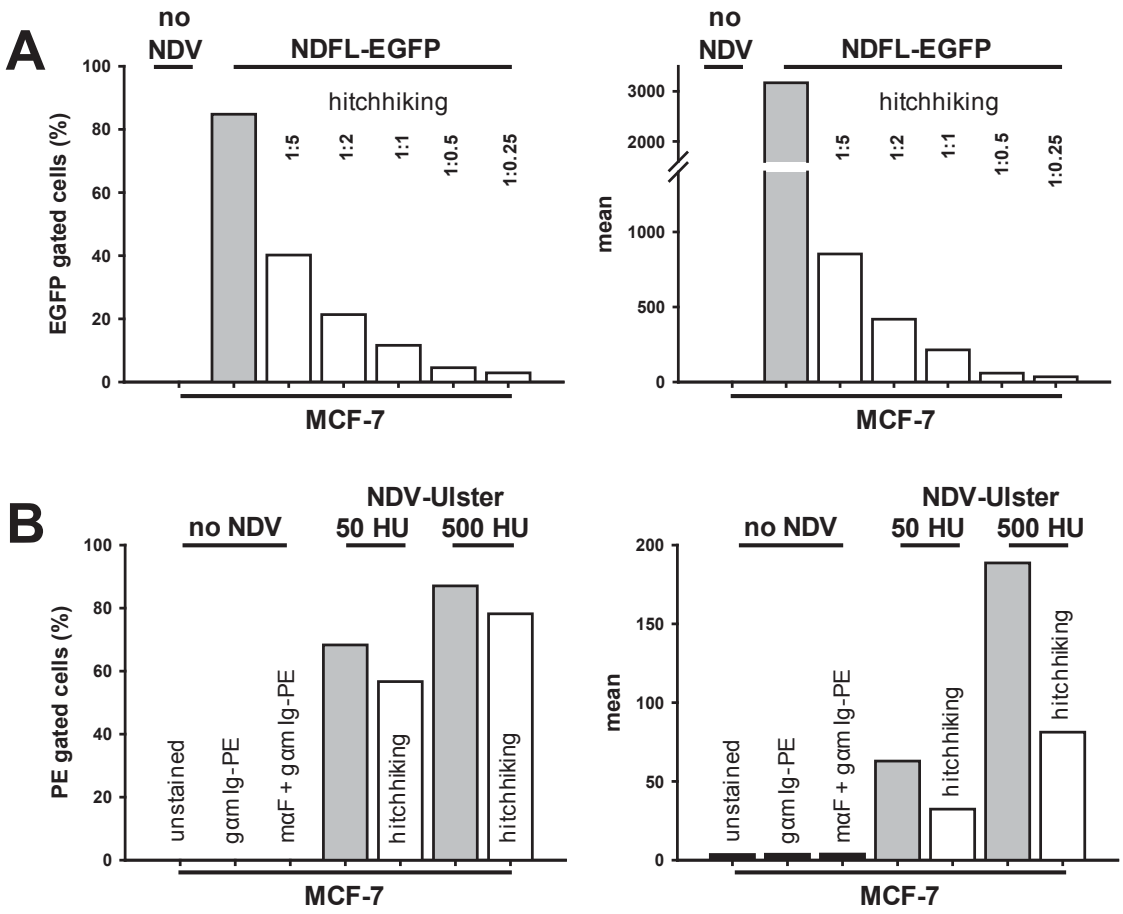


**Figure 83. Flow cytometry analysis of MCF-7 to T cell ratios and impact of NDV doses for optimization of hitchhiking. A**) Hitchhiking of NDV strain NDFL-EGFP (50 HU) on T cells co-cultured with MCF-7 cells was investigated, analyzing different tumor cell to T cell ratios (1:0.25, 1:0.5, 1:1, 1:2, 1:5). The EGFP signal of MCF-7 cells was measured by flow cytometry after 20 h of incubation and the percentage of EGFP-positive cells (left) and the mean of the EGFP positivity (right) are presented and indicate a NDV transfer to tumor cells at all investigated ratios. Thereby, the most efficient transport was revealed at a ratio of 1:5. **B**) Hitchhiking of NDV strain NDV-Ulster on T cells, co-cultured with MCF-7 cells (tumor cell to T cell ratio 1:2) was examined, analyzing different NDV doses (50 HU, 500 HU). The NDV-positive cells (staining for F protein) were then analyzed after a co-culture of 20 h and showed a maximum transport rate using 500 HU of NDV. As controls, MCF-7 cells without NDV (no NDV) and directly modified by NDV (grey bars) were used. Representative data from one of two experiments are shown.

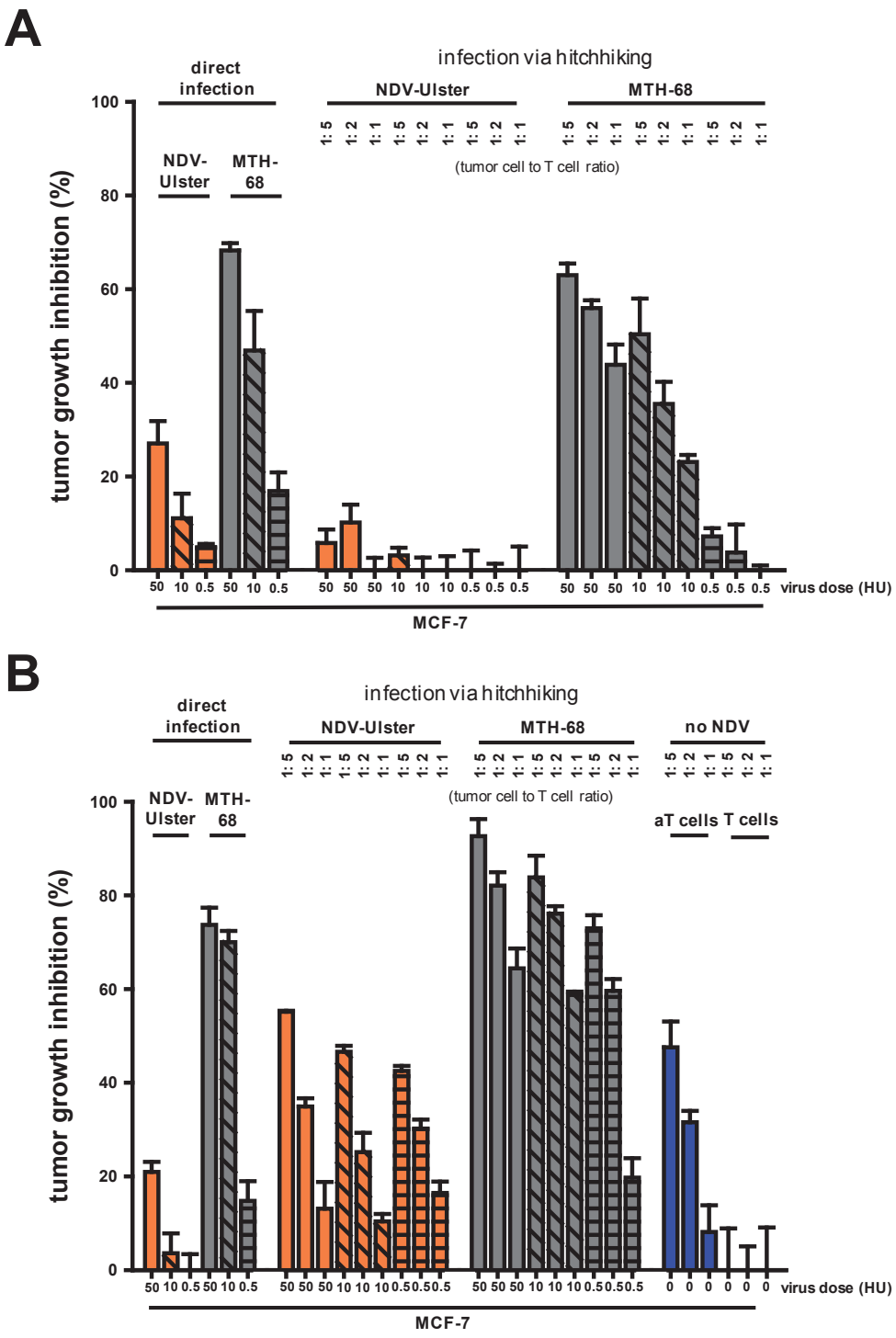


**Figure 84. Tumor cell growth control *in vitro* through T cell-mediated NDV hitchhiking.** Using the tumor neutralization assay, the inhibition of tumor cell growth was determined after 2 d co-culture of MCF-7 cells with virus-modified T cells using the NDV strains NDV-Ulster or MTH-68. For NDV hitchhiking, non-activated T cells (**A**) and activated T cells (aT cells; **B**) were used. Different tumor cell to T cell ratios (1:1, 1:2, 1:5) and NDV doses (0.5 HU, 10 HU, 50 HU) were tested and revealed the most efficient tumor growth control using MTH-68-modified aT cells as NDV carriers. As controls, MCF-7 cells directly infected with the respective NDV strains and MCF-7 cells co-cultured with T cells or aT cells without NDV modification were used. For each individual setting, triplicates were performed. Representative data from one of two experiments are shown. Mean ± SEM

### 8.3.4. Summary on further strategies to influence human tumor cell growth

The presence of the cell adhesion molecule CEACAM6 was shown for different human tumor cell lines derived from breast, colorectal and pancreatic adenocarcinomas and multiple myeloma. Thereby, compared to respective untreated control cells, the inhibition of CEACAM6 on cells of these tumor lines revealed strongly increased functional human T cell responses, indicated through elevated IFNγ levels and tumor cell-directed cytolytic T cell functions. Moreover, in comparison to the parental MCF-7 cell line, a CEACAM6 blockade on flow cytometry-sorted CEACAM6 high MCF-7 cells, resulted in increased IFNγ production by co-cultured patient-derived T cells.

Besides the immunosuppressive role of tumor-expressed CEACAM6, a comparable function was shown for the cell adhesion molecule L1CAM. The inhibition of L1CAM on human MeWo melanoma cells also revealed an increased cytolytic T cell function against the investigated tumor cells. Summarized, these data show that human T cell responses against human tumor cells were functionally suppressed by the molecules CEACAM6 and L1CAM, expressed by tumor cells.

Furthermore, to influence human tumor cell growth *in vitro*, a human T cell-mediated oncolytic viral tumor cell targeting was examined for NDV. Human PB-derived T cells were modified with NDV, while activated T cells were most efficiently loaded with the virus. Thereby, in T cells NDV was not able to replicate and to form infectious progeny virus. Using an *in vitro* co-culture system, the virus-modified T cells were used to transfer NDV in a “hitchhiking”-like process to tumor target cells. The efficiency of NDV transfer via T cells to tumor cells was dependent on the co-culture ratio and the viral dose. Finally, while investigating the tumor growth inhibition, the T cell-mediated transport of NDV could be used to control the tumor growth *in vitro*.

# 9. Discussion

Cancer causes high mortality in terms of several million deaths per year for both men and women and represents therefore a major public health problem all over the world (Jemal et al., 2010). In order to efficiently fight cancer, existing therapeutic strategies have to be optimized and novel approaches will need to be established. To overcome tumor escape, malignant tumors have to be attacked from different angles. Moreover, to achieve a successful intervention, the fact that cancer represents a multifunctional disease that requires the combination of various therapeutic approaches is of central importance. In addition to conventional cancer therapies including surgery, radiation- and chemotherapy, a number of other approaches for cancer treatment exist, such as immunotherapy. Different immunotherapeutic approaches have been performed for cancer treatment. All of them aim to harness and direct immune mechanisms against transformed malignant tumor cells.

Nevertheless, the clinical efficiency of current tumor immunotherapies remains low, in part due to the capacity of tumors to interfere and control immune responses. The identification of mechanisms, that help to down-regulate those tumor-mediated anti-immune responses, and strategies, that efficiently reactivate pre-existing cancer-directed immune cells, are of great importance. In addition, the optimization of specific gene-modified tumor-reactive cells and combinational treatment approaches are of central clinical importance for tumor targeting. Therefore, this thesis focused on different aspects of cancer immune therapeutic interventions, which are separately discussed in the following paragraphs.

## 9.1. Spontaneously induced tumor antigen-reactive T cell responses in melanoma and dysplastic nevi patients

Tumor-reactive memory T cell responses have been discussed to be required for a durable prevention of tumor recurrence and metastasis formation, especially after surgical tumor removal (Côté et al., 2008). They provide a repertoire of functional and potentially protective immune cells that can be therapeutically reactivated (Beckhove et al., 2004). Although, spontaneously induced pre-existing tumor antigen-reactive memory T cells have been extensively studied and shown to be present in patients suffering from various types of cancer including breast, pancreatic and colon carcinomas as well as multiple myeloma and melanoma (Choi et al., 2005; Schmitz-Winnenthal et al., 2005; Mueller-Berghaus et al., 2006; Bonertz et al., 2009; Schuetz et al., 2009), little is known about the regulation of their spontaneous responses. Moreover, the identification of relevant antigens to reactivate pre-existing memory T cell responses is still of central importance for the optimization of cancer treatment, especially for peptide-based immunotherapy.

In the presented thesis the presence and kinetic of spontaneously induced memory T cells was characterized in the peripheral blood (PB) of non-metastasized melanoma patients after primary tumor resection over time. Thereby, T cell responses against a broad variety of different melanoma

TAAs were examined. Spontaneously induced tumor antigen-reactive memory T cell responses can be identified using a 40 h short-term IFNγ ELISPOT assay as detection method. Thereby, it could be shown that the measured T cell reactivity via IFNγ secretion resulted mainly from the $CD45RO^+$ and not the $CD45RO^-$ T cell population (Bonertz et al., 2009). Therefore, spontaneously induced pre-existing memory T cells but not recently primed $CD45RO^-$ naive/effector T cell fractions can be identified as the source of IFNγ secretion during co-culture of peptide-pulsed autologous dendritic cells and T cells. Compared to $CD45RA^+$ T cell fractions, only $CD45RO^+$ memory T cells have the capacity to release IFNγ within 40 h after antigen stimulation. In this way, naive primary immune responses can be excluded as source for IFNγ (Schirrmacher et al., 2003; Sommerfeldt et al., 2006).

Based on these observations, all measured IFNγ cytokine amounts, which were obtained through short-term IFNγ ELISPOT assays in the course of this PhD thesis, present memory T cell-mediated secondary immune responses. However, since total $CD3^+$ T cell populations were used for the investigations instead of purified $CD45RO^+$ memory-like effector T cells, it might be possible that to some degree the presence of tumor-reactive T cells were underestimated. In general, total $CD3^+$ T cell fractions were used, since the elimination of naive T cells was associated with a major general cell loss. In parallel, T cell responses against a large panel of various TAAs have been investigated. Therefore, a high T cell number was necessary to perform the above assays. In addition, the limited amount of cells that can be obtained from a maximum of 50 ml human patient-derived PB, led to the decision to use total $CD3^+$ T cell populations instead of purified memory T cells.

The IFNγ ELISPOT assay is used for monitoring during clinical trials. The assay has an important advantage, since it does not require the expansion of specific T cells before investigation and therefore reflects the *ex vivo* T cell status (Gajewski, 2000). Besides IFNγ, other cytokines and effector molecules produced by activated T cells including TNFα, IL-2 or perforin can be addressed. IFNγ has primarily been investigated, as it is a powerful early produced effector molecule secreted by reactivated effector T cells that, e.g., can directly inhibit human tumor cell growth, while inducing apoptosis (Wall et al., 2003). Using this method, in the PB of non-metastasized melanoma patients, pre-existing T cell responses were revealed against all tested TAAs, which showed a significant increase compared to the control IgG (Fig. 25). Importantly, the frequency of TAA-reactive T cells was significantly increased in the cohort of 36 non-metastasized melanoma patients compared to healthy donors, where TAA-reactive T cell responses were only rarely observed (Fig. 33). This comparable analysis indicated that the detected TAA responses are preferentially limited to the melanoma cohort.

The investigated TAAs represent 13 different antigens that belong to melanocyte linage/differentiation antigens, oncofetal/cancer-testis antigens, atypical antigens and antigens that are over-expressed in melanoma (for references see Tab. 8). In more than 75 % of all analyzed non-metastasized patients spontaneous T cell responses against at least one of the investigated antigens were detected. In contrast to colon carcinoma patients where on average 1.7 TAAs were recognized (Bonertz et al., 2009), interestingly, in the melanoma cohort preferentially responses

against 4 or more antigens were observed, indicating polyvalent and patient-dependent individual T cell responses (Figs. 20 and 21). High T cell reactivities were obtained against all tested polypeptides, whereas the highest response rates - in more than 60 % of patients - were obtained against the melanocyte linage/differentiation antigens Melan-A/MART-1 and Tyrosinase (Fig. 25A). Both antigens represent primary candidates that were and still are extensively studied for immunotherapy of cancer patients, especially for melanoma (Boon et al., 2006). In this context, multiple epitopes that are recognized by CTLs, but also CD4 effector T cells, have been described for Melan-A/MART-1 and Tyrosinase (cf., Cancer Immunity, peptide database, last update of January 2011; www.cancerimmunity.org; see also Valmori et al., 1999; Larrieu et al., 2007). Moreover, these antigens are partially involved in melanin production and therefore not exclusively expressed in melanoma but also in normal melanocytes. While the treatment in metastatic melanoma patients revealed promising results, which is indicated through reported regression of melanoma metastases (Rosenberg et al., 2008), side effects have been described using melanocyte differentiation antigens as targets for immune therapeutic interventions including adoptive immunotherapy. In this context, autoimmune melanocyte destruction was reported in several melanoma patients, as indicated by severe vitiligo in the skin and hair as well as uveitis of the eye (Robinson et al., 2004; Caspi, 2008; Rosenberg et al., 2008). These adverse events are due to the fact that the targeted antigens are not exclusively expressed by tumor cells. Tumor antigen-specific T cells home not only to the tumor to mediate tumor regression but also to melanocytes, which express melanin in healthy tissues including the skin, hair follicle and eye. This indicates that besides the promising results, obtained through known tumor antigens, there is still a central need in identifying new antigens that are more specific to the respective cancer or ideally only specifically expressed by cancer cells.

The antigen NA17-A, might be one candidate, as it represents an atypical protein that is encoded by an intron sequence of the human N-acetyl glucosaminyl-transferase V gene (GnT-V). Due to a cryptic activated promoter within the intron sequence this protein is translated. NA17-A is primarily expressed by melanoma but not in normal tissues and has therefore been described as a tumor-specific antigen (Guilloux et al., 1996). Interestingly, the data presented in this thesis revealed that pre-existing T cell responses against NA17-A were found in more than 40 % of non-metastasized melanoma patients. Therefore, besides Melan-A/MART-1 and Tyrosinase, NA17-A represents the third most common antigen which could be specifically recognized by spontaneous T cell responses (Fig. 25).

In general, during melanoma cohort analysis, high T cell reactivities were detected. Thereby, the response rates were distinctly higher than 20 % for all of the investigated antigens (Fig. 25), in comparison to colon carcinoma patients, where almost all peptide response rates were revealed to be clearly lower than 20 % using the same assay system (Bonertz et al., 2009).

An explanation for the different proportions of colon carcinoma and melanoma patients, that exerted significant T cell reactivities against polypeptides derived from the respective TAAs, can be due to the different medical backgrounds of the two cancer cohorts. The colon carcinoma patients were still tumor-bearing when the PB was taken for investigation of pre-existing tumor antigen-

reactive T cells. In contrast, the melanoma cohort did not have a direct tumor stimulus at the moment of PB investigation for T cell responses, since the patients were non-metastasized and the primary tumor had already been resected.

In order to investigate, how the frequency of TAA-reactive T cells behave over time after primary tumor resection, in non-metastasized melanoma patients different time points after the resection of the primary tumor were analyzed. Surprisingly, the T cell frequencies increased significantly over time up to d60 after the removal of the tumor (cf., Figs. 26 and 27). This observation indicated that the presence of the tumor controlled pre-existing memory T cell responses in the PB. Furthermore, it showed that after tumor removal the cancer-suppressive control was lost, resulting in a strong increase of pre-existing T cell responses. In this context, based on the cancer immunoediting hypothesis (Schreiber et al., 2011; Vesely et al., 2011), the clinically apparent, non-metastasized primary melanoma may represent tumors that have escaped immune control.

The cancer immunoediting hypothesis highlights that the immune system directly interacts with the development of the tumor. Thereby, on the one hand the immune system protects the host against the formation of immunogenic tumors. On the other hand, it edits tumor immunogenicity and promotes tumor growth. In this context, cancer immunoediting represents a dynamic extrinsic process composed of 3 distinct phases: elimination, equilibrium and escape (Schreiber et al., 2011; Vesely et al., 2011). The elimination process is a modernized view of cancer immunosurveillance that has first been hypothesized in content by Burnet and Thomas in the 1950s (Burnet, 1957; Thomas, 1959). Thereby, the innate and adaptive immunity directly fight and protect the organism against unedited developing tumors that were finally destroyed long before they become clinically apparent. If all tumor cells were destructed, the elimination phase represents an endpoint of cancer immunoediting. However, tumor cell variants that may survive the elimination phase can enter the equilibrium, where the adaptive immune system prevents tumor outgrowth. In the equilibrium phase, tumor cells can become functionally dormant and remain clinically unapparent. Since this phase can last for the entire life of the host, it can characterize a second stable endpoint of cancer immunoediting. Finally, due to changes resulting from an active immunoediting process, cancer-induced immunosuppression or immune system failure, tumor cells can escape from immune control resulting in a clinically apparent tumor formation (Schreiber et al., 2011; Vesely et al., 2011). In this line, since cancer immune-based approaches including vaccine therapies for melanoma have to deal with tumors that escaped immune control, it might be explainable why they often revealed limited overall success or even completely failed (Eggermont, 2009; Chi and Dudek, 2011). Based on this condition, one might ask the question, if clinically apparent edited tumors, the targets of cancer therapy that grow in an immunologically unrestricted manner, are still feasible targets for immunotherapy. During the last years, many efforts of various research groups worldwide positively answered the question. For example, Galon et al. (2006) showed that the infiltration, the location and the density of T cells in tumors indicate a major prognostic factor of cancer patient outcome. Moreover, cancer-induced immunosuppressive mechanisms are now better understood (Eggermont, 2009).

Nowadays, it is believed, that the immune system is capable of efficiently fighting the tumor growth when it receives help by powerful therapeutic intervention approaches. The checkpoint blockade of immunosuppressive molecules such as CTLA-4 or PD-1 on T cells represents an important possibility of such an intervention (Korman et al., 2006; Schreiber et al., 2011). For example, the therapy using CTLA-4 blocking Abs revealed a significant survival benefit in metastatic melanoma patients (Hodi et al., 2010; Wolchok et al., 2011). Thereby, the anti-tumor effect obtained through Ab blockade of, e.g., CTLA-4 resulted from increased T cell activation. The positive results of the checkpoint blockade showed also that antigens relevant for tumor targeting are still present in edited tumors and more important that it is still possible to fight cancer in an immunological fashion, even when the escape phase is already entered.

An effective immunotherapy is dependent on the quality and quantity of immune effector cells, including memory T cells (Kaech et al., 2002). In this thesis, it could be shown that high frequencies of pre-existing tumor antigen-reactive memory T cells are present in the PB of non-metastasized melanoma patients while testing a broad variety of different melanoma TAA polypeptides *in vitro* (Figs. 25-27 and 33). After the resection of the tumor, the T cell responses strongly increased, which may implicate a protective relevance, meaning that TAA-reactive T cells are present *in vivo*. In order to provide their functional potential, they have to be reactivated. Based on the produced *in vitro* data, a potent peptide vaccine would result in an efficient memory T cell reactivation *in vivo* using for example long peptides for Melan-A/MART-1, Tyrosinase or NA17-A, which revealed the highest response rates. At later time points above d60, the increased tumor antigen-reactive T cell frequencies declined to basal numbers in the PB. The decrease of TAA-reactive T cell frequencies could be explained by the hypothesis that cells might leave the blood and enter lymphoid immune organs including the bone marrow via circulation. It has been described that TAA-specific memory $CD8^+$ T cells persist in high numbers in the bone marrow (Mahnke et al., 2005). In this context, the bone marrow microenvironment is suggested to have special features for the maintenance of immunological T cell memory. Furthermore, memory T cells have a self-renewal capacity and are characterized by their longevity (Schirrmacher et al., 2003). When they get specifically activated, at any later time point in life, memory T cells can mount efficient immune responses. Importantly, immune responses by memory T cells are faster and stronger than primary responses and their requirements for activation are less strict (Sallusto et al., 2004). It has also been shown that they need lower antigen concentration and are less dependent on co-stimulation than naive T cells (Schirrmacher et al., 2003). For a durable prevention of tumor recurrence and metastasis formation, tumor-reactive memory T cell responses might therefore be required (Côté et al., 2008).

Although, non-metastasized melanoma is considered to be cured after the surgical removal of the primary tumor, still a moderate or intermediate risk remains for novel melanoma or metastases development, decades after apparently successful initial treatment (Cancer Research UK, 2010). Melanoma has a high metastatic potential and melanoma recurrence can occur very late and has been reported after a disease-free interval of 35 years (Tahery and Moy, 1993). Importantly, melanoma tumor dormancy through micrometastases or solitary dormant cells during a tumor

equilibrium state might be, at least in part, responsible for the late cancer recurrence (Townson and Chambers, 2006; Strauss and Thomas, 2010). A high incidence of circulating tumor cells (CTC) in early melanoma, with 32 % in stage I and 42 % in stage II have been reported (Mocellin et al., 2006; Strauss and Thomas, 2010). The early spread of CTCs is usually undetected by current high-resolution imaging techniques and therefore tremendous efforts are currently performed, to optimize sensitive immunocytochemical and molecular assays to detect CTCs at the single-cell stage (for reviews see Pantel et al., 2009; Pantel and Alix-Panabieres, 2010). Moreover, whether CTC contain cancer stem cells is currently under debate, especially for melanoma (Panel et al., 2009; Girouard and Murphy, 2011). Patients with melanoma micrometastases survive without metastatic relapse as long as solitary tumor cells or micrometastases are kept dormant in the immunocompetent host (Thomas, 2008; Strauss and Thomas, 2010). Nevertheless, considering the transmission of melanoma by apparent melanoma disease-free organ donors that had a previous history of melanoma, the presence of dormant tumor cells and in this context the role of a functional and effective immune control becomes obvious. Several case reports exist showing that dormant melanoma cells escaped in an immunosuppressed recipient after organ transplantation. In this line, melanoma is one of the most often reported and lethal donor-derived malignancies with a high tumor-transmission rate of 74 %, thereby showing 58 % mortality (Buell et al., 2004). Since even melanoma patients with early disease can harbor systemic dormant tumor cells that can survive unlimited, it has been advised that patients with early, apparently cured melanoma should not be considered as organ donors (Strauss and Thomas, 2010). The clinical relevance and the prognostic influence of CTCs in early melanoma in immunocompetent hosts are still unclear and therefore require further future investigations (Strauss and Thomas, 2010).

However, the presence of polyvalent spontaneously induced tumor antigen-reactive memory T cells, as detected in non-metastasized melanoma patients (Figs. 18-21, 24-27, 29 and 32-37) might be of importance in controlling potential tumor recurrence caused by CTC or micrometastases, based on the longevity of memory T cells. Furthermore, memory T cells can be boosted for therapeutic purposes at any time by the application of, e.g., peptide vaccines specific for TAAs.

The here presented investigation of spontaneous tumor-reactive memory T cell responses was performed with long synthetic polypeptides composed of 50 amino acids (aa). The strategy to use long polypeptide for T cell stimulation has several advantages, compared to short peptides with exact binding properties (for discussion see Melief and van der Burg, 2008). Thus, vaccination with exact short MHC-binding peptides, preferentially presented by MHC class I molecules (mainly HLA-A2-restricted) reveals a popular approach that is widely used for cancer immunotherapy. But, apart from promising outcomes obtained in melanoma, so far this approach showed disappointing overall success, caused among other reasons, by an induction of only $CD8^+$ T cell responses. Since long peptides are not able to bind directly to MHC molecules, they can induce more effective immune responses as they must be processed by dendritic cells before they can be presented to T cells (Melief and van der Burg, 2008). Therefore, the 50aa long polypeptides, used in this thesis, were constructed to cover at least one known MHC class I, HLA-A2-restricted epitope that has well been described in the literature (cf., Tab. 8). In addition, other putative MHC class I and II epitopes,

predicted by database analysis on the basis of computer algorithms were covered. In order to test, whether HLA-A2 negative patient-derived T cells recognized the polypeptides, patient samples were separated based on the expression of HLA-A2 by flow cytometry, into HLA-$A2^+$ and HLA-$A2^-$ patients. Importantly, TAA-derived polypeptides were recognized by both groups (Fig. 23). In line with this finding, $CD8^+$ as well as $CD4^+$ T cells of the same patient significantly recognized the tested synthetic melanoma polypeptides (Fig. 24). Thus, the designed polypeptides were proved to contain epitopes that can efficiently be recognized by HLA-$A2^+$ and HLA-$A2^-$ T cells. Importantly, the investigation showed that the length of the polypeptides was sufficient to allow an efficient presentation on various HLA alleles.

The use of such polypeptides for cancer immunotherapy approaches has the mature advantage that patients not longer have to be selected according to the expression of defined HLA molecules. Moreover, an important implication might be that more patients and no longer only subsets of patients could benefit from the treatment. Through polyvalent induction of $CD4^+$ and $CD8^+$ T cells, both subsets can contribute together to the anti-tumor response. It has been shown that a synthetic peptide-mediated activation of $CD4^+$ T cells is necessary for the induction and maintenance of efficient anti-tumor memory T cells over time (for discussion see Khazaie et al., 2009). Consequently, the lack of dependence on restricted HLA types might represent an important advantage to minimize the immune escape of cancer cells in a vaccination setting through downregulation of certain HLA alleles. For example, it has been described for melanoma, that HLA-A2 is down-regulated with melanoma disease progression (Kageshita et al., 2001).

The effectiveness of such peptide vaccination approaches can be confirmed by current vaccination studies. Exemplarily, a recent study of stage IV melanoma patients, that combined cancer vaccination with chemotherapy using a telomerase peptide vaccination together with the chemotherapeutic agent temozolomide, showed that the majority of patients (78 %) had telomerase-specific immune responses and developed long-term T cell memory (Kyte et al., 2011). Using this treatment, some patients developed partial tumor regression or showed a stable disease. Interestingly, in one patient a complete remission was reported. Thereby, the telomerase peptide sequence, used for this clinical trial, was selected on the basis of computer algorithms that predicted strong human HLA class I and class II binding motifs that can recruit $CD4^+$ T helper cells and $CD8^+$ CTLs.

Noteworthy, in the presented thesis, in addition to non-metastasized melanoma also T cells of metastasized melanoma patients showed polyvalent and HLA-type independent spontaneous tumor antigen-reactive T cell responses to the constructed synthetic 50aa polypeptides (Figs. 20, 21 and 23). These observations indicate that the polypeptides can be efficiently used in order to induce pre-existing T cell responses in melanoma patients, independent of the disease stage and HLA-type. Importantly, since endogenous responses against human IgG were subtracted, the measured pre-existing T cell frequencies represented TAA-reactive frequencies.

It is unlikely that the detected increased TAA-reactive T cell responses over time after resection of the primary tumor or lesion occurred as an unspecific response or side effect to the surgical intervention. The fact that in PB samples of the same patient before and after surgical resection

TAA-reactive T cell responses specifically increased over time, while TAA-unspecific responses against IgG did not alter in the same magnitude, support this statement (Fig. 29). Moreover, autoimmune markers investigated in the plasma of the patients, before and after resection, did not considerably increase, which also supports indirectly the previous interpretation (cf., Tab. 10). In addition, one would expect that if a T cell response had been induced by the surgical intervention, it would most likely be detectable soon after the resection. Since it is known that after antigen encounter it takes ~4-5 d until clonal expansion is completed and naive T cells have differentiated into effector cells (e.g., Murphy et al., 2008). Comparing the T cell responses in the PB of a patient, before and 13 d after the resection, the IFNγ spot numbers by T cells were not elevated, as shown for both TAA-specific and -unspecific responses (Fig. 29A). But, in agreement with the cumulative data (Fig. 26), the TAA-specific T cell responses of the same patient increased strongly over time up to d 64 after resection, in a significant higher magnitude compared to control IgG (Fig. 29A). This indicates that at later time points after the resection, the cancer/lesion-induced suppression of specific immune responses is no longer taking place and therefore allows the increased manifestation of tumor specific pre-existing memory T cell responses.

Even more interesting was the observation that using the synthetic polypeptides, significantly increased TAA-reactive memory T cell responses were detected in patients with dysplastic nevi lesions, compared to healthy donors (Figs. 22 and 37). Thereby, the frequencies of TAA-reactive T cells in dysplastic nevi patients were intermediate between healthy donors and melanoma patients. Moreover, the revealed T cell responses were higher after resection of the pre-malignant lesion compared to the responses measured before (Figs. 29A and 37). In this context, as already discussed for melanoma, the dysplastic nevi lesions, indicating benign neoplasms of melanocytes, seemed to control pre-existing memory T cell responses in the PB. This observation of a lesion-dependent immune control also indicated that already pre-malignant dysplastic nevi lesions might be edited and escaped immune control. In agreement with other research observations, this data suggests that during melanoma genesis immune tolerance is early induced, in order to favor melanoma growth (Mourmouras et al., 2007). Importantly, in this context, it has been shown that already dysplastic nevi contain mutations that are reported for melanoma including BRAF and NRAS mutations (Poynter et al., 2006; Wu et al., 2007). Therefore, they are placed in a tumor progression lineage with melanoma, intermediate between common nevi and melanoma. Moreover, they present a pre-malignant stage that indicates an increased risk of developing cutaneous melanoma (Edler, 2010). Depending on the study conducted about 25-50 % of melanoma tumors have been shown to derive from a histological associated nevus, thereby often from a dysplastic nevus (Edler, 2010; Ko et al., 2010). Because of their relative small size and questionable malignant potential, melanocytic dysplastic nevi lesions have previously been studied less extensively (Hussein, 2005), but gained more attention during the last years. In this context, a recent study investigated the molecular profiling of dysplastic nevi and identified altered biological processes (Scatolini et al., 2010).

Despite the fact that $CD3^+$ tumor-infiltrating lymphocytes (TILs) were detected in dysplastic nevi in contrast to benign nevi, where they are almost absent (e.g., Hussein et al., 2006; Mourmouras et

al., 2007), little is known about circulating pre-existing melanoma TAA-reactive memory T cells in dysplastic nevi patients. Summarized, this thesis for the first time reports the presence of these T cells in the PB of dysplastic nevi patients. In response to synthetic 50aa melanoma polypeptides the presented data indicated a cell population that could be specifically reactivated through peptide vaccination. Moreover, based on the fact that at least a proportion of melanoma develops from dysplastic nevi, these lesions and the underlying immune reactions through, e.g., pre-existing memory T cell responses may provide further important insights into mechanisms of melanoma progression and may disclose possible future treatment interventions.

In the course of my thesis it additionally could be shown that in the PB of non-metastasized melanoma patients after resection of the primary tumor on average 5 % of the $CD4^+$ T cells were $Foxp3^+$ Treg (Fig. 30). This number was comparable to the Treg percentage detected in the PB of healthy donors and is in accordance with data recently shown by other research groups (e.g., McCarter et al., 2007). In this reports, healthy donors and stage I melanoma patients had comparable amounts of circulating Treg of about 6 % whereas stage IV metastasized patients had a doubling of Treg compared to the other two cohorts. In the PB of the metastasized patients ~12 % circulating Treg were detected, in accordance with a more immunosuppressive phenotype in advanced melanoma. Moreover, it has been shown that TGFβ serum levels were significantly higher in stage I and stage IV melanoma patients compared to healthy donors (McCarter et al., 2007). Thereby, TGFβ levels in stage I patients were intermediate between normal controls and stage IV patients. It is known that Treg mediate their suppressive function preferentially through inhibitory cytokines including TGFβ, which in addition can directly be produced by tumor cells in order to induce an immune suppressive state, while inhibiting immune cell functions (Vignali et al., 2008; Wan and Flavell, 2008; Lohr et al., 2011; Vesely et al., 2011). Moreover, Treg have been described to affect both, innate and acquired immunity and are regarded as the primary mediators of peripheral self tolerance. They are involved in a variety of human disorders such as autoimmune diseases, infectious and inflammatory diseases, allergies, organ transplantation and cancer (for reviews see, e.g., Vignali et al., 2008; Sakaguchi, 2011). Importantly, in melanoma, Treg have been described to induce immune tolerance in order to favor melanoma growth and control immune responses through inhibition of T cell proliferation (Mourmouras et al., 2007; Niu et al., 2011).

In agreement with reports on PB samples of breast and colon carcinoma patients (Bonertz et al., 2009; Ge, 2009), this thesis shows that the depletion of Treg in some investigated non-metastasized melanoma patients after primary tumor resection led to increased recognition rates of TAA polypeptides by tumor antigen-reactive memory T cells (Fig. 32). The data revealed that in these patients pre-existing TAA-specific immune responses were suppressed by Treg. This was observed in ~16 % of all patients investigated. In this line, TAA-reactive T cell responses especially for Melan-A/MART-1, p53 and Tyrosinase were shown to be preferentially controlled by Treg. In contrast to the findings in the melanoma cohort, it has been reported for colon carcinoma that Treg-mediated T cell inhibition was predominantly not observed for the p53 antigen, which was defined as a “Treg-independent antigen” for colon carcinoma (Bonertz et al., 2009). Although, p53-specific

T cells have been reported to be present in a majority of human cancers (e.g., Chikamatsu et al., 1999; Hoffmann et al., 2000; Albers et al., 2005), the Treg-mediated control of those p53-reactive T cell responses seems to differ for the individual cancer cohorts. In agreement with the observation made in this thesis that Melan-A/MART-1 T cell responses were suppressed by Treg, an *in vivo* depletion study of Treg in melanoma patients, that used recombinant IL-2-diphteria toxin fusion protein (ONTAK), led to enhanced immune functions. This was characterized exemplarily through induction of Melan-A/MART-1-specific $CD8^+$ T cells (Mahnke et al., 2007).

Unexpectedly, however, the cumulative data of 36 non-metastasized patients showed that the Treg depletion did not lead to a further increase in the frequency of pre-existing TAA-reactive memory T cells in the investigated cohort in respect to the total patient group. This observation was independent of the time point that was investigated after resection of the primary tumor and was seen for all analyzed TAAs (Figs. 33-35). Furthermore, a reduction of T cell frequencies after Treg depletion was shown to be a result of a co-depletion of conventional T cells, indicated by investigating the depleted cell fraction for the marker proteins CD127 and Foxp3. As previously mentioned by other groups that used for Treg depletion, out of the $CD4^+$ population, a protocol that focused on CD25 high cells, besides Treg conventional T cells were also depleted (Fig. 40; see also, Lahl et al., 2007). Since CD127 is present in the majority of mature T cells but absent on Treg, a flow cytometry staining using Abs against CD127 and Foxp3 allowed the distinction of Treg and conventional T cells. Moreover, the presence of CD127 has shown to be inversely correlated with Foxp3 expression (Liu et al., 2006; Seddiki et al., 2006).

Based on the cumulative analysis no essential role of Treg in controlling spontaneous TAA-reactive T cell responses was observed after surgical removal of the primary tumor. In view of this finding, the biological background of the melanoma patients might be of importance. The reason may be that the studied cohort represented a group of patients that were non-metastasized and the primary tumor was already resected at the time of PB examination. It can therefore be assumed that the analyzed patients were tumor free, with the restriction of a possible presence of undetected dormant CTCs or micrometastases that are most likely immune controlled (see, e.g., Barnhill, 2001; Mocellin et al., 2006; Thomas, 2008; Strauss and Thomas, 2010). In this context, after resection a central tumor-mediated immune suppression mechanism that may include immuno suppressive cellular mediators such as Treg might not longer be functionally active. This interpretation is supported on the one hand by the observation that the frequency of pre-existing memory TAA-reactive T cells significantly increased after tumor resection over time and on the other hand by the fact that Treg depleted T cell responses were not additionally increased. In contrast, as exemplarily shown for colon carcinoma in tumor-bearing patients, Treg depletion led to an increased recognition of most of the investigated TAAs by tumor antigen-specific memory T cells (Bonertz et al., 2009). This observation, however, allow the interpretation that in the tumor-bearing patient cohort pre-existing TAA-specific immune responses were suppressed by Treg (Bonertz et al., 2009).

Besides circulating Treg, tumor-infiltrating Treg have also been reported for several cutaneous melanoma lesions, including dysplastic nevi as well as primary and metastatic lesions

(Mourmouras et al., 2007). Nevertheless, the performance of repeated analyses in some patients, before and after resection, revealed that a depletion of Treg did not result in significantly increased TAA-reactive T cell frequencies, independent if the lesion was present or not (Fig. 37). However, in the presence of the respective lesion, pre-existing Treg with TAA specificities for MDM2, p53, Tyrosinase and Melan-A/-MART-1 as well as for human IgG could be detected in the circulation of dysplastic nevi and melanoma patients (Fig. 39). In contrast, after tumor resection, the number of detected specific Treg strongly decreased, since only Treg with specificities for p53 and IgG could be observed. This observation implicated that functional specific Treg seemed to be reduced after removal of the lesions or that the detection method was not sensitive enough, which may be caused by low cells frequencies. Finally, the investigations showed that even TAA-specific Treg are present in the PB of non-metastasized melanoma and dysplastic nevi patients, while a central role of Treg in controlling pre-existing TAA-reactive memory T cell responses could not be observed. Consequently, the tumor or lesion-mediated suppression of TAA-reactive memory T cell responses might preferentially by facilitated via other effector mechanisms of immunosuppression. Thereby, combinations of soluble and cellular mediators are most likely. Besides Treg, further potent mediators have been described including IDO, TGFβ, CTLA-4, PD-1, MDSCs or M2 macrophages (for recent literature see, e.g., Sakuishi et al., 2010; Sica, 2010; Tarhini and Iqbal, 2010; Goedegebuure et al., 2011; Heitger, 2011; Schreiber et al., 2011; Solito et al., 2011).

Moreover, based on the findings that no specific Treg for NA17-A were detected, irregardless of the dysplastic nevi or melanoma cohort, this 50aa long peptide might be useful in terms of peptide vaccination. The generated synthetic polypeptide efficiently reactivated pre-existing NA17-A-reactive memory T cell responses in dysplastic nevi and melanoma patients without inducing NA17-A-specific Treg (Figs. 22, 25, 29 and 39). In this line, the frequency of NA17-A-reactive T cells significantly increased over time after primary tumor resection (Fig. 27). Importantly, besides the known HLA-A2-restricted epitope that was shown to efficiently induce $CD8^+$ T cell responses (Guilloux et al., 1996; Fonteneau et al., 1997), the long peptide sequence contained further predicted HLA-A2 independent epitopes, that were useful to additionally induce responses of $CD4^+$ T cells (Fig. 24).

Derbinski et al. (2001) showed that tissue-specific antigens like gp100 and Tyrosinase are expressed in adulthood in the thymus by mTECs, in a process termed as “promiscuous gene expression”, that is important for the induction of T cell tolerance to self-antigens and induction of Treg (for review see also Kyewski and Klein, 2006). Nevertheless, promiscuous gene expression for NA17-A has so far not been reported. Moreover, as already discussed, the synthetic long peptide sequence for the atypical peptide NA17-A is partially coded through an intron-based nucleotide sequence and therefore is naturally not translated into a protein (cf., Fig. 16; Guilloux et al., 1996). Especially in melanoma cells, a cryptic promoter within the intron sequence is active and lead to the transcription of a known HLA-A2-restricted epitope (Guilloux et al., 1996) that is comprised by the generated 50aa peptide sequence. HLA-A2-restricted NA17-A peptide vaccination has already been used for clinical trials as part of combinational treatments for melanoma patients. For example, currently a randomized phase II clinical trial that used NA17-A

short peptide vaccination was conducted in patients with metastatic melanoma (http://clinicaltrials.gov /NCT00064168, ID: CDR0000309519). The trial applied a vaccine therapy of peptide-pulsed autologous PBMC together with IL-12, with or without low-dose IL-2. In addition, a peptide mixture of MAGE-3, MART-1, gp100 and NA17-A was used. Furthermore, a multicenter randomized phase III clinical trial with HLA-$A2^+$ primary ocular melanoma patients has been performed using vaccination with NA17-A, Tyrosinase, Melan-A and gp100 short peptides (http://clinicaltrials.gov/NCT00036816, ID: CDR0000069325). Finally, a third study currently started to recruit metastatic melanoma patients. This phase II clinical trial uses a vaccine therapy with MART-1, gp100, MAGE-3 and NA17-A short peptides together with or without IL-12 and the humanized mAb against CD25, daclizumab. Thereby, daclizumab is aimed to deplete $CD4^+CD25^+$ Treg (http://clinicaltrials.gov/NCT01307618, ID: CDR0000696233). However, the effectivity of the individual treatment interventions and a possible superior role of the NA17-A vaccination will be seen in the future.

## 9.2. *In vivo* tumor growth control by optimized TCR transgenic human T cells

Nowadays, adoptive immunotherapy is used for cancer treatment and especially for melanoma revealed promising results (cf., Dudley et al., 2005, 2008). In this context, T cell receptor (TCR) gene therapy gained increased importance for adoptive transfer treatment interventions. In mouse tumor models and initial studies in melanoma patients, the programming of T cells with genes encoding antigen-specific TCR were shown to be functional, although the efficacy in humans in terms of low response rates was limited so far (Xue et al., 2005; Morgan et al., 2006; Johnson et al., 2009). Nevertheless, this method represents a great advantage, since TCRs directed against any desired target antigen, including TAAs, can be generated and introduced into T cells.

To provide self-tolerance under normal conditions in the host, high-avidity T cells are eliminated from the T cell repertoire during the negative selection process that occurs in the thymus (von Boehmer et al., 1989; Robey and Fowlkes, 1994). However, high-avidity T cells might be needed in order to facilitate effective anti-tumor reactions (Kieback and Uckert, 2010). On the one hand, since high-avidity T cells can be generated with this gene transfer method, adoptive transfer of TCR engineered T cells might help to overcome the limitation caused by the self tolerance mechanism. On the other hand, caution should be demanded in the generation of the constructs as long as the target antigen is not exclusively restricted to the tumor and might also be expressed on normal tissues. Under these circumstances, “on-target” toxicity on healthy tissue might be possible (for review see Kieback and Uckert, 2010).

Moreover, the correct pairing of the introduced exogenous TCR chains is crucial in terms of safety aspects and represents currently an important field of research. When introduced into human T cells, the transfer of exogenous TCRs, which consist of two chains, can potentially lead to hybrid/mixed dimer formation with endogenous TCRs. The undesired pairing of the introduced TCR chains with the endogenous chains has two principle consequences. First, it reduces the correct pairing of the introduced engineered TCRs on the cell surface, resulting in a restricted

effectiveness of the treatment. Second, TCRs with unpredictable specificities can occur and may cause “off-target” reactivities, potentially leading to autoimmune reactions, since those transgenic T cells have not been negatively selected in the thymus (Schumacher, 2002; Kieback and Uckert, 2010). Thereby, the general possibility of mispaired hybrid heterodimers could already be shown (Sommermeyer et al., 2006; Heemskerk et al., 2007). Currently, different strategies are investigated to avoid misspairing and promote preferential pairing, such as the modification of the molecular design of the TCR αβ interface or the generation of TCR-like molecules (Voss et al., 2008, 2010; see also Kieback and Uckert, 2010). In order to evaluate the advances made in the generation of TCR transgenic T cells, mouse studies have to be conducted to investigate the *in vivo* potential of those optimized constructs.

Parts of the presented thesis, in a collaboration project, dealed with TCR transgenic T cells with specificities for the antigens MDM2 or gp100 that had been optimized in order to avoid the formation of hybrid TCRs. Thereby, the efficiency of the optimized MDM2 and gp100 TCR transgenic human T cells to control tumor growth was shown for the first time in an *in vivo* murine xenotransplantation model (Voss et al., 2010).

Therefore, as target cell line, cells of the human melanoma line MeWo, established from a lymph node metastasis of a nodular melanoma (Bean et al., 1975; Carey et al., 1976) were used. As melanocytes in the basal layer of the epidermis have been specifically stained with vimentin (Mahrle et al., 1983), the melanocyte-derived origin of the MeWo cells was controlled by analyzing the intermediate-sized filaments vimentin as well as keratins 8 and 18. Vimentin which primarily indicates cells of mesenchymal-derived origin (Franke et al., 1978) was positive in the MeWo cells, whereas keratins 8 and 18 which are used to differentiate cells of epithelial-derived origin were negative (cf., Fig. 41; for reviews see also Moll et al., 1982, 2008; Kurokawa et al., 2011). In addition, the melanocyte antigens gp100 and Melan-A/MART-1 were shown to be positive. Moreover, MeWo cells were revealed to be HLA-A2$^+$ and MDM2$^+$ (Figs. 41, 42 and 45). These observations agreed with the analyses of other groups that also showed positivity of MeWo for HLA-A2, MDM2 and gp100 (cf., Bakker et al., 1994; Schreurs et al., 1998; Pedeux et al., 2002). The presence of these three markers indicated a precondition to be used as target line for recognition by the MDM2 or gp100 TCR engineered T cells, since their TCRs only recognize the respective peptide epitopes in a HLA-A2-restricted manner. In addition, the MeWo cell line has widely been used for studies on the basis of human tumor xenograft mouse models (e.g., Cornil et al., 1989; Skobe et al., 2001; Petrangolini et al., 2003; Schoensiegel et al., 2004). Mouse xenotransplantation models using immunocompromised mice, are important instruments to investigate factors involved in malignant transformation, invasion and metastasis. Moreover, they are used to study responses to therapies including cancer therapeutic approaches *in vivo* (Thallinger et al., 2003; Richmond and Su, 2008). The disadvantages of these models are that the stromal components of the developing tumors are rodent and the hosts are immunodeficient. Nevertheless, since human tumor xenograft models comprise human malignant cells and are reproducible, they present clinically relevant tumor models (Sausville and Newell, 2004; Teicher, 2006).

During the course of the presented thesis, the cells of the line MeWo were injected i.d. onto the flank of NOD-SCID or NSG mice, resulting in a tumor formation in all treated mice. Since the cells were implanted into the tissue of their origin, the performed administration indicated an orthotopic model (Petrangolini et al., 2003). Besides the MeWo parental cells, firefly luciferase stable transfected MeWo cells were used as target line for the xenotransplantation model. The advantages of labeled tumor models are that the tumor growth can be visualized *in vivo* with imaging approaches and metastases can be detected (Teicher, 2006).

The *in vivo* tumor growth control in response to MDM2 or gp100 TCR-redirected T cells was analyzed and showed that human T cells transduced with optimized TCR constructs, in order to avoid the formation of mixed TCR dimers, efficiently controlled the tumor growth. The highest reactivity and strongest control was revealed for the constructs, of a gp100 scTCR that co-expressed a constant α domain and contained an artificial disulfide bond as well as of a MDM2 dcTCR, that comprised a reciprocal Arg/Gly amino acid mutation in the core C-domain interface (Figs. 56 and 58). Correspondingly, the optimized TCR constructs were generated based on two different strategies to prevent the formation of mispaired heterodimers. First, to favor the specific pairing of the MDM2 TCR chains an approach was utilized to modify the molecular design of the TCR αβ interface (Voss et al., 2008). Thereby, the underlying concept was a reciprocal replacement of amino acid residues at the interface of the TCR α and TCR β constant regions. The configurational changes resulted in a selective assembly of the introduced TCR chains with preserved receptor functions including TCR specificity and avidity for antigen fragment ligands (Voss et al., 2008). Moreover, the analyzed high-avidity HLA-A2-restricted MDM2 TCR constructs indicated murine TCRs. Originally, the MDM2 TCR was generated in a partially humanized, HLA-A2.1 transgenic mouse model while performing an immunization with the human MDM2 (81-88) peptide (Stanislawski et al., 2001). This short peptide indicates a tumor antigen that is presented by HLA-A2 and has shown to be recognized by MDM2-specific CTLs (Stanislawski et al., 2001). Moreover, this sequence is integrated in the 50aa long peptide for MDM2 that had successfully been used in order to reactivate pre-existing TAA-reactive memory T cells in the PB of melanoma and dysplastic nevi patients (cf., Figs. 18 and 22). The transforming potential of the ubiquitous self-protein MDM2 resulting by over-expression, leads to the inactivation of the p53 tumor suppressor gene (Momand et al., 1992). In this line, high levels of MDM2 have shown to be present in a number of human tumors (Finlay, 1993; Leach et al., 1993; Freedman and Levine, 1999). In agreement, MDM2 positivity was revealed for a panel of melanoma cell lines as well as for the breast adenocarcinoma cell line MCF-7 (Fig. 41).

It has been further reported that murine TCRs can efficiently replace human TCRs on the human T cell surface, indicating the potential of mouse-derived TCRs in the course of human therapeutic interventions (Sommermeyer et al., 2006). As it might be possible that murine amino acids are immunogenic in humans and cause the elimination of the transferred engineered T cells, human trials have therefore been combined with non-myeloablative lymphodepletion (Kieback and Uckert, 2010). In this line, a clinical trial that used a complete murine TCR showed that the cells can persist in humans (Johnson et al., 2009). Interestingly, Voss et al. (2006) demonstrated that a

humanized version of the MDM2-specific Wt murine TCR revealed diminished functions. Thus, in order to mount equivalent cytotoxicity, the transgenic T cells showed a higher demand for peptide than the murine TCR.

Nevertheless, a crucial requirement for an effective use of TCR gene therapy involving adoptive transfer of TCR gene-modified T cells is the sufficient expression of transferred TCRs. In this direction, it could be shown that murinization of constant regions of human TCRs led to improved chain pairing, elevated TCR expression and function (Cohen et al., 2006). Recently, Sommermeyer and Uckert (2010) identified nine critical amino acid residues that differ between mouse and human constant regions, allowing to generate minimal murinized human TCRs. Those chimeric TCRs show an enhanced expression compared to complete human TCRs. Most likely, minimal murinized therapeutic TCRs will not be immunogenic in humans while preserving the positive effects of murinization.

The second TCR gene-modified T cell approach investigated during this thesis used gp100 specific TCRs. As strategy to promote preferential pairing, Voss et al. (2010) developed a novel 3-domain scTCR approach with murine constant regions that additionally co-expressed a constant murine α domain in order to facilitate a stable and functional TCR expression. The underlying original HLA-A2-restricted gp100 dcTCR that recognizes the gp100 peptide (280-288) has previously been generated (Schaft et al., 2003). The melanoma TAA gp100 is a melanocyte linage/differentiation antigen, from which various epitopes have been described, that can generate antitumor immune responses in melanoma patients. Moreover, it has also successfully been used in clinical trials (Rosenberg et al., 2003; Schwartzentruber et al., 2009).

So far, affinity of scTCR constructs were shown to be reduced compared to full-length TCRs (Zhang et al., 2004). Therefore, of importance is the here presented observation that optimized chimeric gp100 scTCR constructs revealed the highest reactivity in terms of tumor growth control in NOD-SCID mice *in vivo* and were even superior compared to the Wt dcTCR (cf., Fig. 58). In this line, an optimized scTCR with an additional disulfide bond between the constant domains showed the best results. Naturally, the TCR α and β chains are covalently linked by a cysteine disulfide bond between the constant regions (Kieback and Uckert, 2010). Thereby, interestingly, the introduction of a secondary cysteine bridge enhanced the preferential pairing and improved the TCR expression and function (Kuball et al., 2007). In addition, the observation that the tumor growth was even significantly reduced after a secondary tumor challenge in the same animals indicated a persistent and memory T cell response of the transduced TCR engineered T cells *in vivo*. Since the TCR gene-modified T cells showed an effector memory-like phenotype with a CD27 expression in some cells (Fig. 54), the revealed phenotype supported this observation. It has been described that CD27 promote long-term survival and persistence of functional effector memory T cells *in vivo* (Ochsenbein et al., 2004). Therefore, it can be assumed that a fraction of the transferred T cells persisted *in vivo* as a less-differentiated, peripheral effector memory-like T cell subset or gave rise to central memory-like T cells that could home to secondary lymphoid organs (Sallusto et al., 2004; Schwendemann et al., 2005; Romero et al., 2007; Ahmed et al., 2009). Moreover, using optimized scTCR modified T cells, the persistence of effector memory-like

T cells and their ability to exert immediate rapid effector functions might be responsible for the observed stronger tumor growth control of the secondary compared to the primary tumor.

Nevertheless, in none of the *in vivo* experiments the tumor was completely rejected by the therapeutic TCR gene-modified T cells and only a tumor growth control could be observed. This might be due to insufficient presentation of the specific peptide epitopes through the HLA-A2 molecules of the melanoma cells. Additionally, using TCR gp100 transduced T cells, as effector cells, a specific lysis of MeWo cells *in vitro* did not exceed 50 % and normally reclined between 20-50 % (Fig. 77; see also Voss et al., 2010).

The fact, that the here shown combination of a 2 Gy local low dose irradiation of the tumor and adoptive T cell transfer of scTCR gp100 transduced T cells further helped to control the tumor growth compared to the single approaches, indicated the efficiency of combinational treatments. It is well known that irradiation can efficiently kill tumor cells and release tumor antigens that can be presented to T cells (e.g., Watters, 1999; Larsson et al., 2001). The impact of a local low dose irradiation of the tumor for importance of T cell tumor targeting has been shown for the RIP1-Tag5 mouse model of spontaneous insulinomas (Seibel, 2010). Here, a strong infiltration of T cells into the tumor could be detected when the tumor was irradiated locally, thereby irradiation with 2 Gy revealed consistent responses in terms of increased T cell infiltration. That irradiation affected the aberrant tumor vasculature, leading to a normalization of the capillaries accompanied by infiltration of TAA-specific effector T cells, has also previously been shown (Ganss et al., 2002). In agreement, here demonstrated, tumor-infiltrated human $CD45^+$ cells were only detected in the combinational approach of 2 Gy tumor irradiation together with adoptive transfer of TCR engineered T cells (Figs. 69 and 70). However, the low $CD45^+$ cell numbers that were detected inside the tumors might be due to the type of animal model used, since the effect of irradiation might be more pronounced in an immunocompetent environment. It has been shown that during the phase of vasculature normalization and tumor regression, caused by irradiation, besides TAA-specific T cells, further immune cells including macrophages, are strongly involved in the process of tumor rejection (Ganss et al., 2002). Thereby, macrophages trigger the infiltration of T cells by production of nitric oxide (NO). In the absence of macrophages or NO the tumor growth was no longer controlled, independently if T cells were present or not (Seibel, 2010). Since immunodeficient mice including NOD-SCID and NSG have defects in function and activity of immune cells (Shultz et al., 1995, 2005; Zhou et al., 2003), the revealed low infiltration rate of human transgenic T cells into the tumor might be explainable. However, the here presented study was able to show that TCR transgenic T cells, generated in order to avoid hybrid TCR formation, were effective in terms of *in vivo* tumor growth control. Moreover, especially in a combinational setting with local low dose tumor irradiation they obtained promising results. Future studies have to show, whether the *in vitro* optimized TCR constructs that revealed to be functional in animal studies *in vivo* might have a clinical impact.

## 9.3. Tumor-mediated immune suppression through cell adhesion molecules

Malignant tumors escape immune recognition through a panel of different strategies including the reduction of immune recognition, increased resistance to cytotoxic effects of immunity as well as cancer-induced immunosuppression (for recent references see, e.g., Khong and Restifo, 2002; Zitvogel et al., 2006; Schreiber et al., 2011; Vesely et al., 2011). Thereby, tumors suppress immune responses through immunosuppressive cytokines, the recruitment of regulatory immune cells or expression of molecules that are able to mediate inhibitory responses that control the activation status of T cells.

In this context, the cell adhesion molecule CEACAM1 has been discussed in order to facilitate immunosuppressive mechanisms of melanoma cells while developing a resistant phenotype upon recognition by specific T cells (Markel et al., 2006). Thus, homophilic interactions of CEACAM1 molecules, expressed by melanoma cells and activated T cells were shown to be responsible for the inhibition of T cell properties including specific killing activities and IFNγ release. Moreover, it could also be shown that melanoma cells are able to increase their surface CEACAM1 expression in an active process which resulted in enhanced resistance against autologous or allogenic TILs (Markel et al., 2008). CEACAM1 has the ability to recruit Src homology domain 2-containing tyrosine phosphatase-1 (SHP1) to its cytoplasmic tail (Nagaishi et al., 2006), that causes dephosphorylation of the protein tyrosine kinases Lck and ZAP-70, resulting in the inhibition of TCR signaling and thus interfere in T cell activation and cell proliferation (Smith-Garvin et al., 2009). Correspondingly, in T cells CEACAM1 has a predominantly inhibitory function.

Normally, in resting T cells CEACAM1 is stored in intracellular vesicles and only low levels are expressed on the surface of $CD4^+$ cells (Gray-Owen and Blumberg, 2006). But, within minutes after cellular activation high levels of CEACAM1 can be detected on the cell surface of $CD4^+$ and $CD8^+$ T cells (Kammerer et al., 1998; Nakajima et al., 2002). Thereby, the kinetic of CEACAM1 mobilization was shown to be comparable to the early activation molecule CD69. Consequently, CEACAM1 preceded the activation-induced expression of the inhibitory receptor CTLA-4, indicating that CEACAM1-mediated inhibition can function before CTLA-4-mediated inhibition occurs (Gray-Owen and Blumberg, 2006). Furthermore, CEACAM1 has shown to be expressed on T cells also *in vivo* (Morales et al., 1999). However, the reason that only CEACAM1 and no other CEACAM-family members are expressed on T cells may indicate a unique role for CEACAM1 in terms of T cell function (Gray-Owen and Blumberg, 2006).

Accordingly, since with exception of melanoma, many other tumors do not express CEACAM1, during the presented study an immunosuppressive function of further CAMs was addressed. Interestingly, it could be shown that as a result of CEACAM6 and L1CAM expression on tumor cells, human autologous and allogenic TCR-engineered T cell responses against human tumor cells were functionally suppressed. CEACAM6 was detected on a panel of different human adenocarcinoma and multiple myeloma cell lines (Fig. 71). This observation has been confirmed by other groups who detected high levels of CEACAM6 on different cell lines that, e.g., derived from colon, breast, pancreatic or lung cancer (Scholzel et al., 2000; Blumenthal et al., 2007;

Singer et al., 2010). In accordance to the data presented as part of this thesis, a pronounced CEACAM6 presence has been revealed on various adenocarcinoma lines. Moreover, CEACAM6 has shown to be associated with increased potential for metastases formation *in vivo* resulting in reduced survival (Duxbury et al., 2004). Through CEACAM6 inhibition, the ability of pancreatic adenocarcinoma cells to form liver metastases decreased (Duxbury et al., 2004). The present study clearly shows that an inhibition of CEACAM6 on tumor cells revealed increased functional T cell responses, mediated by increased IFNγ secretion. Under this condition, the T cells were competent to accomplish intensified specific tumor cell killing (Figs. 72, 75 and 76). Thereby, the immunosuppressive role of CEACAM6 might be comparable to the verified role of tumor-expressed CEACAM1 in terms of T cell response inhibition and can be interpreted as a mechanism to escape recognition by effector T cells. Moreover, also heterophilic interactions of CEACAM molecules have been shown to occur (Oikawa et al., 1991). Therefore, it might be conceivable that CEACAM6 on the surface of tumor cells exerts T cell inhibition through binding to CEACAM1 molecules on the T cell surface. So far, however, heterophilic interactions between CEACAM1 and CEACAM6 have not been described.

Besides CEACAM6, preliminary data revealed an immunosuppressive role of L1CAM. In accordance to previous studies, cells of the melanoma cell line MeWo showed high L1CAM levels (cf., Figs. 41 and 77; see also Thies et al., 2007). Furthermore, besides melanoma, L1CAM has also been reported for a number of further cancer types including ovarian and colorectal carcinomas and is correlated with an adverse prognosis for the cancer patients (Fogel et al., 2003; Kaifi et al., 2007). Moreover, especially shown for melanoma it has been revealed that L1CAM presence on tumor cells lead to increased proliferation, cell migration and invasive capacities (Meier et al., 2006). Finally, in contrast to Balaian et al. (2000) who reported a co-stimulatory function of L1CAM for T cell activation through homophilic binding of L1CAM molecules, in the present report the specific inhibition of L1CAM on tumor cells revealed a significant increase of cytolytic T cell function against melanoma cells (Fig. 77). This finding may indicate that melanoma cells take advantage not only of CEACAM1 but most likely in addition other CAMs including L1CAM in order to mediate their escape from immune control. To proof this hypothesis, further studies will have to be conducted in the future.

## 9.4. Human tumor cell infection by T cell-transferred Newcastle disease virus

In order to efficiently fight tumor growth, besides the direct use of the immune system through cellular components including TAA-specific T cells, oncolytic virotherapy can additionally be used for cancer intervention. So far, a combination of immune cell and viral therapy for the treatment of cancer demonstrated efficiency in a number of murine- and human-based studies (e.g., Schirrmacher, 2005; Thorne and Contag, 2007; Qiao et al., 2008; Schulze et al., 2009). Despite the knowledge about anti-tumor responses of viruses and viral-transfer vectors, the efficient viral targeting of the tumor tissue represents still a crucial problem. The reason is that, the virus has to transit through several distinct tissues in order to reach the tumor target in a tumor-bearing host.

Therefore, after systemic application the majority of the viral vectors may distribute in various normal tissues and in addition, a part of the virus might also become neutralized in the PB. Consequently, to increase the efficiency of the viral treatments, different approaches have been addressed. For example, the targeting of Newcastle disease virus (NDV) could be shown to be improved using bispecific adapter proteins (Bian et al., 2006). Nevertheless, efficient tumor targeting of oncolytic viruses remains still a major problem.

As part of the presented thesis, the loading of human T cells with NDV was described for the first time in an *in vitro* co-culture system (Pfirschke and Schirrmacher, 2009). In this context, the NDV-loaded T cells were able to transfer the virus in a “hitchhiking”-like process to tumor cells, leading to tumor cell infection and destruction, while affecting the tumor growth behavior. Interestingly, this observation is in agreement with studies of other groups that could show a transfer of retrovirus and vesicular stromatitis virus on blood circulating cells (Cole et al., 2005; Rooney, 2005; Qiao et al., 2008). Based on the revealed transfer mechanism of virus particles, it can be assumed that circulating tumor-homing T cells indicate effective virus carriers in order to facilitate tumor targeting.

In general, oncolytic virotherapy is a strategy for cancer therapy implemented by viruses that feature tumor selective replication, cell lysis of tumor cells, viral spread and the induction of anti-cancer immune responses. However, the effectiveness of the oncolytic cancer virotherapy is primarily based on the characteristic of the virus type used. In this line, for NDV anti-neoplastic and immune stimulatory properties have been reported (Csatary et al., 2004; Schirrmacher, 2005; Freeman et al., 2006; Schirrmacher and Fournier, 2008). Moreover, NDV shows a tumor selective replication, while normal cells induce a strong anti-viral gene expression in response to NDV infections that triggers a virus-resistant phenotype (Wilden et al., 2009). Thus, in response to doubled stranded viral RNA several cellular defense mechanisms are activated in normal cells including type I IFNs. In contrast, it has been shown that in tumor cells the IFN response is often inefficient due to mutations (Wilden et al., 2009).

Furthermore, off importance for cancer treatment are immune stimulatory properties that are induced during virus infection. It has been reported that after efficient and selective replication of NDV in the cell cytoplasm of tumor cells, tumor antigens, immunostimulatory cytokines and danger signals including IFNs and dsRNA are released (Schirrmacher et al., 2003). However, since viruses as single agents might not be sufficient for an optimal use in cancer therapy they have often been used as vectors for cancer gene therapeutic approaches (e.g., Rein et al., 2006; Janke et al., 2007; Zhao et al., 2008). In this combination, they are attractive anti-cancer agents that allow the transfer of genetic material with a therapeutic targeting mechanism. Besides the advantages of viruses, the here presented hitchhiking approach utilizes T cells that are also able to directly fight cancer growth. T cells circulate through the body, can penetrate deep into multilayered tissues and have even shown to cross the blood-brain barrier when they receive the appropriate homing signals (Butcher and Picker, 1996). Once TAA-specific T cells reach tumor cells, which they specifically recognize through antigen presentation, they get activated, gain effector functions followed by the recruitment and activation of additional T cells or further immune cells (Schreiber et al., 2011).

The data of the presented thesis report that T cells can be efficiently modified with different NDV strains (Figs. 78-84). While it has been shown that an amplification of viral M gene expression was detected in activated NDV-modified T cells, the virus could not form infections progeny in the lymphocytes (cf., Fig. 79; see also Pfirschke and Schirrmacher, 2009). In contrast, progeny infectious viral particles accumulated in the supernatant of MCF-7 breast tumor cells (Fig. 79). The effectiveness of the NDV hitchhiking process to tumor cells was shown to depend on the used viral amounts, the T cell to tumor cell ratio, the activation status of the carrier cells, the co-culture time and the virulence of the investigated NDV strain (Figs. 80-84). Even more interesting was the observation that monolayers of human tumor cells could be completely destroyed by the addition of polyclonally activated human T cells that were loaded with oncolytic NDV of strain MTH-68 (Fig. 84). Moreover, the tumor growth control through hitchhiking on activated T cells was superior to non-activated T cells. This finding indicated that the combination of the effectiveness of activated T cells together with the oncolytic viral potential resulted in the optimal tumor growth inhibition. In view of these findings, activated T cells were reported to undergo stronger contacts with tumor cells than non-activated T cells (Bromley et al., 2001). These contacts might help to facilitate a more efficient transfer of the virus to the tumor target, while NDV becomes focused in the contact zone of the stabilized immunological synapse. In addition, much of the cell bound virus might only be loosely attached to the glycocalyx. Therefore, it can be more easily transferred to tumor cells when the T cells undergo strong contacts.

Finally, in a retroviral hitchhiking study, viral transfer to tumor cells was dependent on the enzyme heparanase (Cole et al., 2005). In contrast, T cell-mediated hitchhiking of NDV to tumor cells was proven to be heparanase-independent (Pfirschke and Schirrmacher, 2009). This observation indicated that the mechanisms of NDV transfer in the course of T cell-mediated hitchhiking differ to other viruses. Furthermore, the NDV hitchhiking kinetic was revealed to be faster than the retrovirus or vaccinia virus transfer (cf., Fig. 81, see also Cole et al., 2005; Thorne et al., 2005). The efficiency of NDV hitchhiking using further carrier cells besides human T cells as well as pilot *in vivo* experiments utilizing hitchhiking of NDV have been described (Pfirschke and Schirrmacher, 2009). Future *in vivo* studies will therefore have to show the effect of NDV hitchhiking on TAA-specific T cells and might reveal a positive impact in terms of improved human cancer treatments.

## 9.5. Concluding remarks and future perspectives

Despite the fact that the clinical efficiency of present cancer immune therapeutic interventions is limited, the molecular and regulatory mechanisms that affect the cancer-directed properties of the immune system are currently of great scientific interest. However, detailed mechanisms that influence the potential of tumor immunotherapies still remain poorly understood. Accordingly, the findings revealed during the course of the presented thesis added new aspects to the optimization of cancer immune therapeutic approaches in the areas of peptide-based immunotherapy, adoptive cell transfer of TCR-transgenic T cells, oncolytic virotherapy and cancer-induced immunosuppressive mechanisms.

Adapted from these observations, peptide-based immunotherapies might be appropriate to obtain clinically relevant future results, while using a potent combination of multiple polypeptides that reactivate pre-existing anti-tumor memory T cells. The used peptides should efficiently be able to activate $CD4^+$ and $CD8^+$ tumor-reactive T cell responses while avoiding the reactivation or induction of Treg or further immunosuppressive cells. Thereby, atypical or mutated tumor-specific peptides that are not expressed on normal tissues should preferentially be used. Moreover, a vaccine that will be effective against cancer might not only focus on peptide-based immunotherapy as a monotherapy, rather a combination with mechanisms that block or destroy mediators of cancer-induced immunosuppression might be needed.

In order to obtain effective clinical tumor targeting results, in general, combinational treatments will probably be of central importance for the majority of immune-based approaches. Consequently, as demonstrated during the presented thesis, combinations with oncolytic viruses, low dose irradiation therapies or treatments that inhibit tumor cell-induced immunosuppression, mediated through CAMs could serve as useful treatment additions. To prove the functional relevance of these combinational approaches, further studies will be necessary. This, hopefully, will lead to a better understanding of the tumor disease nature and potentially contribute to the development of functional and effective clinical treatment strategies for improved future cancer immunotherapies.

## 10. References

Abbas AK and Lichtman AH. (2005) Cellular and molecular immunology. Elsevier Saunders, Philadelphia, PA, USA. 1-564 pp.

Acuto O, Di Bartolo V and Michel F. (2008) Tailoring T-cell receptor signals by proximal negative feedback mechanisms. *Nat Rev Immunol*. 8:699-712.

Agarwala SS and Kirkwood JM. (1996) Interferons in melanoma. *Curr Opin Oncol*. 8:167-174.

Aguirre-Ghiso JA. (2007) Models, mechanisms and clinical evidence for cancer dormancy. *Nat Rev Cancer*. 7:834-846.

Ahmed R and Gray D. (1996) Immunological memory and protective immunity: understanding their relation. *Science*. 272:54-60.

Ahmed R, Bevan MJ, Reiner SL and Fearon DT. (2009) The precursors of memory: models and controversies. *Nat Rev Immunol*. 9:662-668.

Albers AE, Ferris RL, Kim GG, Chikamatsu K, DeLeo AB and Whiteside TL. (2005) Immune responses to p53 in patients with cancer: enrichment in tetramer+ p53 peptide-specific T cells and regulatory T cells at tumor sites. *Cancer Immunol Immunother*. 54:1072-1081.

Andrews DM, Maraskovsky E and Smyth MJ. (2008) Cancer vaccines for established cancer: how to make them better? *Immunol Rev*. 222:242-255.

Arnold R, Brenner D, Becker M, Frey CR and Krammer PH. (2006) How T lymphocytes switch between life and death. *Eur J Immunol*. 36:1654-1658.

Arstila TP, Casrouge A, Baron V, Even J, Kanellopoulos J and Kourilsky P. (1999) A direct estimate of the human alphabeta T cell receptor diversity. *Science*. 286:958-961.

Asai T, Storkus WJ, Mueller-Berghaus J, Knapp W, DeLeo AB, Chikamatsu K and Whiteside TL. (2002) In vitro generated cytolytic T lymphocytes reactive against head and neck cancer recognize multiple epitopes presented by HLA-A2, including peptides derived from the p53 and MDM-2 proteins. *Cancer Immun*. 2:3. http://www.cancerimmunity.org/v2p3/020303.pdf.

Atkins MB, Lotze MT, Dutcher JP, Fisher RI, Weiss G, Margolin K, Abrams J, Sznol M, Parkinson D, Hawkins M, Paradise C, Kunkel L and Rosenberg SA. (1999) High-dose recombinant interleukin 2 therapy for patients with metastatic melanoma: analysis of 270 patients treated between 1985 and 1993. *J Clin Oncol*. 17:2105-2116.

Bakker AB, Schreurs MW, de Boer AJ, Kawakami Y, Rosenberg SA, Adema GJ and Figdor CG. (1994) Melanocyte lineage-specific antigen gp100 is recognized by melanoma-derived tumor-infiltrating lymphocytes. *J Exp Med*. 179:1005-1009.

Balaian LB, Moehler T and Montgomery AM. (2000) The human neural cell adhesion molecule L1 functions as a costimulatory molecule in T cell activation. *Eur J Immunol*. 30:938-943.

Balch CM, Gershenwald JE, Soong SJ, Thompson JF, Atkins MB, Byrd DR, Buzaid AC, Cochran AJ, Coit DG, Ding S, Eggermont AM, Flaherty KT, Gimotty PA, Kirkwood JM, McMasters KM, Mihm MC, Jr., Morton DL, Ross MI, Sober AJ and Sondak VK. (2009) Final version of 2009 AJCC melanoma staging and classification. *J Clin Oncol*. 27:6199-6206.

Bandarchi B, Ma L, Navab R, Seth A and Rasty G. (2010) From melanocyte to metastatic malignant melanoma. *Dermatol Res Pract*: Article ID 583748, doi:583710.581155/582010/583748.

Barnhill RL. (2001) The biology of melanoma micrometastases. *Recent Results Cancer Res*. 158:3-13.

Barry M and Bleackley RC. (2002) Cytotoxic T lymphocytes: all roads lead to death. *Nat Rev Immunol*. 2:401-409.

Beadling C, Jacobson-Dunlop E, Hodi FS, Le C, Warrick A, Patterson J, Town A, Harlow A, Cruz F, 3rd, Azar S, Rubin BP, Muller S, West R, Heinrich MC and Corless CL. (2008) KIT gene mutations and copy number in melanoma subtypes. *Clin Cancer Res*. 14:6821-6828.

Bean MA, Bloom BR, Herberman RB, Old LJ, Oettgen HF, Klein G and Terry WD. (1975) Cell-mediated cytotoxicity for bladder carcinoma: evaluation of a workshop. *Cancer Res*. 35:2902-2913.

Becker TC, Coley SM, Wherry EJ and Ahmed R. (2005) Bone marrow is a preferred site for homeostatic proliferation of memory CD8 T cells. *J Immunol*. 174:1269-1273.

Beckhove P, Feuerer M, Dolenc M, Schuetz F, Choi C, Sommerfeldt N, Schwendemann J, Ehlert K, Altevogt P, Bastert G, Schirrmacher V and Umansky V. (2004) Specifically activated memory T cell subsets from cancer patients recognize and reject xenotransplanted autologous tumors. *J Clin Invest*. 114:67-76.

Behrens J and Nelson WJ. (2004) Cell Adhesion. Springer Verlag, Berlin, Heidelberg, New York. 1-481 pp.

Bendle GM, Haanen JB and Schumacher TN. (2009) Preclinical development of T cell receptor gene therapy. *Curr Opin Immunol*. 21:209-214.

Benz C, Heinzel K and Bleul CC. (2004) Homing of immature thymocytes to the subcapsular microenvironment within the thymus is not an absolute requirement for T cell development. *Eur J Immunol*. 34:3652-3663.

Berger C, Jensen MC, Lansdorp PM, Gough M, Elliott C and Riddell SR. (2008) Adoptive transfer of effector CD8+ T cells derived from central memory cells establishes persistent T cell memory in primates. *J Clin Invest*. 118:294-305.

Bevona C, Goggins W, Quinn T, Fullerton J and Tsao H. (2003) Cutaneous melanomas associated with nevi. *Arch Dermatol*. 139:1620-1624; discussion 1624.

Bian H, Fournier P, Peeters B and Schirrmacher V. (2005) Tumor-targeted gene transfer in vivo via recombinant Newcastle disease virus modified by a bispecific fusion protein. *Int J Oncol*. 27:377-384.

Bian H, Wilden H, Fournier P, Peeters B and Schirrmacher V. (2006) In vivo efficacy of systemic tumor targeting of a viral RNA vector with oncolytic properties using a bispecific adapter protein. *Int J Oncol*. 29:1359-1369.

Bjorkman PJ, Saper MA, Samraoui B, Bennett WS, Strominger JL and Wiley DC. (1987a) Structure of the human class I histocompatibility antigen, HLA-A2. *Nature*. 329:506-512.

Bjorkman PJ, Saper MA, Samraoui B, Bennett WS, Strominger JL and Wiley DC. (1987b) The foreign antigen binding site and T cell recognition regions of class I histocompatibility antigens. *Nature*. 329:512-518.

Blumenthal RD, Leon E, Hansen HJ and Goldenberg DM. (2007) Expression patterns of CEACAM5 and CEACAM6 in primary and metastatic cancers. *BMC Cancer*. 7:2; doi:10.1186/1471-2407-1187-1182.

Boiko AD, Razorenova OV, van de Rijn M, Swetter SM, Johnson DL, Ly DP, Butler PD, Yang GP, Joshua B, Kaplan MJ, Longaker MT and Weissman IL. (2010) Human melanoma-initiating cells express neural crest nerve growth factor receptor CD271. *Nature*. 466:133-137.

Bonertz A, Weitz J, Pietsch DH, Rahbari NN, Schlude C, Ge Y, Juenger S, Vlodavsky I, Khazaie K, Jaeger D, Reissfelder C, Antolovic D, Aigner M, Koch M and Beckhove P. (2009) Antigen-specific Tregs control T cell responses against a limited repertoire of tumor antigens in patients with colorectal carcinoma. *J Clin Invest*. 119:3311-3321.

Boon T, Coulie PG, van den Eynde BJ and van der Bruggen P. (2006) Human T cell responses against melanoma. *Annu Rev Immunol*. 24:175-208.

Bopp T, Becker C, Klein M, Klein-Hessling S, Palmetshofer A, Serfling E, Heib V, Becker M, Kubach J, Schmitt S, Stoll S, Schild H, Staege MS, Stassen M, Jonuleit H and Schmitt E. (2007) Cyclic adenosine monophosphate is a key component of regulatory T cell-mediated suppression. *J Exp Med*. 204:1303-1310.

Bos R and Sherman LA. (2010) CD4+ T-cell help in the tumor milieu is required for recruitment and cytolytic function of CD8+ T lymphocytes. *Cancer Res*. 70:8368-8377.

Bousso P, Bhakta NR, Lewis RS and Robey E. (2002) Dynamics of thymocyte-stromal cell interactions visualized by two-photon microscopy. *Science*. 296:1876-1880.

Bromley SK, Burack WR, Johnson KG, Somersalo K, Sims TN, Sumen C, Davis MM, Shaw AS, Allen PM and Dustin ML. (2001) The immunological synapse. *Annu Rev Immunol*. 19:375-396.

Buell JF, Beebe TM, Trofe J, Gross TG, Alloway RR, Hanaway MJ and Woodle ES. (2004) Donor transmitted malignancies. *Ann Transplant*. 9:53-56.

Burnet M. (1957) Cancer: a biological approach. III. Viruses associated with neoplastic conditions. IV. Practical applications. *Br Med J*. 1:841-847.

Butcher EC and Picker LJ. (1996) Lymphocyte homing and homeostasis. *Science*. 272:60-66.

Butler MO, Lee JS, Ansen S, Neuberg D, Hodi FS, Murray AP, Drury L, Berezovskaya A, Mulligan RC, Nadler LM and Hirano N. (2007) Long-lived antitumor CD8+ lymphocytes for adoptive therapy generated using an artificial antigen-presenting cell. *Clin Cancer Res*. 13:1857-1867.

Cancer Research UK. (2010) http://cancerhelp.cancerresearchuk.org/prod_consump/groups/cr_common/@cah/@gen/documents/generalcontent/treating-melanoma.pdf

Carbone FR, Kurts C, Bennett SR, Miller JF and Heath WR. (1998) Cross-presentation: a general mechanism for CTL immunity and tolerance. *Immunol Today*. 19:368-373.

Carey TE, Takahashi T, Resnick LA, Oettgen HF and Old LJ. (1976) Cell surface antigens of human malignant melanoma: mixed hemadsorption assays for humoral immunity to cultured autologous melanoma cells. *Proc Natl Acad Sci U S A*. 73:3278-3282.

Caspi RR. (2008) Immunotherapy of autoimmunity and cancer: the penalty for success. *Nat Rev Immunol*. 8:970-976.

Cassel WA and Garrett RE. (1965) Newcastle Disease Virus as an Antineoplastic Agent. *Cancer*. 18:863-868.

Cassel WA and Murray DR. (1992) A ten-year follow-up on stage II malignant melanoma patients treated postsurgically with Newcastle disease virus oncolysate. *Med Oncol Tumor Pharmacother*. 9:169-171.

Castelli C, Storkus WJ, Maeurer MJ, Martin DM, Huang EC, Pramanik BN, Nagabhushan TL, Parmiani G and Lotze MT. (1995) Mass spectrometric identification of a naturally processed melanoma peptide recognized by CD8+ cytotoxic T lymphocytes. *J Exp Med*. 181:363-368.

Cavallo F, de Giovanni C, Nanni P, Forni G and Lollini PL. (2011) 2011: the immune hallmarks of cancer. *Cancer Immunol Immunother*. 60:319-326.

Cederbom L, Hall H and Ivars F. (2000) CD4+CD25+ regulatory T cells down-regulate co-stimulatory molecules on antigen-presenting cells. *Eur J Immunol*. 30:1538-1543.

CenterWatch. (2011) FDA Approved Drugs for Oncology. http://www.centerwatch.com/drug-information/fda-approvals/drug-areas.aspx?AreaID=12.

Cha MH, Rhim T, Kim KH, Jang AS, Paik YK and Park CS. (2007) Proteomic identification of macrophage migration-inhibitory factor upon exposure to TiO2 particles. *Mol Cell Proteomics*. 6:56-63.

Chai JG, Xue SA, Coe D, Addey C, Bartok I, Scott D, Simpson E, Stauss HJ, Hori S, Sakaguchi S and Dyson J. (2005) Regulatory T cells, derived from naive CD4+CD25- T cells by in vitro Foxp3 gene transfer, can induce transplantation tolerance. *Transplantation*. 79:1310-1316.

Chambers CA and Allison JP. (1999) Costimulatory regulation of T cell function. *Curr Opin Cell Biol*. 11:203-210.

Chen W, Jin W, Hardegen N, Lei KJ, Li L, Marinos N, McGrady G and Wahl SM. (2003) Conversion of peripheral CD4+CD25- naive T cells to CD4+CD25+ regulatory T cells by TGF-beta induction of transcription factor Foxp3. *J Exp Med*. 198:1875-1886.

Chi M and Dudek AZ. (2011) Vaccine therapy for metastatic melanoma: systematic review and meta-analysis of clinical trials. *Melanoma Res*. 21:165-174.

Chikamatsu K, Nakano K, Storkus WJ, Appella E, Lotze MT, Whiteside TL and DeLeo AB. (1999) Generation of anti-p53 cytotoxic T lymphocytes from human peripheral blood using autologous dendritic cells. *Clin Cancer Res*. 5:1281-1288.

Choi C, Witzens M, Bucur M, Feuerer M, Sommerfeldt N, Trojan A, Ho A, Schirrmacher V, Goldschmidt H and Beckhove P. (2005) Enrichment of functional CD8 memory T cells specific for MUC1 in bone marrow of patients with multiple myeloma. *Blood*. 105:2132-2134.

Clark WH, Jr., Elder DE, Guerry Dt, Epstein MN, Greene MH and van Horn M. (1984) A study of tumor progression: the precursor lesions of superficial spreading and nodular melanoma. *Hum Pathol*. 15:1147-1165.

Cohen CJ, Zhao Y, Zheng Z, Rosenberg SA and Morgan RA. (2006) Enhanced antitumor activity of murine-human hybrid T-cell receptor (TCR) in human lymphocytes is associated with improved pairing and TCR/CD3 stability. *Cancer Res*. 66:8878-8886.

Cole C, Qiao J, Kottke T, Diaz RM, Ahmed A, Sanchez-Perez L, Brunn G, Thompson J, Chester J and Vile RG. (2005) Tumor-targeted, systemic delivery of therapeutic viral vectors using hitchhiking on antigen-specific T cells. *Nat Med*. 11:1073-1081.

Collison LW, Workman CJ, Kuo TT, Boyd K, Wang Y, Vignali KM, Cross R, Sehy D, Blumberg RS and Vignali DA. (2007) The inhibitory cytokine IL-35 contributes to regulatory T-cell function. *Nature*. 450:566-569.

Cornil I, Man S, Fernandez B and Kerbel RS. (1989) Enhanced tumorigenicity, melanogenesis, and metastases of a human malignant melanoma after subdermal implantation in nude mice. *J Natl Cancer Inst*. 81:938-944.

Côté AL, Usherwood EJ and Turk MJ. (2008) Tumor-specific T-cell memory: clearing the regulatory T-cell hurdle. *Cancer Res*. 68:1614-1617.

Coyle AJ and Gutierrez-Ramos JC. (2001) The expanding B7 superfamily: increasing complexity in costimulatory signals regulating T cell function. *Nat Immunol*. 2:203-209.

Croft M. (2009) The role of TNF superfamily members in T-cell function and diseases. *Nat Rev Immunol*. 9:271-285.

Csatary LK, Gosztonyi G, Szeberenyi J, Fabian Z, Liszka V, Bodey B and Csatary CM. (2004) MTH-68/H oncolytic viral treatment in human high-grade gliomas. *J Neurooncol*. 67:83-93.

de Witte MA, Jorritsma A, Kaiser A, van den Boom MD, Dokter M, Bendle GM, Haanen JB and Schumacher TN. (2008) Requirements for effective antitumor responses of TCR transduced T cells. *J Immunol*. 181:5128-5136.

Deaglio S, Dwyer KM, Gao W, Friedman D, Usheva A, Erat A, Chen JF, Enjyoji K, Linden J, Oukka M, Kuchroo VK, Strom TB and Robson SC. (2007) Adenosine generation catalyzed by CD39 and CD73 expressed on regulatory T cells mediates immune suppression. *J Exp Med*. 204:1257-1265.

Derbinski J, Schulte A, Kyewski B and Klein L. (2001) Promiscuous gene expression in medullary thymic epithelial cells mirrors the peripheral self. *Nat Immunol*. 2:1032-1039.

Derbinski J, Gaebler J, Brors B, Tierling S, Jonnakuty S, Hergenhahn M, Peltonen L, Walter J and Kyewski B. (2005) Promiscuous gene expression in thymic epithelial cells is regulated at multiple levels. *J Exp Med*. 202:33-45.

Dranoff G. (2004) Cytokines in cancer pathogenesis and cancer therapy. *Nat Rev Cancer*. 4:11-22.

Dudley ME, Wunderlich JR, Yang JC, Sherry RM, Topalian SL, Restifo NP, Royal RE, Kammula U, White DE, Mavroukakis SA, Rogers LJ, Gracia GJ, Jones SA, Mangiameli DP, Pelletier MM, Gea-Banacloche J, Robinson MR, Berman DM, Filie AC, Abati A and Rosenberg SA. (2005) Adoptive cell transfer therapy following non-myeloablative but lymphodepleting chemotherapy for the treatment of patients with refractory metastatic melanoma. *J Clin Oncol*. 23:2346-2357.

Dudley ME, Yang JC, Sherry R, Hughes MS, Royal R, Kammula U, Robbins PF, Huang J, Citrin DE, Leitman SF, Wunderlich J, Restifo NP, Thomasian A, Downey SG, Smith FO, Klapper J, Morton K, Laurencot C, White DE and Rosenberg SA. (2008) Adoptive cell therapy for patients with metastatic melanoma: evaluation of intensive myeloablative chemoradiation preparative regimens. *J Clin Oncol*. 26:5233-5239.

Duxbury MS, Ito H, Zinner MJ, Ashley SW and Whang EE. (2004) CEACAM6 gene silencing impairs anoikis resistance and in vivo metastatic ability of pancreatic adenocarcinoma cells. *Oncogene*. 23:465-473.

Egeblad M, Nakasone ES and Werb Z. (2010) Tumors as organs: complex tissues that interface with the entire organism. *Dev Cell*. 18:884-901.

Eggermont AM. (2009) Immunotherapy: Vaccine trials in melanoma - time for reflection. *Nat Rev Clin Oncol*. 6:256-258.

Elder DE. (2010) Dysplastic naevi: an update. *Histopathology*. 56:112-120.

Ernfors P. (2010) Cellular origin and developmental mechanisms during the formation of skin melanocytes. *Exp Cell Res*. 316:1397-1407.

Fallarino F, Grohmann U, Hwang KW, Orabona C, Vacca C, Bianchi R, Belladonna ML, Fioretti MC, Alegre ML and Puccetti P. (2003) Modulation of tryptophan catabolism by regulatory T cells. *Nat Immunol*. 4:1206-1212.

Feuerer M, Beckhove P, Garbi N, Mahnke Y, Limmer A, Hommel M, Hammerling GJ, Kyewski B, Hamann A, Umansky V and Schirrmacher V. (2003) Bone marrow as a priming site for T-cell responses to blood-borne antigen. *Nat Med*. 9:1151-1157.

Finlay CA. (1993) The mdm-2 oncogene can overcome wild-type p53 suppression of transformed cell growth. *Mol Cell Biol*. 13:301-306.

Fogel M, Gutwein P, Mechtersheimer S, Riedle S, Stoeck A, Smirnov A, Edler L, Ben-Arie A, Huszar M and Altevogt P. (2003) L1 expression as a predictor of progression and survival in patients with uterine and ovarian carcinomas. *Lancet*. 362:869-875.

Fonteneau JF, Le Drean E, Le Guiner S, Gervois N, Diez E and Jotereau F. (1997) Heterogeneity of biologic responses of melanoma-specific CTL. *J Immunol*. 159:2831-2839.

Fontenot JD, Gavin MA and Rudensky AY. (2003) Foxp3 programs the development and function of CD4+CD25+ regulatory T cells. *Nat Immunol*. 4:330-336.

Franke WW, Schmid E, Osborn M and Weber K. (1978) Different intermediate-sized filaments distinguished by immunofluorescence microscopy. *Proc Natl Acad Sci U S A*. 75:5034-5038.

Frauwirth KA, Riley JL, Harris MH, Parry RV, Rathmell JC, Plas DR, Elstrom RL, June CH and Thompson CB. (2002) The CD28 signaling pathway regulates glucose metabolism. *Immunity*. 16:769-777.

Freedman DA and Levine AJ. (1999) Regulation of the p53 protein by the MDM2 oncoprotein - thirty-eighth G.H.A. Clowes Memorial Award Lecture. *Cancer Res*. 59:1-7.

Freeman AI, Zakay-Rones Z, Gomori JM, Linetsky E, Rasooly L, Greenbaum E, Rozenman-Yair S, Panet A, Libson E, Irving CS, Galun E and Siegal T. (2006) Phase I/II trial of intravenous NDV-HUJ oncolytic virus in recurrent glioblastoma multiforme. *Mol Ther*. 13:221-228.

Gajewski TF. (2000) Monitoring specific T-cell responses to melanoma vaccines: ELISPOT, tetramers, and beyond. *Clin Diagn Lab Immunol*. 7:141-144.

Galon J, Costes A, Sanchez-Cabo F, Kirilovsky A, Mlecnik B, Lagorce-Pages C, Tosolini M, Camus M, Berger A, Wind P, Zinzindohoue F, Bruneval P, Cugnenc PH, Trajanoski Z, Fridman WH and Pages F. (2006) Type, density, and location of immune cells within human colorectal tumors predict clinical outcome. *Science*. 313:1960-1964.

Ganss R, Ryschich E, Klar E, Arnold B and Haemmerling GJ. (2002) Combination of T-cell therapy and trigger of inflammation induces remodeling of the vasculature and tumor eradication. *Cancer Res*. 62:1462-1470.

Ge Y. (2009) "From bench to bedside": role of tumour-specific regulatory T cells in breast cancer and exploration of their therapeutic modulation. Faculty of Biology. Ph. D. Thesis. University of Heidelberg, Heidelberg, Germany. 1-127 pp.

Girouard SD and Murphy GF. (2011) Melanoma stem cells: not rare, but well done. *Lab Invest*. 91:647-664.

Goedegebuure P, Mitchem JB, Porembka MR, Tan MC, Belt BA, Wang-Gillam A, Gillanders WE, Hawkins WG and Linehan DC. (2011) Myeloid-Derived Suppressor Cells: General Characteristics and Relevance to Clinical Management of Pancreatic Cancer. *Curr Cancer Drug Targets*. 11:734-751.

Gray-Owen SD and Blumberg RS. (2006) CEACAM1: contact-dependent control of immunity. *Nat Rev Immunol*. 6:433-446.

Guilloux Y, Lucas S, Brichard VG, van Pel A, Viret C, de Plaen E, Brasseur F, Lethe B, Jotereau F and Boon T. (1996) A peptide recognized by human cytolytic T lymphocytes on HLA-A2 melanomas is encoded by an intron sequence of the N-acetylglucosaminyltransferase V gene. *J Exp Med*. 183:1173-1183.

Haabeth OA, Lorvik KB, Hammarstrom C, Donaldson IM, Haraldsen G, Bogen B and Corthay A. (2011) Inflammation driven by tumour-specific Th1 cells protects against B-cell cancer. *Nat Commun*. 2:240; doi:210.1038/ncomms1239.

Hammarstrom S. (1999) The carcinoembryonic antigen (CEA) family: structures, suggested functions and expression in normal and malignant tissues. *Semin Cancer Biol*. 9:67-81.

Hanahan D and Folkman J. (1996) Patterns and emerging mechanisms of the angiogenic switch during tumorigenesis. *Cell*. 86:353-364.

Hanahan D and Weinberg RA. (2000) The hallmarks of cancer. *Cell*. 100:57-70.

Hanahan D and Weinberg RA. (2011) Hallmarks of cancer: the next generation. *Cell*. 144:646-674.

Heemskerk MH, Hagedoorn RS, van der Hoorn MA, van der Veken LT, Hoogeboom M, Kester MG, Willemze R and Falkenburg JH. (2007) Efficiency of T-cell receptor expression in dual-specific T cells is controlled by the intrinsic qualities of the TCR chains within the TCR-CD3 complex. *Blood*. 109:235-243.

Heitger A. (2011) Regulation of expression and function of IDO in human dendritic cells. *Curr Med Chem*. 18:2222-2233.

Hildeman DA, Zhu Y, Mitchell TC, Kappler J and Marrack P. (2002) Molecular mechanisms of activated T cell death in vivo. *Curr Opin Immunol*. 14:354-359.

Hocker T and Tsao H. (2007) Ultraviolet radiation and melanoma: a systematic review and analysis of reported sequence variants. *Hum Mutat*. 28:578-588.

Hodi FS, O'Day SJ, McDermott DF, Weber RW, Sosman JA, Haanen JB, Gonzalez R, Robert C, Schadendorf D, Hassel JC, Akerley W, van den Eertwegh AJ, Lutzky J, Lorigan P, Vaubel JM, Linette GP, Hogg D, Ottensmeier CH, Lebbe C, Peschel C, Quirt I, Clark JI, Wolchok JD, Weber JS, Tian J, Yellin MJ, Nichol GM, Hoos A and Urba WJ. (2010) Improved survival with ipilimumab in patients with metastatic melanoma. *N Engl J Med*. 363:711-723.

Hoffmann TK, Nakano K, Elder EM, Dworacki G, Finkelstein SD, Appella E, Whiteside TL and DeLeo AB. (2000) Generation of T cells specific for the wild-type sequence p53(264-272) peptide in cancer patients: implications for immunoselection of epitope loss variants. *J Immunol*. 165:5938-5944.

Hori S, Nomura T and Sakaguchi S. (2003) Control of regulatory T cell development by the transcription factor Foxp3. *Science*. 299:1057-1061.

Horst AK and Wagener C. (2004) CEA-Related CAMs. *In* Cell Adhesion. Vol. 165. Behrens J and Nelson WJ, editors. Springer Verlag, Berlin, Heidelberg, New York. pp.283-341.

Huppa JB and Davis MM. (2003) T-cell-antigen recognition and the immunological synapse. *Nat Rev Immunol*. 3:973-983.

Hussein MR. (2005) Melanocytic dysplastic naevi occupy the middle ground between benign melanocytic naevi and cutaneous malignant melanomas: emerging clues. *J Clin Pathol*. 58:453-456.

Hussein MR, Elsers DA, Fadel SA and Omar AE. (2006) Immunohistological characterisation of tumour infiltrating lymphocytes in melanocytic skin lesions. *J Clin Pathol*. 59:316-324.

Jaeger E, Chen YT, Drijfhout JW, Karbach J, Ringhoffer M, Jaeger D, Arand M, Wada H, Noguchi Y, Stockert E, Old LJ and Knuth A. (1998) Simultaneous humoral and cellular immune response against cancer-testis antigen NY-ESO-1: definition of human histocompatibility leukocyte antigen (HLA)-A2-binding peptide epitopes. *J Exp Med*. 187:265-270.

Jameson SC, Hogquist KA and Bevan MJ. (1995) Positive selection of thymocytes. *Annu Rev Immunol*. 13:93-126.

Jandus C, Speiser D and Romero P. (2009) Recent advances and hurdles in melanoma immunotherapy. *Pigment Cell Melanoma Res*. 22:711-723.

Janke M, Peeters B, de Leeuw O, Moorman R, Arnold A, Fournier P and Schirrmacher V. (2007) Recombinant Newcastle disease virus (NDV) with inserted gene coding for GM-CSF as a new vector for cancer immunogene therapy. *Gene Ther*. 14:1639-1649.

Jemal A, Siegel R, Xu J and Ward E. (2010) Cancer statistics, 2010. *CA Cancer J Clin*. 60:277-300.

Jensen PE. (2007) Recent advances in antigen processing and presentation. *Nat Immunol*. 8:1041-1048.

Jerant AF, Johnson JT, Sheridan CD and Caffrey TJ. (2000) Early detection and treatment of skin cancer. *Am Fam Physician*. 62:357-368, 375-376, 381-382.

Johnson LA, Morgan RA, Dudley ME, Cassard L, Yang JC, Hughes MS, Kammula US, Royal RE, Sherry RM, Wunderlich JR, Lee CC, Restifo NP, Schwarz SL, Cogdill AP, Bishop RJ, Kim H, Brewer CC, Rudy SF, VanWaes C, Davis JL, Mathur A, Ripley RT, Nathan DA, Laurencot CM and Rosenberg SA. (2009) Gene therapy with human and mouse T-cell receptors mediates cancer regression and targets normal tissues expressing cognate antigen. *Blood*. 114:535-546.

Josefowicz SZ and Rudensky A. (2009) Control of regulatory T cell lineage commitment and maintenance. *Immunity*. 30:616-625.

Kaech SM, Wherry EJ and Ahmed R. (2002) Effector and memory T-cell differentiation: implications for vaccine development. *Nat Rev Immunol*. 2:251-262.

Kageshita T, Kawakami Y and Ono T. (2001) Clinical significance of MART-1 and HLA-A2 expression and CD8+ T cell infiltration in melanocytic lesions in HLA-A2 phenotype patients. *J Dermatol Sci*. 25:36-44.

Kaifi JT, Reichelt U, Quaas A, Schurr PG, Wachowiak R, Yekebas EF, Strate T, Schneider C, Pantel K, Schachner M, Sauter G and Izbicki JR. (2007) L1 is associated with micrometastatic spread and poor outcome in colorectal cancer. *Mod Pathol*. 20:1183-1190.

Kammerer R, Hahn S, Singer BB, Luo JS and von Kleist S. (1998) Biliary glycoprotein (CD66a), a cell adhesion molecule of the immunoglobulin superfamily, on human lymphocytes: structure, expression and involvement in T cell activation. *Eur J Immunol*. 28:3664-3674.

Kammertoens T and Blankenstein T. (2009) Making and circumventing tolerance to cancer. *Eur J Immunol*. 39:2345-2353.

Kaufmann SH. (2007) The contribution of immunology to the rational design of novel antibacterial vaccines. *Nat Rev Microbiol*. 5:491-504.

Kawakami Y, Eliyahu S, Delgado CH, Robbins PF, Sakaguchi K, Appella E, Yannelli JR, Adema GJ, Miki T and Rosenberg SA. (1994a) Identification of a human melanoma antigen recognized by tumor-infiltrating lymphocytes associated with in vivo tumor rejection. *Proc Natl Acad Sci U S A*. 91:6458-6462.

Kawakami Y, Eliyahu S, Sakaguchi K, Robbins PF, Rivoltini L, Yannelli JR, Appella E and Rosenberg SA. (1994b) Identification of the immunodominant peptides of the MART-1 human melanoma antigen recognized by the majority of HLA-A2-restricted tumor infiltrating lymphocytes. *J Exp Med*. 180:347-352.

Kawakami Y, Eliyahu S, Jennings C, Sakaguchi K, Kang X, Southwood S, Robbins PF, Sette A, Appella E and Rosenberg SA. (1995) Recognition of multiple epitopes in the human melanoma antigen gp100 by tumor-infiltrating T lymphocytes associated with in vivo tumor regression. *J Immunol*. 154:3961-3968.

Khazaie K, Bonertz A and Beckhove P. (2009) Current developments with peptide-based human tumor vaccines. *Curr Opin Oncol*. 21:524-530.

Khong HT and Restifo NP. (2002) Natural selection of tumor variants in the generation of "tumor escape" phenotypes. *Nat Immunol*. 3:999-1005.

Khong HT and Rosenberg SA. (2002) Pre-existing immunity to tyrosinase-related protein (TRP)-2, a new TRP-2 isoform, and the NY-ESO-1 melanoma antigen in a patient with a dramatic response to immunotherapy. *J Immunol*. 168:951-956.

Kieback E and Uckert W. (2010) Enhanced T cell receptor gene therapy for cancer. *Expert Opin Biol Ther*. 10:749-762.

Kirkwood JM, Tarhini AA, Panelli MC, Moschos SJ, Zarour HM, Butterfield LH and Gogas HJ. (2008) Next generation of immunotherapy for melanoma. *J Clin Oncol*. 26:3445-3455.

Kisielow P, Teh HS, Bluthmann H and von Boehmer H. (1988) Positive selection of antigen-specific T cells in thymus by restricting MHC molecules. *Nature*. 335:730-733.

Kline J, Brown IE, Zha YY, Blank C, Strickler J, Wouters H, Zhang L and Gajewski TF. (2008) Homeostatic proliferation plus regulatory T-cell depletion promotes potent rejection of B16 melanoma. *Clin Cancer Res*. 14:3156-3167.

Knutson KL and Disis ML. (2005) Augmenting T helper cell immunity in cancer. *Curr Drug Targets Immune Endocr Metabol Disord*. 5:365-371.

Ko JM, Velez NF and Tsao H. (2010) Pathways to melanoma. *Semin Cutan Med Surg*. 29:210-217.

Ko JM and Fisher DE. (2011) A new era: melanoma genetics and therapeutics. *J Pathol*. 223:241-250.

Korman AJ, Peggs KS and Allison JP. (2006) Checkpoint blockade in cancer immunotherapy. *Adv Immunol*. 90:297-339.

Krammer PH, Arnold R and Lavrik IN. (2007) Life and death in peripheral T cells. *Nat Rev Immunol*. 7:532-542.

Kretschmer K, Apostolou I, Jaeckel E, Khazaie K and von Boehmer H. (2006) Making regulatory T cells with defined antigen specificity: role in autoimmunity and cancer. *Immunol Rev*. 212:163-169.

Kroemer G and Jaattela M. (2005) Lysosomes and autophagy in cell death control. *Nat Rev Cancer*. 5:886-897.

Krueger A, Fas SC, Baumann S and Krammer PH. (2003) The role of CD95 in the regulation of peripheral T-cell apoptosis. *Immunol Rev*. 193:58-69.

Kuball J, Dossett ML, Wolfl M, Ho WY, Voss RH, Fowler C and Greenberg PD. (2007) Facilitating matched pairing and expression of TCR chains introduced into human T cells. *Blood*. 109:2331-2338.

Kudchadkar R. (2010) Novel targeted therapies for the treatment of metastatic melanoma. *Ochsner J*. 10:117-124.

Kuespert K, Pils S and Hauck CR. (2006) CEACAMs: their role in physiology and pathophysiology. *Curr Opin Cell Biol*. 18:565-571.

Kuphal S and Bosserhoff A. (2009) Recent progress in understanding the pathology of malignant melanoma. *J Pathol*. 219:400-409.

Kurobe H, Liu C, Ueno T, Saito F, Ohigashi I, Seach N, Arakaki R, Hayashi Y, Kitagawa T, Lipp M, Boyd RL and Takahama Y. (2006) CCR7-dependent cortex-to-medulla migration of positively selected thymocytes is essential for establishing central tolerance. *Immunity*. 24:165-177.

Kurokawa I, Takahashi K, Moll I and Moll R. (2011) Expression of keratins in cutaneous epithelial tumors and related disorders - distribution and clinical significance. *Exp Dermatol*. 20:217-228.

Kyewski B and Derbinski J. (2004) Self-representation in the thymus: an extended view. *Nat Rev Immunol*. 4:688-698.

Kyewski B and Klein L. (2006) A central role for central tolerance. *Annu Rev Immunol*. 24:571-606.

Kyhse-Andersen J. (1984) Electroblotting of multiple gels: a simple apparatus without buffer tank for rapid transfer of proteins from polyacrylamide to nitrocellulose. *J Biochem Biophys Methods*. 10:203-209.

Kyte JA, Gaudernack G, Dueland S, Trachsel S, Julsrud L and Aamdal S. (2011) Telomerase Peptide Vaccination Combined with Temozolomide: A Clinical Trial in Stage IV Melanoma Patients. *Clin Cancer Res*. 17:4568-4580.

LaFlamme SE and Kowalczyk AP. (2008) Cell Junctions, Adhesion, Development, and Disease. Wiley-VCH, Weinheim, Germany. 1-301 pp.

Lahl K, Loddenkemper C, Drouin C, Freyer J, Arnason J, Eberl G, Hamann A, Wagner H, Huehn J and Sparwasser T. (2007) Selective depletion of Foxp3+ regulatory T cells induces a scurfy-like disease. *J Exp Med*. 204:57-63.

Lang K, Bolsen K, Stahl W, Ruzicka T, Sies H, Lehmann P and Fritsch C. (2001) The 5-aminolevulinic acid-induced porphyrin biosynthesis in benign and malignant cells of the skin. *J Photochem Photobiol B*. 65:29-34.

Larrieu P, Ouisse LH, Guilloux Y, Jotereau F and Fonteneau JF. (2007) A HLA-DQ5 restricted Melan-A/MART-1 epitope presented by melanoma tumor cells to CD4+ T lymphocytes. *Cancer Immunol Immunother*. 56:1565-1575.

Larsson M, Fonteneau JF and Bhardwaj N. (2001) Dendritic cells resurrect antigens from dead cells. *Trends Immunol*. 22:141-148.

Lau LL, Jamieson BD, Somasundaram T and Ahmed R. (1994) Cytotoxic T-cell memory without antigen. *Nature*. 369:648-652.

Leach FS, Tokino T, Meltzer P, Burrell M, Oliner JD, Smith S, Hill DE, Sidransky D, Kinzler KW and Vogelstein B. (1993) p53 Mutation and MDM2 amplification in human soft tissue sarcomas. *Cancer Res*. 53:2231-2234.

Liang B, Workman C, Lee J, Chew C, Dale BM, Colonna L, Flores M, Li N, Schweighoffer E, Greenberg S, Tybulewicz V, Vignali D and Clynes R. (2008) Regulatory T cells inhibit dendritic cells by lymphocyte activation gene-3 engagement of MHC class II. *J Immunol*. 180:5916-5926.

Lienard D, Rimoldi D, Marchand M, Dietrich PY, van Baren N, Geldhof C, Batard P, Guillaume P, Ayyoub M, Pittet MJ, Zippelius A, Fleischhauer K, Lejeune F, Cerottini JC, Romero P and Speiser DE. (2004) Ex vivo detectable activation of Melan-A-specific T cells correlating with inflammatory skin reactions in melanoma patients vaccinated with peptides in IFA. *Cancer Immun*. 4:4. http://www.cancerimmunity.org/v4p4/040404.htm.

Liu W, Putnam AL, Xu-Yu Z, Szot GL, Lee MR, Zhu S, Gottlieb PA, Kapranov P, Gingeras TR, Fazekas de St Groth B, Clayberger C, Soper DM, Ziegler SF and Bluestone JA. (2006) CD127 expression inversely correlates with FoxP3 and suppressive function of human CD4+ T reg cells. *J Exp Med*. 203:1701-1711.

Lohr J, Ratliff T, Huppertz A, Ge Y, Dictus C, Ahmadi R, Grau S, Hiraoka N, Eckstein V, Ecker RC, Korff T, von Deimling A, Unterberg A, Beckhove P and Herold-Mende C. (2011) Effector T-Cell Infiltration Positively Impacts Survival of Glioblastoma Patients and Is Impaired by Tumor-Derived TGF-{beta}. *Clin Cancer Res*. 17:4296-4308.

Lu LF, Lind EF, Gondek DC, Bennett KA, Gleeson MW, Pino-Lagos K, Scott ZA, Coyle AJ, Reed JL, van Snick J, Strom TB, Zheng XX and Noelle RJ. (2006) Mast cells are essential intermediaries in regulatory T-cell tolerance. *Nature*. 442:997-1002.

Ma W, Germeau C, Vigneron N, Maernoudt AS, Morel S, Boon T, Coulie PG and van den Eynde BJ. (2004) Two new tumor-specific antigenic peptides encoded by gene MAGE-C2 and presented to cytolytic T lymphocytes by HLA-A2. *Int J Cancer*. 109:698-702.

Mach JP and Pusztaszeri G. (1972) Carcinoembryonic antigen (CEA): demonstration of a partial identity between CEA and a normal glycoprotein. *Immunochemistry*. 9:1031-1034.

Mahabeleshwar GH and Byzova TV. (2007) Angiogenesis in melanoma. *Semin Oncol*. 34:555-565.

Mahnke K, Schonfeld K, Fondel S, Ring S, Karakhanova S, Wiedemeyer K, Bedke T, Johnson TS, Storn V, Schallenberg S and Enk AH. (2007) Depletion of CD4+CD25+ human regulatory T cells in vivo: kinetics of Treg depletion and alterations in immune functions in vivo and in vitro. *Int J Cancer*. 120:2723-2733.

Mahnke YD, Schwendemann J, Beckhove P and Schirrmacher V. (2005) Maintenance of long-term tumour-specific T-cell memory by residual dormant tumour cells. *Immunology*. 115:325-336.

Mahrle G, Bolling R, Osborn M and Weber K. (1983) Intermediate filaments of the vimentin and prekeratin type in human epidermis. *J Invest Dermatol*. 81:46-48.

Markel G, Seidman R, Stern N, Cohen-Sinai T, Izhaki O, Katz G, Besser M, Treves AJ, Blumberg RS, Loewenthal R, Mandelboim O, Orenstein A and Schachter J. (2006) Inhibition of human tumor-infiltrating lymphocyte effector functions by the homophilic carcinoembryonic cell adhesion molecule 1 interactions. *J Immunol*. 177:6062-6071.

Markel G, Seidman R, Cohen Y, Besser MJ, Sinai TC, Treves AJ, Orenstein A, Berger R and Schachter J. (2008) Dynamic expression of protective CEACAM1 on melanoma cells during specific immune attack. *Immunology*. 126:186-200.

Marrack P and Kappler J. (2004) Control of T cell viability. *Annu Rev Immunol*. 22:765-787.

Matzinger P. (1994) Immunology. Memories are made of this? *Nature*. 369:605-606.

Matzinger P. (2002) An innate sense of danger. *Ann N Y Acad Sci*. 961:341-342.

McCarter MD, Baumgartner J, Escobar GA, Richter D, Lewis K, Robinson W, Wilson C, Palmer BE and Gonzalez R. (2007) Immunosuppressive dendritic and regulatory T cells are upregulated in melanoma patients. *Ann Surg Oncol*. 14:2854-2860.

McDermott DF, Sosman JA, Gonzalez R, Hodi FS, Linette GP, Richards J, Jakub JW, Beeram M, Tarantolo S, Agarwala S, Frenette G, Puzanov I, Cranmer L, Lewis K, Kirkwood J, White JM, Xia C, Patel K and Hersh E. (2008) Double-blind randomized phase II study of the combination of sorafenib and dacarbazine in patients with advanced melanoma: a report from the 11715 Study Group. *J Clin Oncol*. 26:2178-2185.

Meier F, Busch S, Gast D, Goppert A, Altevogt P, Maczey E, Riedle S, Garbe C and Schittek B. (2006) The adhesion molecule L1 (CD171) promotes melanoma progression. *Int J Cancer*. 119:549-555.

Melief CJ and van der Burg SH. (2008) Immunotherapy of established (pre)malignant disease by synthetic long peptide vaccines. *Nat Rev Cancer*. 8:351-360.

Miller AJ and Mihm MC, Jr. (2006) Melanoma. *N Engl J Med*. 355:51-65.

Miller JF. (1961) Analysis of the thymus influence in leukaemogenesis. *Nature*. 191:248-249.

Misslitz A, Pabst O, Hintzen G, Ohl L, Kremmer E, Petrie HT and Forster R. (2004) Thymic T cell development and progenitor localization depend on CCR7. *J Exp Med*. 200:481-491.

Mocellin S, Hoon D, Ambrosi A, Nitti D and Rossi CR. (2006) The prognostic value of circulating tumor cells in patients with melanoma: a systematic review and meta-analysis. *Clin Cancer Res*. 12:4605-4613.

Moll R, Franke WW, Schiller DL, Geiger B and Krepler R. (1982) The catalog of human cytokeratins: patterns of expression in normal epithelia, tumors and cultured cells. *Cell*. 31:11-24.

Moll R, Divo M and Langbein L. (2008) The human keratins: biology and pathology. *Histochem Cell Biol*. 129:705-733.

Momand J, Zambetti GP, Olson DC, George D and Levine AJ. (1992) The mdm-2 oncogene product forms a complex with the p53 protein and inhibits p53-mediated transactivation. *Cell*. 69:1237-1245.

Monks CR, Freiberg BA, Kupfer H, Sciaky N and Kupfer A. (1998) Three-dimensional segregation of supramolecular activation clusters in T cells. *Nature*. 395:82-86.

Mora JR and von Andrian UH. (2006) T-cell homing specificity and plasticity: new concepts and future challenges. *Trends Immunol*. 27:235-243.

Morales VM, Christ A, Watt SM, Kim HS, Johnson KW, Utku N, Texieira AM, Mizoguchi A, Mizoguchi E, Russell GJ, Russell SE, Bhan AK, Freeman GJ and Blumberg RS. (1999) Regulation of human intestinal intraepithelial lymphocyte cytolytic function by biliary glycoprotein (CD66a). *J Immunol*. 163:1363-1370.

Morgan RA, Dudley ME, Wunderlich JR, Hughes MS, Yang JC, Sherry RM, Royal RE, Topalian SL, Kammula US, Restifo NP, Zheng Z, Nahvi A, de Vries CR, Rogers-Freezer LJ, Mavroukakis SA and Rosenberg SA. (2006) Cancer regression in patients after transfer of genetically engineered lymphocytes. *Science*. 314:126-129.

Mourmouras V, Fimiani M, Rubegni P, Epistolato MC, Malagnino V, Cardone C, Cosci E, Nisi MC and Miracco C. (2007) Evaluation of tumour-infiltrating CD4+CD25+FOXP3+ regulatory T cells in human cutaneous benign and atypical naevi, melanomas and melanoma metastases. *Br J Dermatol*. 157:531-539.

Mueller-Berghaus J, Ehlert K, Ugurel S, Umansky V, Bucur M, Schirrmacher V, Beckhove P and Schadendorf D. (2006) Melanoma-reactive T cells in the bone marrow of melanoma patients: association with disease stage and disease duration. *Cancer Res*. 66:5997-6001.

Murphy KP, Travers P and Walport M. (2008) Janeway's immunobiology. Garland Science, Taylor and Francis Group, New York, NY, USA. 1-887 pp.

Murray DR, Cassel WA, Torbin AH, Olkowski ZL and Moore ME. (1977) Viral oncolysate in the management of malignant melanoma. II. Clinical studies. *Cancer*. 40:680-686.

Nagaishi T, Pao L, Lin SH, Iijima H, Kaser A, Qiao SW, Chen Z, Glickman J, Najjar SM, Nakajima A, Neel BG and Blumberg RS. (2006) SHP1 phosphatase-dependent T cell inhibition by CEACAM1 adhesion molecule isoforms. *Immunity*. 25:769-781.

Nakajima A, Iijima H, Neurath MF, Nagaishi T, Nieuwenhuis EE, Raychowdhury R, Glickman J, Blau DM, Russell S, Holmes KV and Blumberg RS. (2002) Activation-induced expression of carcinoembryonic antigen-cell adhesion molecule 1 regulates mouse T lymphocyte function. *J Immunol*. 168:1028-1035.

NCI. (2011) National Cancer Institute (NCI) at the National Institute of Health. http:// www.cancer.gov/cancertopics/druginfo/melanoma.

Nelson J and Fuchs E. (2010) Cell-Cell Junctions. Cold Spring Harbor Laboratory Press, New York, NY, USA. 1-443 pp.

Nicholaou T, Ebert LM, Davis ID, McArthur GA, Jackson H, Dimopoulos N, Tan B, Maraskovsky E, Miloradovic L, Hopkins W, Pan L, Venhaus R, Hoffman EW, Chen W and Cebon J. (2009) Regulatory T-cell-mediated attenuation of T-cell responses to the NY-ESO-1 ISCOMATRIX vaccine in patients with advanced malignant melanoma. *Clin Cancer Res*. 15:2166-2173.

Nishikawa H and Sakaguchi S. (2010) Regulatory T cells in tumor immunity. *Int J Cancer*. 127:759-767.

Niu J, Jiang C, Li C, Liu L, Li K, Jian Z and Gao T. (2011) Foxp3 expression in melanoma cells as a possible mechanism of resistance to immune destruction. *Cancer Immunol Immunother*. 60:1109-1118.

Nordlund JJ and Boissy RE. (2001) The biology of melanocytes. *In* The biology of the skin. Freinkel RK and Woodley DT, editors. Parthenon Publishing, New York, NY, USA. pp.113-131.

Ochsenbein AF, Riddell SR, Brown M, Corey L, Baerlocher GM, Lansdorp PM and Greenberg PD. (2004) CD27 expression promotes long-term survival of functional effector-memory CD8+ cytotoxic T lymphocytes in HIV-infected patients. *J Exp Med*. 200:1407-1417.

Oikawa S, Inuzuka C, Kuroki M, Arakawa F, Matsuoka Y, Kosaki G and Nakazato H. (1991) A specific heterotypic cell adhesion activity between members of carcinoembryonic antigen family, W272 and NCA, is mediated by N-domains. *J Biol Chem*. 266:7995-8001.

Okazaki T and Honjo T. (2007) PD-1 and PD-1 ligands: from discovery to clinical application. *Int Immunol*. 19:813-824.

Ostrand-Rosenberg S. (2008) Immune surveillance: a balance between protumor and antitumor immunity. *Curr Opin Genet Dev*. 18:11-18.

Ottaviani S, Zhang Y, Boon T and van der Bruggen P. (2005) A MAGE-1 antigenic peptide recognized by human cytolytic T lymphocytes on HLA-A2 tumor cells. *Cancer Immunol Immunother*. 54:1214-1220.

Pandolfino MC, Viret C, Gervois N, Guilloux Y, Davodeau F, Diez E and Jotereau F. (1992) Specificity, T cell receptor diversity and activation requirements of CD4+ and CD8+ clones derived from human melanoma-infiltrating lymphocytes. *Eur J Immunol*. 22:1795-1802.

Pantel K, Alix-Panabieres C and Riethdorf S. (2009) Cancer micrometastases. *Nat Rev Clin Oncol*. 6:339-351.

Pantel K and Alix-Panabieres C. (2010) Circulating tumour cells in cancer patients: challenges and perspectives. *Trends Mol Med*. 16:398-406.

Parker KC, Bednarek MA and Coligan JE. (1994) Scheme for ranking potential HLA-A2 binding peptides based on independent binding of individual peptide side-chains. *J Immunol*. 152:163-175.

Parmiani G, Castelli C, Dalerba P, Mortarini R, Rivoltini L, Marincola FM and Anichini A. (2002) Cancer immunotherapy with peptide-based vaccines: what have we achieved? Where are we going? *J Natl Cancer Inst*. 94:805-818.

Pascolo S, Schirle M, Gueckel B, Dumrese T, Stumm S, Kayser S, Moris A, Wallwiener D, Rammensee HG and Stevanovic S. (2001) A MAGE-A1 HLA-A A*0201 epitope identified by mass spectrometry. *Cancer Res*. 61:4072-4077.

Pear W, Scott M and Nolan GP. (1997) Generation of high titre, helper-free retroviruses by transient transfection. *In* Methods in Molecular Medicine: Gene Therapy Protocols. Robbins P, editor. Humana Press, Totowa, NJ, USA. pp.41-57.

Pecora AL, Rizvi N, Cohen GI, Meropol NJ, Sterman D, Marshall JL, Goldberg S, Gross P, O'Neil JD, Groene WS, Roberts MS, Rabin H, Bamat MK and Lorence RM. (2002) Phase I trial of intravenous administration of PV701, an oncolytic virus, in patients with advanced solid cancers. *J Clin Oncol*. 20:2251-2266.

Pedeux R, Lefort K, Cuenin C, Cortes U, Kellner K, Dore JF and Nakazawa H. (2002) Specific induction of gadd45 in human melanocytes and melanoma cells after UVB irradiation. *Int J Cancer*. 98:811-816.

Peggs KS, Quezada SA, Chambers CA, Korman AJ and Allison JP. (2009) Blockade of CTLA-4 on both effector and regulatory T cell compartments contributes to the antitumor activity of anti-CTLA-4 antibodies. *J Exp Med*. 206:1717-1725.

Pepper M and Jenkins MK. (2011) Origins of CD4(+) effector and central memory T cells. *Nat Immunol*. 131:467-471.

Peter RU, Worret WI and Nickolay-Kiesthardt J. (1992) Prevalence of dysplastic nevi in healthy young men. *Int J Dermatol*. 31:327-330.

Petrangolini G, Pratesi G, de Cesare M, Supino R, Pisano C, Marcellini M, Giordano V, Laccabue D, Lanzi C and Zunino F. (2003) Antiangiogenic effects of the novel camptothecin ST1481 (gimatecan) in human tumor xenografts. *Mol Cancer Res*. 1:863-870.

Pfirschke C and Schirrmacher V. (2009) Cross-infection of tumor cells by contact with T lymphocytes loaded with Newcastle disease virus. *Int J Oncol*. 34:951-962.

Pietras K and Ostman A. (2010) Hallmarks of cancer: interactions with the tumor stroma. *Exp Cell Res*. 316:1324-1331.

Pignatelli M and Vessey CJ. (1994) Adhesion molecules: novel molecular tools in tumor pathology. *Hum Pathol*. 25:849-856.

Plotkin J, Prockop SE, Lepique A and Petrie HT. (2003) Critical role for CXCR4 signaling in progenitor localization and T cell differentiation in the postnatal thymus. *J Immunol*. 171:4521-4527.

Poynter JN, Elder JT, Fullen DR, Nair RP, Soengas MS, Johnson TM, Redman B, Thomas NE and Gruber SB. (2006) BRAF and NRAS mutations in melanoma and melanocytic nevi. *Melanoma Res*. 16:267-273.

Prlic M and Bevan MJ. (2011) Cutting Edge: {beta}-Catenin Is Dispensable for T Cell Effector Differentiation, Memory Formation, and Recall Responses. *J Immunol*. 187:1542-1546.

Qiao J, Wang H, Kottke T, Diaz RM, Willmon C, Hudacek A, Thompson J, Parato K, Bell J, Naik J, Chester J, Selby P, Harrington K, Melcher A and Vile RG. (2008) Loading of oncolytic vesicular stomatitis virus onto antigen-specific T cells enhances the efficacy of adoptive T-cell therapy of tumors. *Gene Ther*. 15:604-616.

Quezada SA, Simpson TR, Peggs KS, Merghoub T, Vider J, Fan X, Blasberg R, Yagita H, Muranski P, Antony PA, Restifo NP and Allison JP. (2010) Tumor-reactive CD4(+) T cells develop cytotoxic activity and eradicate large established melanoma after transfer into lymphopenic hosts. *J Exp Med*. 207:637-650.

Rammensee H, Bachmann J, Emmerich NP, Bachor OA and Stevanovic S. (1999) SYFPEITHI: database for MHC ligands and peptide motifs. *Immunogenetics*. 50:213-219.

Rathjen FG and Schachner M. (1984) Immunocytological and biochemical characterization of a new neuronal cell surface component (L1 antigen) which is involved in cell adhesion. *Embo J*. 3:1-10.

Rein DT, Breidenbach M and Curiel DT. (2006) Current developments in adenovirus-based cancer gene therapy. *Future Oncol*. 2:137-143.

Ren X, Ye F, Jiang Z, Chu Y, Xiong S and Wang Y. (2007) Involvement of cellular death in TRAIL/DR5-dependent suppression induced by CD4(+)CD25(+) regulatory T cells. *Cell Death Differ*. 14:2076-2084.

Richmond A and Su Y. (2008) Mouse xenograft models vs GEM models for human cancer therapeutics. *Dis Model Mech*. 1:78-82.

Riley JP, Rosenberg SA and Parkhurst MR. (2001) Identification of a new shared HLA-A2.1 restricted epitope from the melanoma antigen tyrosinase. *J Immunother*. 24:212-220.

Ring S, Oliver SJ, Cronstein BN, Enk AH and Mahnke K. (2009) CD4+CD25+ regulatory T cells suppress contact hypersensitivity reactions through a CD39, adenosine-dependent mechanism. *J Allergy Clin Immunol*. 123:1287-1296 e1282.

Robb RJ, Munck A and Smith KA. (1981) T cell growth factor receptors. Quantitation, specificity, and biological relevance. *J Exp Med*. 154:1455-1474.

Robey E and Fowlkes BJ. (1994) Selective events in T cell development. *Annu Rev Immunol*. 12:675-705.

Robinson MR, Chan CC, Yang JC, Rubin BI, Gracia GJ, Sen HN, Csaky KG and Rosenberg SA. (2004) Cytotoxic T lymphocyte-associated antigen 4 blockade in patients with metastatic melanoma: a new cause of uveitis. *J Immunother*. 27:478-479.

Romero P, Zippelius A, Kurth I, Pittet MJ, Touvrey C, Iancu EM, Corthesy P, Devevre E, Speiser DE and Rufer N. (2007) Four functionally distinct populations of human effector-memory CD8+ T lymphocytes. *J Immunol*. 178:4112-4119.

Rooney CM. (2005) Hitchhiker's guide to the T cell. *Nat Med*. 11:1051-1052.

Rosenberg SA. (1999) A new era for cancer immunotherapy based on the genes that encode cancer antigens. *Immunity*. 10:281-287.

Rosenberg SA, Yang JC, Schwartzentruber DJ, Hwu P, Topalian SL, Sherry RM, Restifo NP, Wunderlich JR, Seipp CA, Rogers-Freezer L, Morton KE, Mavroukakis SA, Gritz L, Panicali DL and White DE. (2003) Recombinant fowlpox viruses encoding the anchor-modified gp100 melanoma

antigen can generate antitumor immune responses in patients with metastatic melanoma. *Clin Cancer Res*. 9:2973-2980.

Rosenberg SA, Yang JC and Restifo NP. (2004) Cancer immunotherapy: moving beyond current vaccines. *Nat Med*. 10:909-915.

Rosenberg SA, Restifo NP, Yang JC, Morgan RA and Dudley ME. (2008) Adoptive cell transfer: a clinical path to effective cancer immunotherapy. *Nat Rev Cancer*. 8:299-308.

Sakaguchi S. (2004) Naturally arising CD4+ regulatory t cells for immunologic self-tolerance and negative control of immune responses. *Annu Rev Immunol*. 22:531-562.

Sallusto F, Lenig D, Forster R, Lipp M and Lanzavecchia A. (1999) Two subsets of memory T lymphocytes with distinct homing potentials and effector functions. *Nature*. 401:708-712.

Sallusto F, Geginat J and Lanzavecchia A. (2004) Central memory and effector memory T cell subsets: function, generation, and maintenance. *Annu Rev Immunol*. 22:745-763.

Sausville EA and Newell DR. (2004) Preclinical models in cancer drug discovery and development - Introduction. *Eur J Cancer*. 40:783-784.

Scatolini M, Grand MM, Grosso E, Venesio T, Pisacane A, Balsamo A, Sirovich R, Risio M and Chiorino G. (2010) Altered molecular pathways in melanocytic lesions. *Int J Cancer*. 126:1869-1881.

Schaefer MK and Altevogt P. (2010) L1CAM malfunction in the nervous system and human carcinomas. *Cell Mol Life Sci*. 67:2425-2437.

Schaft N, Willemsen RA, de Vries J, Lankiewicz B, Essers BW, Gratama JW, Figdor CG, Bolhuis RL, Debets R and Adema GJ. (2003) Peptide fine specificity of anti-glycoprotein 100 CTL is preserved following transfer of engineered TCR alpha beta genes into primary human T lymphocytes. *J Immunol*. 170:2186-2194.

Schatton T, Murphy GF, Frank NY, Yamaura K, Waaga-Gasser AM, Gasser M, Zhan Q, Jordan S, Duncan LM, Weishaupt C, Fuhlbrigge RC, Kupper TS, Sayegh MH and Frank MH. (2008) Identification of cells initiating human melanomas. *Nature*. 451:345-349.

Schirrmacher V and von Hoegen P. (1993) Importance of tumor cell membrane intergrity and viability for CTL activation by cancer vaccines. *Immunol Cell Biol*. 2:183-196.

Schirrmacher V, Haas C, Bonifer R, Ahlert T, Gerhards R and Ertel C. (1999) Human tumor cell modification by virus infection: an efficient and safe way to produce cancer vaccine with pleiotropic immune stimulatory properties when using Newcastle disease virus. *Gene Ther*. 6:63-73.

Schirrmacher V, Feuerer M, Fournier P, Ahlert T, Umansky V and Beckhove P. (2003) T-cell priming in bone marrow: the potential for long-lasting protective anti-tumor immunity. *Trends Mol Med*. 9:526-534.

Schirrmacher V. (2005) Clinical trials of antitumor vaccination with an autologous tumor cell vaccine modified by virus infection: improvement of patient survival based on improved antitumor immune memory. *Cancer Immunol Immunother*. 54:587-598.

Schirrmacher V and Fournier P. (2008) Newcastle Disease Virus: a promising vector for viral therapy of cancer. *In* Viral Therapy of Cancer. Harrington K, Pandha H and Vile RG, editors. John Wiley & Sons Ltd., Chichester, UK. pp.171-186.

Schirrmacher V and Fournier P. (2009) Newcastle disease virus: a promising vector for viral therapy, immune therapy, and gene therapy of cancer. *Methods Mol Biol*. 542:565-605.

Schmitt CJ, Franke WW, Goerdt S, Falkowska-Hansen B, Rickelt S and Peitsch WK. (2007) Homo- and heterotypic cell contacts in malignant melanoma cells and desmoglein 2 as a novel solitary surface glycoprotein. *J Invest Dermatol*. 127:2191-2206.

Schmitt M and Pawlita M. (2009) High-throughput detection and multiplex identification of cell contaminations. *Nucleic Acids Res*. 37:e119; doi:110.1093/nar/gkp1581.

Schmitz-Winnenthal FH, Volk C, Z'Graggen K, Galindo L, Nummer D, Ziouta Y, Bucur M, Weitz J, Schirrmacher V, Buchler MW and Beckhove P. (2005) High frequencies of functional tumor-reactive T cells in bone marrow and blood of pancreatic cancer patients. *Cancer Res*. 65:10079-10087.

Schmitz I, Krueger A, Baumann S, Schulze-Bergkamen H, Krammer PH and Kirchhoff S. (2003) An IL-2-dependent switch between CD95 signaling pathways sensitizes primary human T cells toward CD95-mediated activation-induced cell death. *J Immunol*. 171:2930-2936.

Schoensiegel F, Paschen A, Sieger S, Eskerski H, Mier W, Rothfels H, Kleinschmidt J, Schadendorf D and Haberkorn U. (2004) MIA (melanoma inhibitory activity) promoter mediated tissue-specific suicide gene therapy of malignant melanoma. *Cancer Gene Ther*. 11:408-418.

Scholzel S, Zimmermann W, Schwarzkopf G, Grunert F, Rogaczewski B and Thompson J. (2000) Carcinoembryonic antigen family members CEACAM6 and CEACAM7 are differentially expressed in normal tissues and oppositely deregulated in hyperplastic colorectal polyps and early adenomas. *Am J Pathol*. 156:595-605.

Schreiber RD, Old LJ and Smyth MJ. (2011) Cancer immunoediting: integrating immunity's roles in cancer suppression and promotion. *Science*. 331:1565-1570.

Schreurs MW, de Boer AJ, Figdor CG and Adema GJ. (1998) Genetic vaccination against the melanocyte lineage-specific antigen gp100 induces cytotoxic T lymphocyte-mediated tumor protection. *Cancer Res*. 58:2509-2514.

Schuetz F, Ehlert K, Ge Y, Schneeweiss A, Rom J, Inzkirweli N, Sohn C, Schirrmacher V and Beckhove P. (2009) Treatment of advanced metastasized breast cancer with bone marrow-derived tumour-reactive memory T cells: a pilot clinical study. *Cancer Immunol Immunother*. 58:887-900.

Schulze T, Kemmner W, Weitz J, Wernecke KD, Schirrmacher V and Schlag PM. (2009) Efficiency of adjuvant active specific immunization with Newcastle disease virus modified tumor cells in colorectal cancer patients following resection of liver metastases: results of a prospective randomized trial. *Cancer Immunol Immunother*. 58:61-69.

Schumacher TN. (2002) T-cell-receptor gene therapy. *Nat Rev Immunol*. 2:512-519.

Schwartzentruber DJ, Lawson DL, Richards J, Conry RM, Miller D, Triesman J, Gailani F, Riley LB, Vena D and Hwu P. (2009) A phase III multi-institutional randomized study of immunization with the gp100:209-217(210M) peptide followed by high-dose IL-2 compared with high-dose IL-2 alone in patients with metastatic melanoma. *J Clin Oncol*. 27, ASCO Annual Meeting; suppl.; abstract CRA9011.

Schwendemann J, Choi C, Schirrmacher V and Beckhove P. (2005) Dynamic differentiation of activated human peripheral blood CD8+ and CD4+ effector memory T cells. *J Immunol*. 175:1433-1439.

Seddiki N, Santner-Nanan B, Martinson J, Zaunders J, Sasson S, Landay A, Solomon M, Selby W, Alexander SI, Nanan R, Kelleher A and Fazekas de St Groth B. (2006) Expression of interleukin (IL)-2 and IL-7 receptors discriminates between human regulatory and activated T cells. *J Exp Med*. 203:1693-1700.

Seibel TJ. (2010) Local low dose irradiation triggers tumor infiltration by adoptively transferred and host T lymphocytes and enhances immunotherapy in mice. Faculty of Biology. Ph. D. Thesis. University of Heidelberg, Heidelberg, Germany. 1-111 pp.

Shultz LD, Schweitzer PA, Christianson SW, Gott B, Schweitzer IB, Tennent B, McKenna S, Mobraaten L, Rajan TV and Greiner DL. (1995) Multiple defects in innate and adaptive immunologic function in NOD/LtSz-scid mice. *J Immunol*. 154:180-191.

Shultz LD, Lyons BL, Burzenski LM, Gott B, Chen X, Chaleff S, Kotb M, Gillies SD, King M, Mangada J, Greiner DL and Handgretinger R. (2005) Human lymphoid and myeloid cell development in NOD/LtSz-scid IL2R gamma null mice engrafted with mobilized human hemopoietic stem cells. *J Immunol*. 174:6477-6489.

Sica A. (2010) Role of tumour-associated macrophages in cancer-related inflammation. *Exp Oncol*. 32:153-158.

Singer BB, Scheffrahn I, Kammerer R, Suttorp N, Ergun S and Slevogt H. (2010) Deregulation of the CEACAM expression pattern causes undifferentiated cell growth in human lung adenocarcinoma cells. *PLoS One*. 5:e8747; doi:8710.1371/journal.pone.0008747.

Sinkovics JG and Horvath JC. (2000) Newcastle disease virus (NDV): brief history of its oncolytic strains. *J Clin Virol*. 16:1-15.

Skobe M, Hamberg LM, Hawighorst T, Schirner M, Wolf GL, Alitalo K and Detmar M. (2001) Concurrent induction of lymphangiogenesis, angiogenesis, and macrophage recruitment by vascular endothelial growth factor-C in melanoma. *Am J Pathol*. 159:893-903.

Smith-Garvin JE, Koretzky GA and Jordan MS. (2009) T cell activation. *Annu Rev Immunol*. 27:591-619.

Smith KA. (1984) Interleukin 2. *Annu Rev Immunol*. 2:319-333.

Smyth MJ, Dunn GP and Schreiber RD. (2006) Cancer immunosurveillance and immunoediting: the roles of immunity in suppressing tumor development and shaping tumor immunogenicity. *Adv Immunol*. 90:1-50.

Solito S, Bronte V and Mandruzzato S. (2011) Antigen specificity of immune suppression by myeloid-derived suppressor cells. *J Leukoc Biol*. 90:31-36.

Sommerfeldt N, Schutz F, Sohn C, Forster J, Schirrmacher V and Beckhove P. (2006) The shaping of a polyvalent and highly individual T-cell repertoire in the bone marrow of breast cancer patients. *Cancer Res*. 66:8258-8265.

Sommermeyer D, Neudorfer J, Weinhold M, Leisegang M, Engels B, Noessner E, Heemskerk MH, Charo J, Schendel DJ, Blankenstein T, Bernhard H and Uckert W. (2006) Designer T cells by T cell receptor replacement. *Eur J Immunol*. 36:3052-3059.

Sommermeyer D and Uckert W. (2010) Minimal amino acid exchange in human TCR constant regions fosters improved function of TCR gene-modified T cells. *J Immunol*. 184:6223-6231.

Soneoka Y, Cannon PM, Ramsdale EE, Griffiths JC, Romano G, Kingsman SM and Kingsman AJ. (1995) A transient three-plasmid expression system for the production of high titer retroviral vectors. *Nucleic Acids Res*. 23:628-633.

Sprent J and Miller JF. (1976a) Fate of H2-activated T lymphocytes in syngeneic hosts. II. Residence in recirculating lymphocyte pool and capacity to migrate to allografts. *Cell Immunol*. 21:303-313.

Sprent J and Miller JF. (1976b) Fate of H2-activated T lymphocytes in syngeneic hosts. III. Differentiation into long-lived recirculating memory cells. *Cell Immunol*. 21:314-326.

Stanislawski T, Voss RH, Lotz C, Sadovnikova E, Willemsen RA, Kuball J, Ruppert T, Bolhuis RL, Melief CJ, Huber C, Stauss HJ and Theobald M. (2001) Circumventing tolerance to a human MDM2-derived tumor antigen by TCR gene transfer. *Nat Immunol*. 2:962-970.

Strasser A and Pellegrini M. (2004) T-lymphocyte death during shutdown of an immune response. *Trends Immunol*. 25:610-615.

Strauss DC and Thomas JM. (2010) Transmission of donor melanoma by organ transplantation. *Lancet Oncol*. 11:790-796.

Swain SL, Hu H and Huston G. (1999) Class II-independent generation of CD4 memory T cells from effectors. *Science*. 286:1381-1383.

Swift S, Lorens J, Achacoso P and Nolan GP. (2001) Rapid production of retroviruses for efficient gene delivery to mammalian cells using 293T cell-based systems. *Curr Protoc Immunol*. Chapter 10:Unit 10 17C; doi: 10.1002/0471142735.im0471141017cs0471142731.

Tahery DP and Moy RL. (1993) Recurrent malignant melanoma following a 35-year disease-free interval. *J Dermatol Surg Oncol*. 19:161-163.

Takahama Y. (2006) Journey through the thymus: stromal guides for T-cell development and selection. *Nat Rev Immunol*. 6:127-135.

Tarhini AA and Agarwala SS. (2006) Cutaneous melanoma: available therapy for metastatic disease. *Dermatol Ther*. 19:19-25.

Tarhini AA and Iqbal F. (2010) CTLA-4 blockade: therapeutic potential in cancer treatments. *Onco Targets Ther*. 3:15-25.

Taylor JJ and Jenkins MK. (2011) CD4(+) memory T cell survival. *Curr Opin Immunol*. 23:319-323.

Teft WA, Kirchhof MG and Madrenas J. (2006) A molecular perspective of CTLA-4 function. *Annu Rev Immunol*. 24:65-97.

Teicher BA. (2006) Tumor models for efficacy determination. *Mol Cancer Ther*. 5:2435-2443.

Thallinger C, Wolschek MF, Wacheck V, Maierhofer H, Gunsberg P, Polterauer P, Pehamberger H, Monia BP, Selzer E, Wolff K and Jansen B. (2003) Mcl-1 antisense therapy chemosensitizes human melanoma in a SCID mouse xenotransplantation model. *J Invest Dermatol*. 120:1081-1086.

Theobald M, Biggs J, Dittmer D, Levine AJ and Sherman LA. (1995) Targeting p53 as a general tumor antigen. *Proc Natl Acad Sci U S A*. 92:11993-11997.

Thies A, Mauer S, Fodstad O and Schumacher U. (2007) Clinically proven markers of metastasis predict metastatic spread of human melanoma cells engrafted in scid mice. *Br J Cancer*. 96:609-616.

Thomas JM. (2008) Prognostic false-positivity of the sentinel node in melanoma. *Nat Clin Pract Oncol*. 5:18-23.

Thomas L. (1959) Discussion to P. B. Medawar's paper. *In* Cellular and Humoral Aspects of the Hypersensitive States. Lawrence H, editor. Hoeber-Harper, New York, NY, USA. pp.529-532.

Thorne SH, Hwang TH and Kirn DH. (2005) Vaccinia virus and oncolytic virotherapy of cancer. *Curr Opin Mol Ther*. 7:359-365.

Thorne SH and Contag CH. (2007) Combining immune cell and viral therapy for the treatment of cancer. *Cell Mol Life Sci*. 64:1449-1451.

Thornton AM and Shevach EM. (2000) Suppressor effector function of CD4+CD25+ immunoregulatory T cells is antigen nonspecific. *J Immunol*. 164:183-190.

Townson JL and Chambers AF. (2006) Dormancy of solitary metastatic cells. *Cell Cycle*. 5:1744-1750.

Tsao H, Zhang X, Benoit E and Haluska FG. (1998) Identification of PTEN/MMAC1 alterations in uncultured melanomas and melanoma cell lines. *Oncogene*. 16:3397-3402.

Ueno T, Saito F, Gray DH, Kuse S, Hieshima K, Nakano H, Kakiuchi T, Lipp M, Boyd RL and Takahama Y. (2004) CCR7 signals are essential for cortex-medulla migration of developing thymocytes. *J Exp Med*. 200:493-505.

Valmori D, Pittet MJ, Vonarbourg C, Rimoldi D, Lienard D, Speiser D, Dunbar R, Cerundolo V, Cerottini JC and Romero P. (1999) Analysis of the cytolytic T lymphocyte response of melanoma patients to the naturally HLA-A*0201-associated tyrosinase peptide 368-376. *Cancer Res*. 59:4050-4055.

van den Eynde B, Peeters O, de Backer O, Gaugler B, Lucas S and Boon T. (1995) A new family of genes coding for an antigen recognized by autologous cytolytic T lymphocytes on a human melanoma. *J Exp Med*. 182:689-698.

van der Bruggen P, Traversari C, Chomez P, Lurquin C, de Plaen E, van den Eynde B, Knuth A and Boon T. (1991) A gene encoding an antigen recognized by cytolytic T lymphocytes on a human melanoma. *Science*. 254:1643-1647.

Vesely MD, Kershaw MH, Schreiber RD and Smyth MJ. (2011) Natural innate and adaptive immunity to cancer. *Annu Rev Immunol*. 29:235-271.

Vignali DA, Collison LW and Workman CJ. (2008) How regulatory T cells work. *Nat Rev Immunol*. 8:523-532.

von Bergwelt-Baildon MS, Vonderheide RH, Maecker B, Hirano N, Anderson KS, Butler MO, Xia Z, Zeng WY, Wucherpfennig KW, Nadler LM and Schultze JL. (2002) Human primary and memory cytotoxic T lymphocyte responses are efficiently induced by means of CD40-activated B cells as antigen-presenting cells: potential for clinical application. *Blood*. 99:3319-3325.

von Boehmer H, Teh HS and Kisielow P. (1989) The thymus selects the useful, neglects the useless and destroys the harmful. *Immunol Today*. 10:57-61.

von Boehmer H and Fehling HJ. (1997) Structure and function of the pre-T cell receptor. *Annu Rev Immunol*. 15:433-452.

von Herrath MG and Harrison LC. (2003) Antigen-induced regulatory T cells in autoimmunity. *Nat Rev Immunol*. 3:223-232.

von Kleist S, Chavanel G and Burtin P. (1972) Identification of an antigen from normal human tissue that crossreacts with the carcinoembryonic antigen. *Proc Natl Acad Sci U S A*. 69:2492-2494.

Voss RH, Kuball J, Engel R, Guillaume P, Romero P, Huber C and Theobald M. (2006) Redirection of T cells by delivering a transgenic mouse-derived MDM2 tumor antigen-specific TCR and its humanized derivative is governed by the CD8 coreceptor and affects natural human TCR expression. *Immunol Res*. 34:67-87.

Voss RH, Willemsen RA, Kuball J, Grabowski M, Engel R, Intan RS, Guillaume P, Romero P, Huber C and Theobald M. (2008) Molecular design of the Calphabeta interface favors specific pairing of introduced TCRalphabeta in human T cells. *J Immunol*. 180:391-401.

Voss RH, Thomas S, Pfirschke C, Hauptrock B, Klobuch S, Kuball J, Grabowski M, Engel R, Guillaume P, Romero P, Huber C, Beckhove P and Theobald M. (2010) Coexpression of the T-cell receptor constant alpha domain triggers tumor reactivity of single-chain TCR-transduced human T cells. *Blood*. 115:5154-5163.

Wall L, Burke F, Barton C, Smyth J and Balkwill F. (2003) IFN-gamma induces apoptosis in ovarian cancer cells in vivo and in vitro. *Clin Cancer Res*. 9:2487-2496.

Walton SM, Gerlinger M, de la Rosa O, Nuber N, Knights A, Gati A, Laumer M, Strauss L, Exner C, Schaefer N, Urosevic M, Dummer R, Tiercy JM, Mackensen A, Jaeger E, Levy F, Knuth A, Jaeger D and Zippelius A. (2006) Spontaneous CD8 T cell responses against the melanocyte differentiation antigen RAB38/NY-MEL-1 in melanoma patients. *J Immunol*. 177:8212-8218.

Wan YY and Flavell RA. (2008) TGF-beta and regulatory T cell in immunity and autoimmunity. *J Clin Immunol*. 28:647-659.

Wang HY, Lee DA, Peng G, Guo Z, Li Y, Kiniwa Y, Shevach EM and Wang RF. (2004) Tumor-specific human CD4+ regulatory T cells and their ligands: implications for immunotherapy. *Immunity*. 20:107-118.

Watters D. (1999) Molecular mechanisms of ionizing radiation-induced apoptosis. *Immunology and cell biology*. 77:263-271.

Watts TH and DeBenedette MA. (1999) T cell co-stimulatory molecules other than CD28. *Curr Opin Immunol*. 11:286-293.

Weaver CT, Harrington LE, Mangan PR, Gavrieli M and Murphy KM. (2006) Th17: an effector CD4 T cell lineage with regulatory T cell ties. *Immunity*. 24:677-688.

Weber K and Osborn M. (1969) The reliability of molecular weight determinations by dodecyl sulfate-polyacrylamide gel electrophoresis. *J Biol Chem*. 244:4406-4412.

Weijtens ME, Willemsen RA, Hart EH and Bolhuis RL. (1998) A retroviral vector system 'STITCH' in combination with an optimized single chain antibody chimeric receptor gene structure allows efficient gene transduction and expression in human T lymphocytes. *Gene Ther*. 5:1195-1203.

Whiteman DC, Pavan WJ and Bastian BC. (2011) The Melanomas: A synthesis of epidemiological, clinical, histopathological, genetic, and biological aspects, supporting distinct subtypes, causal pathways, and cells of origin. *Pigment Cell Melanoma Res*.

WHO. (2011) World Health Organization. Fact sheet No. 297, http://www.who.int/mediacentre/factsheets/fs297/en/index.html.

Wilden H, Fournier P, Zawatzky R and Schirrmacher V. (2009) Expression of RIG-I, IRF3, IFN-beta and IRF7 determines resistance or susceptibility of cells to infection by Newcastle Disease Virus. *Int J Oncol*. 34:971-982.

Willemsen RA, Debets R, Chames P and Bolhuis RL. (2003) Genetic engineering of T cell specificity for immunotherapy of cancer. *Hum Immunol*. 64:56-68.

Woelfel T, van Pel A, Brichard V, Schneider J, Seliger B, Meyer zum Buschenfelde KH and Boon T. (1994) Two tyrosinase nonapeptides recognized on HLA-A2 melanomas by autologous cytolytic T lymphocytes. *Eur J Immunol*. 24:759-764.

Wolchok JD, Thomas L, Bondarenko IN, O'Day S, Weber JS, Garbe C, Francis S, Ibrahim RA, Hoos A and Robert C. (2011) Phase III randomized study of ipilimumab (IPI) plus dacarbazine (DTIC) versus DTIC alone as first-line treatment in patients with unresectable stage III or IV melanoma. *J Clin Oncol*. 29, ASCO Annual Meeting; suppl.; abstract LBA5.

Wu J, Rosenbaum E, Begum S and Westra WH. (2007) Distribution of BRAF T1799A(V600E) mutations across various types of benign nevi: implications for melanocytic tumorigenesis. *Am J Dermatopathol*. 29:534-537.

Xue SA, Gao L, Hart D, Gillmore R, Qasim W, Thrasher A, Apperley J, Engels B, Uckert W, Morris E and Stauss H. (2005) Elimination of human leukemia cells in NOD/SCID mice by WT1-TCR gene-transduced human T cells. *Blood*. 106:3062-3067.

Yee C. (2005) Adoptive T cell therapy: Addressing challenges in cancer immunotherapy. *J Transl Med*. 3:17.

Yewdell JW, Reits E and Neefjes J. (2003) Making sense of mass destruction: quantitating MHC class I antigen presentation. *Nat Rev Immunol*. 3:952-961.

Zhang T, He X, Tsang TC and Harris DT. (2004) Transgenic TCR expression: comparison of single chain with full-length receptor constructs for T-cell function. *Cancer Gene Ther*. 11:487-496.

Zhao H, Janke M, Fournier P and Schirrmacher V. (2008) Recombinant Newcastle disease virus expressing human interleukin-2 serves as a potential candidate for tumor therapy. *Virus Res*. 136:75-80.

Zhou L, Chong MM and Littman DR. (2009) Plasticity of CD4+ T cell lineage differentiation. *Immunity*. 30:646-655.

Zhou W, Ohdan H, Tanaka Y, Hara H, Tokita D, Onoe T and Asahara T. (2003) NOD/SCID mice engrafted with human peripheral blood lymphocytes can be a model for investigating B cells responding to blood group A carbohydrate determinant. *Transpl Immunol*. 12:9-18.

Zhu J and Paul WE. (2008) CD4 T cells: fates, functions, and faults. *Blood*. 112:1557-1569.

Zielinski CE, Corti D, Mele F, Pinto D, Lanzavecchia A and Sallusto F. (2011) Dissecting the human immunologic memory for pathogens. *Immunol Rev*. 240:40-51.

Zinkernagel RM, Callahan GN, Althage A, Cooper S, Klein PA and Klein J. (1978) On the thymus in the differentiation of "H-2 self-recognition" by T cells: evidence for dual recognition? *J Exp Med*. 147:882-896.

Zitvogel L, Tesniere A and Kroemer G. (2006) Cancer despite immunosurveillance: immunoselection and immunosubversion. *Nat Rev Immunol*. 6:715-727.

Zou W and Restifo NP. (2010) T(H)17 cells in tumour immunity and immunotherapy. *Nat Rev Immunol*. 10:248-256.

Zuklys S, Balciunaite G, Agarwal A, Fasler-Kan E, Palmer E and Hollander GA. (2000) Normal thymic architecture and negative selection are associated with Aire expression, the gene defective in the autoimmune-polyendocrinopathy-candidiasis-ectodermal dystrophy (APECED). *J Immunol*. 165:1976-1983.

## 11. Acknowledgements

First of all I would like to sincerely thank my supervisor and mentor **Prof. Dr. Philipp Beckhove**, for his guidance and enthusiasm during the whole period of my PhD thesis. His encouragement and support to attend both national and international scientific meetings and the possibility to work in intensive collaborations introduced me to a fascinating field of research.

I am also grateful to my second thesis referee **Prof. Dr. Stefan Wölfl** (Department of Biology, Institute for Pharmacy and Molecular Biotechnology, University of Heidelberg) and the other members of my thesis committee **Prof. Dr. Viktor Umansky** (Clinical Cooperation Unit Dermato-Oncology, DKFZ) and **Prof. Dr. Karsten Mahnke** (Department of Dermatology, University of Heidelberg) for taking the time to evaluate my work.

During my thesis, I had the change to collaborate and work with **Dr. Ralf-Holger Voss** and his group (Department of Hematology and Oncology, University of Mainz). I would like to thank him for introducing me to the field of TCR transgenic research, for teaching me the required methods and all the critical and helpful scientific discussions.

Similarly, I want to acknowledge **Prof. Dr. Alexander Enk** and **Dr. Christoffer Gebhardt** (Department of Dermatology, University Hospital Heidelberg) for providing the peripheral blood samples and informations of the analyzed melanoma and dysplastic nevi patients.

Furthermore, I would like to thank **Prof. Dr. Volker Schirrmacher** and **Dr. Philippe Fournier** (both former Division of Cellular Immunology, DKFZ) for teaching me how to work with Newcastle disease virus, for all helpful and interesting discussions as well as valuable advices.

I would not have managed to perform the experiments and analysis without the help and guidance of my colleagues from the Unit of Translational Immunology at the DKFZ. In particular, I would like to thank **Dr. Andreas Bonertz**, **Dr. Yingzi Ge** and **Maria Xydia** for the excellent scientific advice, support, helpful discussions and for the review of this manuscript.

My gratitude also go to **Mariana Bucur** and **Simone Jünger** as well as **Annette Arnold** and **Andreas Griesbach** for their enthusiastic and excellent technical assistance. Special thanks go to our secretaries **Bianca Dornseiff** and **Irmtraud Williams** for their kind support. Further, I want to thank the other current and former colleagues from our group, in particular **Felix Klug**, **Nisit Khandelwal**, **Anna-Lena Krause**, **Dr. Kim Pietsch**, **Jasmin Quandt**, **Dr. Tobias Seibel**, **Hans-Henning Schmidt**, **Christoph Schlude** and **Dr. Serpil Tanriverdi-Akhisaroglu** for the great and friendly atmosphere in the lab and for their assistance at all times.

Similarly, I want to acknowledge **Dr. Jing Ni** for the help with mouse experiments and **Dr. Holger Wilden** for support of real-time PCR investigations (both former Division of Cellular Immunology, DKFZ). Moreover, I thank **Günter Küblbeck** for help with molecular methods as well as **Dr. Dominik Djandji**, **Dr**. **Carmen Henrich** and **Dr. Tewfik Miloud** (all Division of Molecular Immunology, DKFZ) for the introduction to the IVIS100 *in vivo* imaging system. I am also grateful to **Dr. Alexei Salnikov** and **Dr. Gerhard Moldenhauer** (both Unit of Translational Immunology, DKFZ) who kindly supported me by antibody-related histological questions.

Special thanks go to the people who work in the **Animal Facility** and the **Flow Cytometry Unit** of the DKFZ for great collaborations.

My special gratitude goes to my family, especially my **parents**, who supported me during the whole course of my study of biology and my doctoral thesis research.

Last but not least my deepest thanks go to **Steffen** for his immeasurable continual support and for always believing in me. Without his encouragement I would never have come this far.

## 12. Declaration

Herewith I, Christina Pfirschke, declare that I have completed this thesis single-handedly without the unauthorized help of a second party. Any help that I have received in my research work and the preparation of the thesis itself has been acknowledged.

Heidelberg, 11.08.2011

Christina Pfirschke

# 13. Appendix

## 13.1. Plasmid map of pBullet_IRESpuro-[NcoI]

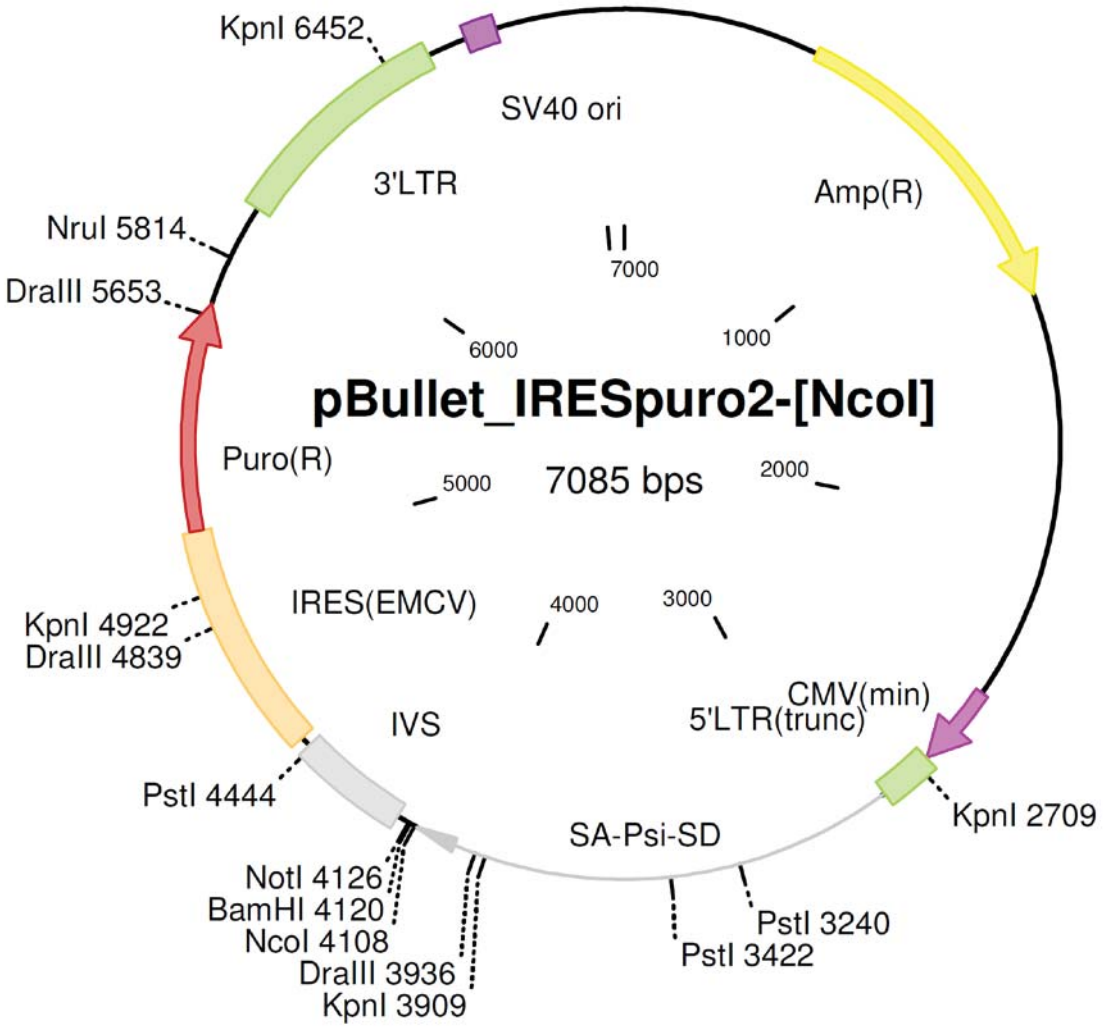


```
Molecule:       pBullet_IRESpuro2-[NcoI],  7085 bps DNA Circular
File Name:      pBu_IRESpuro2-[NcoI].cm5,  dated 04 Nov 2008

Description:    pBullet with IRES-puromycin cassette

Notes:          IVS-IRES-puromycin2 BamHI/[XbaI]-fragment cloned from pIRESpuro2
                (Clontech) into pBullet (Dr. Ralph Willemsen, Erasmus University,
                Rotterdam, NL) via BamHI/[NotI].

                Internal NcoI in puromycin silenced

                Multiple cloning sites: NcoI must be used
                NcoI / BamHI
                NcoI / NotI

                Corresponding author: Dr. Ralf-Holger Voss
                (hvoss@uni-mainz.de or rh.voss@gmx.de)
```

### 13.2. Plasmid map of pBullet_IRESneo-[NcoI]

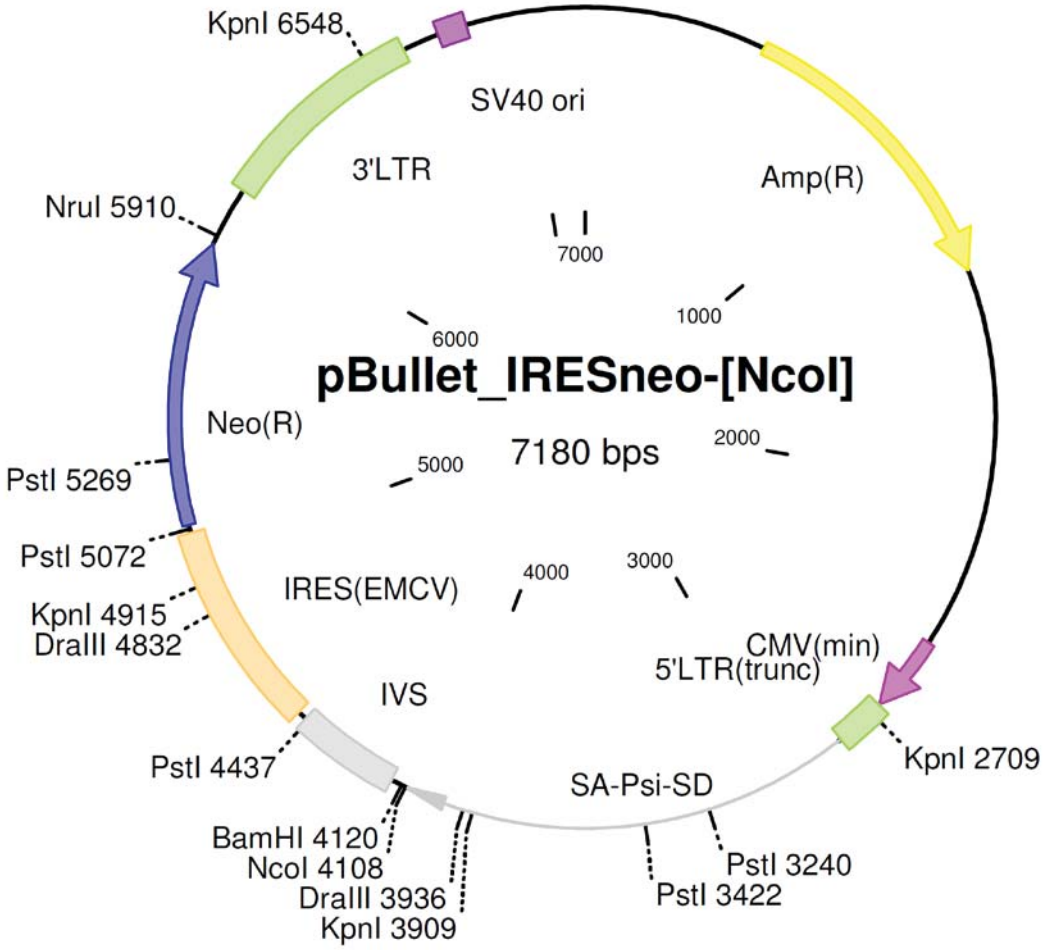


```
Molecule:       pBullet_IRESneo-[NcoI],  7180 bps DNA Circular
File Name:      pBu_IRESneo-[NcoI].cm5,  dated 25 Sep 2008

Description:    pBullet with IRES-neomycin cassette

Notes:          IVS-IRES-neomycin BamHI/[XbaI]-fragment cloned from pIRESneo (Clontech)
                into pBullet (Dr. Ralph Willemsen, Erasmus University, Rotterdam, NL)
                via BamHI/[NotI]

                Internal NcoI in neomycin silenced

                Multiple cloning sites: NcoI must be used
                NcoI / BamHI

                Corresponding author: Dr. Ralf-Holger Voss
                (hvoss@uni-mainz.de or rh.voss@gmx.de)
```

### 13.3. Plasmid map of pBullet_Mu Wta TCR MDM2_IRESpuro

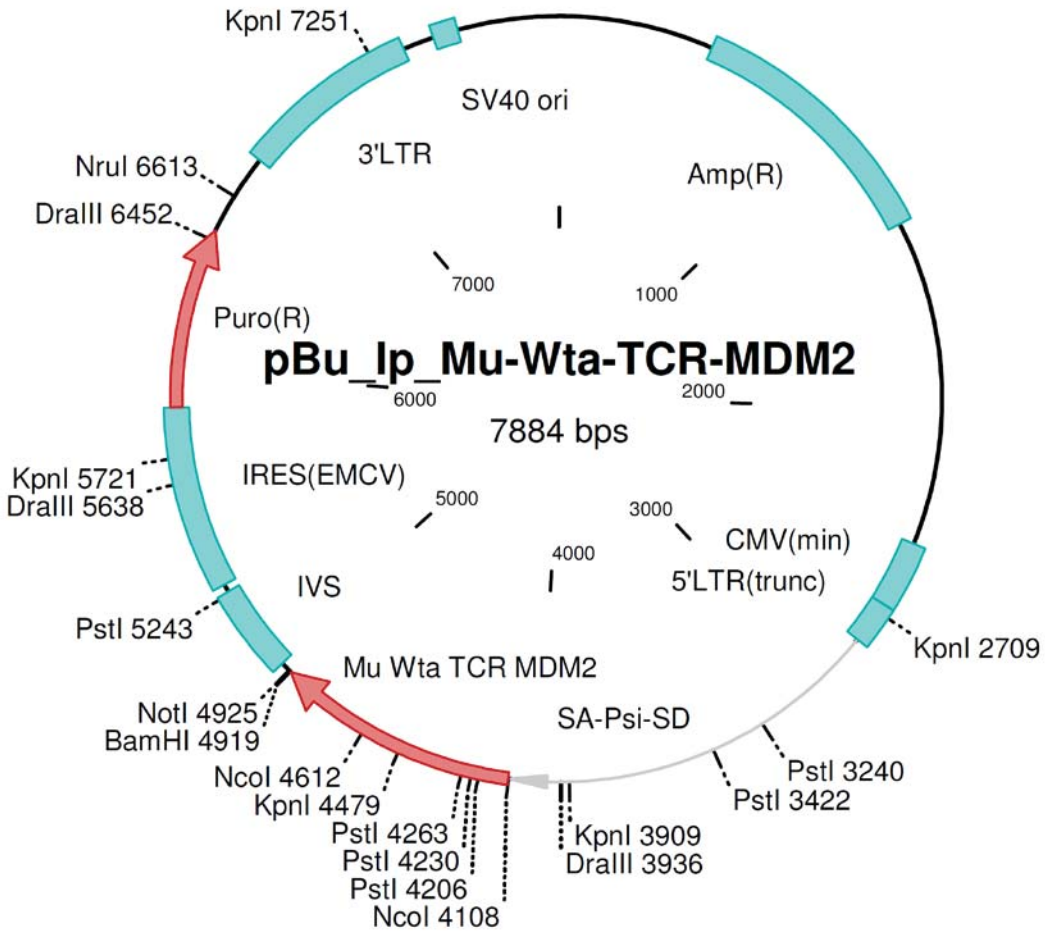


```
Molecule:       pBu_Ip_Mu-Wta-TCR-MDM2,  7884 bps DNA Circular
File Name:      pBu_Ip_Mu-Wta-TCR-MDM2.cm5,  dated 24 Nov 2008

Description:    Ligation of Mu TCRa MDM2 into pBu_Ip_NcoI/BamHI

Notes:          Vector molecule:  pBu_Ip_NcoI/BamHI
                   Fragment ends: BamHI and NcoI
                   Fragment size: 7073
                Insert molecule:  Mu TCRa MDM2
                   Fragment ends: NcoI and BamHI
                   Fragment size: 811

                Author: Dr. Ralf-Holger Voss (rh.voss@gmx.de)

                Original vector: Retroviral vector pBullet (Dr. Ralph Willemsen)
```

### 13.4. Plasmid map of pBullet_Mu Wtb TCR MDM2_IRESneo

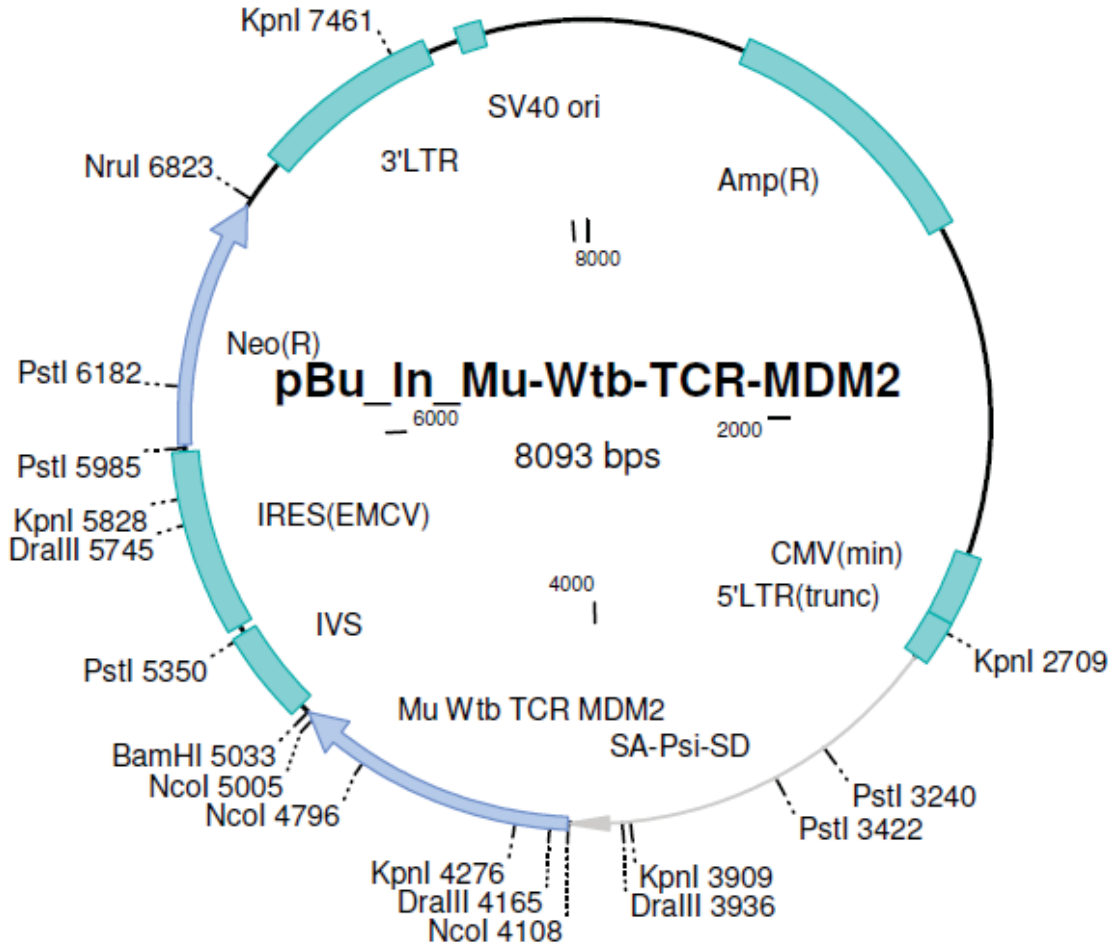


```
Molecule:       pBu_In_Mu-Wtb-TCR-MDM2,  8093 bps DNA Circular
File Name:      pBu_In_Mu-Wtb-TCR-MDM2.cm5,  dated 24 Nov 2008

Description:    Ligation of Mu Wtb TCR MDM2 into pBu_In_NcoI/BamHI

Notes:          Vector molecule:  pBu_In_NcoI/BamHI
                   Fragment ends: BamHI and NcoI
                   Fragment size: 7168
                Insert molecule:  Mu Wtb TCR MDM2
                   Fragment ends: NcoI and BamHI
                   Fragment size: 925

                Author: Dr. Ralf-Holger Voss (rh.voss@gmx.de)

                Original vector: Retroviral vector pBullet (Dr. Ralph Willemsen)
```

## 13.5. Plasmid map of pBullet_Mu Mta TCR MDM2 G85.1caR_IRESpuro

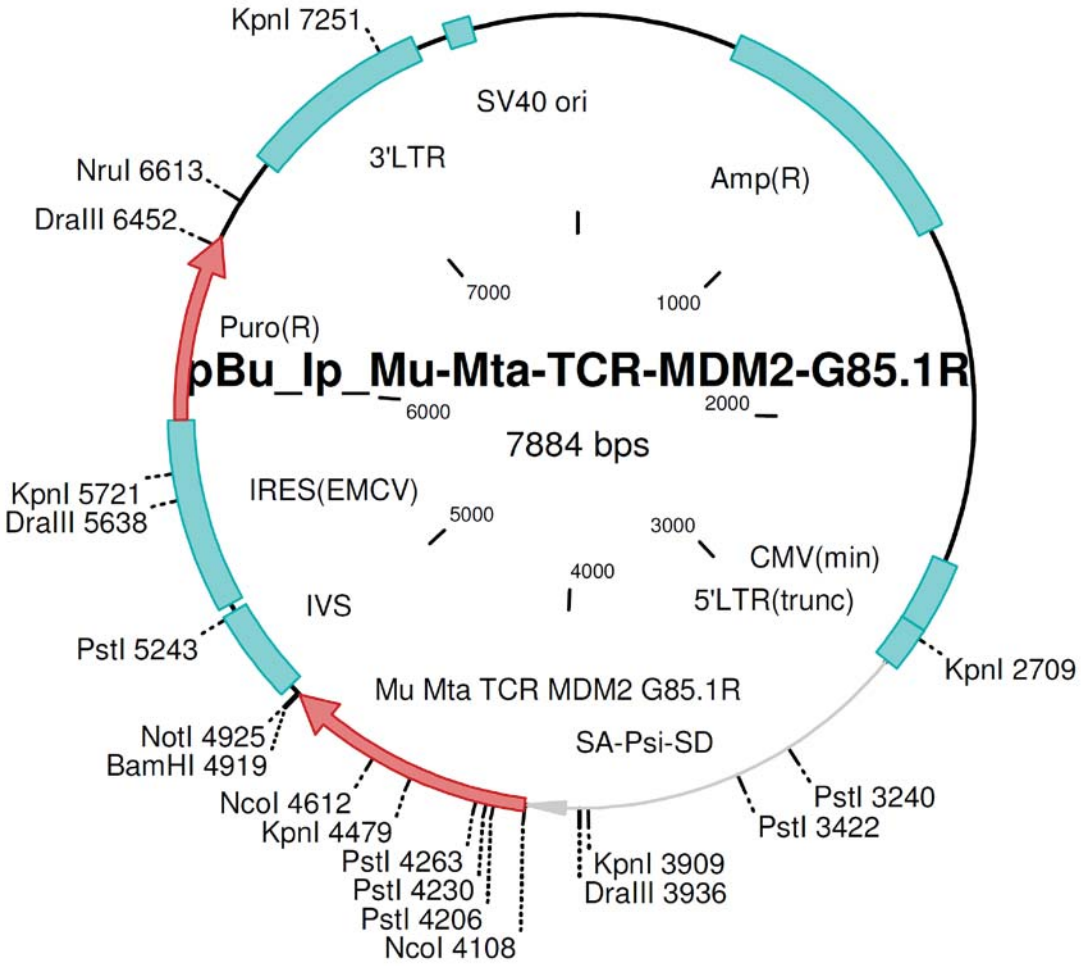


```
Molecule:       pBu_Ip_Mu-Mta-TCR-MDM2-G85.1R,  7884 bps DNA Circular
File Name:      pBu_Ip_Mu-Mta-TCR-MDM2-G85.1R.cm5,  dated 24 Nov 2008

Description:    Ligation of Mu Mta TCR MDM2 G85.1R into pBu_Ip_NcoI/BamHI

Notes:          Vector molecule:  pBu_Ip_NcoI/BamHI
                   Fragment ends: BamHI and NcoI
                   Fragment size: 7073
                Insert molecule:  Mu Mta TCR MDM2 G85.1R
                   Fragment ends: NcoI and BamHI
                   Fragment size: 811

                Author: Dr. Ralf-Holger Voss (rh.voss@gmx.de)

                TCR C-domain numbering according to IMGT

                Original vector: Retroviral vector pBullet (Dr. Ralph Willemsen)
```

### 13.6. Plasmid map of pBullet_Mu Mtb TCR MDM2 R88cbG_IRESneo

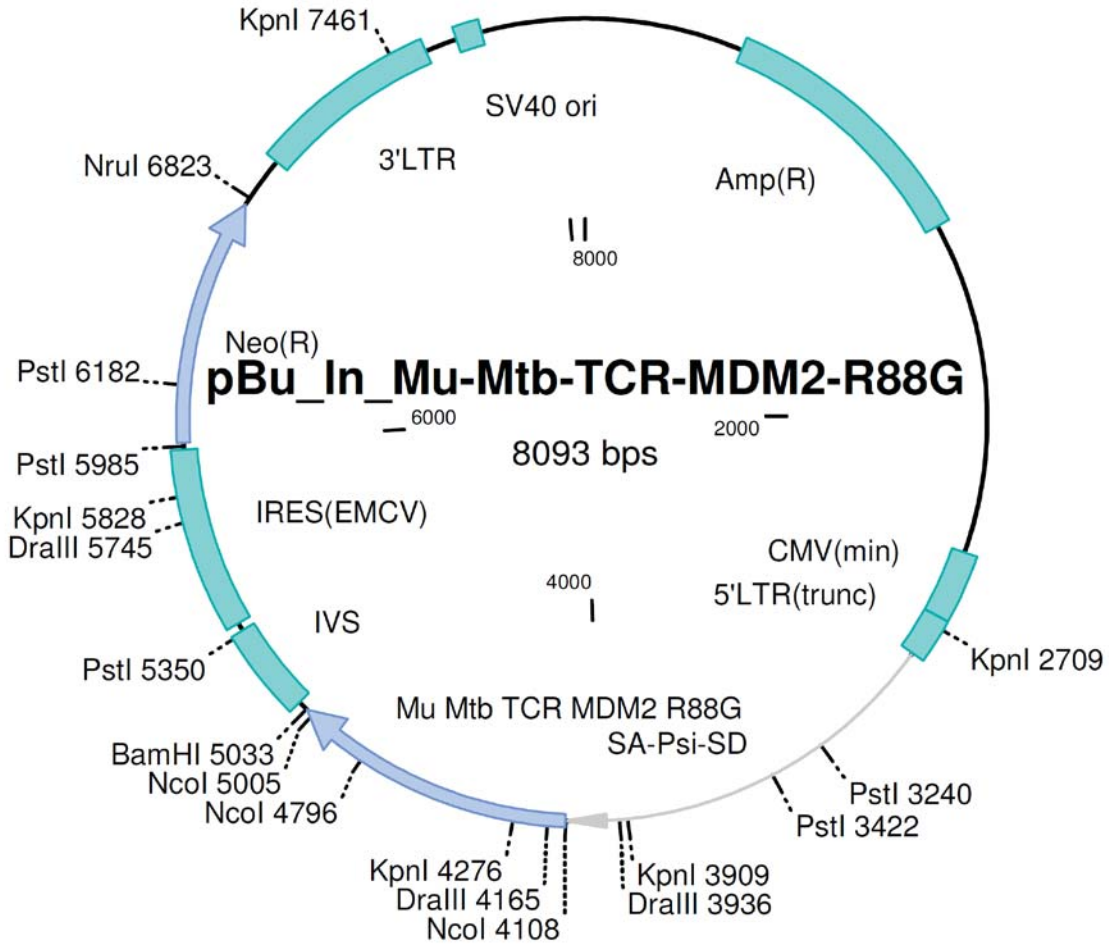


```
Molecule:       pBu_In_Mu-Mtb-TCR-MDM2-R88G,  8093 bps DNA Circular
File Name:      pBu_In_Mu-Mtb-TCR-R88G.cm5,  dated 24 Nov 2008

Description:    Ligation of Mu Mtb TCR MDM2 R88G into pBu_In_NcoI/BamHI

Notes:          Vector molecule:  pBu_In_NcoI/BamHI
                   Fragment ends: BamHI and NcoI
                   Fragment size: 7168
                Insert molecule:  Mu Mtb TCR MDM2 R88G
                   Fragment ends: NcoI and BamHI
                   Fragment size: 925

                Author: Dr. Ralf-Holger Voss (rh.voss@gmx.de)

                TCR C-domain numbering according to IMGT

                Original vector: Retroviral vector pBullet (Dr. Ralph Willemsen)
```

## 13.7. Plasmid map of pBullet_Hu Wta TCR gp100_IRESpuro

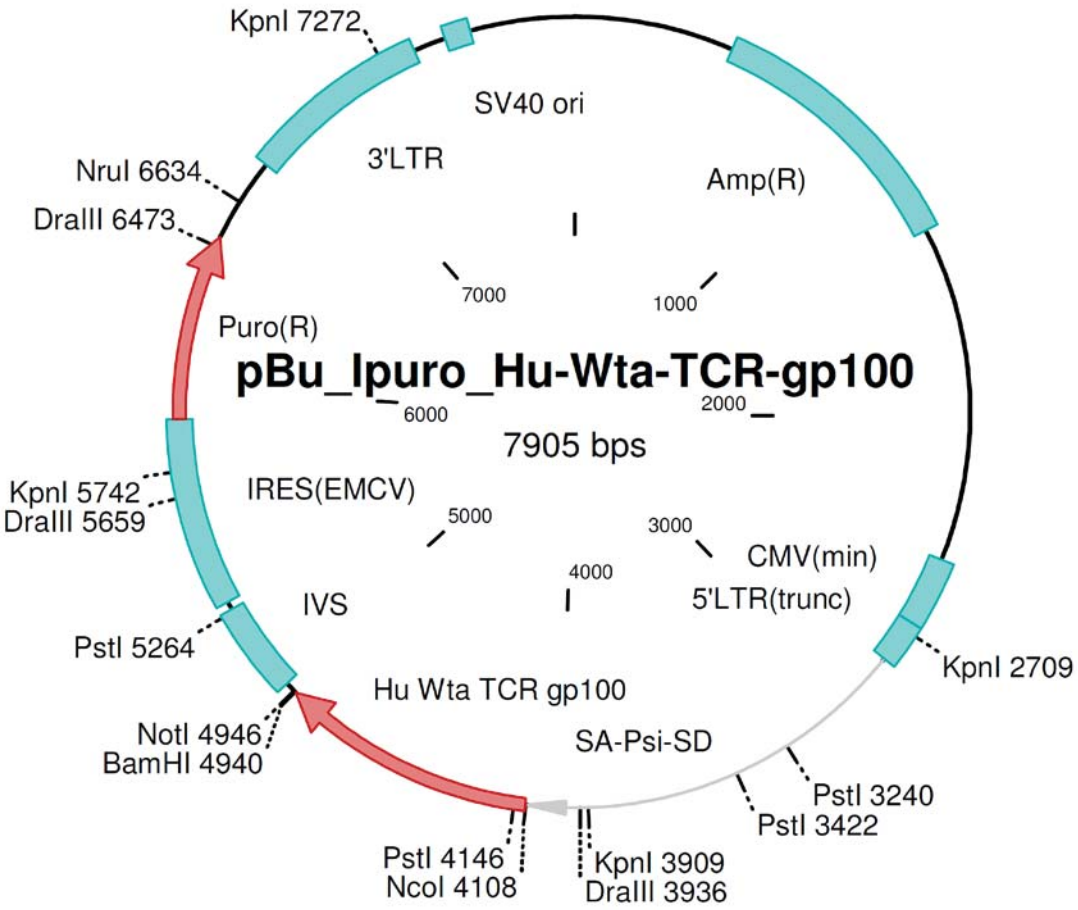


```
Molecule:       pBu_Ipuro_Hu-Wta-TCR-gp100,  7905 bps DNA Circular
File Name:      pBu_Ipuro_Hu-Wta-TCR-gp100.cm5,  dated 25 Nov 2008

Description:    Ligation of Hu Wta TCR gp100  into pBu_Ip

Notes:          Vector molecule:  pBu_Ip
                   Fragment ends: BamHI and NcoI
                   Fragment size: 7073
                Insert molecule:  Hu Wta TCR gp100
                   Fragment ends: NcoI and BamHI
                   Fragment size: 832

                Sequencing: MEG 254/255

                Author: Dr. Ralf-Holger Voss (rh.voss@gmx.de)

                Original vector: Retroviral vector pBullet (Dr. Ralph Willemsen)
```

### 13.8. Plasmid map of pBullet_Hu Wtb TCR gp100_IRESneo

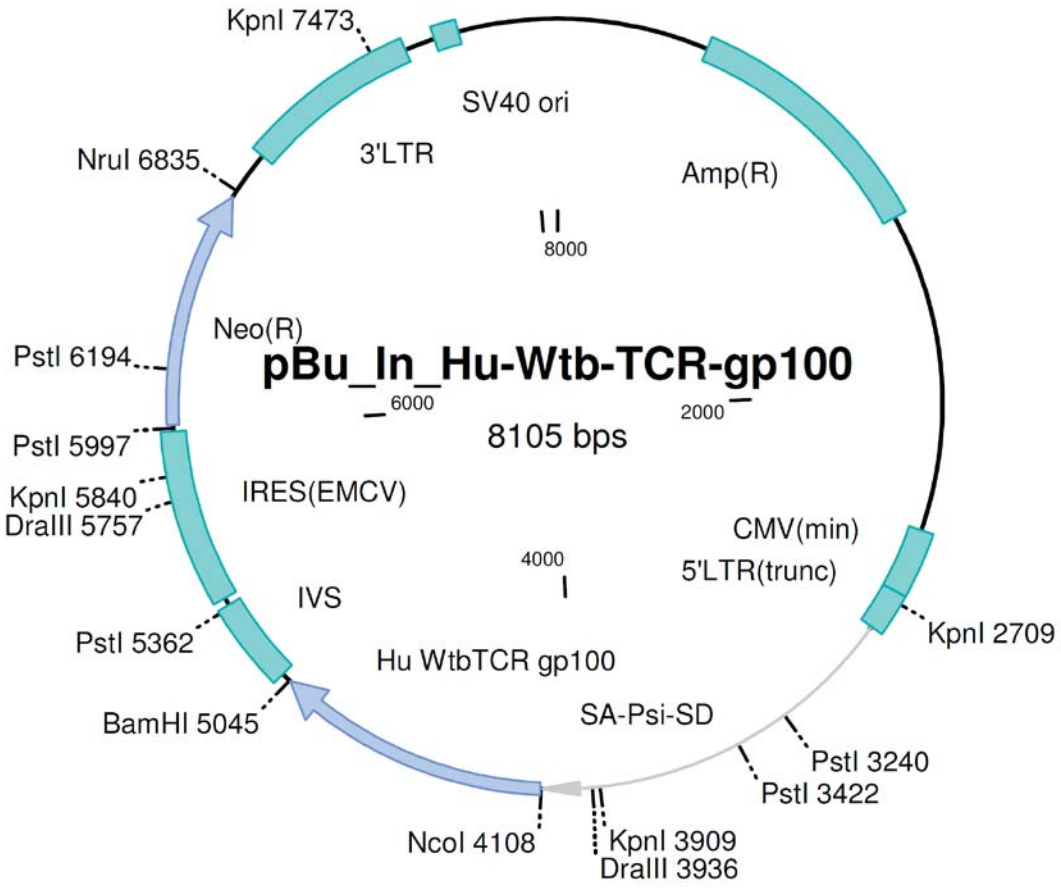


```
Molecule:       pBu_In_Hu-Wtb-TCR-gp100,  8105 bps DNA Circular
File Name:      pBu_In_Hu-Wtb-TCR-gp100.cm5,  dated 25 Nov 2008

Description:    Ligation of Hu Wt TCRb gp100 into pBu_In

Notes:          Vector molecule:  pBu_In
                   Fragment ends: BamHI and NcoI
                   Fragment size: 7168
                Insert molecule:  Hu Wt TCRb gp100
                   Fragment ends: NcoI and BamHI
                   Fragment size: 937

                Sequenzierung: MEG 256/257

                Author: Dr. Ralf-Holger Voss (rh.voss@gmx.de)

                Original vector: Retroviral vector pBullet (Dr. Ralph Willemsen)
```

## 13.9. Plasmid map of pBullet_Mu Ca T84caC_IRESpuro

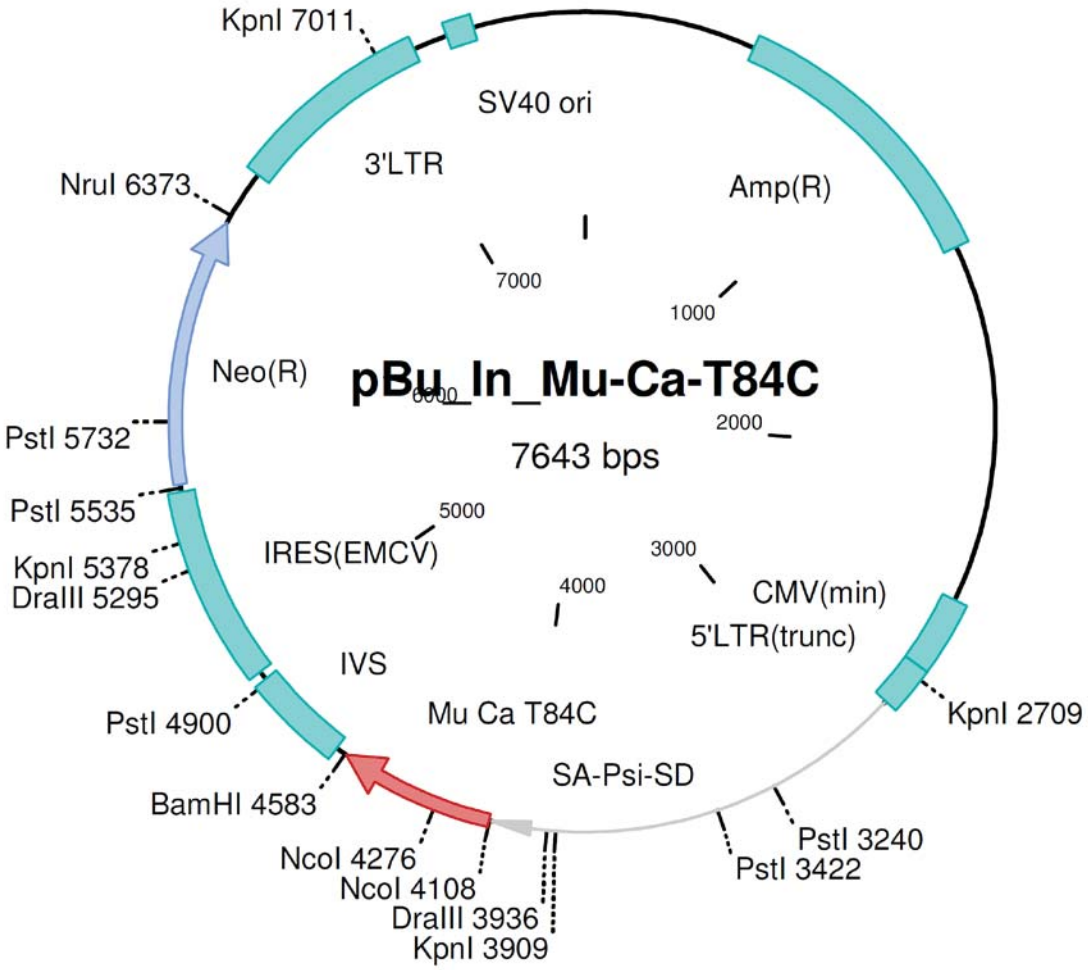


```
Molecule:       pBu_In_Mu-Ca-T84C,  7643 bps DNA Circular
File Name:      pBu_In_Mu-Ca-T84C.cm5,  dated 23 Nov 2008

Description:    Ligation of Mu Ca T84C into pBu_In

Notes:          Vector molecule:  pBu_In
                   Fragment ends: BamHI and NcoI
                   Fragment size: 7168
                Insert molecule:  Mu Ca T84C
                   Fragment ends: NcoI and BamHI
                   Fragment size: 475

                Sequencing: MEG 274/275

                Author: Dr. Ralf-Holger Voss (rh.voss@gmx.de)

                Original vector: Retroviral vector pBullet (Dr. Ralph Willemsen)
```

### 13.10. Plasmid map of pBullet_Hu Chim scTCR gp100 Mu Cb S79cbC_IRESneo

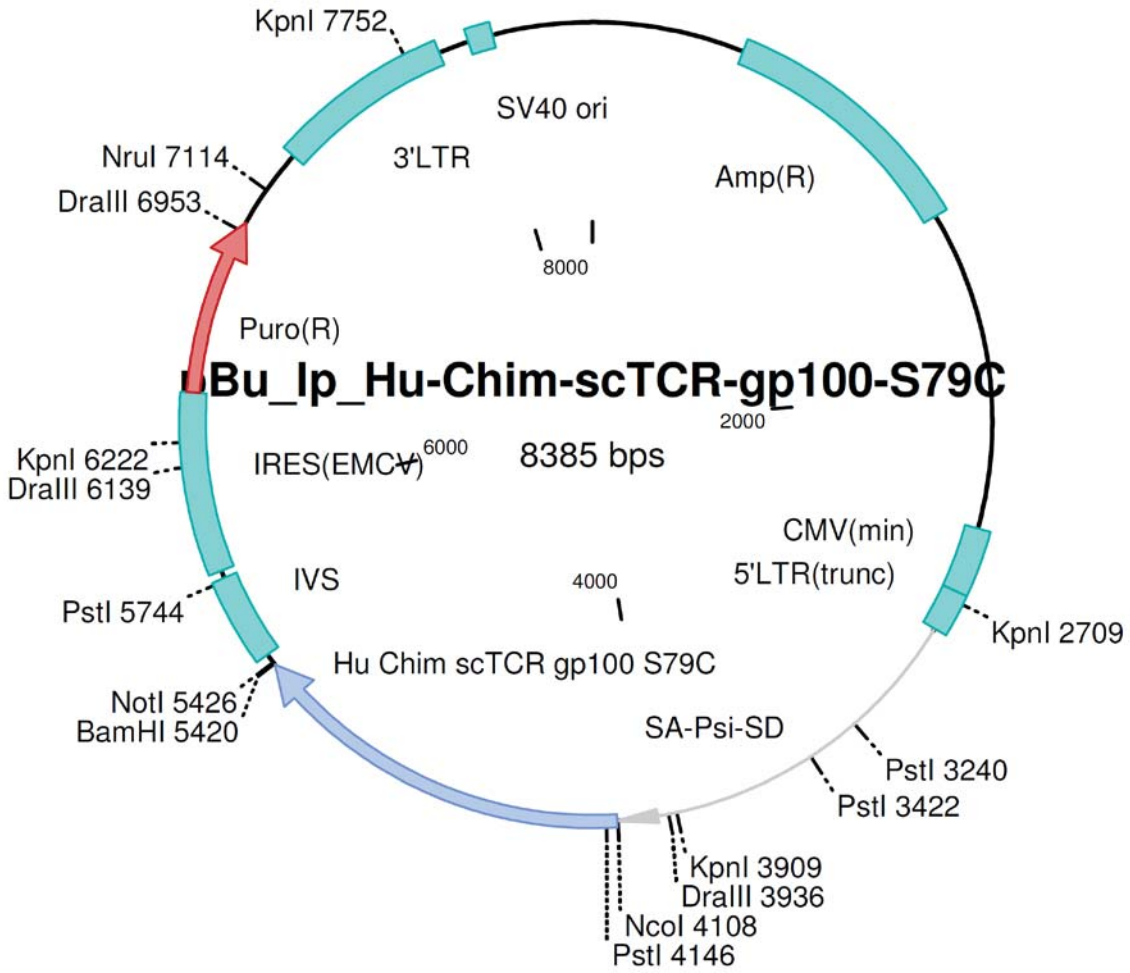


```
Molecule:       pBu_Ip_Hu-Chim-scTCR-gp100-S79C,  8385 bps DNA Circular
File Name:      pBu_Ip_Hu-Chim-scTCR-gp100-S79C.cm5,  dated 25 Nov 2008

Description:    Ligation of Hu Chim scTCR S79C into pBu_Ip

Notes:          Vector molecule:  pBu_Ip
                   Fragment ends: BamHI and NcoI
                   Fragment size: 7073
                Insert molecule:  Hu Chim scTCR S79C
                   Fragment ends: NcoI and BamHI
                   Fragment size: 1312

                Sequencing: MEG 276/277

                Author: Dr. Ralf-Holger Voss (rh.voss@gmx.de)

                Original vector: Retroviral vector pBullet (Dr. Ralph Willemsen)
```

### 13.11. Plasmid map of pBullet_eGFP_IRESneo

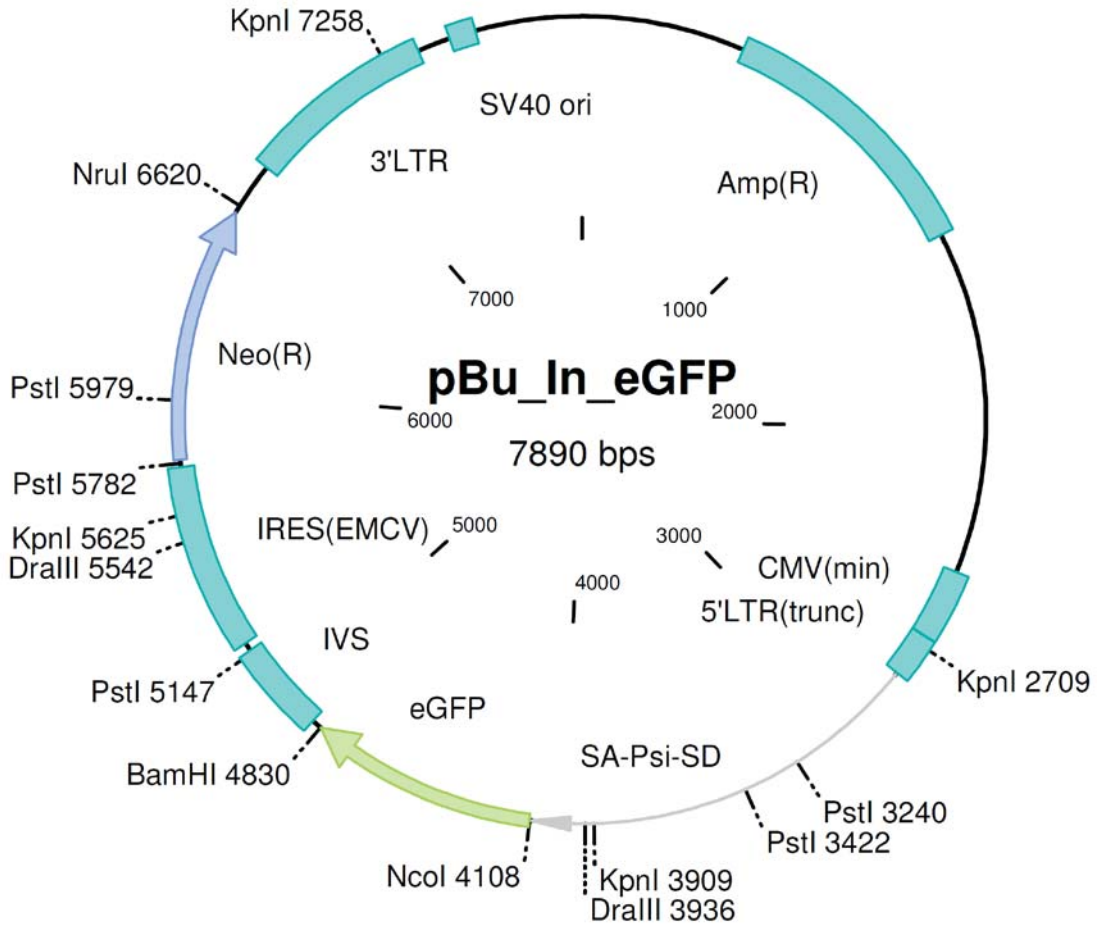


```
Molecule:       pBu_In_eGFP,  7890 bps DNA Circular
File Name:      pBu_In_eGFP.cm5,  dated 25 Nov 2008

Description:    Ligation of eGFP into pBu_In

Notes:          Vector molecule:  pBu_In
                   Fragment ends: BamHI and NcoI
                   Fragment size: 7168
                Insert molecule:  eGFP (enhanced GFP taken from pEGFP-N1 (Clontech))
                   Fragment ends: NcoI and BamHI
                   Fragment size: 722

                Author: Dr. Ralf-Holger Voss (rh.voss@gmx.de)

                Original vector: Retroviral vector pBullet (Dr. Ralph Willemsen)
```

### 13.12. Predicted HLA-A2-negative sequences (MHC class I- and II-restricted)

For all generated 50aa polypeptides possible HLA-A2-negative epitope sequences were predicted via Syfpeithi database (cf., Tab. 8).

**GAGE-1**:
MSWRGRSTYR PRPRRYVEPP EMIGPMRPEQ FSDEVEPATP EEGEPATQRQ (1-50)

*HLA-A*01*
1 M S W R G R S T Y
7 S T Y R P R P R R Y
6 R S T Y R P R P R R Y
*HLA-A*03*
1 M S W R G R S T Y
10 R P R P R R Y V E
22 M I G P M R P E Q F
*HLA-A*1101*
7 S T Y R P R P R R
6 R S T Y R P R P R
1 M S W R G R S T Y R
*HLA-A*2402*
15 R Y V E P P E M I
22 M I G P M R P E Q F
*HLA-A*26*
34 E V E P A T P E E
34 E V E P A T P E E G
*HLA-A*6801*
7 S T Y R P R P R R
1 M S W R G R S T Y R
*HLA-B*0702*
18 E P P E M I G P M
*HLA-B*08*
10 R P R P R R Y V
10 R P R P R R Y V E
*HLA-B*1501*
1 M S W R G R S T Y
*HLA-B*18*
33 D E V E P A T P E
33 D E V E P A T P
*HLA-B*2705*
14 R R Y V E P P E M
*HLA-B*2709*
14 R R Y V E P P E M
9 Y R P R P R R Y V
*HLA-B*37*
23 I G P M R P E Q F
*HLA-B*3801*
14 R R Y V E P P E M I
*HLA-B*4001*
17 V E P P E M I G P
*HLA-B*4101*
17 V E P P E M I G P
*HLA-B*4402*
17 V E P P E M I G P M
*HLA-B*4501*
17 V E P P E M I G P
*HLA-B*5001*
33 D E V E P A T P E
*HLA-B*5101*
27 R P E Q F S D E V
10 R P R P R R Y V
*HLA-DRB1*0101*
20 P E M I G P M R P E Q F S D E
*HLA-DRB1*0401*
28 P E Q F S D E V E P A T P E E
*HLA-DRB1*1101*
6 R S T Y R P R P R R Y V E P P
13 P R R Y V E P P E M I G P M R
*HLA-DRB1*1501*
14 R R Y V E P P E M I G P M R P

**gp100/pmel17**:
SITGSLGPLL DGTATLRLVK RQVPLDCVLY RYGSFSVTLD IVQGIESAEI (449-498)

*HLA-A*01*
472 P L D C V L Y R
471 V P L D C V L Y R Y
469 R Q V P L D C V L Y
470 Q V P L D C V L Y R Y
468 K R Q V P L D C V L Y
*HLA-A*1101*
460 G T A T L R L V K
460 G T A T L R L V K R
470 Q V P L D C V L Y R
456 P L L D G T A T L R
*HLA-A*2402*
479 R Y G S F S V T L
485 V T L D I V Q G I
*HLA-A*26*
488 D I V Q G I E S A
448 E S I T G S L G P L
*HLA-A*6801*
461 T A T L R L V K R
457 L L D G T A T L R
484 S V T L D I V Q G
460 G T A T L R L V K R
456 P L L D G T A T L R
470 Q V P L D C V L Y R
460 G T A T L R L V K
*HLA-B*0702*
455 G P L L D G T A T L
*HLA-B*08*
466 L V K R Q V P L
465 R L V K R Q V P L
*HLA-B*1402*
464 L R L V K R Q V
468 K R Q V P L D C
459 D G T A T L R L
*HLA-B*1501*
472 P L D C V L Y R Y
470 Q V P L D C V L Y
475 C V L Y R Y G S F
469 R Q V P L D C V L Y
*HLA-B*18*
459 D G T A T L R L
*HLA-B*2705*
469 R Q V P L D C V L
465 R L V K R Q V P L
*HLA-B*2709*
468 K R Q V P L D C V
465 R L V K R Q V P L
469 R Q V P L D C V L
479 R Y G S F S V T L
*HLA-B*37*
458 L D G T A T L R L
475 C V L Y R Y G S F
465 R L V K R Q V P L
*HLA-B*3801*
478 Y R Y G S F S V T L
464 L R L V K R Q V P L
468 K R Q V P L D C V L
457 L L D G T A T L R L
450 I T G S L G P L L
*HLA-B*3901*
468 K R Q V P L D C V
479 R Y G S F S V T L
*HLA-B*3902*
469 R Q V P L D C V L
*HLA-B*4001*
465 R L V K R Q V P L
479 R Y G S F S V T L
*HLA-B*4701*
458 L D G T A T L R L
469 R Q V P L D C V L
*HLA-B*4901*
458 L D G T A T L R L
*HLA-B*5001*
488 D I V Q G I E S A
*HLA-B*5101*
459 D G T A T L R L V
*HLA-DRB1*0101*
484 S V T L D I V Q G I E S A E I
*HLA-DRB1*0301*
453 S L G P L L D G T A T L R L V
482 S F S V T L D I V Q G I E S A
468 K R Q V P L D C V L Y R Y G S
*HLA-DRB1*0701*
455 G P L L D G T A T L R L V K R
*HLA-DRB1*1101*
461 T A T L R L V K R Q V P L D C
*HLA-DRB1*1501*
474 D C V L Y R Y G S F S V T L D

**MAGE-A1**:
PARYEFLWGP RALAETSYVK VLEYVIKVSA RVRFFFPSLR EAALREEEEG (259-308)

*HLA-A*01*
274 T S Y V K V L E Y
273 E T S Y V K V L E Y
272 A E T S Y V K V L E Y
*HLA-A*03*
270 A L A E T S Y V K
276 Y V K V L E Y V I K
289 R V R F F F P S L R
282 Y V I K V S A R V R
*HLA-A*1101*
295 P S L R E A A L R
276 Y V K V L E Y V I K
282 Y V I K V S A R V R
*HLA-A*2402*
263 E F L W G P R A L
275 S Y V K V L E Y V I
293 F F P S L R E A A L
*HLA-A*26*
273 E T S Y V K V L E Y
*HLA-A*6801*
276 Y V K V L E Y V I K
282 Y V I K V S A R V R
*HLA-B*0702*
294 F P S L R E A A L
*HLA-B*08*
287 S A R V R F F F
294 F P S L R E A A L
*HLA-B*1402*
290 V R F F F P S L
302 L R E E E E G V
*HLA-B*1501*
285 K V S A R V R F F F
*HLA-B*1510*
263 E F L W G P R A L
*HLA-B*18*
272 A E T S Y V K V L
298 R E A A L R E E E
275 S Y V K V L E Y
*HLA-B*2705*
290 V R F F F P S L R
268 P R A L A E T S Y
*HLA-B*2709*
289 R V R F F F P S L
*HLA-B*37*
272 A E T S Y V K V L
285 K V S A R V R F F
*HLA-B*3801*
288 A R V R F F F P S L
*HLA-B*4001*
272 A E T S Y V K V L
*HLA-B*4101*
262 Y E F L W G P R A
280 L E Y V I K V S A
*HLA-B*4402*
272 A E T S Y V K V L
262 Y E F L W G P R A L
*HLA-B*4501*
262 Y E F L W G P R A
280 L E Y V I K V S A
272 A E T S Y V K V L
292 F F F P S L R E A
*HLA-B*4901*
272 A E T S Y V K V L
*HLA-B*5001*
262 Y E F L W G P R A
280 L E Y V I K V S A
*HLA-B*5101*
271 L A E T S Y V K V
*HLA-DRB1*0101*
259 P A R Y E F L W G P R A L A E
*HLA-DRB1*0301*
281 E Y V I K V S A R V R F F F P
291 R F F F P S L R E A A L R E E
*HLA-DRB1*0701*
279 V L E Y V I K V S A R V R F F
*HLA-DRB1*1101*
277 V K V L E Y V I K V S A R V R
261 R Y E F L W G P R A L A E T S
290 V R F F F P S L R E A A L R E
259 P A R Y E F L W G P R A L A E
*HLA-DRB1*1501*
287 S A R V R F F F P S L R E A A

**MAGE-C2**:
WGPRAHSESI KKKVLEFLAK LNNTVPSSFP SWYKDALKDV EERVQATIDT (301-350)

*HLA-A*01*
323 N T V P S S F P S W Y
*HLA-A*03*
320 K L N N T V P S S F
*HLA-A*1101*
330 P S W Y K D A L K
326 P S S F P S W Y K
*HLA-A*2402*
313 K V L E F L A K L
328 S F P S W Y K D A L
*HLA-A*26*
308 E S I K K K V L E F
*HLA-A*6801*
335 D A L K D V E E R
339 D V E E R V Q A T I
*HLA-B*0702*
329 F P S W Y K D A L
*HLA-B*08*
309 S I K K K V L E
308 E S I K K K V L
311 K K K V L E F L
330 P S W Y K D A L
309 S I K K K V L E F
307 S E S I K K K V L
310 I K K K V L E F L

*HLA-B*1501*
320 K L N N T V P S S F
324 T V P S S F P S W Y
*HLA-B*18*
307 S E S I K K K V L
*HLA-B*2705*
303 P R A H S E S I K
304 R A H S E S I K K
313 K V L E F L A K L
*HLA-B*2709*
313 K V L E F L A K L
*HLA-B*37*
307 S E S I K K K V L
*HLA-B*3902*
310 I K K K V L E F L
*HLA-B*4001*
307 S E S I K K K V L
*HLA-B*4402*
307 S E S I K K K V L
*HLA-B*4701*
313 K V L E F L A K L
*HLA-B*4901*
340 V E E R V Q A T I
*HLA-B*5001*
338 K D V E E R V Q A

*HLA-B*5101*
302 G P R A H S E S I
318 L A K L N N T V
*HLA-DRB1*0301*
326 P S S F P S W Y K D A L K D V
*HLA-DRB1*1501*
311 K K K V L E F L A K L N N T V

**MDM2**:
KEVLFYLGQY IMTKRLYDEK QQHIVYCSND LLGDLFGVPS FSVKEHRKIY (51-100)

*HLA-A*01*
67 Y D E K Q Q H I V Y
66 L Y D E K Q Q H I V Y
91 F S V K E H R K I Y
*HLA-A*1101*
62 M T K R L Y D E K
89 P S F S V K E H R K
*HLA-A*2402*
66 L Y D E K Q Q H I
90 S F S V K E H R K I
*HLA-A*26*
52 E V L F Y L G Q Y
*HLA-A*6801*
52 E V L F Y L G Q Y
57 L G Q Y I M T K R
56 Y L G Q Y I M T K R

*HLA-B*1501*
92 S V K E H R K I Y
58 G Q Y I M T K R L Y
65 R L Y D E K Q Q H I
*HLA-B*18*
68 D E K Q Q H I V Y
84 D L F G V P S F
*HLA-B*37*
79 N D L L G D L F
83 G D L F G V P S F
*HLA-B*3801*
72 Q H I V Y C S N D L
*HLA-B*3902*
58 G Q Y I M T K R L
*HLA-B*4402*
68 D E K Q Q H I V Y
51 K E V L F Y L G Q Y

*HLA-B*4701*
83 G D L F G V P S F
*HLA-B*4901*
66 L Y D E K Q Q H I
*HLA-DRB1*0101*
79 N D L L G D L F G V P S F S V
*HLA-DRB1*0301*
71 Q Q H I V Y C S N D L L G D L
*HLA-DRB1*0701*
82 L G D L F G V P S F S V K E H

**Melan-A/MART-1**:
GHGHSYTTAE EAAGIGILTV ILGVLLLIGC WYCRRRNGYR ALMDKSLHVG (16-65)

*HLA-A*03*
39 V L L L I G C W Y
38 G V L L L I G C W Y
*HLA-A*1101*
33 L T V I L G V L L L
*HLA-A*2402*
35 V I L G V L L L I
34 T V I L G V L L L
53 G Y R A L M D K S L
*HLA-A*26*
34 T V I L G V L L L
33 L T V I L G V L L L
*HLA-B*1402*
34 T V I L G V L L L
54 Y R A L M D K S L
35 V I L G V L L L
50 R R N G Y R A L
*HLA-B*1501*
39 V L L L I G C W Y
38 G V L L L I G C W Y
*HLA-B*18*
25 E E A A G I G I L
*HLA-B*2705*
49 R R R N G Y R A L
50 R R N G Y R A L M
*HLA-B*2709*
49 R R R N G Y R A L
50 R R N G Y R A L M
*HLA-B*37*
33 L T V I L G V L
25 E E A A G I G I L
*HLA-B*3801*
48 C R R R N G Y R A L
32 I L T V I L G V L L
*HLA-B*3901*
54 Y R A L M D K S L
*HLA-B*4001*
25 E E A A G I G I L
34 T V I L G V L L L
*HLA-B*4402*
25 E E A A G I G I L
24 A E E A A G I G I
24 A E E A A G I G I L
*HLA-B*4501*
25 E E A A G I G I L
*HLA-B*4701*
49 R R R N G Y R A L
*HLA-B*4901*
24 A E E A A G I G I
*HLA-B*5001*
20 S Y T T A E E A A
*HLA-B*5101*
27 A A G I G I L T V
23 T A E E A A G I
26 E A A G I G I L
*HLA-DRB1*0101*
30 I G I L T V I L G V L L L I G
*HLA-DRB1*0401*
51 R N G Y R A L M D K S L H V G
*HLA-DRB1*0701*
51 R N G Y R A L M D K S L H V G
18 G H S Y T T A E E A A G I G I
*HLA-DRB1*1501*
30 I G I L T V I L G V L L L I G

**MIF**:
LMAFGGSSEP CALCSLHSIG KIGGAQNRSY SKLLCGLLAE RLRISPDRVY (47-96)

*HLA-A*01*
53 S S E P C A L C S
*HLA-A*03*
78 K L L C G L L A E
87 R L R I S P D R V Y
58 A L C S L H S I G K
*HLA-A*1101*
53 S S E P C A L C S
58 A L C S L H S I G K
*HLA-A*2402*
75 S Y S K L L C G L
75 S Y S K L L C G L L
*HLA-A*6801*
79 L L C G L L A E R
78 K L L C G L L A E R
58 A L C S L H S I G K
*HLA-B*08*
83 L L A E R L R I
76 Y S K L L C G L
76 Y S K L L C G L L
*HLA-B*1402*
73 N R S Y S K L L C
73 N R S Y S K L L
88 L R I S P D R V
*HLA-B*1501*
87 R L R I S P D R V Y
*HLA-B*1510*
51 G G S S E P C A L
*HLA-B*18*
54 S E P C A L C S L
*HLA-B*2705*
86 E R L R I S P D R
88 L R I S P D R V Y
*HLA-B*2709*
82 G L L A E R L R I
*HLA-B*37*
54 S E P C A L C S L
85 A E R L R I S P D
*HLA-B*3901*
62 L H S I G K I G G
*HLA-B*3902*
71 A Q N R S Y S K L
*HLA-B*4001*
54 S E P C A L C S L
*HLA-B*4402*
54 S E P C A L C S L
85 A E R L R I S P D
71 A Q N R S Y S K L L
*HLA-B*4501*
85 A E R L R I S P D
*HLA-B*4701*
80 L C G L L A E R L
*HLA-B*4901*
54 S E P C A L C S L
82 G L L A E R L R I
*HLA-B*5101*
57 C A L C S L H S I
*HLA-DRB1*0101*
77 S K L L C G L L A E R L R I S
*HLA-DRB1*0301*
65 I G K I G G A Q N R S Y S K L
*HLA-DRB1*0701*
47 L M A F G G S S E P C A L C S
*HLA-DRB1*1101*
59 L C S L H S I G K I G G A Q N
81 C G L L A E R L R I S P D R V

**NA17-A**:
MVLPDVFIRC VVFCLTVVCW TWVPLRGPSS PGSYRKWMCF SESQVQPTQK (1-50)

*HLA-A*01*
26 R G P S S P G S Y
25 L R G P S S P G S Y
24 P L R G P S S P G S Y
*HLA-A*03*
5 D V F I R C V V F
10 C V V F C L T V V C
*HLA-A*1101*
42 E S Q V Q P T Q K
17 V V C W T W V P L R
*HLA-A*2402*
6 V F I R C V V F C L
*HLA-A*26*
5 D V F I R C V V F
5 D V F I R C V V F C
*HLA-A*6801*
1 M V L P D V F I R
17 V V C W T W V P L R
*HLA-B*0702*
30 S P G S Y R K W M
3 L P D V F I R C V V
*HLA-B*08*
7 F I R C V V F C L
*HLA-B*1402*
5 D V F I R C V V F
8 I R C V V F C L
*HLA-B*1501*
5 D V F I R C V V F
*HLA-B*18*
5 D V F I R C V V F
*HLA-B*2705*
28 P S S P G S Y R K
*HLA-B*37*
41 S E S Q V Q P T
*HLA-B*3901*
17 V V C W T W V P L
*HLA-B*4001*
17 V V C W T W V P L
*HLA-B*4402*
28 P S S P G S Y R K W
*HLA-B*4701*
4 P D V F I R C V V
*HLA-B*5101*
3 L P D V F I R C V
23 V P L R G P S S
*HLA-DRB1*0101*
19 C W T W V P L R G P S S P G S
*HLA-DRB1*0301*
14 C L T V V C W T W V P L R G P
*HLA-DRB1*0401*
19 C W T W V P L R G P S S P G S
*HLA-DRB1*0701*
34 Y R K W M C F S E S Q V Q P T
*HLA-DRB1*1101*
17 V V C W T W V P L R G P S S P
*HLA-DRB1*1501*
14 C L T V V C W T W V P L R G P

**NY-ESO-1**:
FTVSGNILTI RLTAADHRQL QLSISSCLQQ LSLLMWITQC FLPVFLAQPP (126-175)

*HLA-A*01*
139 A A D H R Q L Q L
139 A A D H R Q L Q L S
139 A A D H R Q L Q L S I
*HLA-A*03*
134 T I R L T A A D H
127 T V S G N I L T I
134 T I R L T A A D H R
*HLA-A*1101*
128 V S G N I L T I R
126 F T V S G N I L T
127 T V S G N I L T I R
*HLA-A*26*
162 I T Q C F L P V F
126 F T V S G N I L T I
147 L S I S S C L Q Q L
161 W I T Q C F L P V F
*HLA-A*6801*
128 V S G N I L T I R
127 T V S G N I L T I R
134 T I R L T A A D H R
*HLA-B*08*
139 A A D H R Q L Q L
*HLA-B*1402*
150 S S C L Q Q L S L
142 H R Q L Q L S I
151 S C L Q Q L S L
*HLA-B*1501*
158 L L M W I T Q C F
157 S L L M W I T Q C F
*HLA-B*2705*
135 I R L T A A D H R
*HLA-B*37*
140 A D H R Q L Q L
146 Q L S I S S C L
139 A A D H R Q L Q L
*HLA-B*3801*
138 T A A D H R Q L Q L
149 I S S C L Q Q L S L
141 D H R Q L Q L S I
139 A A D H R Q L Q L
*HLA-B*3901*
141 D H R Q L Q L S I
163 T Q C F L P V F L
*HLA-B*3902*
145 L Q L S I S S C L
163 T Q C F L P V F L
143 R Q L Q L S I S S
*HLA-B*4001*
163 T Q C F L P V F L
139 A A D H R Q L Q L
129 S G N I L T I R L
*HLA-B*4101*
131 N I L T I R L T A
*HLA-B*4701*
129 S G N I L T I R L
145 L Q L S I S S C L
*HLA-B*4901*
127 T V S G N I L T I
*HLA-DRB1*0301*
156 L S L L M W I T Q C F L P V F
155 Q L S L L M W I T Q C F L P V
*HLA-DRB1*0401*
134 T I R L T A A D H R Q L Q L S
156 L S L L M W I T Q C F L P V F
*HLA-DRB1*0701*
142 H R Q L Q L S I S S C L Q Q L

**p53**:
TAKSVTCTYS PALNKMFCQL AKTCPVQLWV DSTPPPGTRV RAMAIYKQSQ (118-167)

*HLA-A*01*
154 G T R V R A M A I Y
*HLA-A*03*
156 R V R A M A I Y K
136 Q L A K T C P V Q L
*HLA-A*1101*
124 C T Y S P A L N K
156 R V R A M A I Y K
149 S T P P P G T R V R
*HLA-A*2402*
125 T Y S P A L N K M
125 T Y S P A L N K M F
*HLA-A*26*
121 S V T C T Y S P A L
*HLA-A*6801*
148 D S T P P P G T R
149 S T P P P G T R V R
*HLA-B*0702*
151 P P P G T R V R A
*HLA-B*08*
130 L N K M F C Q L
137 L A K T C P V Q L
154 G T R V R A M A I
*HLA-B*4001*
137 L A K T C P V Q L
*HLA-B*5101*
137 L A K T C P V Q L
*HLA-DRB1*0101*
131 N K M F C Q L A K T C P V Q L
*HLA-DRB1*0701*
119 A K S V T C T Y S P A L N K M
123 T C T Y S P A L N K M F C Q L
*HLA-DRB1*1101*
131 N K M F C Q L A K T C P V Q L
*HLA-DRB1*1501*
134 F C Q L A K T C P V Q L W V D
140 T C P V Q L W V D S T P P P G

**RAB38/NY-Mel-1**:
ATIGVDFALK VLHWDPETVV RLQLWDIAGQ ERFGNMTRVY YREAM GAFIV (40-89)

*HLA-A*01*
71 R F G N M T R V Y
70 E R F G N M T R V Y
69 Q E R F G N M T R V Y
70 E R F G N M T R V Y Y
*HLA-A*03*
77 R V Y Y R E A M G
*HLA-A*1101*
40 A T I G V D F A L K
*HLA-A*2402*
79 Y Y R E A M G A F
53 W D P E T V V R L
78 V Y Y R E A M G A F
79 Y Y R E A M G A F I
*HLA-A*26*
56 E T V V R L Q L W
43 G V D F A L K V L
40 A T I G V D F A L
70 E R F G N M T R V Y
56 E T V V R L Q L W D
*HLA-A*6801*
40 A T I G V D F A L K
*HLA-B*0702*
54 D P E T V V R L Q L
*HLA-B*1402*
38 Y R A T I G V D F
70 E R F G N M T R V
59 V R L Q L W D I
44 V D F A L K V L
*HLA-B*1501*
50 V L H W D P E T V
62 Q L W D I A G Q E
71 R F G N M T R V Y
71 R F G N M T R V Y Y
*HLA-B*1510*
53 W D P E T V V R L
*HLA-B*18*
55 P E T V V R L Q L
54 D P E T V V R L
56 E T V V R L Q L
65 D I A G Q E R F
*HLA-B*2705*
70 E R F G N M T R V
76 T R V Y Y R E A M
*HLA-B*2709*
70 E R F G N M T R V
76 T R V Y Y R E A M
*HLA-B*37*
44 V D F A L K V L
53 W D P E T V V R L
*HLA-B*3801*
52 H W D P E T V V R L
*HLA-B*4001*
55 P E T V V R L Q L
53 W D P E T V V R L
*HLA-B*4402*
55 P E T V V R L Q L
40 A T I G V D F A L
55 P E T V V R L Q L W
*HLA-B*4701*
53 W D P E T V V R L
64 W D I A G Q E R F
*HLA-B*4901*
81 R E A M G A F I V
*HLA-B*5101*
42 I G V D F A L K V
54 D P E T V V R L
*HLA-DRB1*0301*
48 L K V L H W D P E T V V R L Q
69 Q E R F G N M T R V Y Y R E A
*HLA-DRB1*1101*
69 Q E R F G N M T R V Y Y R E A
72 F G N M T R V Y Y R E A M G A
*HLA-DRB1*1501*
47 A L K V L H W D P E T V V R L

**TRP2**:

ALPHSAANDP IFVVISNRLL YNATTNILEH VRKEKATKEL PSLHVLVLHS (381-430)

*HLA-A*01*
393 V V I S N R L L Y
392 F V V I S N R L L Y
391 I F V V I S N R L L Y
*HLA-A*03*
398 R L L Y N A T T N
410 H V R K E K A T K
407 I L E H V R K E K
393 V V I S N R L L Y
406 N I L E H V R K E K
*HLA-A*1101*
410 H V R K E K A T K
404 T T N I L E H V R K
403 A T T N I L E H V R
*HLA-A*2402*
400 L Y N A T T N I L
391 I F V V I S N R L
391 I F V V I S N R L L
*HLA-A*26*
393 V V I S N R L L Y
392 F V V I S N R L L Y
419 E L P S L H V L V L
414 E K A T K E L P S L
*HLA-A*6801*
390 P I F V V I S N R
404 T T N I L E H V R
404 T T N I L E H V R K
403 A T T N I L E H V R
409 E H V R K E K A T K
*HLA-B*0702*
420 L P S L H V L V L
382 L P H S A A N D P I
419 E L P S L H V L V L
*HLA-B*08*
411 V R K E K A T K
416 A T K E L P S L
413 K E K A T K E L
411 V R K E K A T K E
*HLA-B*1402*
420 L P S L H V L V L
421 P S L H V L V L
*HLA-B*1501*
393 V V I S N R L L Y
392 F V V I S N R L L Y
*HLA-B*1510*
391 I F V V I S N R L
*HLA-B*18*
418 K E L P S L H V L
413 K E K A T K E L
*HLA-B*37*
413 K E K A T K E L
418 K E L P S L H V L
420 L P S L H V L V L
*HLA-B*3801*
383 P H S A A N D P I F
411 V R K E K A T K E L
383 P H S A A N D P I
*HLA-B*3902*
412 R K E K A T K E L
418 K E L P S L H V L
*HLA-B*4001*
418 K E L P S L H V L
420 L P S L H V L V L
*HLA-B*4101*
408 L E H V R K E K A
413 K E K A T K E L P
418 K E L P S L H V L
*HLA-B*4402*
418 K E L P S L H V L
387 A N D P I F V V I
373 H S F L N G T N A L
*HLA-B*4501*
408 L E H V R K E K A
413 K E K A T K E L P
418 K E L P S L H V L
*HLA-B*4901*
418 K E L P S L H V L
403 A T T N I L E H V
417 T K E L P S L H V
*HLA-B*5001*
408 L E H V R K E K A
*HLA-B*5101*
420 L P S L H V L V L
386 A A N D P I F V V
385 S A A N D P I F V
420 L P S L H V L V
386 A A N D P I F V
*HLA-DRB1*0101*
388 N D P I F V V I S N R L L Y N
*HLA-DRB1*0301*
390 P I F V V I S N R L L Y N A T
389 D P I F V V I S N R L L Y N A
*HLA-DRB1*0401*
389 D P I F V V I S N R L L Y N A
388 N D P I F V V I S N R L L Y N
*HLA-DRB1*0701*
389 D P I F V V I S N R L L Y N A
397 N R L L Y N A T T N I L E H V
388 N D P I F V V I S N R L L Y N
*HLA-DRB1*1101*
405 T N I L E H V R K E K A T K E

**Tyrosinase**:
MLLAVLYCLL WSFQTSAGHF PRACVSSKNL MEKECCPPWS GDRSPCGQLS (1-50)

*HLA-A*03*
4 A V L Y C L L W S F
24 C V S S K N L M E K
*HLA-A*1101*
25 V S S K N L M E K
24 C V S S K N L M E K
*HLA-A*2402*
12 S F Q T S A G H F
*HLA-A*26*
4 A V L Y C L L W S F
*HLA-A*6801*
14 Q T S A G H F P R
24 C V S S K N L M E K
*HLA-B*1402*
1 M L L A V L Y C L
42 D R S P C G Q L
*HLA-B*1501*
5 V L Y C L L W S F
4 A V L Y C L L W S F
*HLA-B*1510*
18 G H F P R A C V S
*HLA-B*18*
31 M E K E C C P P W
*HLA-B*2709*
22 R A C V S S K N L
41 G D R S P C G Q L
*HLA-B*37*
41 G D R S P C G Q L
*HLA-B*3801*
21 P R A C V S S K N L
*HLA-B*4402*
31 M E K E C C P P W
*HLA-B*4701*
41 G D R S P C G Q L
*HLA-B*5001*
31 M E K E C C P P W
9 L L W S F Q T S A
15 T S A G H F P R A
33 K E C C P P W S G
*HLA-B*5101*
3 L A V L Y C L L
*HLA-DRB1*0101*
10 L W S F Q T S A G H F P R A C
*HLA-DRB1*0401*
4 A V L Y C L L W S F Q T S A G
*HLA-DRB1*1501*
7 Y C L L W S F Q T S A G H F P

### 13.13. Predicted HLA-A2-restricted sequences

For all generated 50aa polypeptides, possible HLA-A2-restricted epitope sequences were predicted via Syfpeithi database (cf., Tab. 8).

**GAGE-1**:
MSWRGRSTYR PRPRRYVEPP EMIGPMRPEQ FSDEVEPATP EEGEPATQRQ (1-50)

*HLA-A*0201*

| | |
|---|---|
| 9 | Y R P R P R R Y V |

**gp100/pmel17**:
SITGSLGPLL DGTATLRLVK RQVPLDCVLY RYGSFSVTLD IVQGIESAEI (449-498)

*HLA-A*0201*

| | |
|---|---|
| 456 | P L L D G T A T L |
| 449 | S I T G S L G P L |
| 457 | L L D G T A T L R L |

**MAGE-A1**:
PARYEFLWGP RALAETSYVK VLEYVIKVSA RVRFFFPSLR EAALREEEEG (259-308)

*HLA-A*0201*

| | |
|---|---|
| 278 | K V L E Y V I K V |
| 270 | A L A E T S Y V K V |

**MAGE-C2**:
WGPRAHSESI KKKVLEFLAK LNNTVPSSFP SWYKDALKDV EERVQATIDT (301-350)

*HLA-A*0201*

| | |
|---|---|
| 313 | K V L E F L A K L |
| 317 | F L A K L N N T V |
| 309 | S I K K K V L E F L |

**MDM2**:
KEVLFYLGQY IMTKRLYDEK QQHIVYCSND LLGDLFGVPS FSVKEHRKIY (51-100)

*HLA-A*0201*

| | |
|---|---|
| 80 | D L L G D L F G V |

**Melan-A/MART-1**:
GHGHSYTTAE EAAGIGILTV ILGVLLLIGC WYCRRRNGYR ALMDKSLHVG (16-65)

*HLA-A*0201*

| | |
|---|---|
| 31 | G I L T V I L G V |
| 35 | V I L G V L L L I |
| 31 | G I L T V I L G V L |

**MIF**:
LMAFGGSSEP CALCSLHSIG KIGGAQNRSY SKLLCGLLAE RLRISPDRVY (47-96)

*HLA-A*0201*

| | |
|---|---|
| 79 | L L C G L L A E R |
| 79 | L L C G L L A E R L |

**NA17-A**:
MVLPDVFIRC VVFCLTVVCW TWVPLRGPSS PGSYRKWMCF SESQVQPTQK (1-50)

*HLA-A*0201*

| | |
|---|---|
| 7 | F I R C V V F C L |
| 2 | V L P D V F I R C V |

**NY-ESO-1**:
FTVSGNILTI RLTAADHRQL QLSISSCLQQ LSLLMWITQC FLPVFLAQPP (126-175)

*HLA-A*0201*

| | |
|---|---|
| 148 | S I S S C L Q Q L |
| 127 | T V S G N I L T I |
| 158 | L L M W I T Q C F L |
| 126 | F T V S G N I L T I |

**p53**:
TAKSVTCTYS PALNKMFCQL AKTCPVQLWV DSTPPPGTRV RAMAIYKQSQ (118-167)

*HLA-A*0201*

| | |
|---|---|
| 129 | A L N K M F C Q L |
| 132 | K M F C Q L A K T |
| 136 | Q L A K T C P V Q L |

**RAB38/NY-Mel-1**:
ATIGVDFALK VLHWDPETVV RLQLWDIAGQ ERFGNMTRVY YREAM GAFIV (40-89)

*HLA-A*0201*

| | |
|---|---|
| 50 | V L H W D P E T V |
| 40 | A T I G V D F A L |

**TRP2**:
ALPHSAANDP IFVVISNRLL YNATTNILEH VRKEKATKEL PSLHVLVLHS (381-430)

*HLA-A*0201*

| | |
|---|---|
| 399 | L L Y N A T T N I L |
| 385 | S A A N D P I F V V |

**Tyrosinase**:
MLLAVLYCLL WSFQTSAGHF PRACVSSKNL MEKECCPPWS GDRSPCGQLS (1-50)

*HLA-A*0201*

| | |
|---|---|
| 1 | M L L A V L Y C L |
| 2 | L L A V L Y C L L |
| 1 | M L L A V L Y C L L |